JOINTED ROCK MASS DEFORMABILITY:

A PROBABILISTIC APPROACH

by

WILLIAM SIMON DERSHOWITZ

SBCE, Massachusetts Institute of Technology

Cambridge, Massachusetts

(1977)

Submitted in partial fulfillment
of the requirements for the
degree of

Master of Science

at the

Massachusetts Institute of Technology

June, 1979

© William Simon Dershowitz 1979

Signature of Author.....
Department of Civil Engineering
June, 1979

Certified by.....
Thesis Supervisor

Certified by.....
Thesis Supervisor

Accepted by.....
Chairman, Department Committee on Graduate Students
of the Department of Civil Engineering

OF TECHNOLOGY
JUL 12 1979
LIBRARIES

JOINTED ROCK MASS DEFORMABILITY - A PROBABILISTIC APPROACH

BY

WILLIAM SIMON DERSHOWITZ

Submitted to the Department of Civil Engineering on May 24, 1979, in partial fulfillment of the requirements for the degree of Master of Science.

ABSTRACT

Rock mass deformability is usually predicted with empirical correlations such as Deere (1967)'s correlation with RQD or with large scale field tests. This is due in part to the failure of current models to adequately represent the mechanism of rock mass deformation and the variability of rock masses.

The thesis presents a critique of current modeling concepts and proposes improvements. The proposed methods depend upon more accurate description of rock mass geometry and the mechanics of deformation.

The description of rock mass geometry is improved through the use of probabilistic models of joint geometry. Distributions for joint spacing, length, and orientation are presented and discussed. The descriptions proposed rely exclusively on commonly measured parameters.

Deformation is separated into intact rock and normal and shear joint deformation components. Separate treatment of these allows coherent analysis of the factors affecting deformability.

Finally, the thesis presents examples of the use of probabilistic models. Model results are compared to the results of similar deterministic models, and to Deere's correlation. Model results under different boundary conditions and assumptions are studied and the sensitivity of deformation to different conditions is assessed.

Name and Title of Thesis Supervisors: Gregory B. Baecher
Assistant Professor of
Civil Engineering

Herbert H. Einstein
Associate Professor of
Civil Engineering

ACKNOWLEDGMENTS

I would like to extend my deepest gratitude to Professors Herbert Einstein and Gregory Baecher for their encouragement and guidance. Although the ideas presented in the thesis are my own, they could never have been developed without their assistance and advice.

I would also like to thank the U.S. Bureau of Mines which provided the funding under which this thesis was produced.

Elizabeth Manzi typed the final manuscript and Jim Turlo drafted most of the figures. I appreciate the long nights they spent in helping me meet my deadlines.

Most of all, I would like to thank my love, Susan Hankin, who has made all the hard work worthwhile.

TABLE OF CONTENTS

	Page
TITLE PAGE	1
ABSTRACT	2
ACKNOWLEDGEMENTS	3
TABLE OF CONTENTS	4
LIST OF FIGURES	7
LIST OF TABLES	14
CHAPTER 1: INTRODUCTION	15
1.1 Statement of Problem	15
1.2 Subjects to be Explored	15
1.3 Thesis Structure	16
CHAPTER 2: MODELS FOR ROCK MASS DEFORMATION	17
2.1 Introduction	17
2.2 Models Based on Elasticity Theory	19
2.3 Models Based on Elasto-Plasticity Concept	40
2.4 Discussion	46
2.5 Summary	48
CHAPTER 3: PROBABILISTIC DESCRIPTION OF ROCK MASSES.	49
3.1 Introduction	49
3.2 Types of Description	52
3.3 Rock Mass Properties of Interest	54
3.4 Description of Joint Geometry	55
3.5 Description of Deformability Properties	104
3.6 Summary of Distributional Forms	107

Page

CHAPTER 4: PROBABILISTIC MODELS FOR ROCK MASS DEFORMATION 109

4.1 Introduction 109

4.2 Assumptions used in Probabilistic Models . . 109

4.3 Computational Stratagies for Probabilistic Models 111

4.4 Model 1 - Constrained Cylinder 114

4.5 Model 2 - Boundary Element Model 144

4.6 Conclusions 155

CHAPTER 5: EXAMPLES OF APPLICATION OF PROBABILISTIC MODELS 157

5.1 Introduction 157

5.2 Chapter Structure 157

5.3 Parameter Study of Rock Mass Deformation-Deterministic Assumptions 158

5.4 Parameter Study of Rock Mass Deformation-Probabilistic Assumptions 165

5.5 Comparison of Probabilistic and Deterministic Results 175

5.6 Effect of Boundary Conditions 177

5.7 Validity of Assumptions 183

5.8 RQD - $\hat{E}/E$ Correlation 184

5.9 Conclusions 195

CHAPTER 6: SUMMARY AND CONCLUSIONS 197

6.1 Summary 197

6.2 Conclusions 197

Page

REFERENCES 201

APPENDIX A: ROCK MASS DEFORMABILITY LITERATURE . . . 209

A.1 Description of Joints 209

A.2 RQD 216

A.3 Rock Mass Modulus of Deformation 220

A.4 Joint Stiffness 238

APPENDIX B: ORIENTATION LITERATURE 253

B.1 Graphical Representation of Orientation Data 253

B.2 Clustering 262

B.3 Distributions of Orientation Data 269

B.4 Orientation Sampling Bias 277

APPENDIX C: FITTING ORIENTATION DATA 283

C.1 Introduction 283

C.2 Fitting Procedure 284

C.3 Results 290

C.4 Conclusions 290

LIST OF FIGURES

Figure Number	Title	Page
2.2.1	Linear Elastic Stress-Strain Curve	20
2.2.2	Plane Stress and Plane Strain	22
2.2.3	Triaxial Case	25
2.2.4	Isotropic Linear-Elastic Half-Space	27
2.2.5	Anisotropic Linear-Elastic Half-Space	29
2.2.6	Goodman et. al. (1968) Joint Geometry	33
2.2.7	Kulhawy (1978) Joint Geometry	36
2.2.8	Hungr & Coates (1978) Results	38
2.2.9	Burman & Hammett (1976) Model	39
2.3.1	Elasto-Plastic Stress-Strain Curve	41
2.3.2	Typical Plate Jacking Test Results (Deere, 1967)	42
2.3.3	Elasto-Plastic Stress-Strain Approximated by Elastic Properties - Iida (1968) Method	45
3.1.1	Spatial Variability of Rock Mass Properties	50
3.1.2	Statistical Variability of Rock Mass Properties	51
3.4.1	Discontinuity Planes in Space	56
3.4.2	Joint Spacing	58
3.4.3	Joint Spacing from Cores	60
3.4.4	Joint Spacing from Surface Surveys	61
3.4.5	Exponential Distribution of Spacing	63
3.4.6	Joint Traces	65
3.4.7	Joint Traces for Differently Shaped Joint Planes	67

Figure Number	Title	Page
3.4.8	Distribution of Trace Lengths-Circular Joints with Random Intersections with Sampling Surface	68
3.4.9	Trace Length Bias from Orientation of Sampling Line	69
3.4.10	Persistence	72
3.4.11	Cartesian, Cylindrical, and Spherical Coordinates	76
3.4.12	Joint Orientations as Unit Vectors on a Unit Hemisphere	78
3.4.13	Probability Distributions as Frequencies	79
3.4.14	Spherical and Planar Distributions	81
3.4.15	Axes for Three-Dimensional Plots	84
3.4.16	3D Representation of Uniform Distribution on a Sphere	85
3.4.17	Fisher Distribution Density Function (Mardia, 1972)	88
3.4.18	Three Dimensional Representation of Fisher Distribution (κ=5)	89
3.4.19	3D Representation of Bivariate Fisher Distribution	93
3.4.20	3D Representation of Bingham Distribution ($k_1 = -5; k_2 = -3$)	96
3.4.21	Surface of Sphere Approximated by Plane for Highly Concentrated Distribution	98
3.4.22	3D Representation of Normal Distribution on a Plane (Maranhao, 1968)	99
3.4.23	Deterministic Spacing Model and RQD	101
3.4.24	Inclined Joint Sets and RQD	103
4.4.1	Constrained Cylinder Concept	115

Figure Number	Title	Page
4.4.2	Stress Concentrations in Jointed Rock (Maury, 1970)	118
4.4.3	Interference due to Large Intact Rock and Rock Joint Deformation	119 120
4.4.4	Interference between Intersecting Rock Joints	120
4.4.5	Two and Three Dimensional Geometric Parameters	121
4.4.6	Mohr's Circle of Stresses	126
4.4.7	Calculation of Vertical Displacement by Vectorial Addition	128
4.4.8	Constrained Cylinder Model Cases	130
4.4.9	Unconstrained 2-D Cylinder Boundary Conditions and Geometry	132
4.4.10	Triaxial 2-D Cylinder Boundary Conditions and Geometry	136
4.4.11	Strain Dependent 2-D Cylinger Boundary Conditions and Geometry	140
4.4.12	Boundary Conditions & Geometry-Strain Dependent 3 Dimensional Cylinder	143
4.5.1	Boundary Element Model Concept	145
4.5.2	Spacing-Persistence Relationship	147
4.5.3	Joint Placement Process	149
4.5.4	Non-Linear Elastic Behavior	151
5.3.1	Constrained Cylinder Model with Parameters to be studied (Deterministic Geometry)	159
5.3.2	Rock Mass Deformability as a Function of Dip ϕ and spacing s (Deterministic Geometry	161
5.3.3	Rock Mass Deformability for Different Values of Stiffness (Deterministic Geometry)	162

Figure Number	Title	Page
5.3.4	Rock Mass Model with Fixed Boundaries	164
5.4.1	Constrained Cylinder Model with Parameters to be Studied - Probabilistic Orientation	167
5.4.2	Rock Mass Deformability as a Function of Mean Dip ϕ and Dispersion κ (Probabilistic Geometry)	168
5.4.3	Rock Mass Deformability as a Function of Dip ϕ and Spacing s (Probabilistic Geometry)	170
5.4.4	Standard Deviation of Rock Mass Deformability as a Function of Dip ϕ and Dispersion κ (Probabilistic Geometry)	171
5.4.5	Rock Mass Deformability for Different Values of Stiffness (Probabilistic Geometry)	172
5.4.6	Joint Interference-Non-Parallel Joints	174
5.5.1	Comparison of Deterministic and Probabilistic Rock Mass Deformability Predictions	176
5.6.1	Rock Mass Deformability for Different Boundary Conditions (Deterministic Geometry)	179
5.6.2	Unconfined Cylinder, Constant Stress Triaxial, and Lateral Strain Dependent Triaxial Boundary Conditions	180
5.8.1	RQD as a Function of dip ϕ and spacing s (Deterministic Geometry)	186
5.8.2	Rock Mass Deformability as a Function of Dip ϕ and Spacing s (Deterministic Geometry)	187
5.8.3	Rock Mass Deformability Predicted from RQD for Different Values of Dip ϕ and Spacing s (Deterministic Geometry)	188

Figure Number	Title	Page
5.8.4	Rock Mass Deformability for Different Values of Stiffness (Deterministic Geometry)	189
5.8.5	Rock Mass Deformability Relation to RQD: Model Results and Deere's (1967) Correlation	182
5.8.6	RQD as a Function of Dip ϕ and Dispersion κ (Probabilistic Geometry)	191
5.8.7	Rock Mass Deformability as a Function of Mean Dip ϕ and Dispersion κ (Probabilistic Geometry)	192
5.8.8	Rock Mass Deformability Predicted From RQD (Probabilistic Geometry)	193
A.1.1	Sedimentary Joint Plane Types (Bassarab, 1975)	211
A.1.2	RQD-Fracture Frequency Relationship (Deere, 1967)	214
A.1.3	RQD-Velocity Ratio V_f/V_1 Correlation (Deere, 1967)	215
A.2.1	Model for RQD Process (Kulhawy, 1978)	221
A.2.2	Spacing-RQD Correlation Predcited from Model (Kulhawy, 1978)	222
A.2.3	Alternative RQD Sampling Process Models	223
A.2.4	Comparison of Kulhawy (1978) Model for RQD with Empirical Results (Deere, 1967) and Mathematical Model (Priest & Hudson, 1975)	224
A.3.1	Typical Plate Jacking Test Results (Deere, 1967)	226
A.3.2	RQD Correlation to Modulus Ratio E/E From Field Tests (Coon & Merritt, 1970)	230
A.3.3	Method for Weighting RQD According to Stress Distribution (Deere, 1967)	231
A.3.4	RQD Correlation to Velocity Ratio (Deere, 1967)	233

Figure Number	Title	Page
A.3.5	Joint Orientation Effects on RQD and Velocity Ratio V_f/V_1	235
A.3.6	Geomechanics Classification Index System (Bieniawski, 1975)	236
A.3.7	Geomechanics Classification Correlation with Modulus Ratio $\hat{E}/E$ (Bieniawski,1975)	237
A.3.8	Joint Weathering Index Weighting Factors (Boughton,1968)	239
A.3.9	Joint Weathering Index Correlation with Rock Mass Modulus of Deformability (Boughton, 1968)	240
A.4.1	Typical Results of Triaxial Test on Rock Joint (Rosso, 1976)	243
A.4.2	Typical Results of Direct Shear Test on Rock Joint (Rosso, 1976)	245
B.1.1	Meaning of Orientation (θ,ϕ) as a Point on Surface of Sphere	254
B.1.2	Frequency Polygons for Dip (Cawsey, 1977)	256
B.1.3	Non-Circularity Problem of Frequency Polygons.	257
B.1.4	Rose Diagrams (Chayes, 1949)	258
B.1.5	Computer Generated Rectangular Plot (Robertson & Piteau, 1971)	259
B.1.6	Stereonet(Billings, 1972)	261
B.1.7	Strike Line Plot (Steffan & Jennings, 1974)	263
B.2.1	Clustering from Frequency Polygons (Cawsey, 1977)	264

Figure Number	Title	Page
B.2.2	Stereoplot of Joint Cluster Divided between Two Hemispheres	266
B.2.3	Clustering from Rectangular Plot (Steffan & Jennings, 1974)	267
B.3.1	Observed Types of Orientation Distributions (Mardia, 1972)	270
B.3.2	Reference Frame and Mean Orientation	272
B.3.3	Fisher Distribution on Surface of Sphere	274
B.4.1	Dip Measurement Error as a Function of Dip (Cruden & Charlesworth, 1976)	280
B.4.2	Strike Measurement Error as a Function of Dip (Cruden & Charlesworth, 1976)	281
C.2.1	Determination of Joint Cluster Boundaries from Stereonet	287

LIST OF TABLES

Table Number	Title	Page
3.4.1	Conversion Between Joint Orientation Representation Systems	75
3.4.2	Spherical and Planar Distributions	80
3.6.1	Mathematical Forms to be Used in Probabilistic Models for Rock Joints	108
A.4.1	Goodman(1970) Stiffness Values	247
A.4.2	Hungr & Coates(1978) Stiffness Values	248
A.4.2	Rosso(1974) Stiffness Values	249
A.4.4	Kulhawy(1978) Stiffness Values	250
C.2.1	Mathematical Forms of Distributions Fit	285
C.3.1	Results of Goodness of Fit Tests of Orientation Distributions	291

LIST OF TABLES

Table Number	Title	Page
3.4.1	Conversion Between Joint Orientation Representation Systems	75
3.4.2	Spherical and Planar Distributions	80
3.6.1	Mathematical Forms to be Used in Probabilistic Models for Rock Joints	108
A.4.1	Goodman(1970) Stiffness Values	247
A.4.2	Hungr & Coates(1978) Stiffness Values	248
A.4.2	Rosso(1974) Stiffness Values	249
A.4.4	Kulhawy(1978) Stiffness Values	250
C.2.1	Mathematical Forms of Distributions Fit	285
C.3.1	Results of Goodness of Fit Tests of Orientation Distributions	291

CHAPTER 1

INTRODUCTION

1.1 Statement of Problem

Rock mass deformability predictions are usually needed for the design of large structures in rock. The prediction of rock deformability has in the past relied heavily upon the results of large scale field testing programs and prototype monitoring. Such testing programs are expensive and are impractical for many projects. The types of information available from such programs are also limited. The development of less expensive empirical or analytic techniques for the assesment of rock mass deformability depends upon improved understanding of the nature of rock mass deformation.

Theoretical modeling is one technique which can help to improve the understanding of rock mass deformation behavior. Mathematical models can be used to study the effect of different geologic, geometric, and material conditions on rock mass deformability. The use of mathematical models, however, requires careful consideration of the assumptions, parameters, and analysis methods used.

1.2 Subjects to be Explored

This thesis explores mathematical models which have been developed for rock mass deformation, and presents new probabilistic models for rock mass deformation. Models are studied

and applied to determine their advantages and limitations, and to determine the critical assumptions for each model.

The parameters chosen to represent rock properties can have a significant effect upon model behavior. The selection of deterministic or probabilistic parameters can also be important. The use of different types of parameters and the use of deterministic and probabilistic parameters will be explored to determine how rock mass properties can best be rep-represented in deformation models.

1.3 Thesis Structure

Chapter 2 presents a literature survey of available models for rock mass deformation, and discusses their advantages and limitations. Parameter representation and its consequences is discussed in Chapter 3. Chapter 4 introduces new models for rock mass deformability which incorporate principles of parameter description developed in Chapter 3. The models developed in Chapter 4 are applied in Chapter 5 to demonstrate how mathematical models can be used in the study of rock mass deformation behavior. Chapter 6 presents conclusions.

CHAPTER 2

MODELS FOR ROCK MASS DEFORMATION

2.1 Introduction

2.1.1 Types of Models in Literature

Rock mass deformability models in the literature rely on two basic theories of material behavior. The majority of models rely on elasticity theory, while a small minority are based on the more complex elasto-plasticity approach. These theories are commonly accepted, and are described in such basic textbooks as Timoshenko & Young (1941) and Scott (1963).

In general, models in the literature represent rock masses as deterministic continua, despite the variability, uncertainty and discontinuituous nature of rock masses. To a certain extent these assumptions are necessary for simplicity. On the other hand in some cases they represent an unnecessary restriction on the usefulness of the models. The models developed in Chapter 4 attempt, to some extent, to overcome these restrictions.

2.1.2 Chapter Structure

This chapter presents models in the literature and the theories and assumptions on which they are based. Section 2.2 discusses elasticity theory and the models derived from it. Elasto-plasticity theory and elasto-plastic models are analyzed in Section 2.3. Conclusions are found in Section 2.4.

3) Strain Compatibility. Strain compatibility is a corrollary of the assumption of continuity. If a body is continuous, and volumes conserved, all strains must be compatible.

4) Small Strains. In order to simplify analysis, most solutions of elastic problems assume small strains. Elasticity could occur for large strains, but it would not necessarily be described by the standard elastic equations.

The generalized elastic relations are

$$[\sigma] = [C]\ \{\varepsilon\} \qquad \text{where } [\sigma] = \text{stress field}$$

(2.2.1)

$$[C] = \text{deformability matrix}$$

$$\{\varepsilon\} = \text{strain field}$$

in three dimensions (2.2.1)

$$\begin{bmatrix} \sigma_{11} & \sigma_{12} & \sigma_{13} \\ \sigma_{21} & \sigma_{22} & \sigma_{23} \\ \sigma_{31} & \sigma_{32} & \sigma_{33} \end{bmatrix} = \begin{bmatrix} C_{11} & C_{12} & C_{13} \\ C_{21} & C_{22} & C_{23} \\ C_{31} & C_{32} & C_{33} \end{bmatrix} \begin{bmatrix} \varepsilon_{11} & \varepsilon_{12} & \varepsilon_{13} \\ \varepsilon_{21} & \varepsilon_{22} & \varepsilon_{23} \\ \varepsilon_{31} & \varepsilon_{32} & \varepsilon_{33} \end{bmatrix}$$

(2.2.2) (2.2.2)

In linear elasticity the elastic constant matrix is dependent upon only two coefficients, Young's modulus [E] and Poissons ratio [ν]. Where [C] independent of the reference frame, and properties are therefore non-directional, the properties are "isotropic." Where [C] is dependent upon reference frame,

2.2 Models Based on Elasticity Theory

2.2.1 Elasticity Theory

Elasticity theory is perhaps the most widely used basis for modelling behavior.The basic assumption of elasticity theory is that

> "there exists a unique unstressed state of the body, to which the body returns when all stresses are removed." (Fung, 1965)

This assumption requires only that all strains which occur under stress be recovered upon removal of the stress. In addition, however, elastic equations are generally developed on the basis of several additional assumptions.

1) Linear Elasticity In the original development of elasticity theory by Hooke (1678) the relationship between stress and strain is assumed to be linear This assumption is maintained in all of the models in this chapter (Figure 2.2.1).

2) Continuity. Mathematical development of elastic relations has generally been conducted on the basis of continuity. Although continuity is required for the development of equations, the theory can be used for discontinua. Separate theoretical development has not been conducted for discontinuous elastic bodies, but elastic equations have been applied successfully to some discontinua.

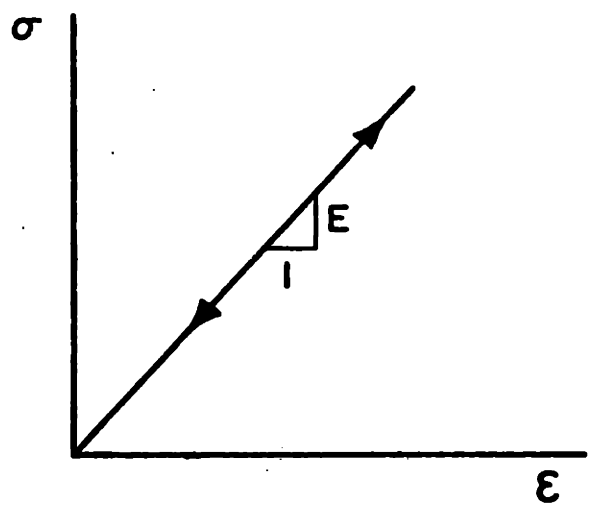

Figure 2.2.1 Linear Elastic Stress-Strain Curve

the properties are "anisotropic." Both isotropic and anisotropic models have been used for rock masses. For further discussion of elastic theory see Timashenko (1950), Fung (1965) or Fung (1977).

2.2.2 Models

This section presents elastic models which have been used for rock masses. First, standard, general elastic models are presented Then, closed form solutions developed especially for rock mass problems are discussed. Finally, finite element models for more complex rock mass problems are analyzed.

General Models

The general anisotropic three dimensional representation of elasticity given above presents considerable problems of solution. Two dimensional boundary condition assumptions are frequently used to facilitate analysis. The most common two dimensional geometries are plane strain and plain stress (Figure 2.2.2).

For the isotropic plane stress condition:

$$\begin{bmatrix} \sigma_{11} & \sigma_{12} & 0 \\ \sigma_{12} & \sigma_{22} & 0 \\ 0 & 0 & 0 \end{bmatrix} \qquad \begin{bmatrix} \lambda + 2\mu & \lambda & \lambda \\ \lambda & \lambda + 2\mu & \\ \lambda & \lambda & \lambda + 2\mu \end{bmatrix} \qquad \begin{bmatrix} \varepsilon_{11} & \varepsilon_{12} & 0 \\ \varepsilon_{21} & \varepsilon_{22} & 0 \\ 0 & 0 & \varepsilon \end{bmatrix}$$

where $\lambda = E\nu/[(1-2\nu)(1+\nu)]$

$\mu = E/[2(1+\nu)]$

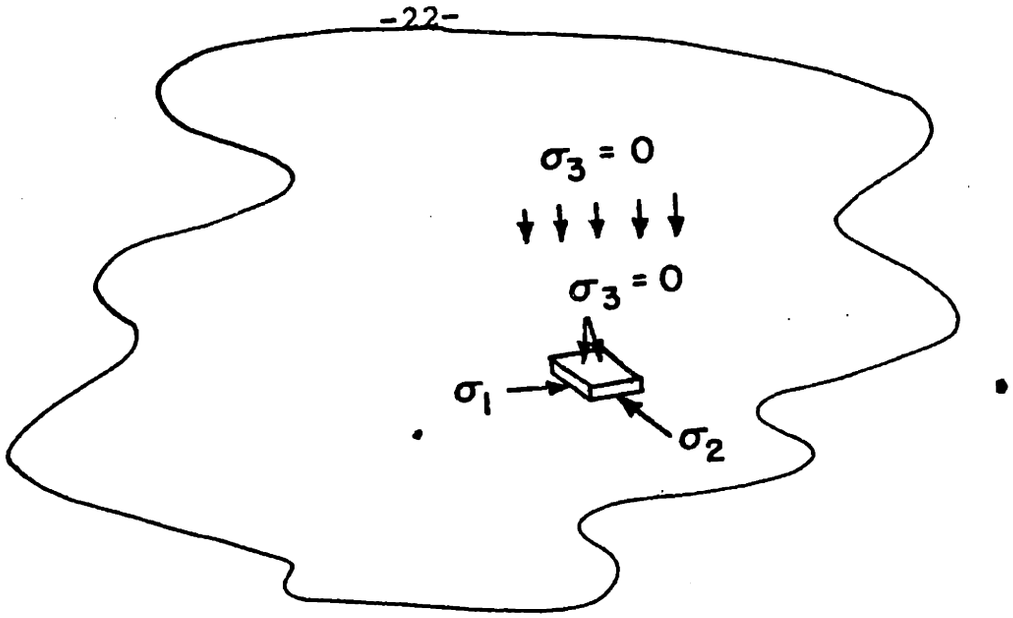

PLANE STRESS

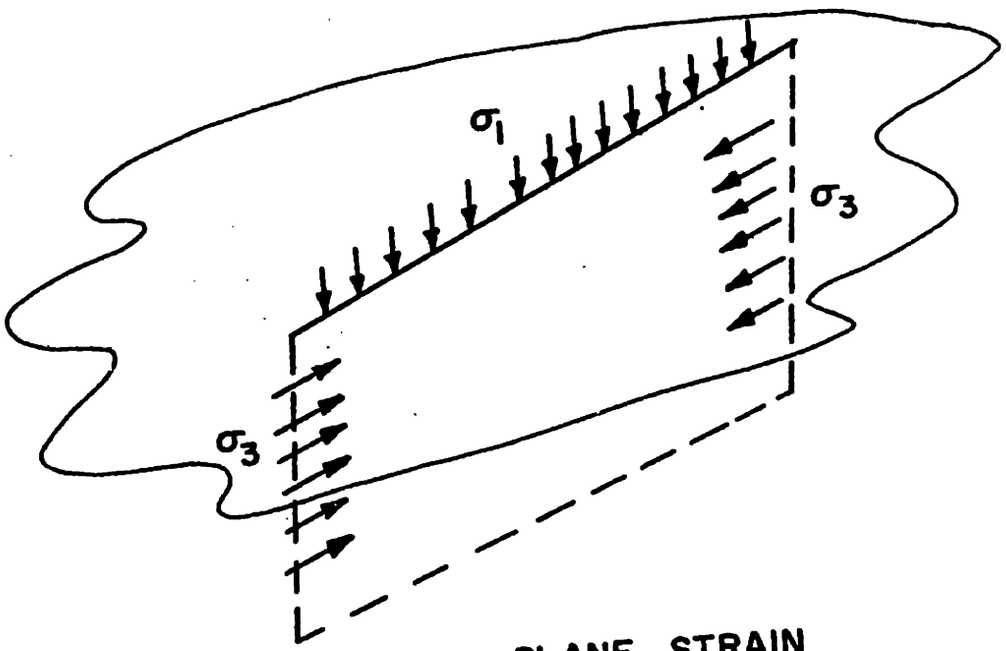

PLANE STRAIN

Figure 2.2.2 Plane Stress and Plane Strain

so

$$\varepsilon_{11} = \frac{1}{E}(\sigma_{11} - \nu\sigma_{22})$$

$$\varepsilon_{22} = \frac{1}{E}(\sigma_{22} - \nu\sigma_{22})$$

$$\varepsilon_{33} = \frac{-\nu}{E}(\sigma_{11} + \sigma_{22})$$

$$\varepsilon_{12} = \varepsilon_{21} = \frac{(1+\nu)}{E}(\sigma_{12})$$

(2.2.3) (2.2.3)

For the isotropic plane strain condition:

$$\begin{bmatrix} \sigma_{11} & \sigma_{12} & 0 \\ \sigma_{12} & \sigma_{22} & 0 \\ 0 & 0 & \sigma \end{bmatrix} = \begin{bmatrix} \lambda+2\mu & \lambda & \lambda \\ \lambda & \lambda+2\mu & \lambda \\ \lambda & \lambda & \lambda+2\mu \end{bmatrix} \begin{bmatrix} \varepsilon_{11} & \varepsilon_{12} & 0 \\ \varepsilon_{21} & \varepsilon_{22} & 0 \\ 0 & 0 & 0 \end{bmatrix}$$

where

$$\lambda = E\nu/[(1-2\nu)(1+\nu)]$$

$$\mu = E/[2(1+\nu)]$$

so

$$\varepsilon_{11} = \frac{1}{E}[(1-\nu^2)\sigma_{11} - \nu(1+\nu)\sigma_{22}]$$

$$\varepsilon_{22} = \frac{1}{E}[(1-\nu^2)\sigma_{22} - \nu(1+\nu)\sigma_{11}]$$

$$\varepsilon_{12} = \varepsilon_{21} = \frac{1}{E}(1+\nu)\sigma_{21}$$

(2.2.4) (2.2.4)

Three dimensional problems can be analyzed in a simplified manner if two stresses are assumed to be equal

$$\sigma_{22} = \sigma_{33} \tag{2.2.5}$$

and only principal stresses are considered. This is the "triaxial" case (Figure 2.2.3).

$$\begin{bmatrix} \sigma_{11} & 0 & 0 \\ 0 & \sigma_{33} & 0 \\ 0 & 0 & \sigma_{33} \end{bmatrix} = \begin{bmatrix} \lambda+2\mu & \lambda & \lambda \\ \lambda & \lambda+2\mu & \lambda \\ \lambda & \lambda & \lambda+2\mu \end{bmatrix} \begin{bmatrix} \varepsilon_{11} & 0 & 0 \\ 0 & \varepsilon_{22} & 0 \\ 0 & 0 & \varepsilon_{33} \end{bmatrix}$$

(2.2.6)

so

$$\varepsilon_{11} = \frac{1}{E}\left[\sigma_{11} - 2\nu\sigma_{33}\right]$$

$$\varepsilon_{33} = \varepsilon_{22} = \frac{1}{E}\left[\sigma_{33} - \nu(\sigma_{33} + \sigma_{11})\right]$$

(2.2.6)

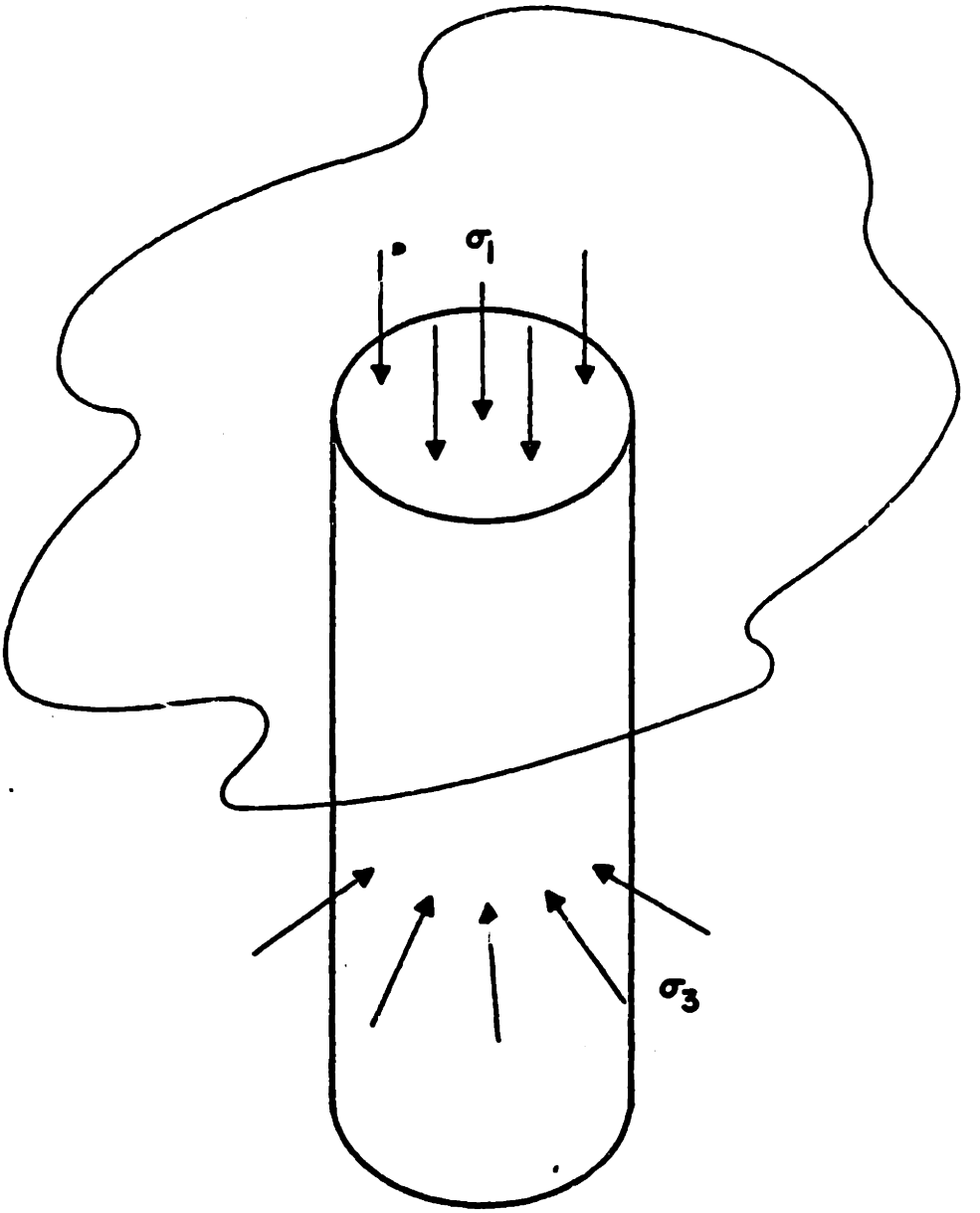

Figure 2.2.3 Triaxial Case

Three dimensional problems can also be solved by assumption of an isotropic linear elastic half space (Figure 2.2.4) in which lateral stresses are the result only of vertical loading. For an elastic half space, strain and stress vary throughout the body. What is of primary interest in the elastic half space model is vertical displacement at the surface.

$$\rho = \frac{P(1-\nu^2)}{B_z A^{\frac{1}{2}} E} \qquad (2.2.7)$$

(Boussinesq, 1883)

where P = total load

A = loaded area

B_z = shape factor for rigid loaded area ≈ 1

ρ = surface displacement (2.2.7)

The four solutions above are possible due to simplified geometries and the assumption of isotropic properties. These restrictions, and particularly the assumption of isotropic properties severely limit the applicability of the model to rock mass problems. The discontinuous nature of rock does not necessarily restrict the use of these solutions, even though they are based upon continuity. Rock joints do, however, introduce a significant amount of anisotropy which must be taken into account in analyses.

For purposes of analysis, vertical deformation ε_v is frequently all that is desired. Rock mass vertical deformability is frequently expressed in terms of vertical elastic constants E_v and ν_v alone, where E_v and ν_v expresses rock

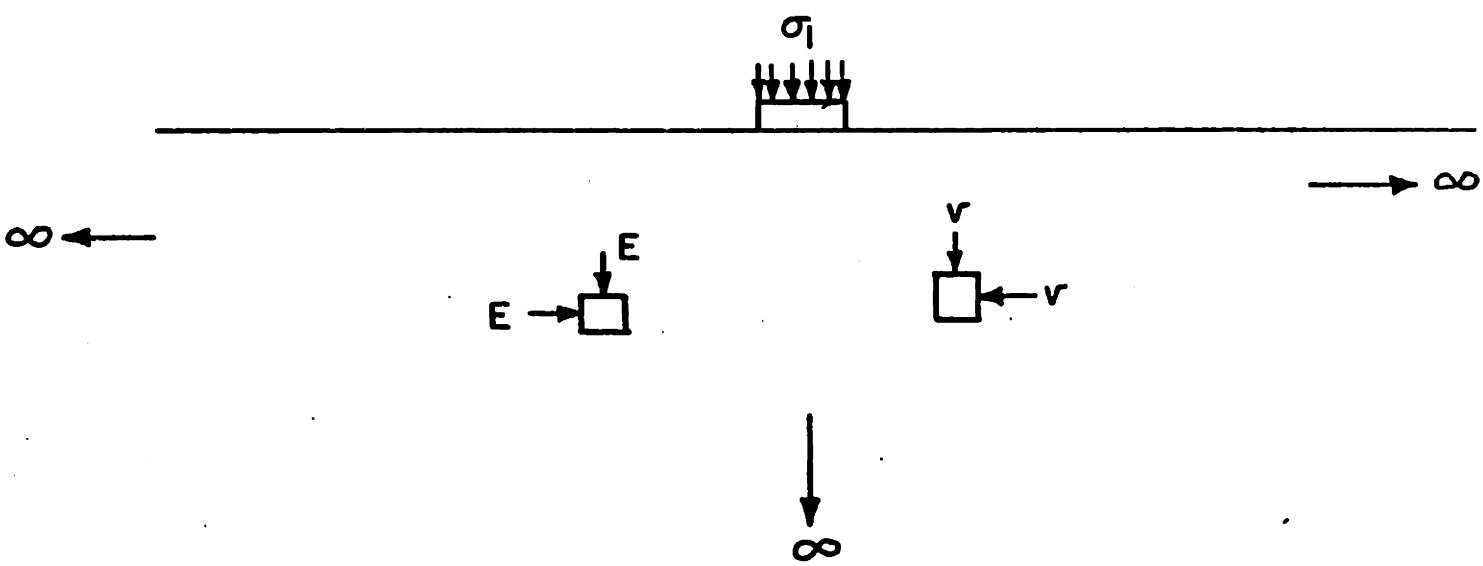

Figure 2.2.4 Isotropic Linear-Elastic Half-Space

mass deformability for vertical loading (principal stress direction vertical). Youngs modulus and Poisson's ratio will be denoted $\hat{E}$ and $\hat{\nu}$. In most cases, however, even where E is anisotropic, ν is not, so Poisson's ratio can be represented in the general form as ν. Some anisotropic solutions for elastic problems have been developed.

For an anisotropic half space in which the principal loading direction is vertical and properties are the same in all lateral directions but different in the vertical directions (Figure 2.2.5).

$$[E] = \begin{bmatrix} E_v & & \\ & E_h & \\ & & E_h \end{bmatrix}$$

(2.2.8)

$$[\nu] = \begin{bmatrix} \nu_v & \nu_{vh} & \nu_{vh} \\ \nu_{vh} & \nu_h & \nu_{hh} \\ \nu_{vh} & \nu_n & \nu_{hh} \end{bmatrix}$$

where

E_v = Vertical Young's Modules

E_h = Horizontal Young's Modulus

ν_v = Vertical Poisson's Ratio

ν_h = Horizontal Poisson's Ratio (2.2.8)

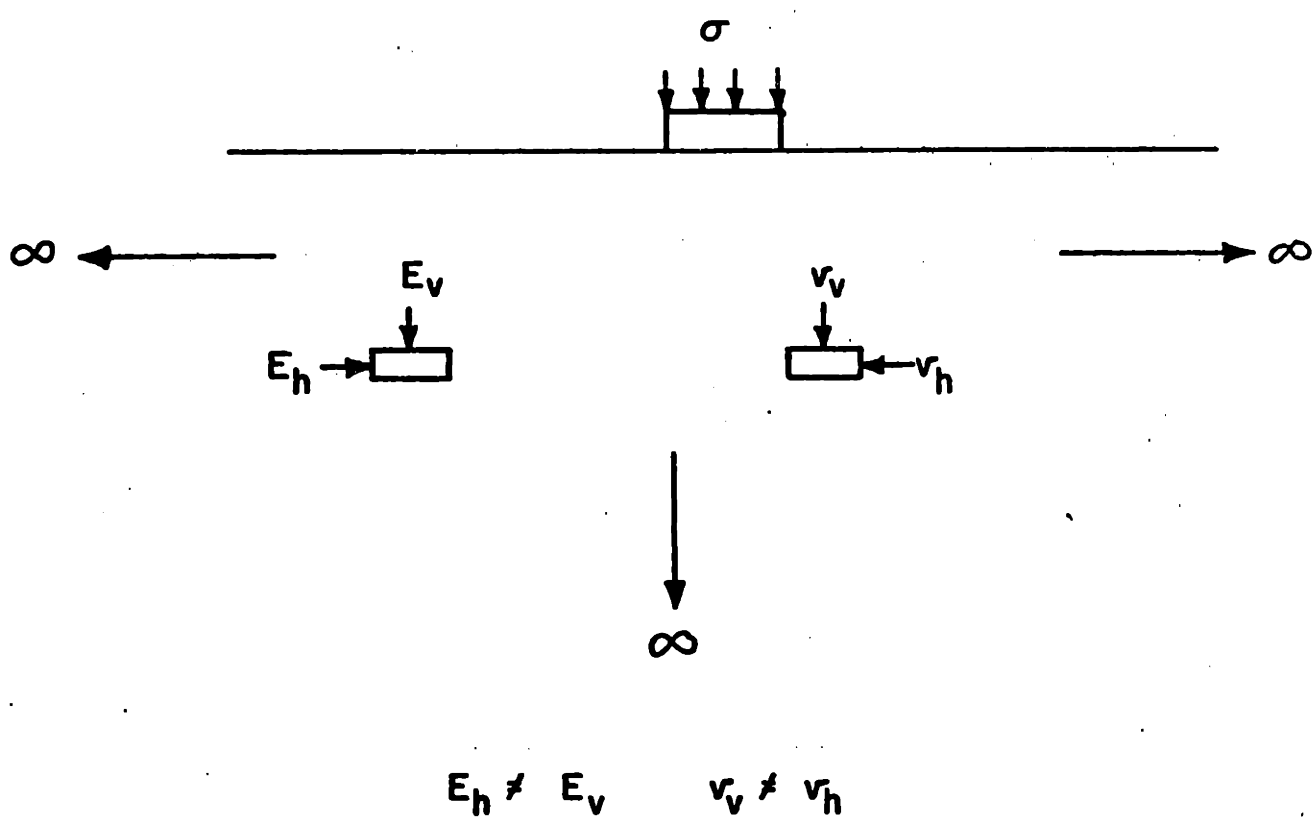

Figure 2.2.5 Anisotropic Linear-Elastic Half-Space

$$\beta^2 \text{ positive: } \rho_z = \frac{P(c + G_{hz})d\delta(\delta^2 - \beta^2)}{2rG_{hz}[c + d(\delta + \beta)^2][c + d(\delta - \beta)^2]}$$

$$\beta^2 \text{ negative: } \rho_z = \frac{P\ (ad)1/2}{2r(ad - c^2)}$$

$$\beta^2 \text{ zero: } \quad \rho_z = \frac{P(c + G_{hz})d^{\ 3}}{2rG_{zh}(c + d\delta^2)^2}$$

(2.2.9)

The appropriate equation to use is defined by

$$\beta^2 = \frac{ad - c^2 - 2cG_{zh} - 2G_{zh}(ad)1/2}{4G_{zh}d}$$

in which

$$a = \frac{E_h(1 - \nu_{hz}\nu_{zh})}{(1 + \nu_{hh})(1 - \nu_{hh} - 2\nu_{hz}\nu_{zh})}$$

$$c = \frac{E_h \; zh}{1 - \nu_{hh} - 2\nu_{hz}\nu_{zh}}$$

$$d = \frac{}{\nu_{hz}(1 - \nu_{hh} - 2\nu_{hz}\nu_{zh}}$$

$$\delta^2 = \frac{ad - c^2 - 2cG_{zh} + G_{zh}(ad)1/2}{4G_{zh}d}$$

These solutions are subject to the following limitations:

$$1 - \nu_{hh} - 2\nu_{hz}\nu_{zh} > 0$$

$$1 - \nu_{hh} > 0$$

$$1 + \nu_{hh} > 0$$

The use of the anisotropic linear elastic half space model is limited primarily by the lack of relation between anisotropic elastic constants and measureable rock properties. Commonly measured rock deformability parameters include intact rock E_i, and ν_i, and rock joint stiffnesses k_s and k_n.

Goodman, Taylor and Brekke (1968) developed a method to derive "equivalent" anisotropic elastic constants for use in the anisotropic linear elastic half-space model. They assumed simple rock mass geometry containing only one joint set, evenly spaced, and parallel to the surface (Figure 2.2.6). Equivalent elastic moduli in the vertical direction are found by summing vertical deformation due to joints and intact rock for a unit length.

$$\varepsilon_{vt} = \varepsilon_{vj} + \varepsilon_{vi} \qquad (2.2.10)$$

where

ε_{vt} = total vertical deformation for a unit height of rock mass

ε_{vj} = vertical deformations of joint for a unit height of rock mass

ε_{vi} = vertical deformation of intact rock for a unit height of rock mass

(2.2.10)

Goodman et al. assumed that intact rock deformations are controlled by isotropic elastic constants E_i and ν_i, and that rock joints are controlled by joint stiffness k_s and k_n where

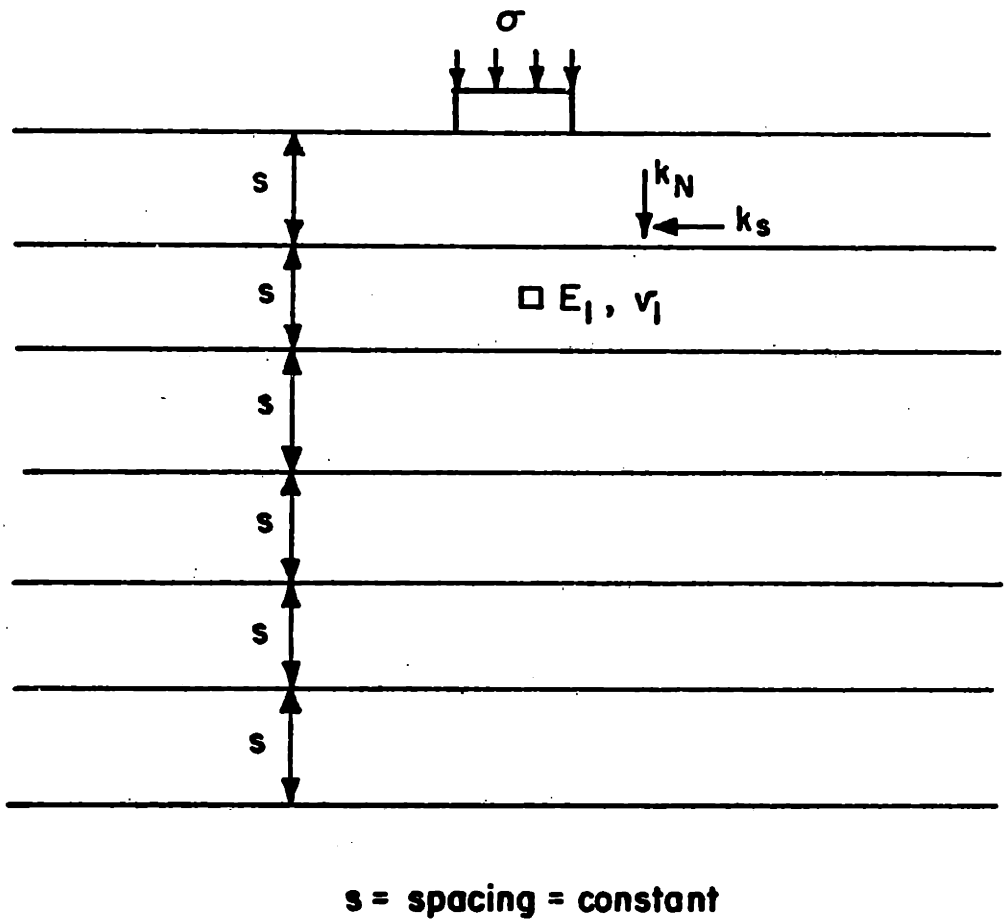

Figure 2.2.6 Goodman et. al.(1968)Joint Geometry

$k_s = \tau_s/\delta_s$ where τ_s = shear stress on joint

$k_N = \sigma_N/\delta_N$ δ_s = shear deformation of joint

σ_N = normal stress on joint

δ_N = normal deformation of joint

(2.2.11)

(2.2.11)

Equivalent elastic constants are

Vertical (normal to joint set)

$$E_v = \left[\frac{1}{E_i} - \frac{1}{sk_N}\right]^{-1}$$

$$\nu_v = \nu_i \, E_v/E_i$$

(2.2.12)

(2.2.12)

Horizontal (shear to joint set)

$$G_H = \left[\frac{1}{G_i} - \frac{1}{sk_s}\right]^{-1}$$

$$\nu_H = \nu_i$$

where E_v, ν_v = Young's modulus, Poisson's ratio in vertical direction

E_i, ν_i = Young's modulus, Poisson's ratio of intact rock

G_N, ν_H = Shear modulus, Poisson's ratio in horizontal direction

s = Joint spacing. $s=1/\lambda$ where λ = number of joints per unit length

These equivalent elastic constants can be plugged directly into the simple anisotropic linear elastic half space model.

Kulhawy (1978) extended the concept of equivalent elastic constants to three dimensions by the same principles that Goodman, et al. used. His joint geometry consisted of three orthagonal joint sets (Figure 2.2.7).

$$E_x = \left[\frac{1}{E_i} + \frac{1}{S_x k_{Nx}}\right]^{-1}$$

$$G_x = \left[\frac{1}{G_i} + \frac{1}{S_x k_{Sx}} + \frac{1}{S_y k_{Sy}}\right]^{-1}$$

$$\nu_{xy} = \nu_i E_x / E_i \qquad (2.2.13)$$

where E_i, G_i, ν_i are intact rock Young's modulus, Shear modulus, and Poisson's ratio.

E_x, G_x, ν_{xy} are rock mass anisotropic Young's modulus, shear modulus, and Poisson's ratio in direction x

Both Goodman, et al. and Kulhawy rely upon closed form solutions for their anisotropic elastic models. This considerably limits the flexibility of their analyses. The finite element method and other numerical techniques allow approximate solutions of more complex elastic models. Finite element programs utilizing arbitrarily selected and "equivalent" anisotropic elastic solution have been developed by Duncan and Goodman (1968), Hungr and Coates (1978) and others. The finite element method is extremely flexible and can give solutions for a wide range of boundary conditions

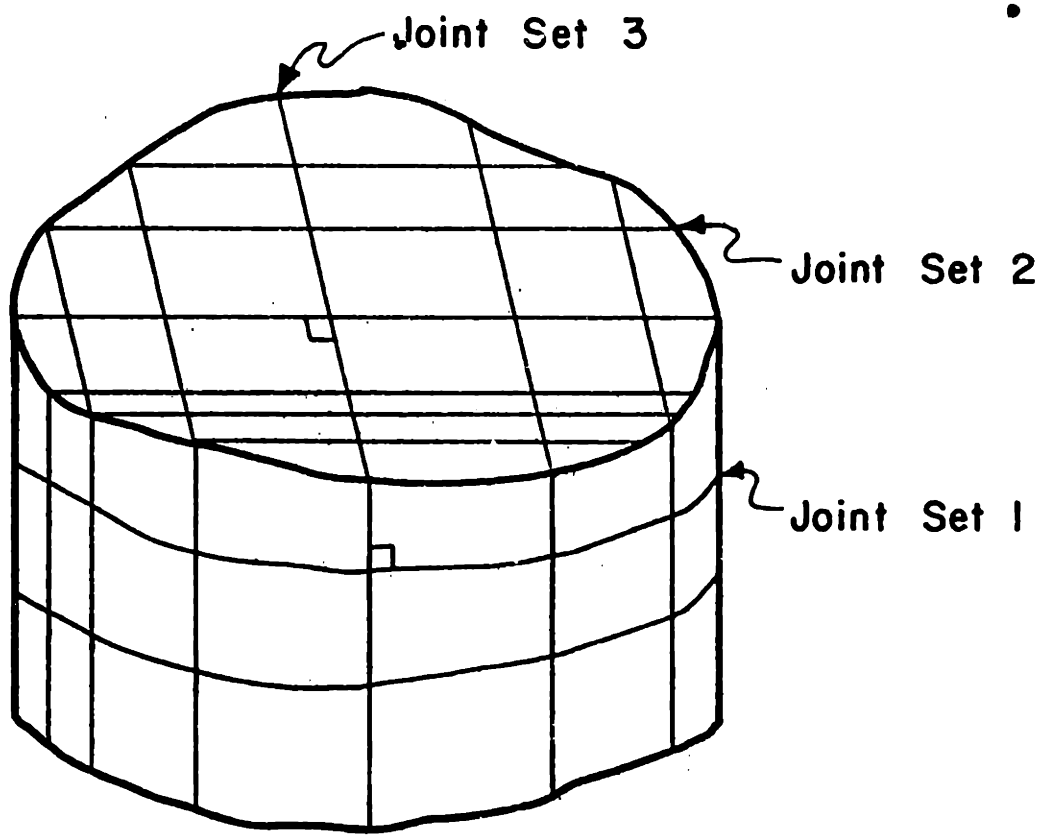

Figure 2.2.7 Kulhawy(1978) Joint Geometry

if elastic properties are known. Using "equivalent" elastic properties, Hungr and Coates studied the effect of variation of direction of anisotropic axes upon deformation. Their results are shown in Figure 2.2.8.

A non-homogeneous elastic body is one in which properties vary from point to point. Rock masses are in fact non-homogeneous, with different properties for rock joints and intact rock. A direct approach to the application of elastic theory to rock masses would therefore be to model them as non-homogeneous linear-elastic bodies. Unfortunately, closed form solutions for non-homogeneous elastic problems are rare. It is possible, however, to solve non-homogeneous elastic problems through the use of the finite element method.

Burman and Hammett (1976), for example, modeled rock masses as non-homogeneous bodies with different elastic properties for intact rock and for rock joints. (Figure 2.2.9). They assumed a plane strain geometry, and studied the effect of rotation of the principal stress directions. They simplified geometry by assuming all rock joints were horizontal, equally spaced, and of equal width. They chose elastic property for intact rock from lab tests and for rock joints arbitrarily. More complicated geometries could also be studied with the finite element method.

The primary problem with the finite element method is cost. In addition, Burman and Hammett's results are limited by their arbitrary selection of elastic constants for joints.

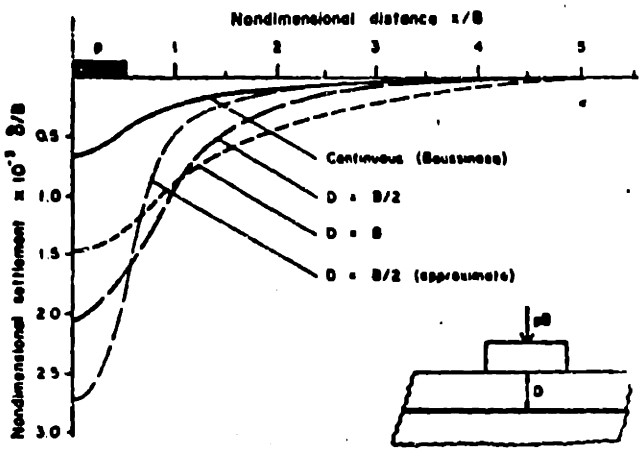

FIG. 1. Surface settlements of a uniform strip load resting on a rock mass with a single horizontal joint. Note: The following nondimensional material properties were assumed: $E/p = 3000$, $\nu = 0.2$, $k_n B/E = 400$ and $k_s B/E = 400$.

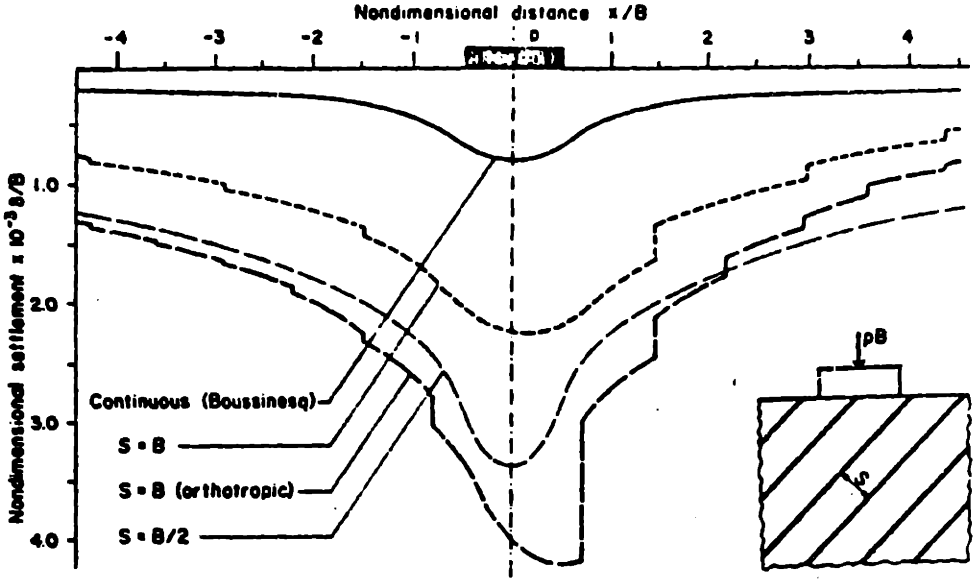

FIG. 2. Settlements of a strip load on a rock mass with a joint set dipping at 45°.

Figure 2.2.8 Hungr&Coates(1978) Results

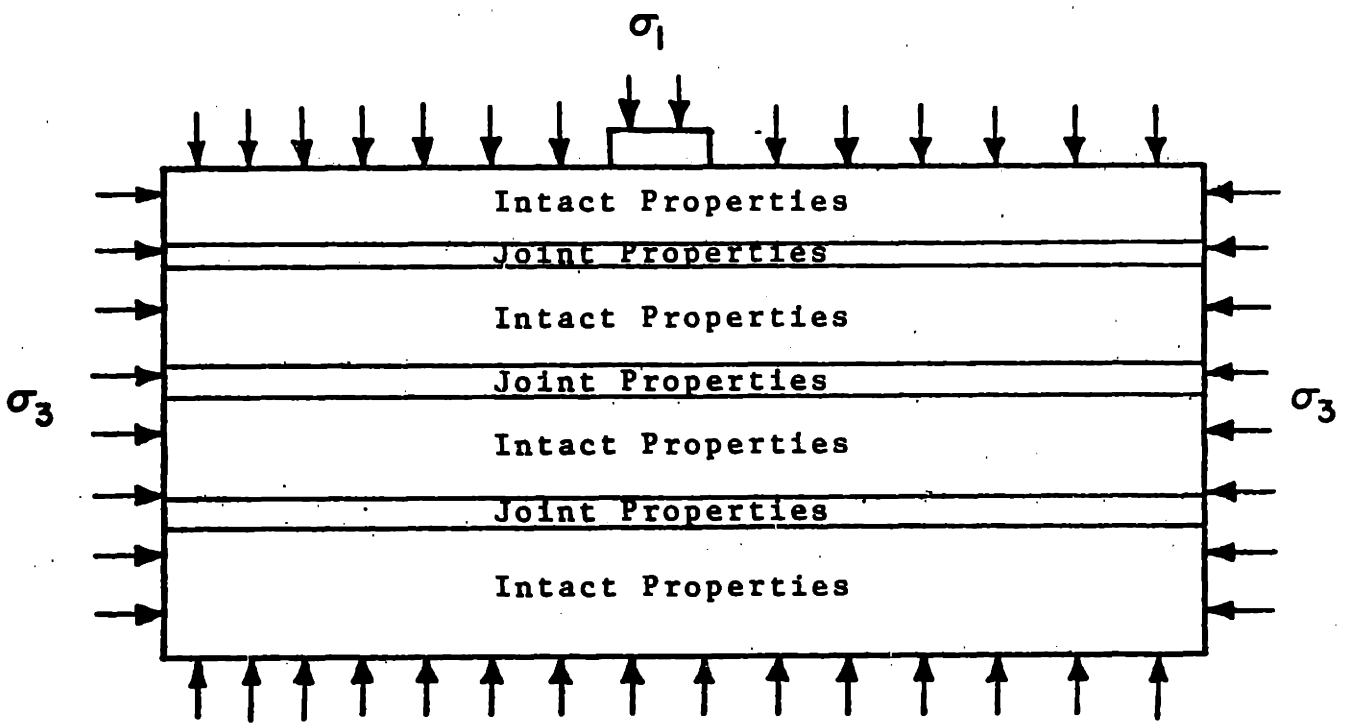

Intact Properties: $E_{intact}, \nu_{intact}, G_{intact}$
Joint Properties : $E_{joint}, \nu_{joint}, G_{joint}$

Figure 2.2.9 Burman & Hammett (1976) Model

All models based upon elastic theory are limited by the assumptions of elastic theory. The use of continuity, strain compatibility, small strains, and linear elasticity can restrict the usefullness of models. In addition inelastic (non-recoverable) strains do occur in rock masses, primarily along rock joints. Another concept, elasto-plasticity, is available to model this behavior.

2.3 Models Based on Elasto-Plasticity Concept

2.3.1 Elasto-Plasticity Theory

Elasto-plasticity theory states that there are two types of deformation:recoverable (elastic) and unrecoverable (plastic). An elasto-plastic stress-strain curve is shown in Figure 2.3.1. Typical rock mass behavior includes both elastic and plastic deformations, as illustrated by the plate-jacking test curve in Figure 2.3.2. Triaxial tests on intact rock indicate that intact rock, in fact, behaves elastically in usual stress ranges. Therefore, plastic behavior is largely due to non-recoverable deformation on rock joints.

Rock masses can therefore be modeled as elasto-plastic bodies. Deformation consists of two components, an elastic component and a plastic component.

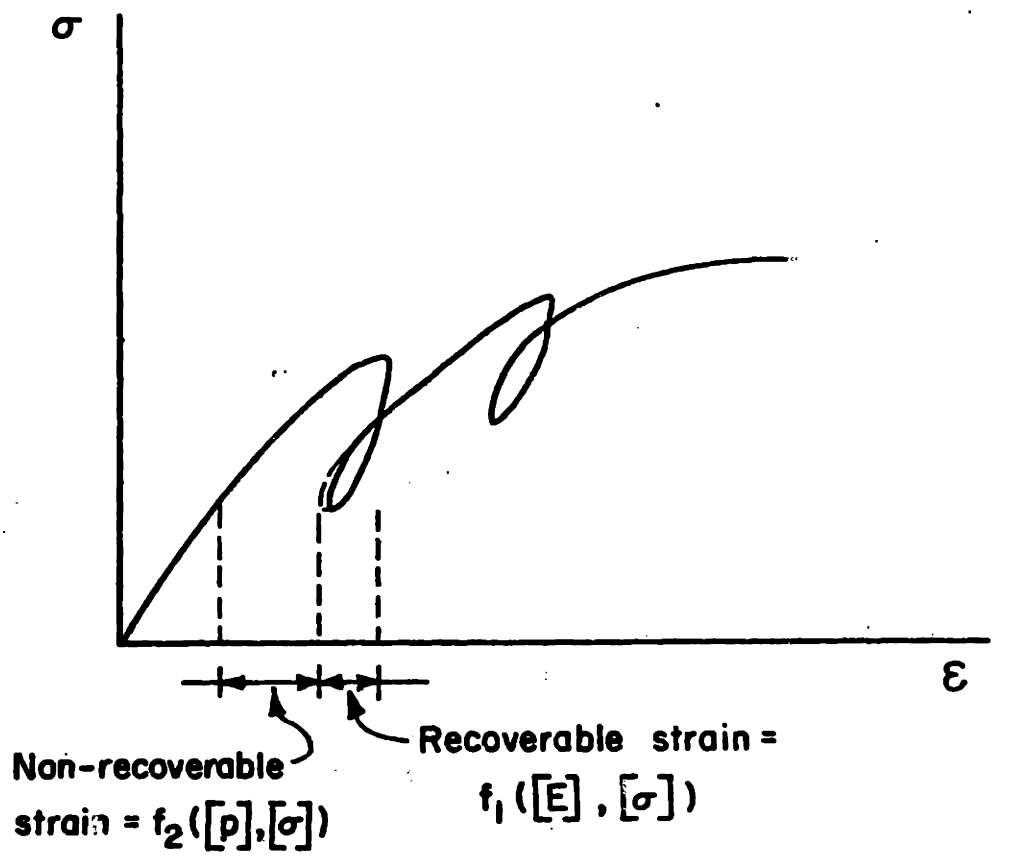

Figure 2.3.1 Elasto-Plastic Stress-Strain Curve

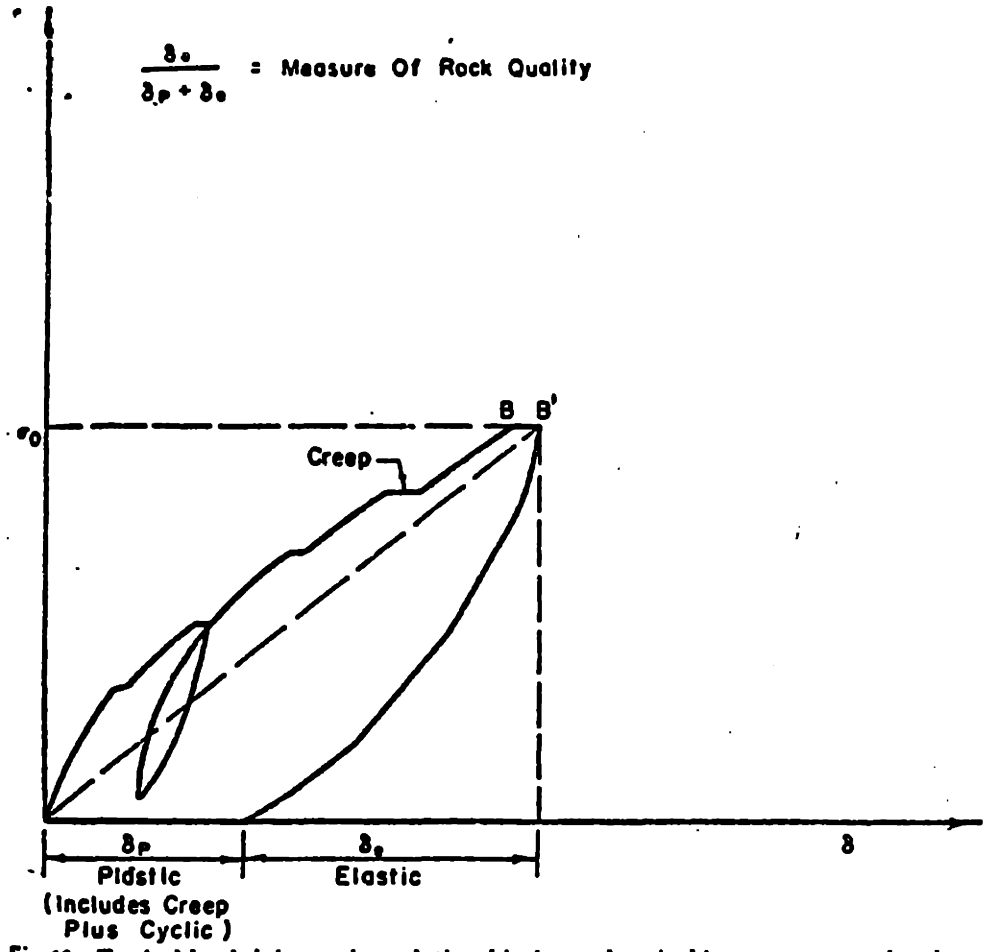

Fig. 10—Typical load-deformation relationship for a plate jacking or pressure chamber test.

Figure 2.3.2 Typical Plate Jacking Test Results (Deere, 1967)

$$[E] = f_1([C],[\sigma]) + f_2([P],[\sigma])$$

where

$[E]$ = Strain Matrix

$[C]$ = Elastic Modulus Matrix

$[\sigma]$ = Stress State Matrix

$[P]$ = Plastic Modulus Matrix

f_1 = Elastic Function

f_2 = Plastic Function

(2.3.1) (2.3.1)

In a generalized elasto-plastic model developed by Roberds and Einstein (1978), plastic behavior is divided into parts -- time dependent (viscous) and non-time dependent.

$$[E] = f_1([C],[\sigma]) + f_2([P_1],[\sigma]) + f_3([P_2],[\sigma]),t)$$

where

$[P_1]$ = Non-Viscous Plastic Modulus Matrix

f_2 = Non-Viscous Plastic Function

$[P_2]$ = Viscous Plastic Modulus Matrix

f_3 = Viscous Plastic Function

t = time (2.3.2)

The development of elasto-plastic theory requires the same general assumptions as elastic theory, except that inelastic strains are permitted. The use of elasto-plastic models, however, require the determination of appropriate plastic behaviors f_2 and f_3 and appropriate plastic parameters

$[P_1]$ and $[P_2]$. This can represent a significant limitation to the use of elasto-plastic theory.

Solutions for elasto-plastic behavior can be found in Calladine (1969), Crandall and Dahl (1959) and Drucker (1959). Solutions are, unfortunately, generally quite complex, and require solutions by advanced numerical methods.

2.3.2 Models

This section presents two of the many possible elasto-plastic models. Iida (1968) developed his model on the basis of an analogy between microscopic elasto-plastic behavior in metals and macroscopic elasto-plastic behavior in rock masses. Roberds and Einstein (1977) developed their model by analyzing deformation behavior of intact rock, rock joints, and joint fill separately. Many other models could be developed, based upon elasto-plasticity, but discussion will be limited to these two models.

Iida (1968) modeled elasto-plastic behavior by using anisotropic elastic properties which vary with stress level as illustrated in Figure 2.3.3. Iida's derivation relied upon assumptions of plastic behavior (elastic- ideally plastic) behavior, yield criterion (Tresca or von Mises) and rock joint geometry (orthagonal, deterministic).

Iida's model does not use any geologically measurable rock mass properties, but depends instead upon parameters developed especially for his formulation. Solution of his model requires the use of advanced finite element techniques.

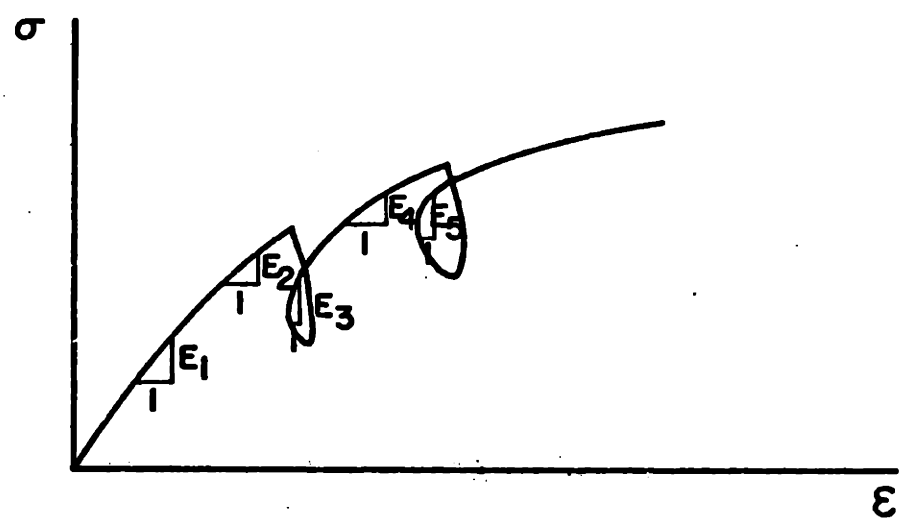

$E_i = f([\sigma], [\varepsilon])$

(Conceptual)

Figure 2.3.3 Elasto-Plastic Stress-Strain Approximated by Elastic Properties- Iida(1968) method

Iida did not implement his model.

Roberds and Einstein (1977) developed a "general purpose elasto-visco-plastic critical state behavioral model." Their model develops general mass properties as a combination of : elastic intact rock , elasto-visco-plastic discontinuity interfaces, elasto-visco-plastic clay discontinuity fill. Separate models are developed for each component, and the solution can be carried out by iterative finite-elements. Roberds and Einstein model each component (intact, joint, fill) separately, and attempt to determine appropriate parameters and representation by comparison of observed deformation (intact, joint etc.) and time behavior.

2.4 Discussion

The models presented in this chapter have differences in method but maintain the same basic approach. Whether elastic or elasto-plastic, linear, non-linear, isotropic or anisotropic all the models relied upon the model of rock masses as continuous, deterministic bodies with small strains.

Continuum -- Rock masses are filled with discontinuities. On the other hand, rock masses can be viewed as continua containing discontinua. And therefore, even from the macroscopic level, it is not necessarily bad to model rock as a continuum provided the effect of discontinuities upon behavior is incorporated into the description of the continuum. This is done implicitly in most of the models, and explicitly in Roberds and Einstein's model.

Determinism -- As will be shown in Chapter 3, uncertainty and spatial variability play significant roles in rock mass behavior. Models in this chapter all ignore these effects. This can result in significant errors.

Small Strains -- The development of linear-elastic and simple elasto-plastic concepts required assumptions of small strains. For most situations, this is not usually a significant constraint, but should be kept in mind in application of model results.

Variation between models in this chapter is primarily in the level of complexity of the model. Simple models such as the isotropic linear elastic half space have the advantages of ease of analysis, interpretation and application. More complex models are more difficult to analyze and apply but use more realistic descriptions of behavior and are therefore more accurate. Both simple and complex analysis have their places.

Where a simple straightforward first level approximation is desired, simple models are better suited. The rock mass modulus of elasticity from the linear elastic half space model, $\hat{E}$, is frequently used to describe deformability qualitatively, and is sometimes given as an output from more complex analyses.

Where the effect of different factors upon behavior is desired, the complex model providing the most complete description of the deformation mechanism is better suited.

Study of rock joint orientation's effect upon deformability is therefore best conducted with that model which best describes the relationship of rock joints to overall rock mass deformation.

2.5 Summary

This chapter presented models for rock mass deformation based upon several different theories, concepts and assumptions. All of the models used deterministic descriptions of rock mass properties. Chapter 3 presents probabilistic alternatives for rock mass descriptions. Models based upon probabilistic properties are developed in Chapter 4.

CHAPTER 3

PROBABILISTIC DESCRIPTION OF ROCK MASSES

3.1 Introduction

Most of the rock mass models in the previous chapter rely upon deterministic parameters. That is, for any given rock mass, they assume that the rock mass properties are constant throughout and that the rock mass properties are completely known. This chapter will develop the concept of probabilistic rock mass description, which acknowledges that the true character of rock is variable, both spatially and statistically.

Probabilistic description is an importnat aid to understanding of rock mass deformation behavior. Probabilistic description can take into account many factors which must be neglected in deterministic descriptions:

- Spatial Variability - occurs where different values of parameters exists at the same time in different regions of a rock mass. Spatial variability is illustrated in Figure 3.1.1. Spatial variability can be very important where behavior is controlled to a considerable extent by extreme rather than mean values of parameters. This is frequently the case with rock masses.

- Statistical (Parameter) Uncertainty - occurs where the true values of parameters are unknown. Statistical uncertainty is ellucidated in Figure 3.1.2. Statistical

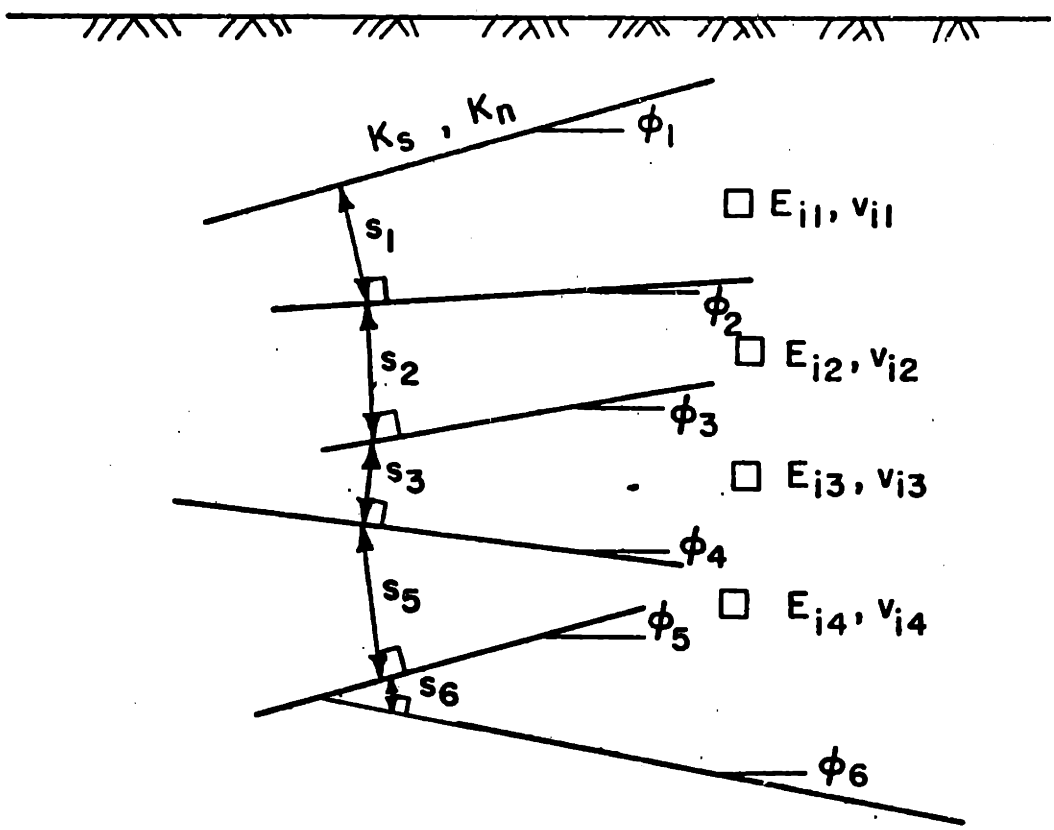

Properties are different at every point in space

Figure 3.1.1 Spatial Variability of Rock Mass Properties

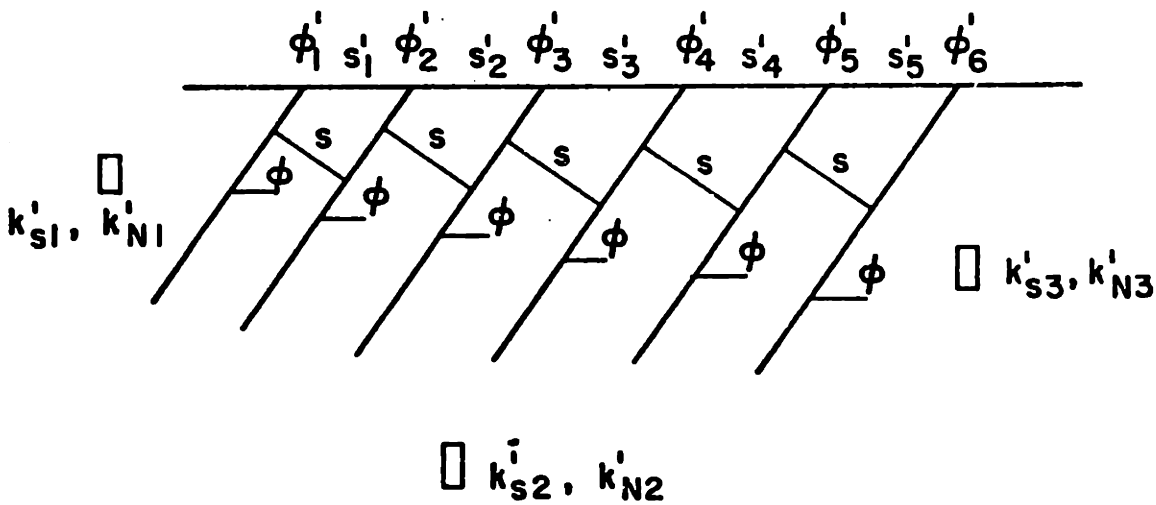

Measured	ϕ_i',	s_i' ,	k_{si}' ,	k_{ni}'	variable
True	ϕ ,	s ,	k_s ,	k_n	constant

Figure 3.1.2 Statistical Variability of Rock Mass Properties

uncertainty results from measurement and sampling errors, biases, and other effects. Statistical uncertainty in rock masses can be largely due to the difficulty of the sampling and measurement process.

- Model Uncertainty - occurs when the mechanism of behavior is unknown. Confidence in predictions then depends upon confidence in assumptions. Rock mass deformation has considerable behavioral uncertainty.

3.2 Types of Description

There are at least four ways to describe parameters. These include deterministic, deterministic with bounds, second-moment probabilistic and fully probabilistic.

Deterministic description provides only an estimate of central tendency. This may be a mean, mode, median, or maximum likelihood estimate. Deterministic description provides no sense of the likelihood of the specified value, or of the range of alternate values. An example of deterministic descriptions is the statement "all rock joints are horizontal within the mass." Deterministic parameters can be simply entered into analyses, and deterministic predictions of behavior will result.

Deterministic descriptions with bounds specify both the central tendency of behavior and upper and lower bounds. Bounds provide an estimate of the extreme values that could be expected. They provide no estimate of how likely those

extreme values may be or how likely or frequent other values between the bounds may be. An example of deterministic description with bounds is the statement "The joint dip is between 5°E and 5°W, and the expected value is 0°." Bounds on input values result in bounds on predictions of behavior.

Second Moment descriptions provide information both on central tendencies and upon the likelihood of bounds. Bounds are represented by standard deviations. For example "The mean dip is 0°, and the standard deviation is 5°." Standard deviations bounds can be represented as percentile bounds by assumption of a distributional form. One standard deviation, according to the normal distribution is 66%. Therefore, if the normal distribution were implicitly assumed, the above statement could be read. "There is a 66% chance that the dip lies between 5°E and 5°W, and the expected dip is 0°."

Fully probabilistic descriptions specify a complete distribution of values. The likelihood of every possible value is specified. The likelihood can express spatial variability, statistical (parameter) uncertainty, model uncertainty, or any combination. Complete probabilistic description has the advantages of generality and completeness, but suffers from the difficulty of finding appropriate distributional forms and of fitting distribution parameters. An example of probabilistic description is "The joint dip is Fisher distributed about 0° with a dispersion parameter of 5 ." Probabilistic descriptions may be used in analyses to produce probabilistic

predictions of behavior.

3.3 Rock Mass Properties of Interest

Parameters used to describe rock masses fall broadly into two categories: material property parameters and joint geometry parameters. Young's modulus of elasticity, E, Poisson's ratio, ν, and joint stiffnesses, k_s and k_n are material properties. They describe the behavior of material under stress or temperature. Fracture frequency, joint orientation and joint size are joint geometry parameters. They describe the geometry of the rock mass.

Description of rock mass properties depends to a certain extent on models for rock masses. Descriptions are not intrinsic properties of rock, but are rather parameters derived for particular models, or for particular measurement methods. An example of the former is Youngs modulus of Elasticity, E, an example of the latter joint spacing. Young's modulus is a parameter developed as part of Elasticity Theory. It can, however, be measured in rock without respect to the requirement of elasticity theory. Beause it is an elastic theory parameter, its value and interpretation depend upon the use of that theory. How well E can be used to describe rock depends upon how well elasticity theory describes rock.

Joint spacing s is measured in boreholes or surface surveys. When spacings are used to describe rock masses, however, a model for rock joints is implicitly used. Joints

are seen as planes of finite size, and width, with some spatial relationship. The use of joint spacing therefore depends upon how well the assumed joint model fits reality. The testing procedure used to measure spacing has considerable effect upon measured spacing because spacing is a property of the measurement process rather than of the rock mass.

Two important observations about the relationhsip of rock mass descriptions to assumed models can be found from the above examples.

1. The interpretation of descriptors depend upon the validity and limitations of the model and the description.
2. The measurement of descriptor values is dependent upon the validity of the model used by the descriptor and upon the measurement process.

3.4 Description of Joint Geometry

Joint geometry plays a significant role in rock mass deformation. Aspects of joint geometry covered here include spacing, length, orientation, persistence, and Deere's "Rock Quality Designation," (Deere, 1967). For the present purposes, a model of joints as planar disks (possibly circular) of random size, location, and orientation has been adopted (Figure 3.4.1.) Geometric descriptions of jointing are defined within the context of this model.

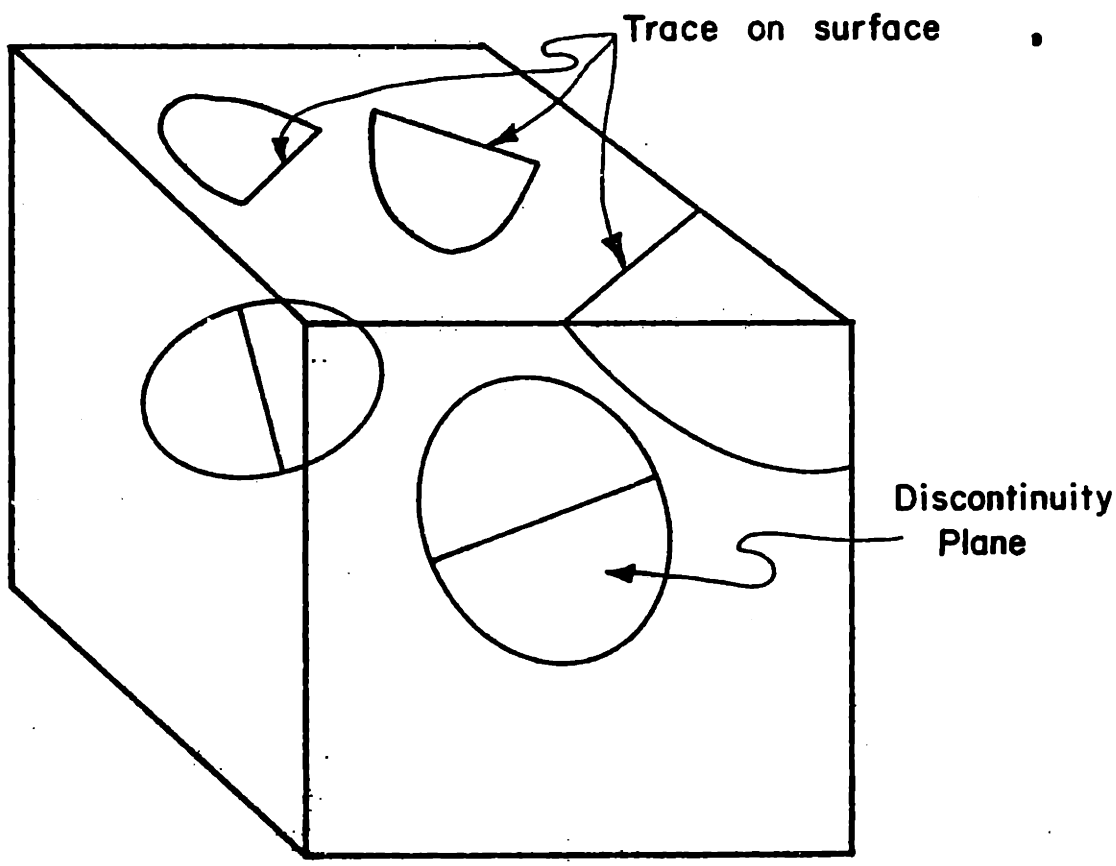

Figure 3.4.1 Discontinuity Planes in Space

3.4.1 Joint Spacing

Joint spacing is, simply enough, the distance between adjacent joints in space. This concept is illustrated in Figure 3.4.2. In rock masses, the overall spacing of joints within a rock mass is frequently represented deterministicly by the mean joint spacing, s_m, where

$$s_m = \frac{1}{(N-1)} \sum_{i=1}^{N-1} d(j_i, j_{i+1}) \tag{3.4.1}$$

where N = number of joints and d (j_i, j_i+1) = distance between joint i and joint i + 1.

In this thesis the true spacing will be defined as the perpendicular spacing between joints.

Joint spacings are normally measured along line surveys on the surface of a rock mass or in borings into a rock mass. The joint spacing therefore represents not the perpendicular distance between joints defined in Figure 3.4.2, but the spacing as measured along the sampling line. This difference is due to the effect of the joint orientation on the measured joint spacing. For perfectly horizontal joints, the true (perpendicular) spacing of joints can be found by vertical borings, but almost no joints will be observed in a horizontal surface survey. For perfectly vertical joints, the true spacing of joints can be found by surface survey if the survey line is perpendicular to the joint set. But a vertical boring would

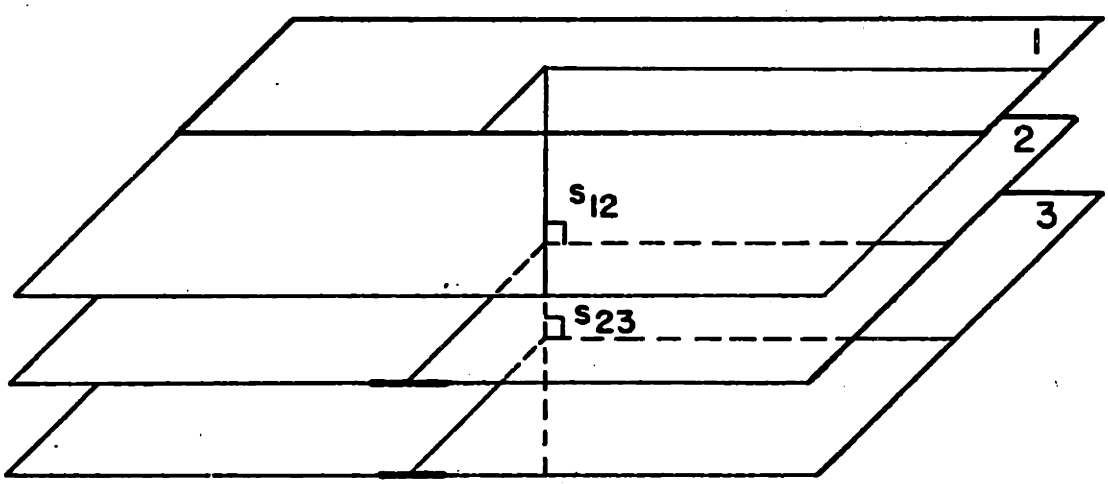

Figure 3.4.2 Joint Spacing

find an infinite distance between joints. This is illustrated in Figure 3.4.3. Rock joints are inclined at angles other than the perfect vertical or horizontal. For vertical borings the measured joint spacing s' can be related to the true joint spacing by

$$s = s'/\cos\phi \tag{3.4.2}$$

where ϕ = joint dip (angle from the horizontal).

For surface surveys, a similar approach can be used. $s = s'/\sin\phi$. This is illustrated in Figure 3.4.4.

The deterministic description of spacing within a rock mass, s_m should be found as the average of true spacings, rather than as the average of measured spacings.

$$s_m = (N)^{-1} \sum_{i=1}^{N} s_i \tag{3.4.3}$$

where s_m = mean spacing
s_i = true spacing
N = No.of spacings measured

Joint spacing can also be represented probabilistically. One approach is to calculate mean spacing and upper and lower bounds. This is adequate where the actual spatial variability of spacing is not important. In many deformation models, however, the spatial variability is important.

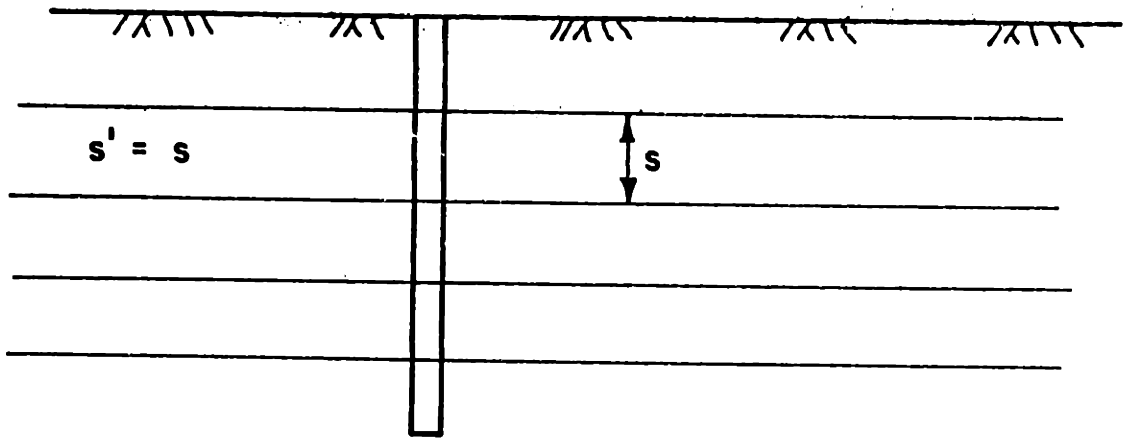

HORIZONTAL JOINT SET

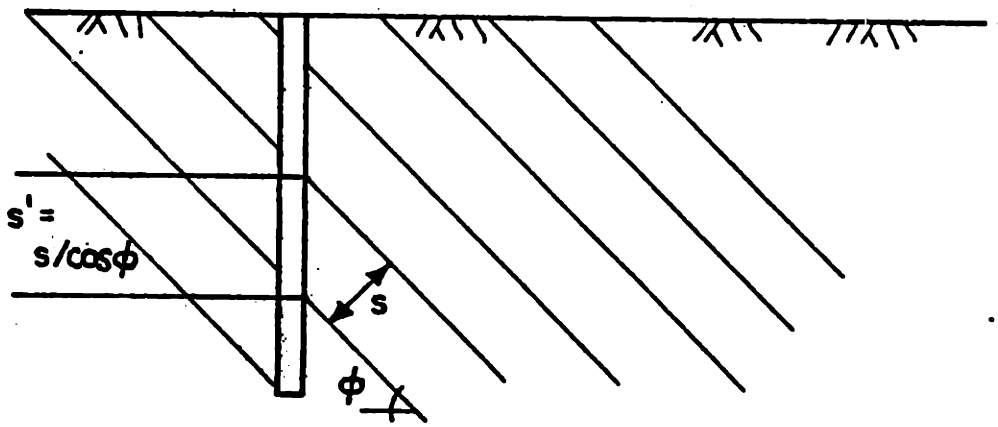

INCLINED JOINT SET

Figure 3.4.3 Joint Spacing from Cores

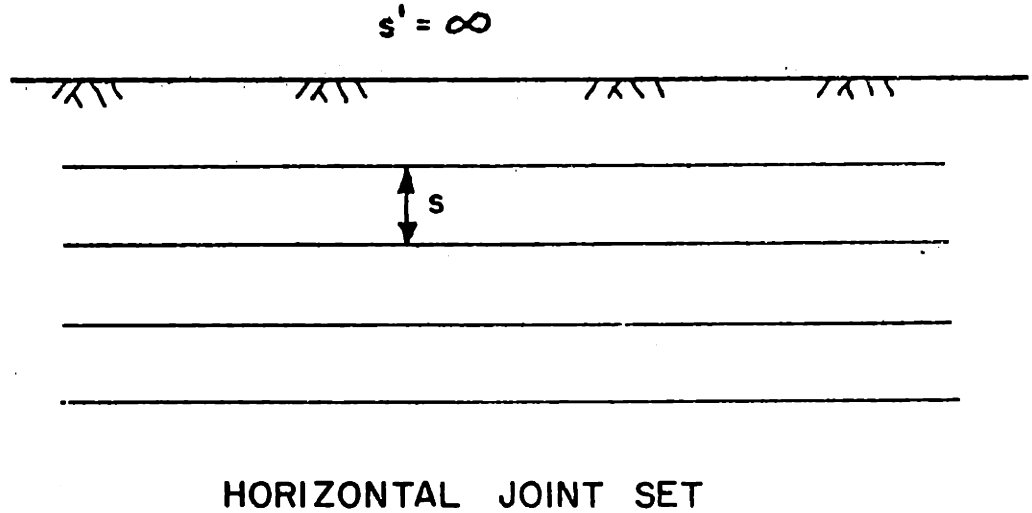

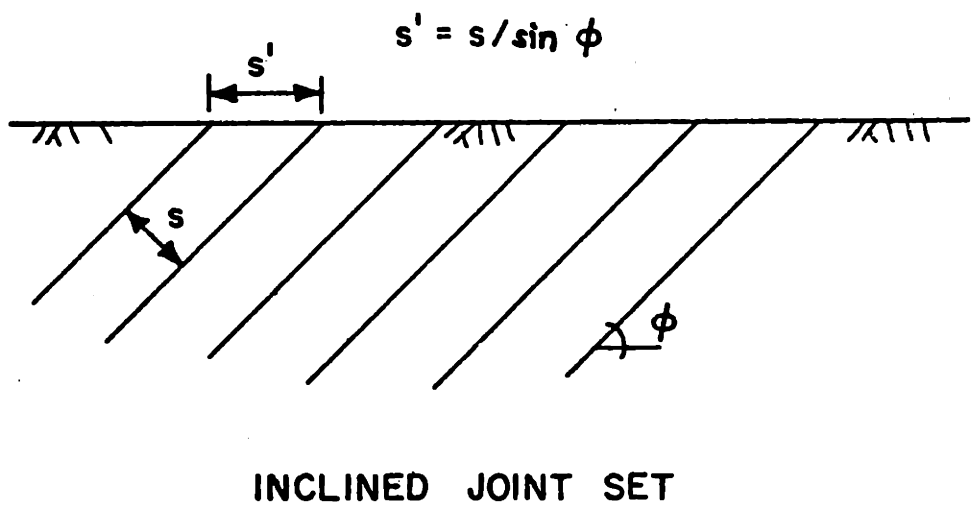

Figure 3.4.4 Joint Spacing from Surface Surveys

The most complete representation of spacing is the use of a parametric distribution. Experimented work by Call et al. (1976), Priest and Hudson (1976) and Lanney (1978) seems to indicate the best model to be the exponential distribution.

$$f_s(s) = \lambda e^{-\lambda s} \tag{3.4.4}$$

The mean of this distribution is $1/\lambda = s_m$ (mean spacing). The standard deviation of the exponential distribution is $1/\lambda$. Researchers have fit the exponential distribution to joint spacings, in general, without regard to the orientation of the sampling line. Therefore, for a sampling line perpendicular to all joints, and therefore measuring true spacings, the exponential distribution could also be expected to fit. In addition, a Poisson plane model for joint planes developed by Veneziano (1978) predict both an exponential distribution for spacing and independence of the distributional form of spacing with respect to the orientation of the sampling line. While the model does not prove the validity of the exponential distribution, it does lend credence to its use.

The exponential distribution for spacing data has the shape shown in Figure 3.4.5. The simple relationship between mean and standard deviation indicates that the scatter between spacings is larger for greater spacings. Normal and log normal

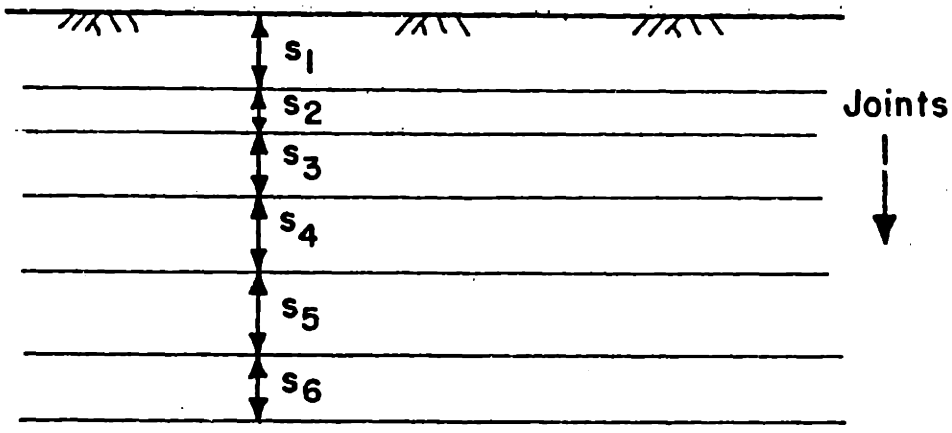

SPACING PROCESS

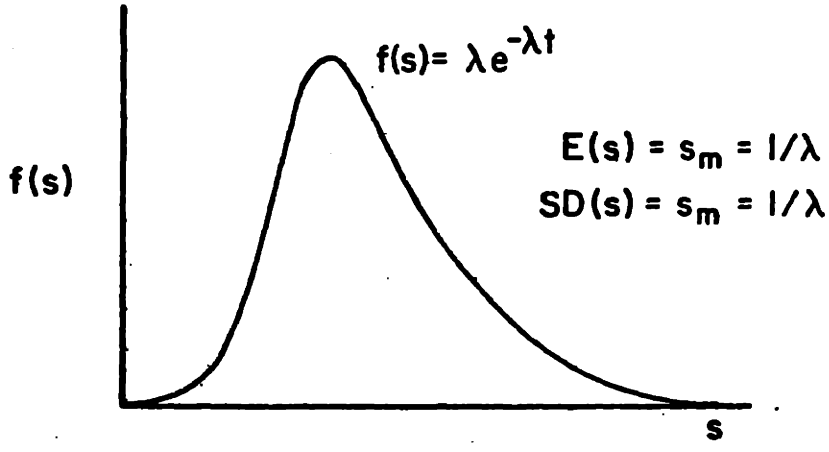

SPACING DISTRIBUTION

Figure 3.4.5 Exponential Distribution of Spacing

distributions have also been fit to spacing data with limited success (Steffan et al., 1970; Bridges, 1976; Barton, 1977).

3.4.2 Joint Length

Size is one of the more difficult aspects of joint geometry to describe. Since joints are contained within rock masses, it is impossible to completely ascertain their three dimensional extent. The only easily measureable indicator of joint size is trace length, the length of an intersection between a joint and the rock mass surface (Figure 3.4.6).

The interpretation of joint trace length depends upon assumptions of joint shape, and the relationship of the joint trace to the joint. If the joint trace can be assumed to be the diagonal of a square or rhomboidal joint, the joint surface area can be found simply from

(3.4.5) $$A_j = 1/2\ l^2$$

where A_j = joint area

l = joint trace length

If the trace can be assumed to be the diameter of a circular joint,

(3.4.6) $$A_j = \pi/4\ l^2$$

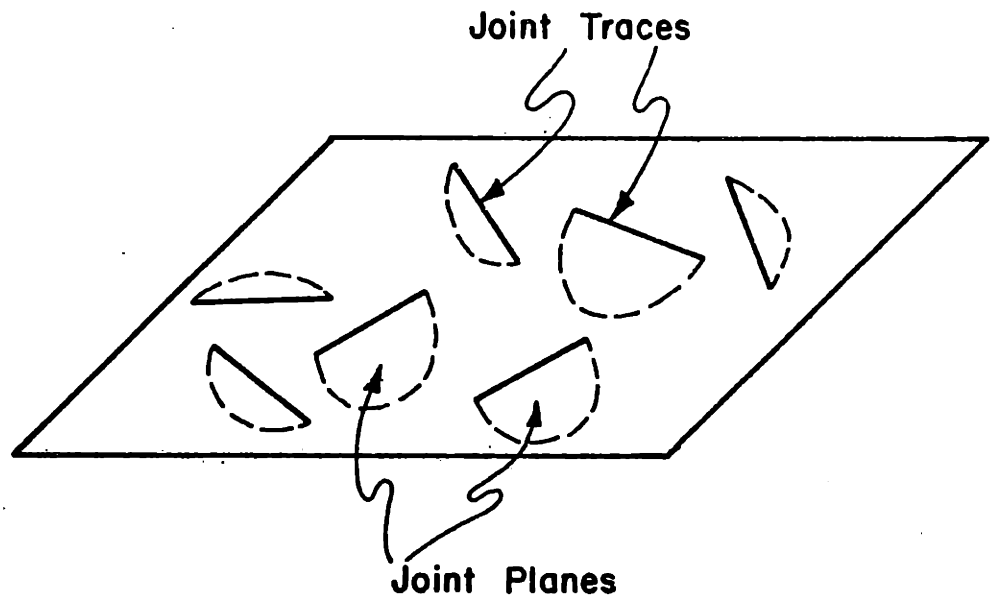

Figure 3.4.6 Joint Traces

More complicated assumptions of joint shape and of the relationship of the joint trace to the joint result in more complicated relations between joint trace and joint size. (See Figure 3.4.7).

Ultimately, of course, even for fixed joint shapes, the location of the joint trace within the joint must be variable. The relationship between the joint trace and joint size is therefore inevitably probabilistic. Figure 3.4.8 shows the distribution of trace lengths for circular joints.

Measurement of trace length on the surface of a rock is subject to many sampling biases. Shorter joints are less frequently intersected in surveys, and are therefore underrepresented in samples of trace length. Larger joints disappear under ground-cover or back into the rock. This adds to the difficulty of interpretation of joint trace data. More research is required to determine what is, in fact, the correct shape for rock joints, what is the relationship between trace length and joint size, and what corrections should be applied to correct for sampling biases in studies of trace length.

In addition, where joint trace lengths are correlated to joint orientations, trace length may be biased according to the orientation of the sampling line, just as spacing is (Figure 3.4.9).

Joint trace length for a rock mass is represented deterministicly by a mean joint length l_m representing the arithmetric average of observed joint lengths. The true mean

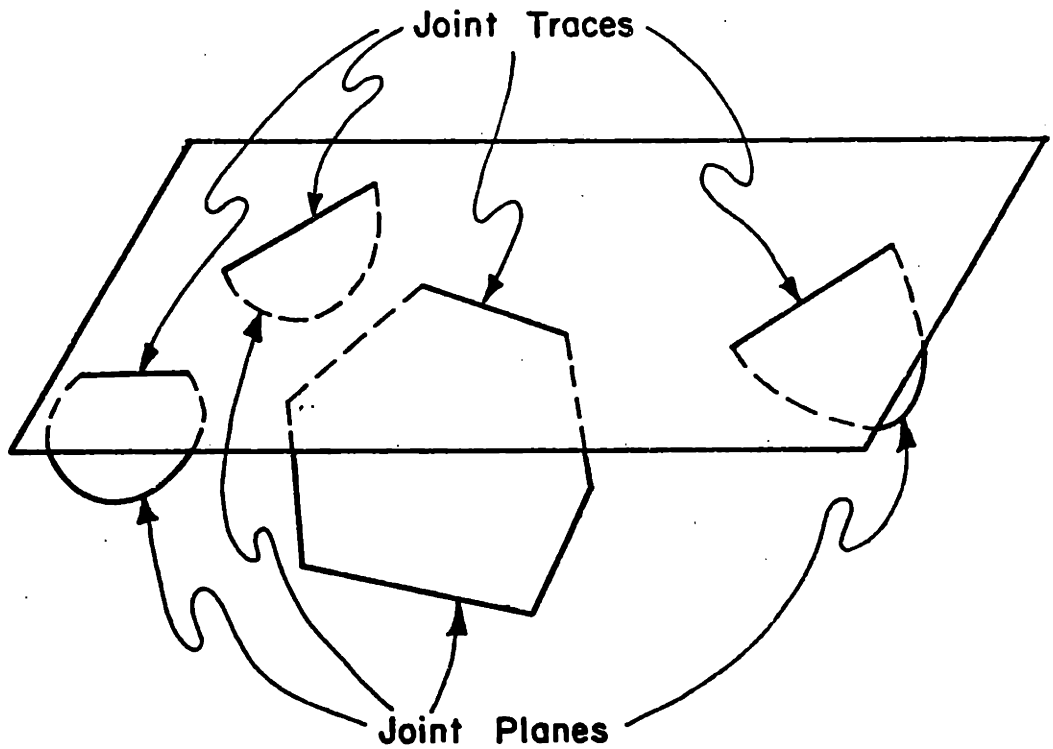

Figure 3.4.7 Joint Traces for Differently Shaped Joint Planes

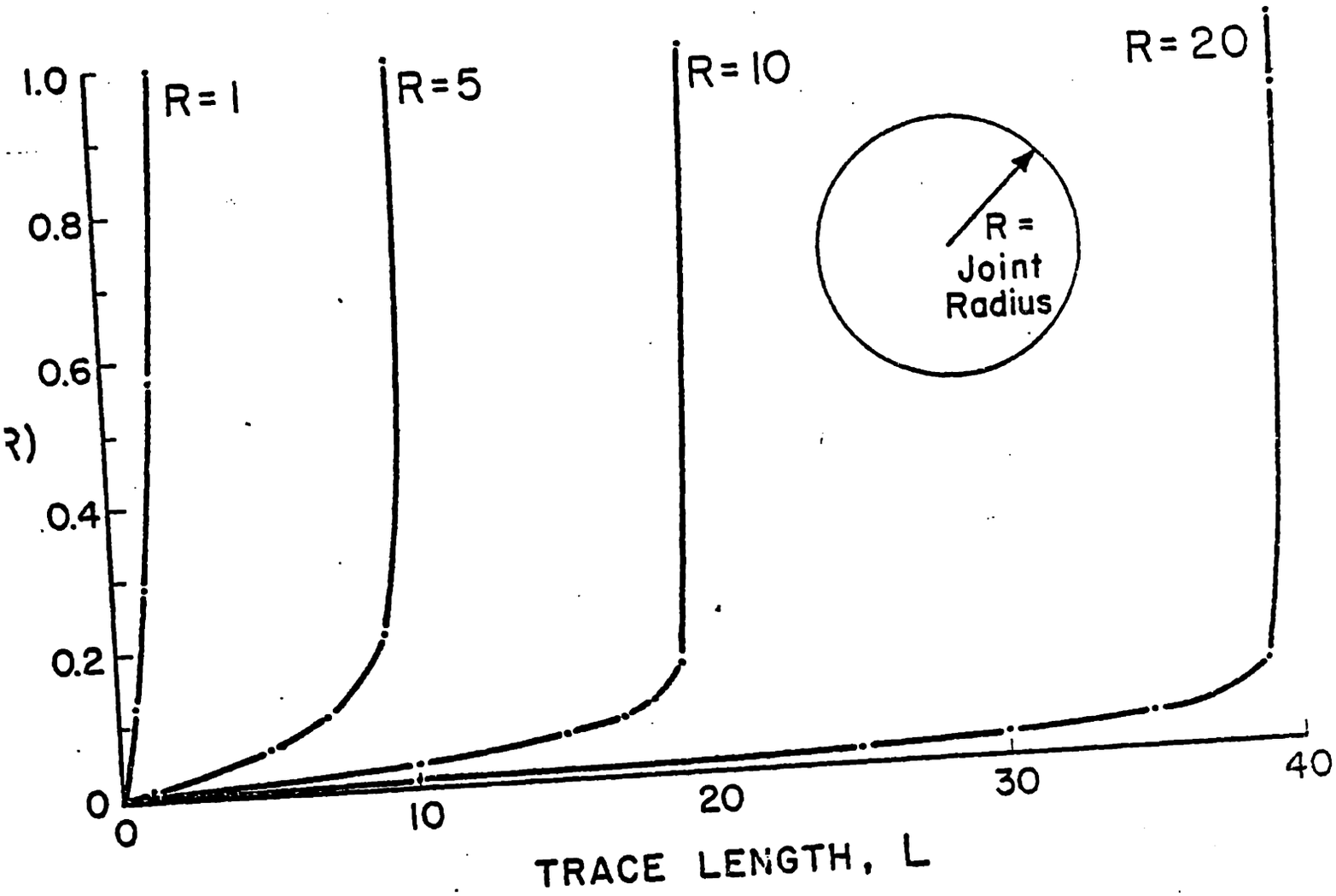

Figure 3.4.8 Distribution of Trace Lengths-
Circular Joints with Random
Intersections with Sampling Surface

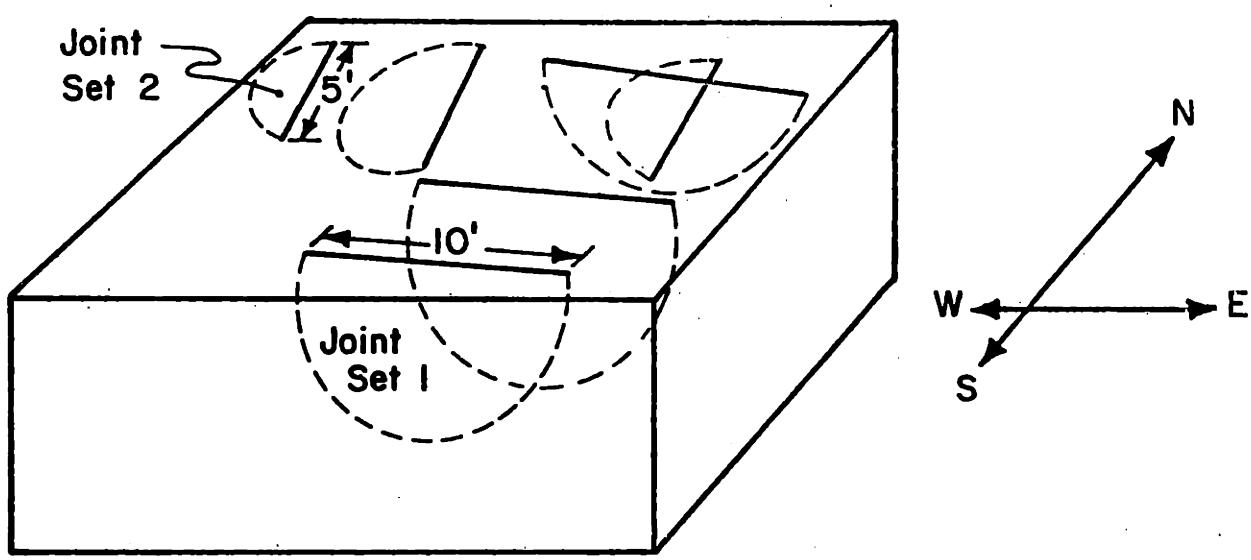

North-South line survey:
Trace Length=10'
East-West line survey:
Trace Length=5'

Figure 3.4.9 Trace Length Bias from Orientation of Sampling Line

depends upon joint shape and sampling biases. There is considerable question, therefore, as to the correct use of mean trace length statistics.

Several researchers have looked for ways to describe the variability in trace length observations. Robertson (1970) proposed that joint trace lengths could best be described by the exponential distribution. McMahon (1974), Barton (1976), Bridges (1976), and Lanney (1978) all conclude that joint trace lengths are lognormally distributed

$$(3.4.7) \qquad f(l) = \frac{l^{-1}}{\sqrt{2\pi}\,\sigma_{\ln l}} \exp\{-\tfrac{1}{2}[\frac{\ln(l/m_l)}{\sigma_{\ln l}}]^2\}$$

where l = trace length, m_l = mean trace length, and $\sigma_{\ln l}$ = standard deviation of log of trace length.

Distributions of trace length are all fit of course, to observed trace length. Because of bias and sampling problems it is difficult to derive the distribution of true trace lengths. It is even more difficult to derive the distribution of true joint size.

3.4.3 Persistence

Persistence, like joint length, is highly dependent upon the model assumptions used to define the measure. Persistence is a general measure of joint continuity. In the definition used here persistence represents relationship between open and closed portions of the same joint plane. This is illustrated

in Figure 3.4.10. For other definitions see Stagg and Zienkiewicz (1968). The existence of joint planes and the existence of open and closed portions thereof is, in fact, a critical and debatable assumption. In discussion of joint size in the previous section, it was assumed that a joint ended when it became closed. But what about cases such as that illustrated in Figure 3.4.10, where several open joints are clearly coplanar?

Persistence can have a very significant effect upon rock mass behavior, so it is important to take the phenomenon into account. Where several joint segments are coplanar, they may act as a single joint under high stresses, and the entire plane may open under some loadings (See Glynn, 1979).

The most common way to describe joint continuity or persistence is as a ratio of open and closed joint lengths.

$$P = \frac{l_o}{(l_o + l_c)} \times 100\% \qquad (3.4.8)$$

where P = persistence in percent

l_o = open joint length

l_c = closed joint length

Persistence is frequently desired as a measure of open or closed <u>area</u> ratios rather than length ratios. This requires the use of assumptions for joint shape. For square or circular joints

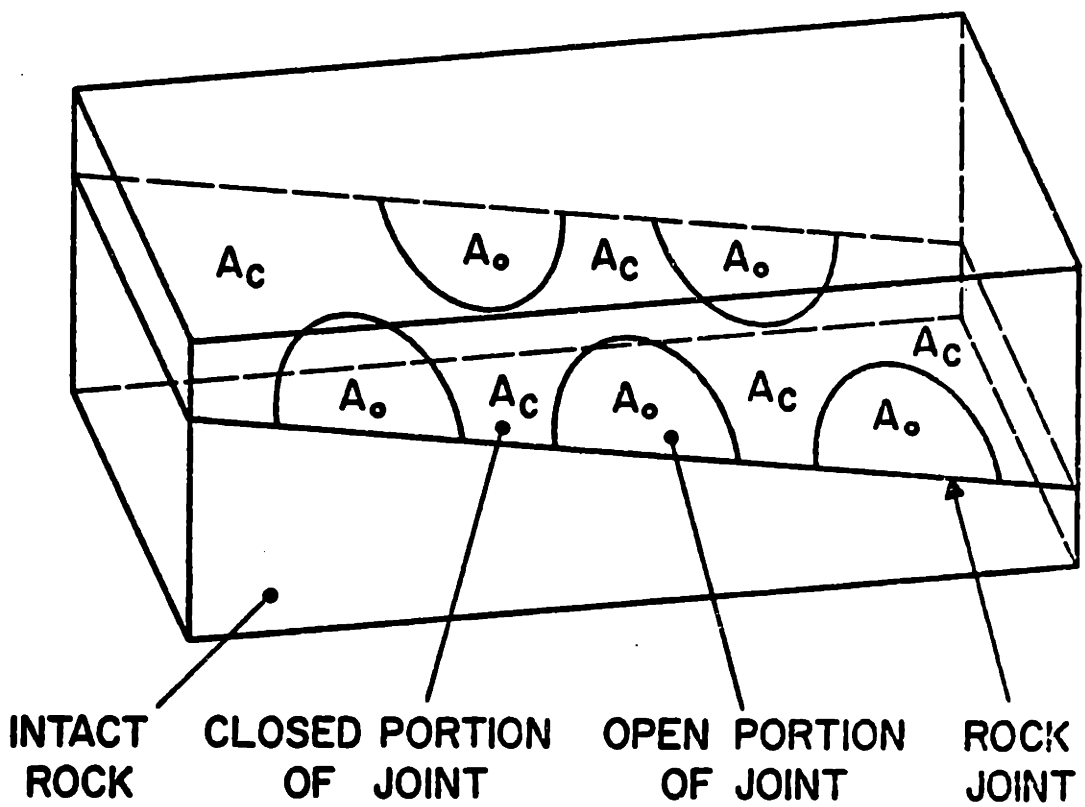

A_o=OPEN AREA OF JOINT

A_c=CLOSED AREA OF JOINT

PERSISTENCE $P=A_o/(A_o+A_c)$

Figure 3.4.10 Persistence

$$P' = \frac{l_o^2}{(l_o + l_c)^2} \tag{3.4.9}$$

where P' = persistence in terms of area

Mean persistence can be used as a deterministic description of persistance. Little work has been done toward the determination of a probabilistic description of persistence. Possible distributions include the normal, lognormal, exponential, and gamma.

Joint Intensity (Baecher, Lanney, and Einstein,1967) is a combination of spacing and persistence:

$$I = l_j/A \tag{3.4.10}$$

where I = joint intensity
l_j = total length of joints on sampled surface
A = area of sampled surface

3.4.4 Joint Orientation

Joint orientation or attitude is an essential aspect of joint geometry, and has a significant effect upon measurement of all other aspects of joint geometry. Description of joint orientation is complicated by the fact that orientation must be described in three dimensions, while other aspects such as spacing or size can be simplified to one or two

dimensions.

The orientation of planes in three-space can be described in several basic systems. Goelogists generally represent orientation by strike or azimuth (dip direction) and dip. Mathematicians may represent orientations by unit vectors either parallel to the dip of the joint or perpendicular to the joint in upper or lower hemisphere. Unit vectors may be represented in either cartesian coordinates, (x,y,z), cylindrical coordinates (r,θ,z), or spherical coordinates (r,θ,ϕ). (Figure 3.4.11). Table 3.4.1 presents conversions among the major representation systems.

Measurement of orientation is subject to many biases and errors. These are discussed in Appendix B. These biases can significantly affect the perception of orientation trends. A particularly poignant example of this is the work of Robertson and Piteau (1975). When they attempted to correct for bias and measurement error effect, they found that their inferences on (θ,ϕ) were changed in many cases by a factor of greater than 5!

Joint orientation can be described deterministicly by a mean orientation. This orientation may be the orientation of the resultant vector found by adding together all joint poles.

DIP DIRECTION θ	DIP ϕ	STRIKE	DIP	AZIMUTH	DIP	LOWER HEMISPHERE POLE DIP DIRECTION	DIP
θ = (0 to 90)	ϕ	(90-θ)W	ϕ E	270 + θ	ϕ	θ + 180	90 - ϕ
θ = (90 to 180)	ϕ	(θ-90)E	ϕ E	θ - 90	ϕ	θ + 180	90 - ϕ
θ = (180 to 270)	ϕ	(270-θ)W	ϕ W	θ - 90	ϕ	θ - 180	90 - ϕ
θ = (270 to 360)	ϕ	(θ-270)E	ϕ W	θ - 90	ϕ	θ - 180	90 - ϕ

Table 3.4.1 Conversion between Joint Orientation Representation Systems

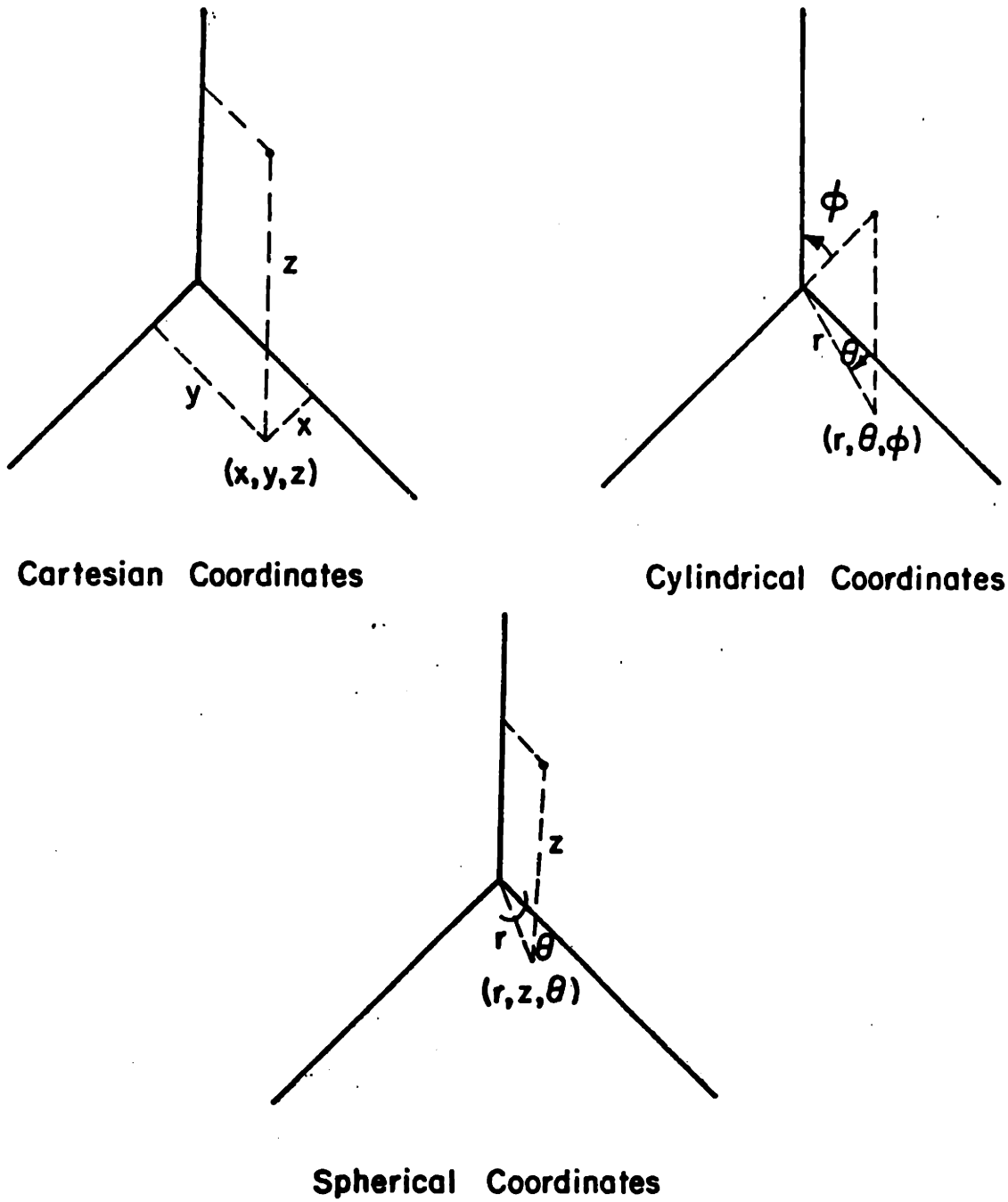

Figure 3.4.11 Cartesian, Cylindrical, and Spherical Coordinates

(3.4.11) $$R = \Sigma l_i^2 + \Sigma m_i^2 + \Sigma n_i^2$$

where R = Resultant vector, and l_i, m_i, n_i are the components of the unit vector in cartesian coordinates (Kiraly, 1969).

Probabilistic description of joint orientations requires description of a collection of unit vectors. These unit vectors may be seen as points on a unit hemisphere as shown in Figure 3.4.12. The problem of description of points on a unit hemisphere is intrinsically different from the problem of description of points on a plane. Thus, such planar distributions as the normal, exponential, lognormal, and gamma cannot be directly applied to the problem of description of points on a unit hemisphere.

Probability distributions by definition describe the frequency of occurrence of points or events. This frequency can be visualized geometrically as a density of points over an area or length.

(3.4.12) $$Pr(x + \Delta x, y + \Delta y) = f(x,y)dA$$

This is illustrated in Figure 3.4.13. On a plane, the areas over which frequencies are calculated can be found simply from

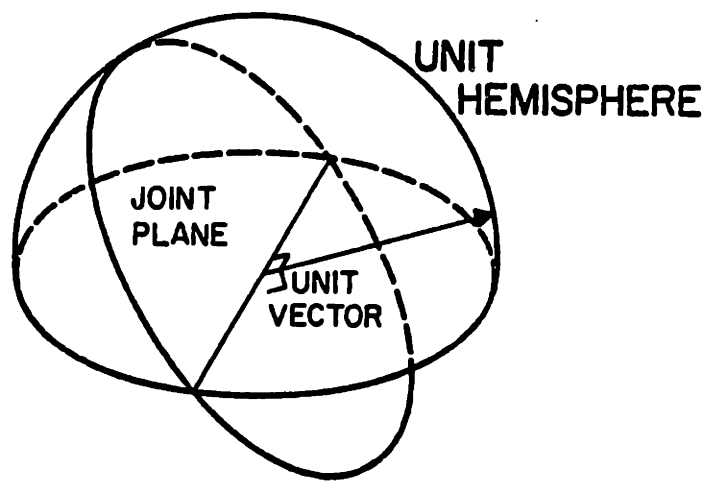

Figure 3.4.12 Joint Orientations as Unit Vectors on a Unit Hemisphere

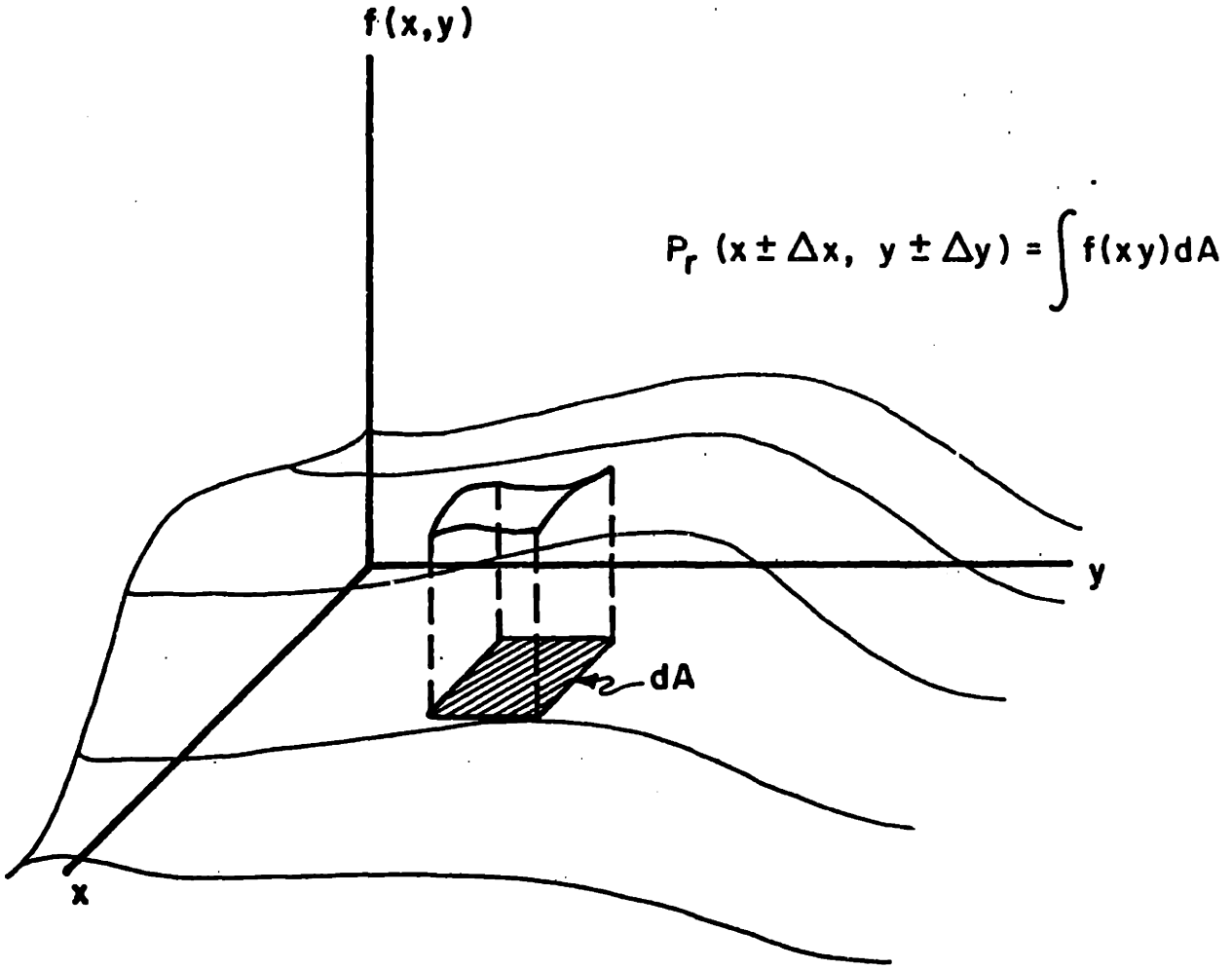

Figure 3.4.13 Probability Distributions as Frequencies

NAME	DISTRIBUTION OF $\{\phi\}$	DISTRIBUTION ON UNIT PLANAR SURFACE	DISTRIBUTION ON UNIT RADIUS SPHERICAL SURFACE
Uniform	$f(\phi) = \frac{1}{2\pi}$	$f(\phi) = \frac{1}{2\pi}$	$f(\phi) = \frac{1}{2\pi}\sin\phi$
Sine	$f(\phi) = \frac{\sin\phi}{2\pi}$	$f(\phi) = \frac{\sin\phi}{2\pi}$	$f(\phi) = \frac{1}{2\pi}$
Normal	$f(\phi) = \frac{\exp[-\frac{1}{2}(\frac{\phi-\phi_m}{\sigma_\phi})^2]}{\sqrt{2\pi}\sigma_\phi}$	$f(\phi) = \frac{\exp[-\frac{1}{2}(\frac{\phi-\phi_m}{\sigma_\phi})^2]}{\sqrt{2\pi}\sigma_\phi}$	$f(\phi) = \frac{\exp(g(\phi))}{C\sin\phi}$ $g(\phi)$ = distribution related to mean and variance C = constant
Bingham	$f(\phi) = \frac{\sin^2\phi\exp[\kappa\sin^2\phi]}{C}$	$f(\phi) = \frac{\sin^2\phi\exp[\kappa\sin^2\phi]}{C}$	$f(\phi) = \frac{\exp[\kappa\sin^2\phi]\sin\phi}{C}$

Table 3.4.2 Spherical and Planar Distributions

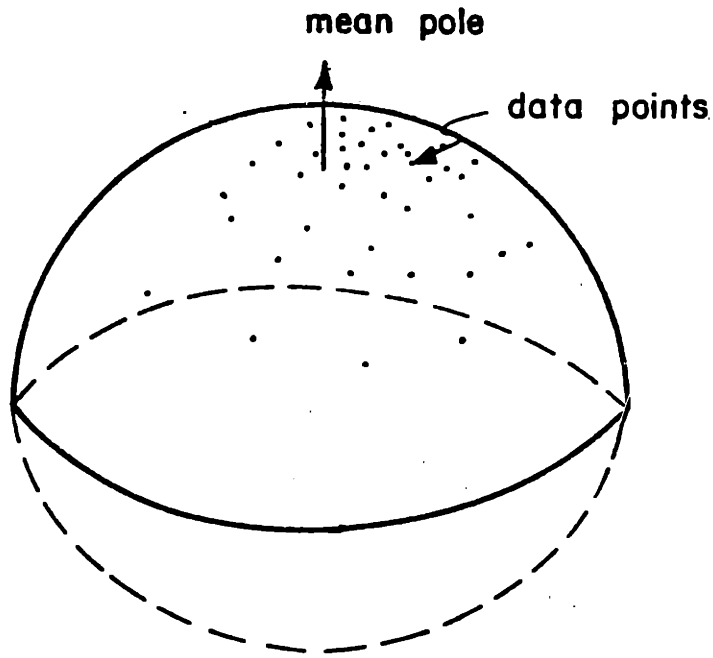

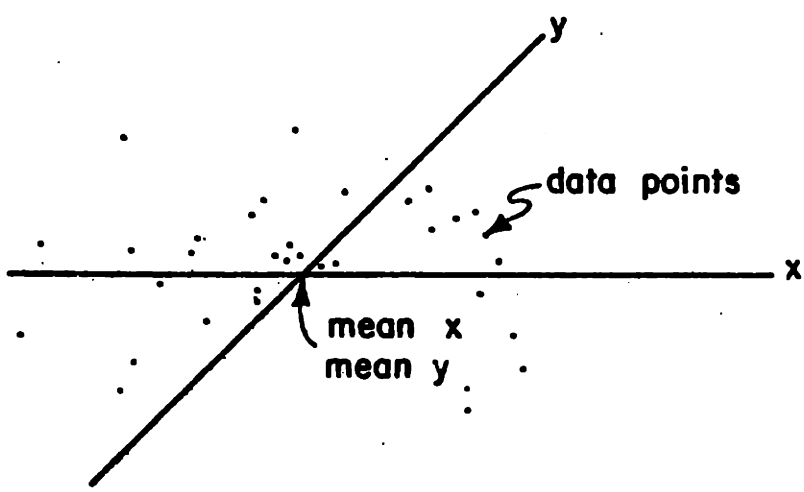

Figure 3.4.14 Spherical and Planar Distributions

(3.4.13) $$dA = dxdy$$

Areas on unit hemispheres, on the other hand are, in spherical coordinates,

(3.4.14) $$dA = \sin\phi d\phi d\theta$$

This difference results in a different class of distributions, the <u>spherical distribution</u>, to describe frequencies on spherical surfaces. The development of these spherical distributions is discussed in Appendix B. Table 3.4.2 shows the difference between spherical and planar distributions. Figure 3.4.14 illustrates the difference graphically.

No single spherical distribution has yet been found which can adequately describe the spatial and statistical variability of joints. Only five distributions have been found which have potential as models for rock orientation distributions. These and the Uniform, Fisher, Bivariate Fisher, Bingham, and Bivariate Normal. These are presented below. Attempts to fit distirbution to orientation data are described in Appendix C.

<u>Uniform Distribution</u>

The uniform distribution suggests that joint poles have no

preferred orientation. The distribution has limited applicability to real data, where preferred orientations are common, but it does have the advantage of simplicity, and can serve as an approximation for extremely diffuse distributions.

The uniform distribution implies that the point density of poles on the surface of unit hemisphere is constant. Thus,

(3.4.15) $$f(\theta,\phi) = \frac{1}{2\pi}\, dA$$ where $\frac{1}{2\pi}$ is a normalization constant to normalize the area of a unit sphere to 1.

The distribution on (θ,ϕ) is

(3.4.16) $$f(\theta,\phi) = \frac{1}{2\pi} \sin\phi d\theta d\phi$$

Figure 3.4.16 is a three dimensional representation of the uniform distribution on the surface of a sphere. The axes for the plot, and for all subsequent 3-D plots are shown in Figure 3.4.15 .

Since the uniform distribution is constant over the entire unit hemisphere, no parameters need be fit for the uniform distribution. Validity of the uniform distribution can be tested by using the χ^2 statistical test to determine whether a preferred orientation does, in fact, exist.

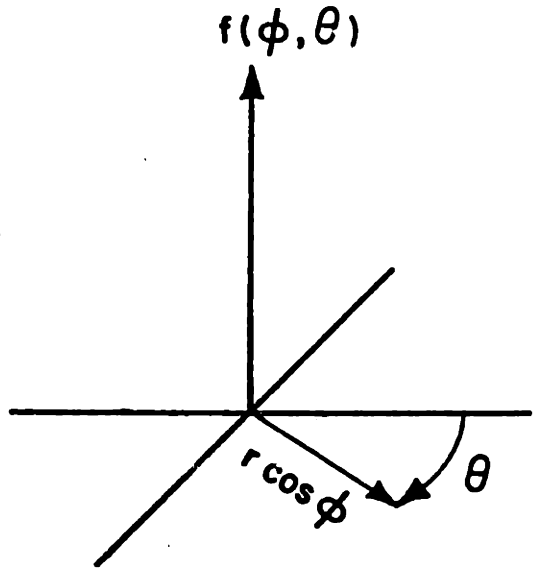

Figure 3.4.15 Axes for Three-Dimensional Plots.

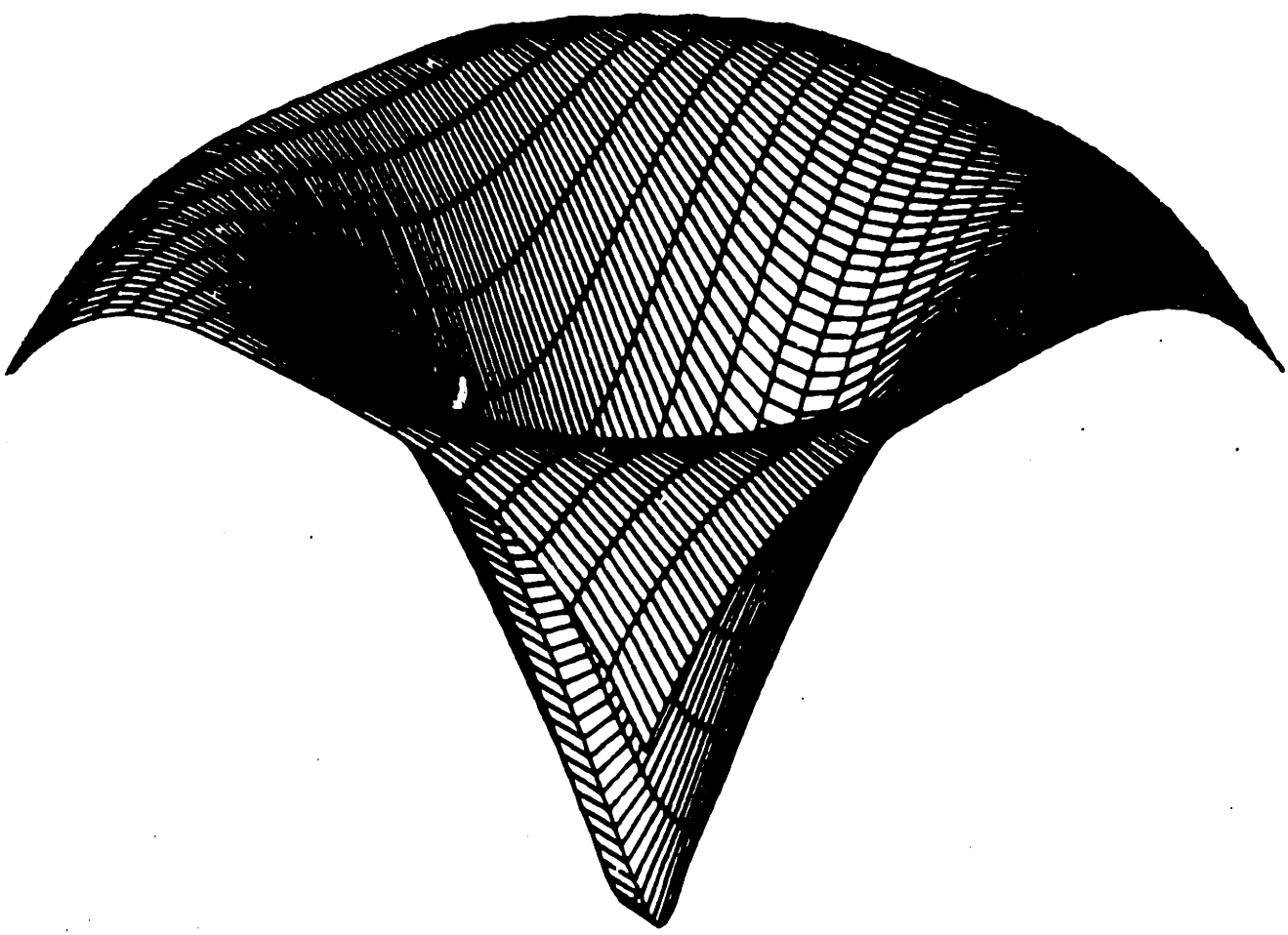

Figure 3.4.16 3D Representation of Uniform Distribution on a Sphere

Fisher Distribution

The Fisher distribution is an analog of the normal on the surface of a sphere. On a plane, the normal distribution can be represented by

$$(3.4.17) \qquad f_x(x) = C_1 \exp\{-\tfrac{1}{2}[\frac{x-x_m}{C_2}]^2\}$$

where C_1 and C_2 are constants related to the mean (x_m) and standard deviation of x.

According to Fisher (1953), this could also be represented by

$$(3.4.18) \qquad f_x(x) = C_1 e^{C_2 \cos x} dx$$

On a sphere, substituting unit length x by unit area $d\theta d\phi \sin\phi$,

$$(3.4.19) \qquad f(\theta,\phi) = C_1 \epsilon^{\kappa\cos\phi} \sin\phi d\theta d\phi$$

Here, the normalizing constant for a sphere is

$$(3.4.20) \qquad C_1 = \kappa/(4\pi \sinh\kappa)$$

The parameter κ is a measure of dispersion about the mean pole, at (0,0). For joint data, which is distributed on a unit hemisphere, the normalizing constant is:

$$C_1 = (1 - e^{-2\kappa})^{-1} \tag{3.4.21}$$

For mean orientations other than (0,0), transformation of coordinates can be used to relate (θ,ϕ) about the mean pole to (θ',ϕ') in the reference frame.

Figure 3.4.17 shows density as a function of ϕ for several different values of dispersion κ. Figure 3.4.18 is a three-dimensional representation of the Fisher distribution for $\kappa = 5$.

Fitting the Fisher distribution involves two stages. First, the mean pole must be found, and coordinates must be transformed into the frame of the mean pole. The mean pole may be found from the orientation of the resultant vector R, as discussed above. Or the mean pole can be found by solving for the eigenvectors of the covariance matrix of direction cosines (Kiraly, 1969).

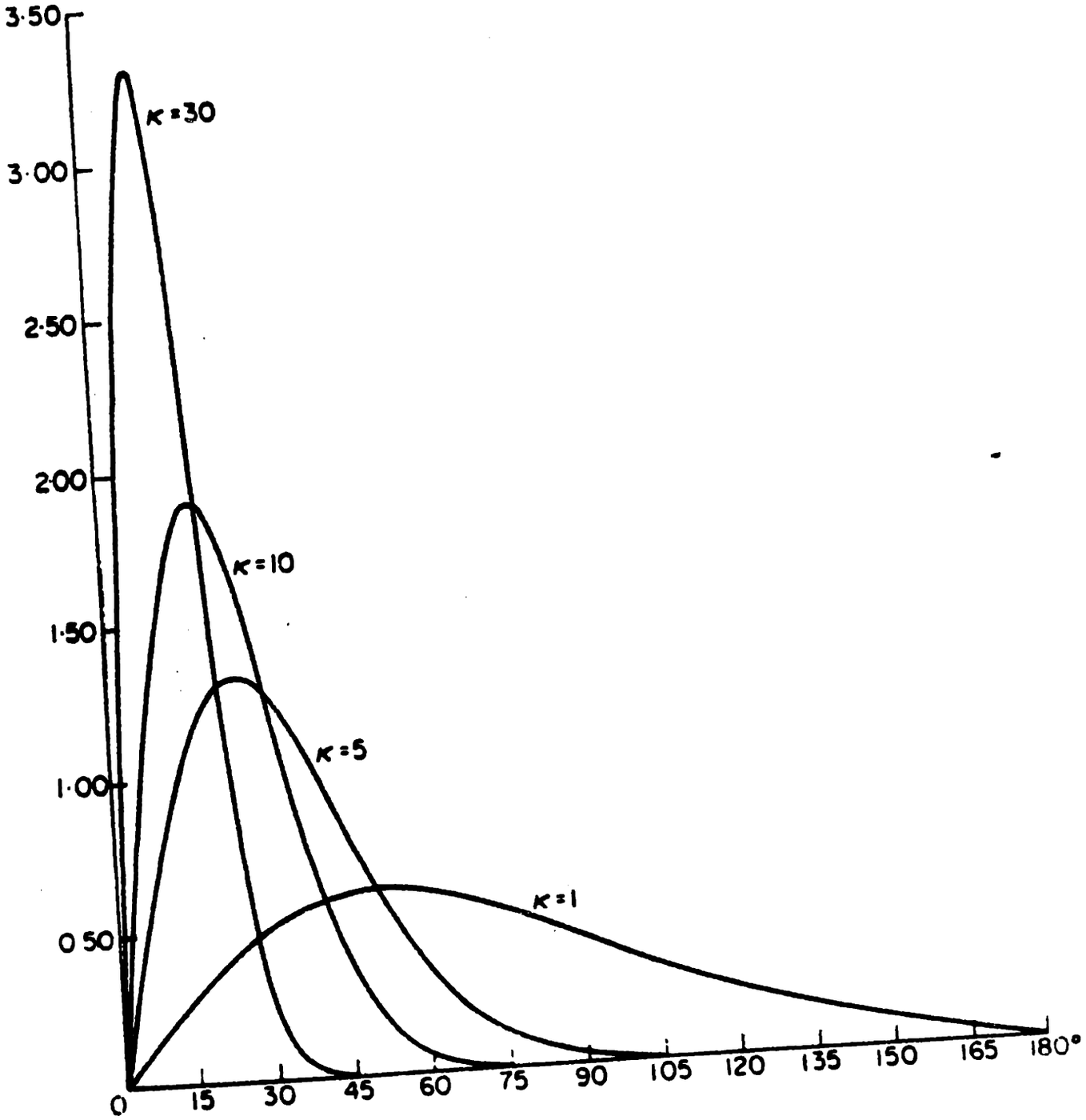

Figure 3.4.17 Fisher Distribution Density Function (Mardia,1972)

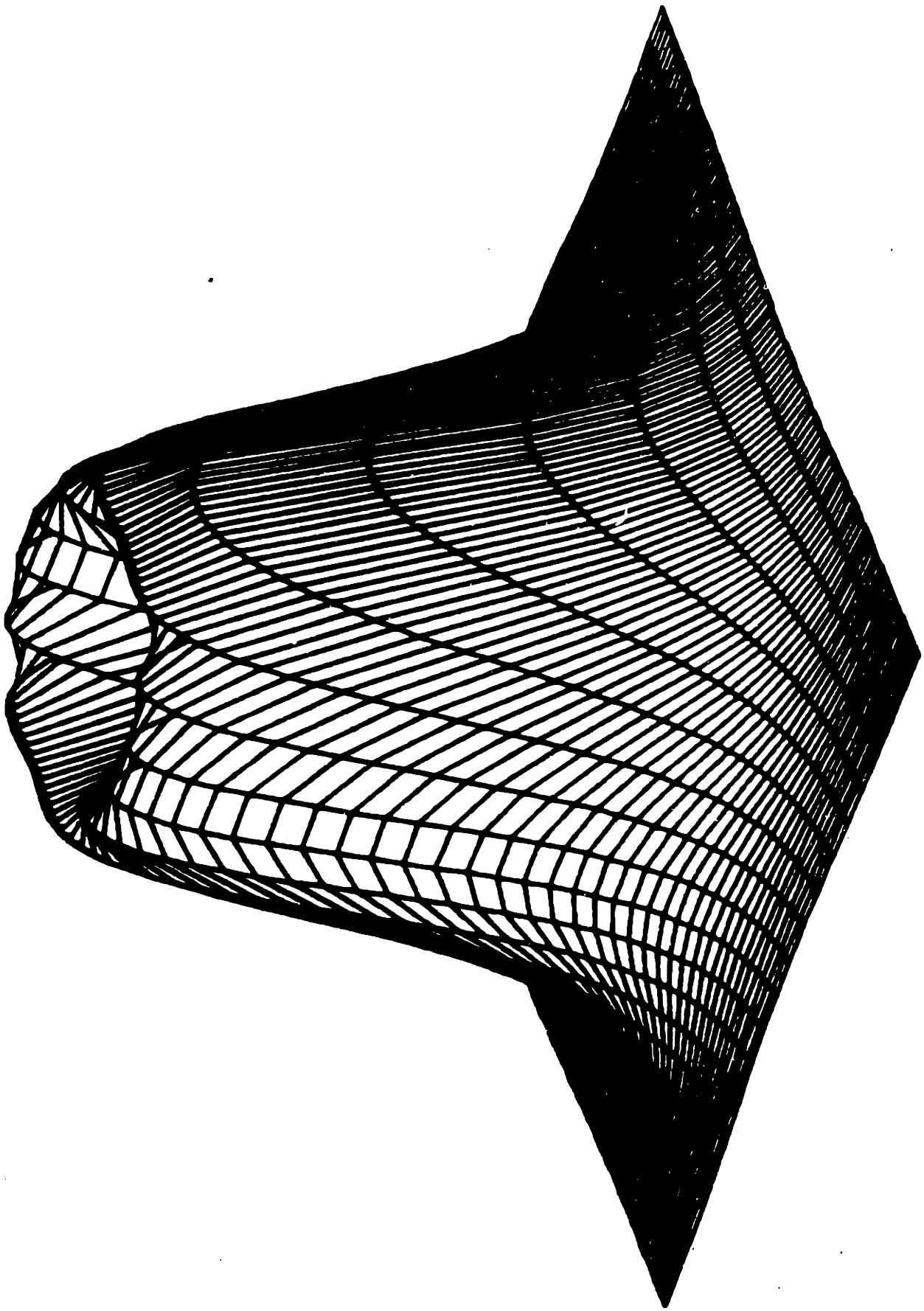

Figure 3.4.18 **Three Dimensional Representation of Fisher Distribution (K=5)**

1) Represent all poles (θ, ϕ) by direction cosines, the Cartesian coordinates of the pole

$$
\begin{aligned}
l &= \cos\phi\sin\theta \\
m &= \cos\phi\cos\theta \\
n &= \sin\phi
\end{aligned}
\tag{3.4.22}
$$

2) Construct the covariance matrix of direction cosines

$$
[x] = \begin{bmatrix} \Sigma\, l_i^{\,2} & \Sigma\, l_i m_i & \Sigma\, l_i n_i \\ \Sigma\, m_i l_i & \Sigma\, m_i^{\,2} & \Sigma\, m_i n_i \\ \Sigma\, n_i l_i & \Sigma\, n_i m_i & \Sigma\, n_i^{\,2} \end{bmatrix}
\tag{3.4.23}
$$

3) Solve for the eigenvectors of $[x]$. The principal eigenvector of the covariance matrix is the mean pole. The minor eigenvectors are major and minor axes of the data set.

4) Transform pole into the reference frame

$$
\begin{aligned}
l_i' &= l_i x_1 + m_i y_1 + n_i z_1 \\
m_i' &= l_i x_2 + m_i y_2 + n_i z_2 \\
n_i' &= l_i x_3 + m_i y_3 + n_i z_3
\end{aligned}
\tag{3.4.24}
$$

where (l_i', m_i', n_i') are transformed direction cosines, (x_1, y_1, z_1), (x_2, y_2, z_2) and (x_3, y_3, z_3) are the major and minor axes and the mean pole, and (l_i, m_i, n_i) are direction cosines.

5) Reconvert direction cosines to (θ, ϕ)

$$\phi' = \arcsin(n') \qquad (3.4.25)$$
$$\theta = \arctan(l'/m')$$

The second stage is to determine the maximum likelihood estimator for the dispersion of the Fisher distribution. This is

$$\coth \kappa = 1/\kappa = \frac{\Sigma \cos\phi}{N} \qquad (3.4.26)$$

where N = number of data points

For $\kappa > 3$, this can be approximated by

$$\kappa = \frac{|R|}{N} \qquad (3.4.27)$$

where R = resultant vector.

The Fisher distribution density is independent of azimuth around the mean pole and is therefore "axisymmetric." The distribution, though three dimensional, is simplified by this fact. This simplifies the fitting of data to the distribution, and the application of the distribution, but severely limits the generality of the distribution.

Bivariate Fisher

The Bivariate Fisher is a biaxially symmetric extension of the Fisher distribution developed by the author. The form

of the Bivariate Fisher is,

$$(3.4.28) \qquad f(\theta,\phi) = C_1 \exp[(\kappa_1 \sin^2\theta + \kappa_2 \cos^2\theta)\cos\phi]\sin\phi d\theta d\phi$$

where C_1 is a normalization constant over the surface of a hemisphere, and κ_1 and κ_2 are dispersion parameters along major and minor principal axes.

The Bivariate Fisher has not been solved analytically, so the parameters C_1, κ_1, and κ_2 must be found by numerical techniques. C_1 is found by

$$(3.4.29) \qquad C_1 = [\iint f(\theta,\phi)d\theta d\phi\ ]^{-1}$$

Dispersion parameters κ_1 and κ_2 may be found by maximization of log likelihoods. Axes for the Bivariate Fisher are found by the same method of eigenvecotrs as was used for the Fisher distribution.

The Bivariate Fisher distribution is illustrated in Figure 3.4.19. The Bivariate Fisher has considerably greater flexibility than the Fisher distribution, since it can model both

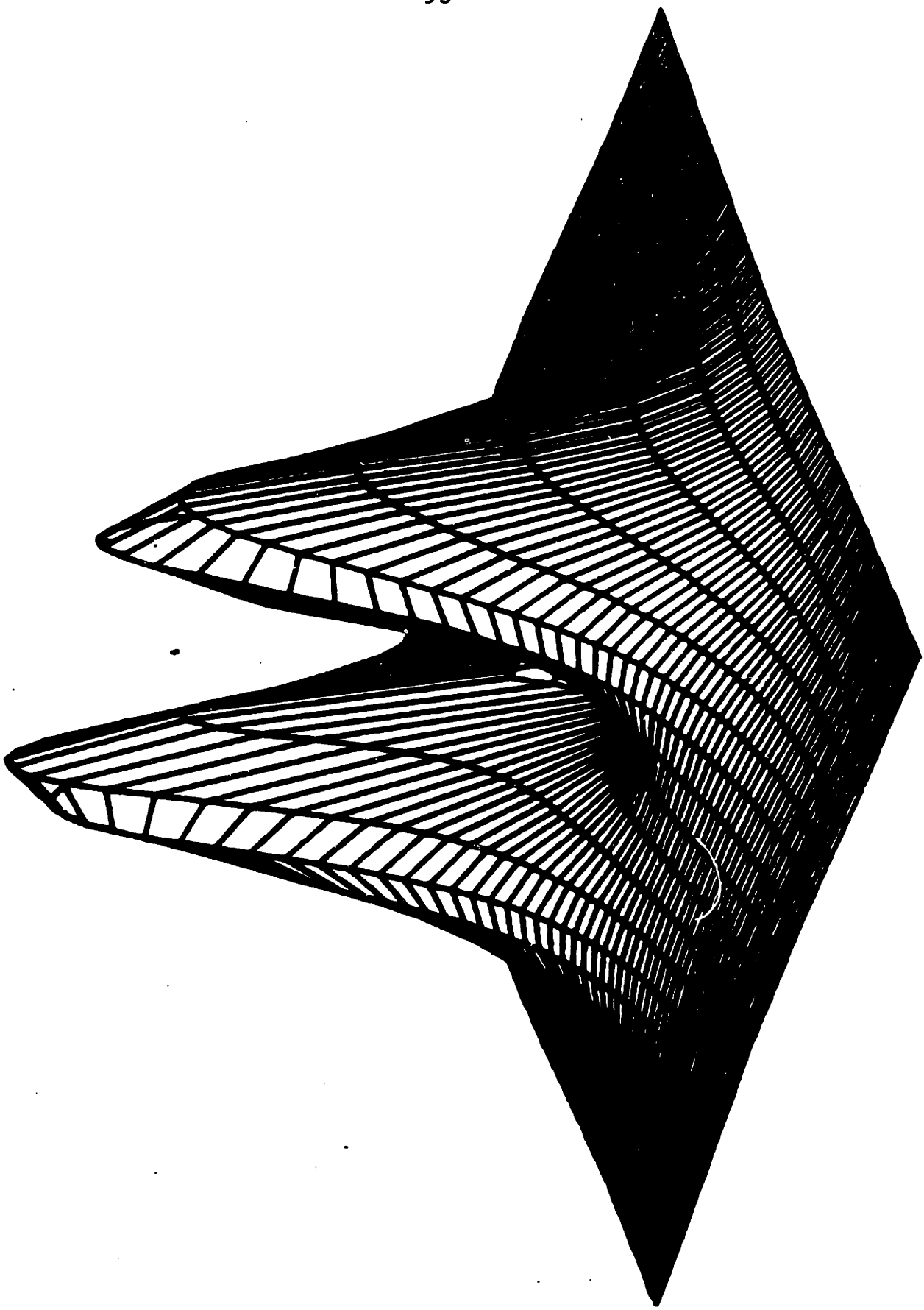

Figure 3.4.19 3D Representation of Bivariate Fisher Distribution

axially and biaxially symmetric conditions. For $\kappa_1 = \kappa_2$, the Bivariate Fisher reduces to the Fisher distribution.

Bingham Distribution

Bingham's distribution is a general biaxially symmetric distribution on the sphere. The distribution has dispersion parameters, κ_1 and κ_2. Unlike the Bivariate Fisher, however, the Bingham decays as

$$e^{\kappa \sin^2 \phi} \quad \text{instead of}$$

$$e^{\kappa \cos \phi} \quad \text{as the Fisher.}$$

This difference is important since the behavior of the tails of distributions may be critical. The form of the Bingham is

$$(3.4.30) \qquad f(\theta,\phi) = C_1 \exp[(\kappa_1 \sin^2\theta + \kappa_2 \cos^2\theta)\sin^2\phi]\sin\phi d\theta d\phi$$

The normalizing constant C_1 can be determined analytically by use of confluent hypergeometric functions (see Bingham, 1964), but the solution is extremely cumbersome. C_1 can be more easily determined by numerical approximation.

(3.4.31) $$C_1 = [\iint f(\theta,\phi)\,d\theta\,d\phi]^{-1}$$

Figure 3.4.20 illustrates the Bingham in three dimensions. When $\kappa_1 = \kappa_2$, the Bingham reduces to an axisymmetric form

(3.4.32) $$f(\theta,\phi) = C_1\, e^{\kappa \sin^2\phi} \sin\phi\, d\theta\, d\phi$$

Axes for the Bingham distribution can be found by the same method used for the Fisher and Bivariate Fisher Distribution Dispersion parameters κ_1 and κ_2 can be found analytically by use of inverse confluent hypergeometric functions on the eigenvalue of the covariance matrix. A more tractable solution is the use of numerical log-likelihood maximization techniques. For further discussion of the Bingham distribution, see Bingham (1964) or Mardia (1972).

Bivariate Normal

The Bivariate Normal distribution is a standard distribution for data defined on a plane (see, for example, Benjamin and Cornell, 1970). The form of the bivariate normal is

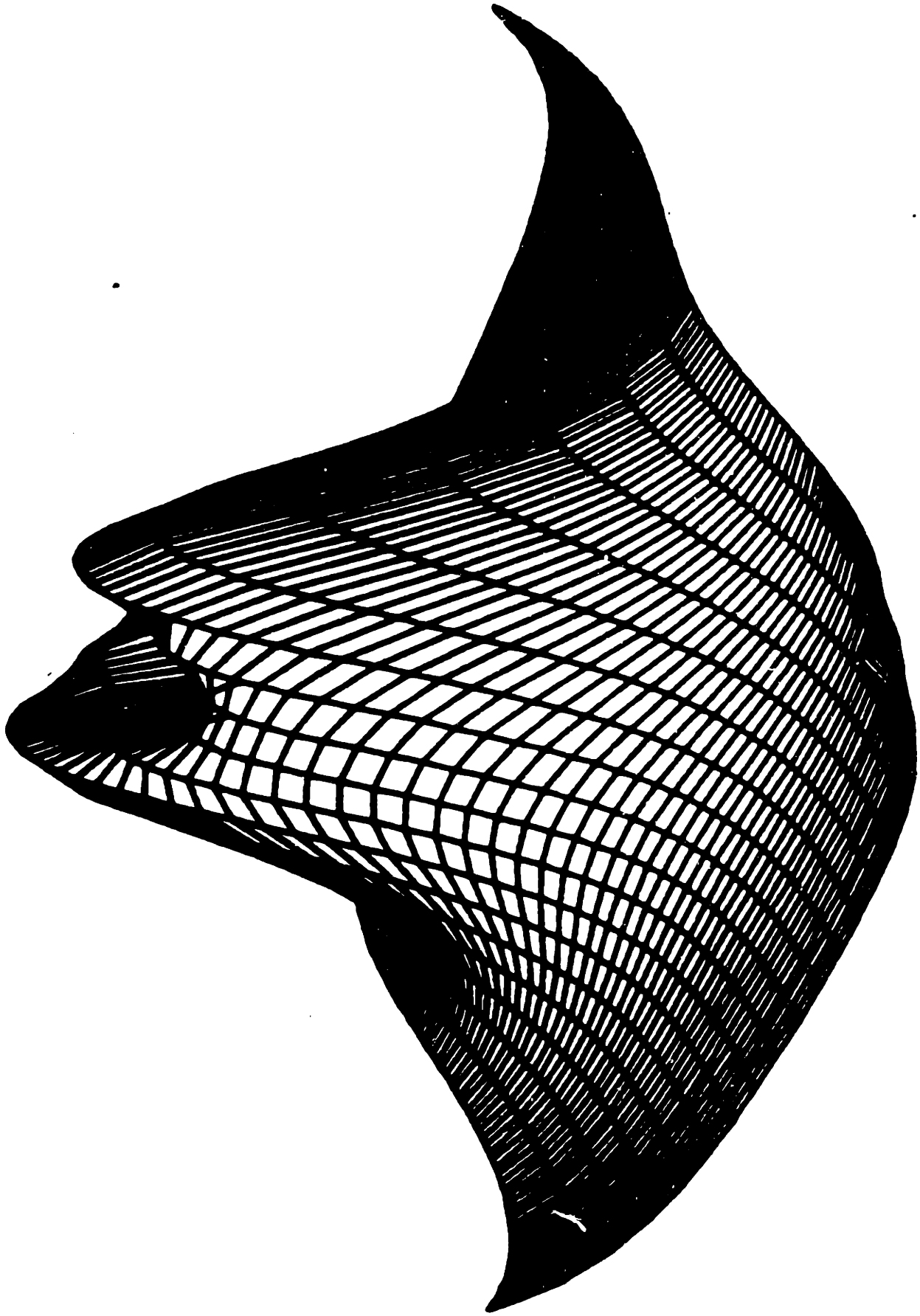

Figure 3.4.20 3D Representation of Bingham Distribution ($\kappa_1=-5, \kappa_2=-3$)

$$(3.4.33) \qquad f(\theta,\phi) = \frac{1}{2\pi\sigma_\theta\sigma_\phi} \exp\{-\tfrac{1}{2}(\frac{\theta^2}{\sigma_\theta^2} + \frac{\phi^2}{\sigma_\phi^2})\}$$

The bivariate normal distribution is a planar distribution and is therefore improper for spherical data. For low dispersion joints sets, however, the surface of the sphere can be approximated by a plane. (Figure 3.4.21). This allows the use of the bivariate normal distribution for low dispersion joint sets.

The bivariate normal distribution has advantages. Maximum likelihood estimates for the parameters of the Bivariate normal distribution are the sample means and covariances. In addition, the bivariate normal distribution has been studied and developed to an extent unrivaled by any spherical distribution.

The bivariate normal distribution on the plane is illustrated in Figure 3.4.22.

3.4.5 Rock Quality Designation (RQD)

RQD is a rock mass quality and geometry index derived from the logging of cores. As such, its definition and measurement are simple, but its interpretation is complex. The development of RQD and other index properties is

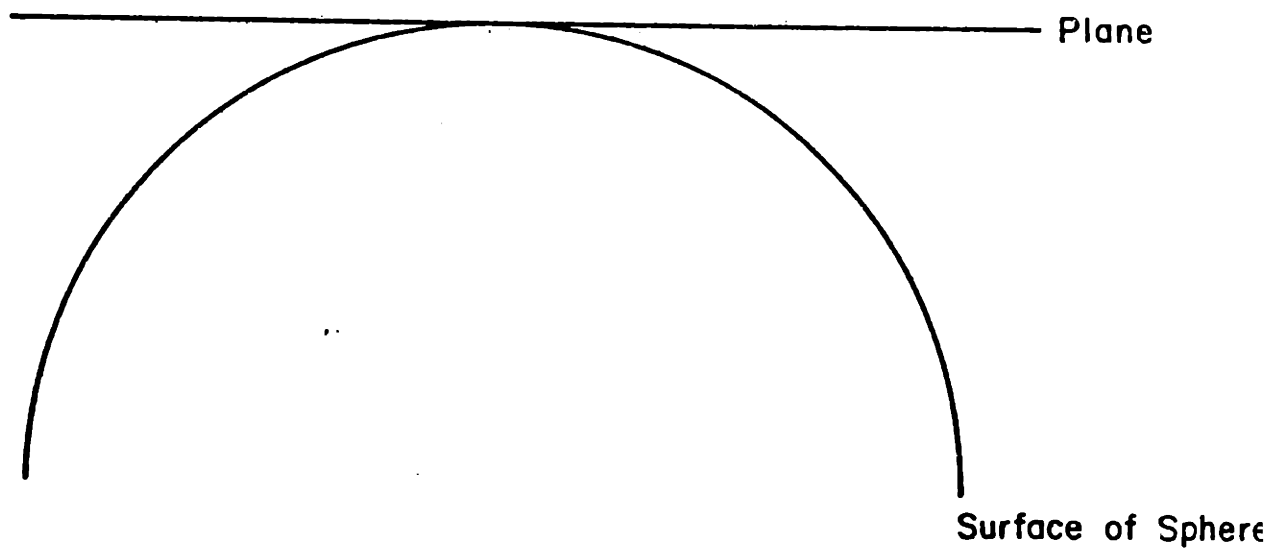

Figure 3.4.21 Surface of Sphere Approximated by Plane for Highly Concentrated Distribution.

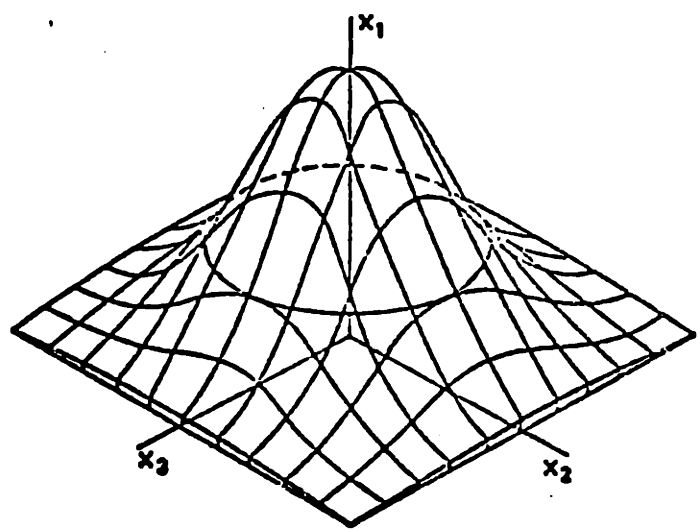

Figure 3.4.22 3D Representation of Normal Distribution on a Plane (Maranhão,1968)

described in greater detail in Appendix A.

Deere (1967) defined RQD as the ratio of the total length of recovered intact rock pieces of length greater than 4" (0.1m) to the total length of core. Mathematically, this can be expressed as

$$\text{(3.4.34)} \qquad RQD = \frac{100}{L} \sum_{i=1}^{N} l_i$$

where l_i are recovered intact lengths of greater than 0.1m, and

L is the length of the core.

The interpretation of RQD in terms of rock joint geometry is important because it is, perhaps, the easiest and most widely used measure of rock joint geometry.

According to deterministic models in which rock joint spacing is constant, RQD is constrained to values of either 0 or 100%. (Figure 3.4.23). Clearly this is false, since measured RQD values vary continuously from 0 to 100%. A probabilistic description of rock mass geometry which takes the variability of joint spacing into account is therefore necessary. Priest and Hudson (1977) developed such a model, based upon an exponential distribution for spacing. (Appendix A) The basic relation they derived between spacing and RQD is

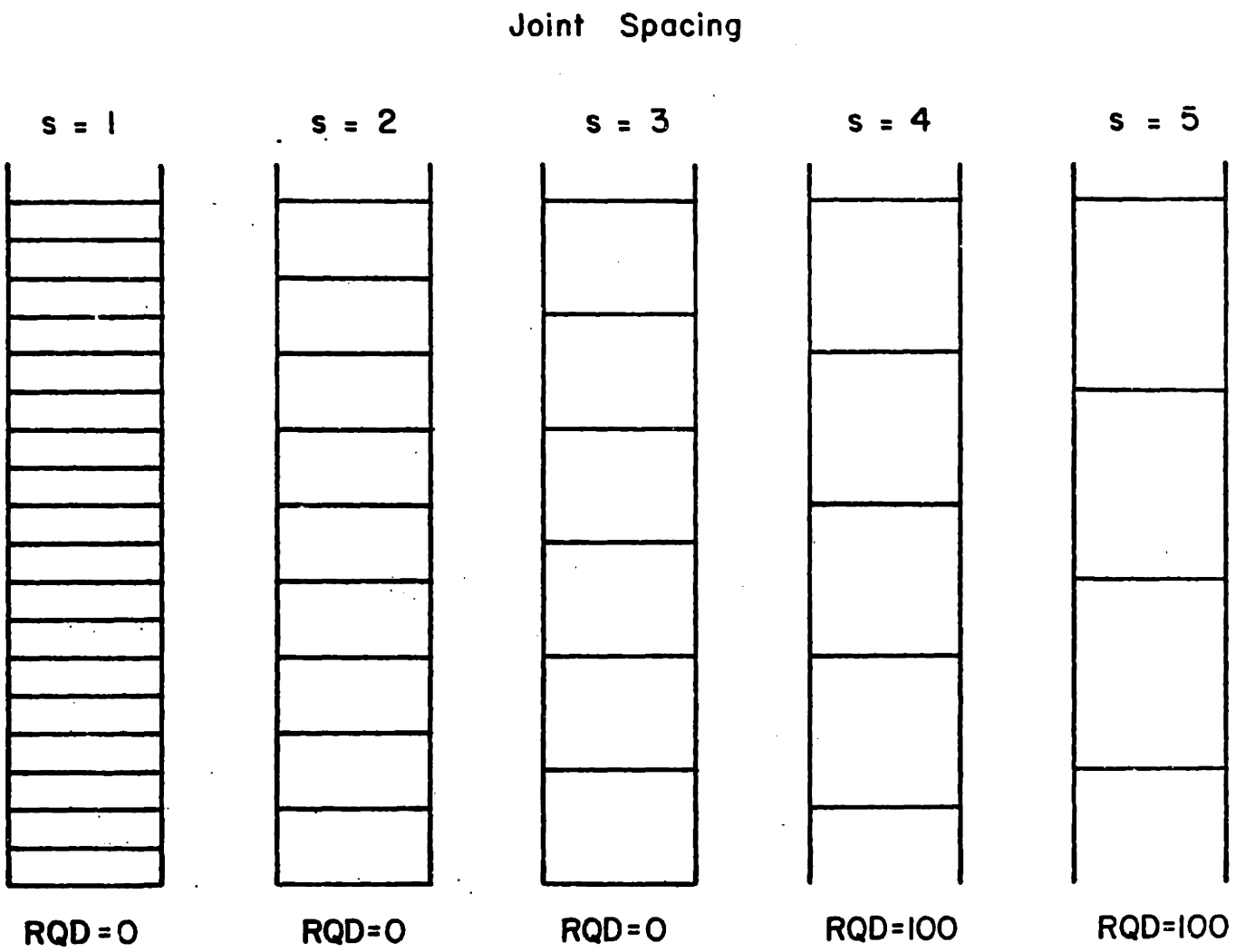

Figure 3.4.23 Deterministic Spacing Model and RQD

(3.4.35) $RQD = 100e^{-\lambda/10}(1 + \lambda/10)$ where $\lambda = s_m^{-1}$, and

s_m = true joint spacing.

This model is only valid for perfectly horizontal joint sets and vertical boreholes where the true (perpendicular) and measured spacings are identical and the joint orientation does not vary. For application of Priest and Hudson's model to situations where these conditions do not hold, it was necessary to develop a probabilistic extension of the model.

The first logical extension is the assumption of joint inclined at a constant dip ϕ. This situation is illustrated in Figure 3.4.24. Here frequency λ can be found from the observed mean spacing

(3.4.36) $s'_m = s_m/\cos\phi$ where s_m = true joint spacing

s'_m = measured spacing

ϕ = dip angle

(3.4.37) $\lambda = \cos\phi/s_m$

(3.4.38) $RQD(\phi) = 100(1 + 0.1\cos\phi/s_m)e^{-0.1\cos\phi/s_m}$

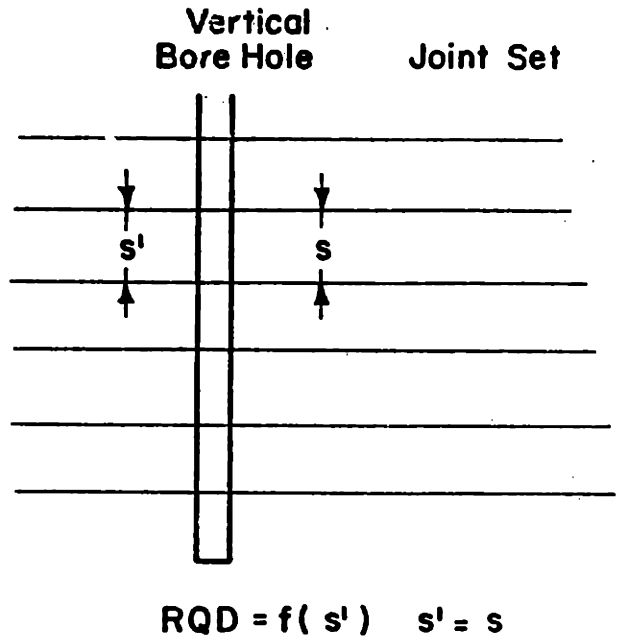

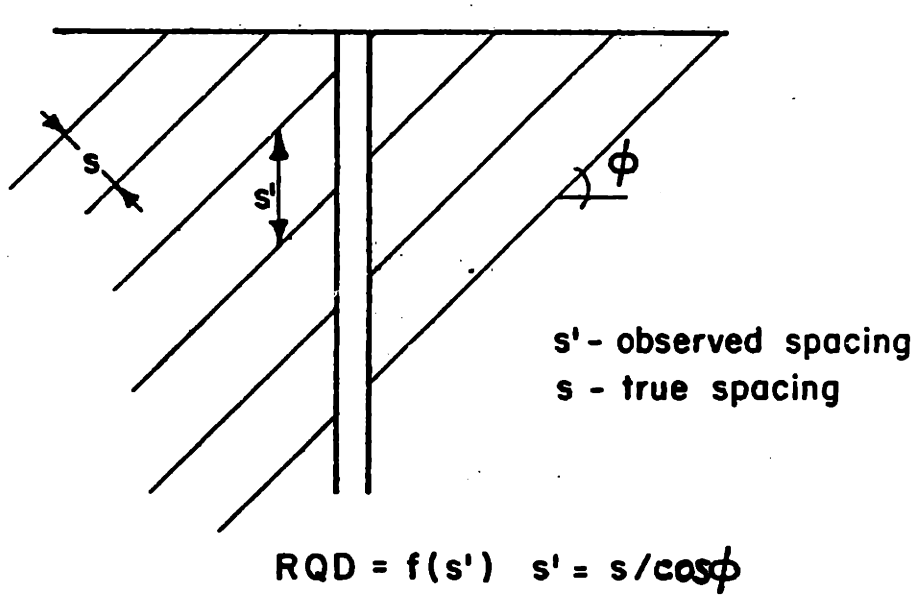

Figure 3.4.24 Inclined Joint Sets and RQD

For variable orientations, RQD can be found from

$$(3.4.39) \qquad E[RQD] = \int_0^{90} RQD(\phi) f(\phi) d\phi \qquad \text{where } f(\phi) = \text{distribution of dip angles.}$$

This model for RQD is limited to situations in which joint spacing can be modeled by the exponential distribution and the joint orientation can be modeled by a distribution $f(\phi)$. In addition, rock must be hard and unweathered, and joint openings must be small. The RQD model depends upon high quality corings in which all pieces >0.1m are recovered. The use of this probabilistic description of RQD will be demonstrated in Chapter 5.

3.5 Description of Deformability Properties

Description of rock mass deformability is difficult because of the great number of factors effecting deformability. These include, joint geometry, material properties, and boundary conditions. Here we will be concerned with the description of the rock mass material properties which affect deformability. Description of material properties is dependent upon the model chosen to describe behavior. Rock mass behavior is generally described in terms of elasticity theory.

Some researchers have described behavior in terms of intact rock deformation according to elasticity theory and rock joint deformation according to stress-displacement (stiffness) theory.

According to elasticity theory, the critical material properties governing deformation are Youngs modulus, E, and Poisson's ratio, ν, where

(3.5.1) $[\sigma] = [C]\{\varepsilon\}$ where $[\sigma]$ = stress matrix

$[C]$ = material property matrix dependent only on E, ν and boundary conditions

$\{\varepsilon\}$ = strain matrix.

Stiffness theory states that strains can be related to stresses on the joint plane by

(3.5.2) $[\sigma] = [K]\{\delta\}$ where $[K]$ = stiffness matrix, and

$\{\delta\}$ = displacement matrix.

The value of [K] is

$$(3.5.3) \qquad [K] = \begin{bmatrix} k_{nn} & k_{s} \\ k_{sn} & k_{ss} \end{bmatrix}$$

Off-diagonal terms are generally assumed to be zero (see Roberds, 1979), so

$$(3.5.4) \qquad [K] = \begin{bmatrix} k_n & 0 \\ 0 & k_s \end{bmatrix}$$

Stiffness can be represented by two parameters k_s and k_n, while elastic deformation can be represented by two parameters E and ν. The measurement of these parameters is discussed in Appendix A.

The use of material property descriptors E, ν, k_s and k_n depends in assumptions of the validity of the models from which those parameters are derived and of the validity of chose values of the parameters. Material property parameters are subject to sampling and statistical uncertianties and spatial variability just as joint geometry parameters are. It is appropriate, therefore, to consider probabilistic methods for description of material property parameters.

Unfortunately, little work has been done to date on the probabilistic modeling of material properties. Work by Yip (1979) provides a beginning for development of appropriate distributional forms for material properties. Until conclusive

results are found, however, material properties can best be represented by deterministic estimates, with bounds or by a normal distribution. The normal distribution is selected because, although little is known of the correct distribution, the normal distribution is generally appropriate where random errors are expected.

The use of bounds on expected values can provide bounds on estimates of mass deformability. Distributions of material properties can be used in probabilistic deformation models to determine distributions of expected behavior.

3.6 Summary of Distributional Forms

The use of probabilistic description for rock mass properties offers many advantages. Probabilistic descriptions can take into account the spatial variability of values, sampling errors and biases, and statistical uncertainty. Models designed to take the probabilistic nature of rock mass properties into account provide a significantly more complete description of expected behavior. Such models will be developed in Chapter 4. Table 3.6.1 summarizes mathematical forms used in the probabilistic description of rock mass properties.

ASPECT	DISTRIBUTION	MATHEMATICAL FORM
Length	Exponential	$\lambda e^{-\lambda t}$
Spacing	Exponential	$\lambda e^{-\lambda t}$
Orientation	Fisher	$\frac{\kappa}{4\pi \sinh \kappa} e^{\kappa \cos\phi} \sin\phi$

Table 3.6.1 Mathematical Forms to be used in Probabilistic Models for Rock Joints

CHAPTER 4

PROBABILISTIC MODELS FOR ROCK MASS DEFORMATION

4.1 Introduction

Deformation models using probabilistic description of rock mass properties have attractive attributes. First, they yield quantitative expressions of the level of uncertainty associated with predicted deformations. This uncertainty can result from statistical uncertainty spatial variability (stochastic uncertainty), and model error. Second, they yield more accurate estimates of behavior over spatial variation. To the extent that the mechanistic model is non-linear, average spatial properties do not lead to expected behavior. For non-linear relations the mean of a function does not necessarily equal the function of the mean.

This chapter will briefly discuss the nature of probabilistic models, and will then present two probabilistic models for rock mass deformation. Probabilistic models developed in this chapter will be compared with deterministic models developed in Chapter 2.

4.2 Assumptions used in Probabilistic Models

All models, both probabilistic and deterministic, depend entirely upon the assumptions used in the construction of the models. Critical assumptions for rock mass deformation models include material property relations, geometric

description, and boundary conditions.

Material Properties: Deterministic models discussed in Chapter 2 rely on elastic and elasto plastic theories with deterministic parameters for the description of material properties. Probabilistic models developed here will rely on the same assumptions for the description of the intact portion of the rock masses. Stress Displacement (stiffness) relations, will be used for joints within the rock masses. Deterministic stiffness parameters will be used. This is partially due to ignorance of proper probabilistic forms for material property parameters and partially due to the degree of computational difficulty introduced by the use of probabilistic parameters for deformability. The problem of uncertainty in material properties is handled through sensitivity studies to determine the effects of variation in E, ν, k_s, and k_n on prediction.

Use of elastic assumptions results in the same constraints upon the applicability of probabilistic models as it does for the models in Chapter 2. Linear elastic theory requires small strains, strain compatability, and completely recoverable deformations.

The models developed here use the probabilistic description of joint geometry developed in Chapter 3. Distributions for joint spacing, length, and orientation were selected on the basis of field studies cited in Chapter 3 and mathematical convenience. Spacing and length are both assumed to be

exponentially distributed; joint orientation, Fisher distributed. Input parameters for these distributions, and therefore for the models, are standard geological properties which can be measured in the field.

The behavior of models is sensitive to assumed boundary conditions. Both models developed here are general, and can be adapted to a variety of boundary conditions. Since actual boundary conditions are unknown, the most useful boundary condition is that which causes the model to best duplicate observed behavior.

4.3 Computation Strategies for Probabilistic Models

This section will discuss four major computational strategies for probabilistic predictions. These are: Closed form solution of output distributions, Monte-Carlo simulation of output distributions, closed form second moment solutions, and second moment solution by numerical integration.

4.3.1 Closed Form Solutions

The most accurate and complete method for probabilistic analysis of model results is the closed form solution of output distributions. Closed form techniques manipulate input densities and the structural relations of a model to result in exact density functions. Typically, this is done by a transformation of variables.

(4.3.1) $$f_y(y) = f_x(g^{-1}(y))J(x,y)$$ where x = input

$y = g(x)$

$g(x)$ = structural relation

J = Jacobian Transformation.

Additional techniques can be found in any standard probability text such as Benjamin and Cornell (1970).

The disadvantage of closed form solutions is that even with the use of statistical techniques they are frequently intractable. This is especially true for more complex physical relations and input parameter distributions.

4.3.2 Monte Carlo Solutions

Where closed form solution for output distributions proves intractable numerical techniques such as Monte Carlo simulation can be used. These numerical techniques randomly generate input parameters according to given distributions and aggregate deterministic outputs to find distributions. The method has advantages. Firstly, it requires little mathematical sophistication. Secondly, it provides complete distribution of outputs. Thirdly, it is sufficiently flexible and general that different input distributions can be used without complete reorganization, which would be required for closed form solutions.

Limitations of Monte Carlo techniques include the limitation of accuracy imposed by cost and the amount of error

introduced by simulation. With large numbers of iterations, Monte-Carlo results approach closed form results, except for a predictable increase in uncertainty due to the simulation process. Restraints on the number of iterations imposed by cost, however can result in significant errors in distributional results. Another limitation results from the fact that Monte Carlo techniques mask the process by which the distribution of results is obtained. This occurs because Monte Carlo results amalgamate the variations induced by spatial and parametric variability and model uncertainty numerically. In addition, the masking of underlying causes of uncertainty and inaccuracy cause Monte Carlo results to be difficult to interpret and frequently to appear more precise than they really are.

4.3.3 Closed Form Second Moment Solutions

Even where it is not possible to determine the distribution of results in closed form, it is sometimes possible to determine second moments of results. This is because of the power of statistical and mathematical techniques (e.g., Taylor series) for solution of second moments. Second moment solutions provide information about the mean and standard deviation of results. In many cases that is all that is required.

Second moment methods can almost always be used to find the mean (First Moment), regardless if the complexity of input parameters and physical relationships. For simple input

parameters, approximate methods must be used for variance (second moment). For complex situations, second moments cannot be found without the use of numerical techniques.

4.3.4 Second Moment Solutions by Numerical Integration

For more complicated problems, second moments can be found by numerical integration. This technique has the advantage of precision comparable to that of closed form second moment solution with considerably less effort. Second moment solution by integration can be performed for almost any degree of complexity. Numerical integration techniques such as Newton's method and Simpson's rule are implemented on most computer systems. These techniques can be used to achieve any desired level of precision.

4.4 Model 1 - Constrained Cylinder

4.4.1 Description of Model

Figure 4.4.1 illustrates the concept of the constrained cylinder model. The model utilizes deterministic relations for the rock mass deformation process and is designed for use with either deterministic or probabilistic input parameters. The model is probabilistic to the extent that, for probabilistic descriptions of material properties or joint geometry, the model produces probabilistic results.

The constrained cylinder model separates the rock mass deformation into two components--deformation of intact rock and deformation of joints. Deformation of intact rock is assumed to occur according to simple elastic theory.

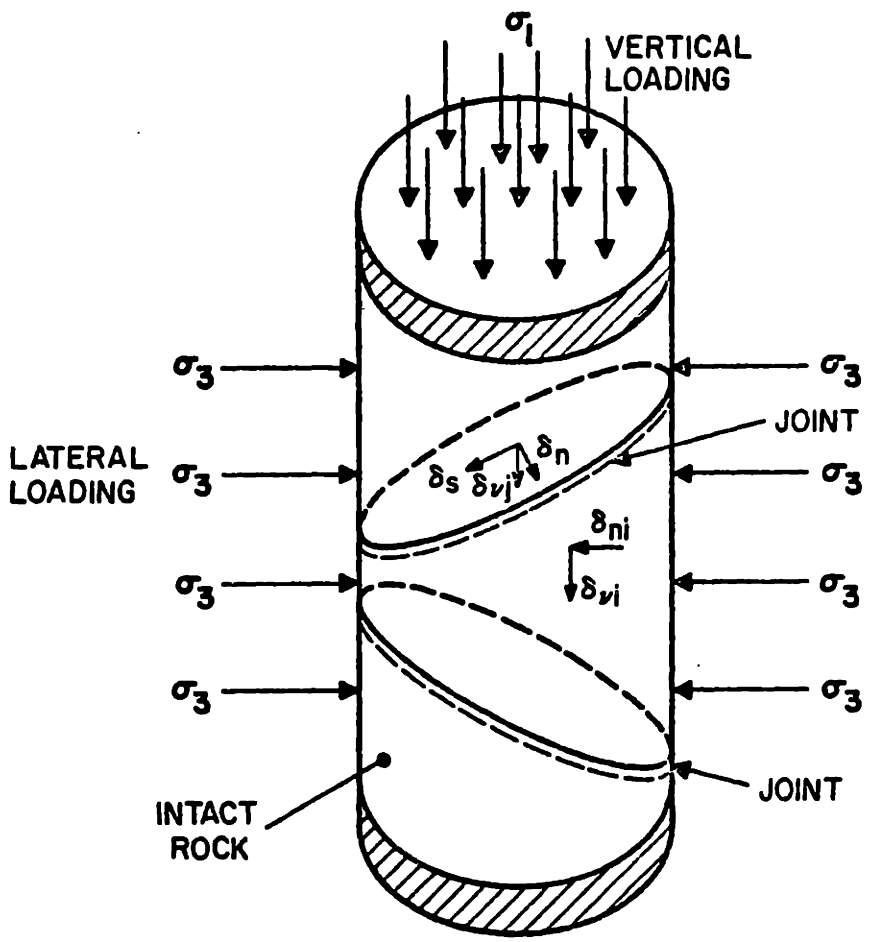

δ_s = SHEAR DEFORMATION OF JOINT

δ_n = NORMAL DEFORMATION OF JOINT

δ_{vj} = VERTICAL COMPONENT OF δ_s, δ_n

δ_{vi} = VERTICAL DEFORMATION OF INTACT ROCK

δ_{ni} = HORIZONTAL DEFORMATION OF INTACT ROCK

Figure 4.4.1 Constrained Cylinder Concept

Deformation of rock joints is assumed to occur according to stress-displacement (stiffness) theory. In the model, applied stresses in the vertical and horizontal directions are converted through elasticity and stiffness relations to vertical and lateral deformations. Total deformation is taken as the sum of these.

Inputs to the model are joint geometry, stiffnesses, and elastic properties. Various boundary conditions can be used. Each different set of boundary conditions is considered a model case.

The cylindrical form of the model can be analyzed in either two or three dimensions. (Figure 4.4.5) This allows a variety of boundary conditions, and conceptualization of the model as a triaxial test.

4.4.2 Assumptions and Consequences

Since both input joint geometries and boundary conditions are model variables, the critical model assumptions involve deformation relations for intact rock and joints, and the interrelation of deformations.

1. Linear Elastic Stress-Strain Relations for Intact Rock Blocks

   Linear Elastic assumptions for intact rock blocks rely upon low strain within the blocks, strain compatability, and no permanent deformation. All of these assumptions have been verified for intact rock samples at low stress levels.

2. Stiffness Stress-Displacement Relation for Rock Joint

Although stiffness relations for rock joints are generally accepted, the difficulty involved in obtaining unique values for stiffness parameters casts some doubt on their applicability. The model relies upon linear stiffness relations. Work by Kulhawy (1975) and others, discussed in Appendix A, indicates that non-linear stiffness relations may be more appropriate for large stress ranges. For small stress ranges, however, linear stiffness relations appear to be a reasonable approximation.

3. Uniform Stress State

The model assumes that a uniform state of stress related to applied stresses and boundary conditions exists throughout the cylinders. Thus stress concentrations on joints and in intact rock are neglected. This assumption considerably simplifies computations, since it allows calculation of intact rock deformation simply on the basis of applied stress, and calculation of joint deformations by simple application of Mohr's Circle to transform stresses onto the plane of the joint. Although this assumption is critical for model tractability, it is of limited validity. Studies by Maury (1970), Seeler (1978) and others have shown that significant stress concentrations do in fact occur in jointed rock masses. (Figure 4.4.2) The amount of error introduced by this assumption is unknown.

4. Independence of Joint and Intact Rock Deformation

Separate calculations of intact rock and rock joint deformations depends upon the independene of joint and intact rock deformation processes. For small deformations, this assumption is valid. For larger deformations, however, rock joint and intact rock shapes may be significantly distorted and the assumption would not hold (Figure 4.4.3).

5. Independence of Joint Deformations

Normal displacements along joints can reasonable be expected to have little effect upon adjacent and intersecting joints. Shear displacement can be expected to have significant interactions, however. This is illustrated in Figure 4.4.4. Compatibility between intact rock blocks affected by shear deformation of joints imposes significant kinematic con-

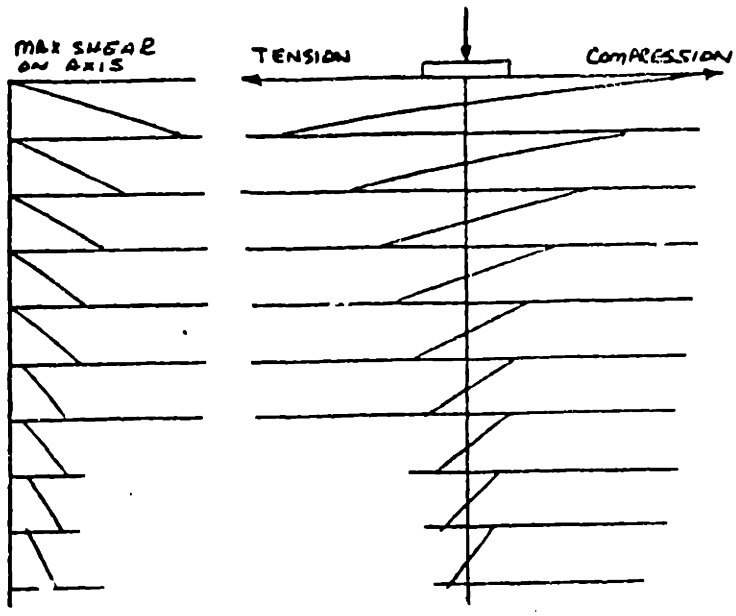

Theoretical Results

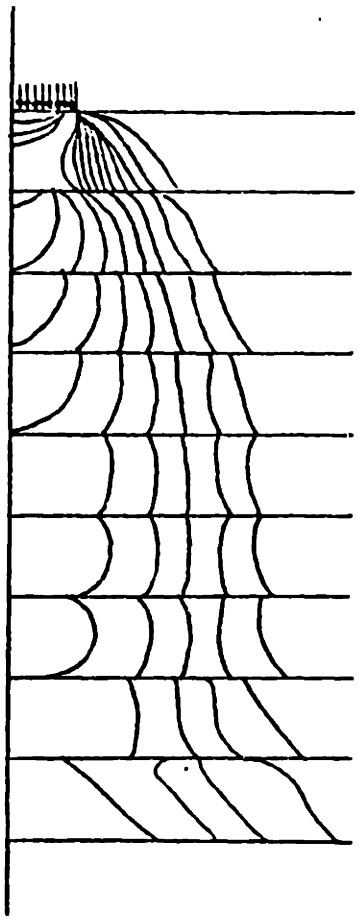

Experimental Results

Figure 4.4.2 Stress Concentrations in Jointed Rock (Maury, 1970)

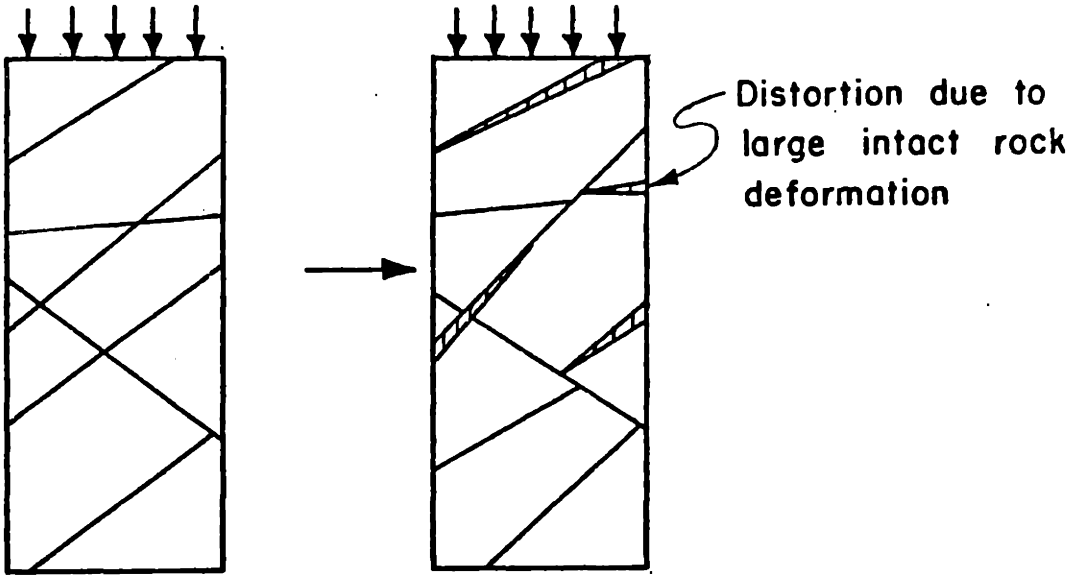

Figure 4.4.3 Interference due to Large Intact Rock and Rock Joint Deformation

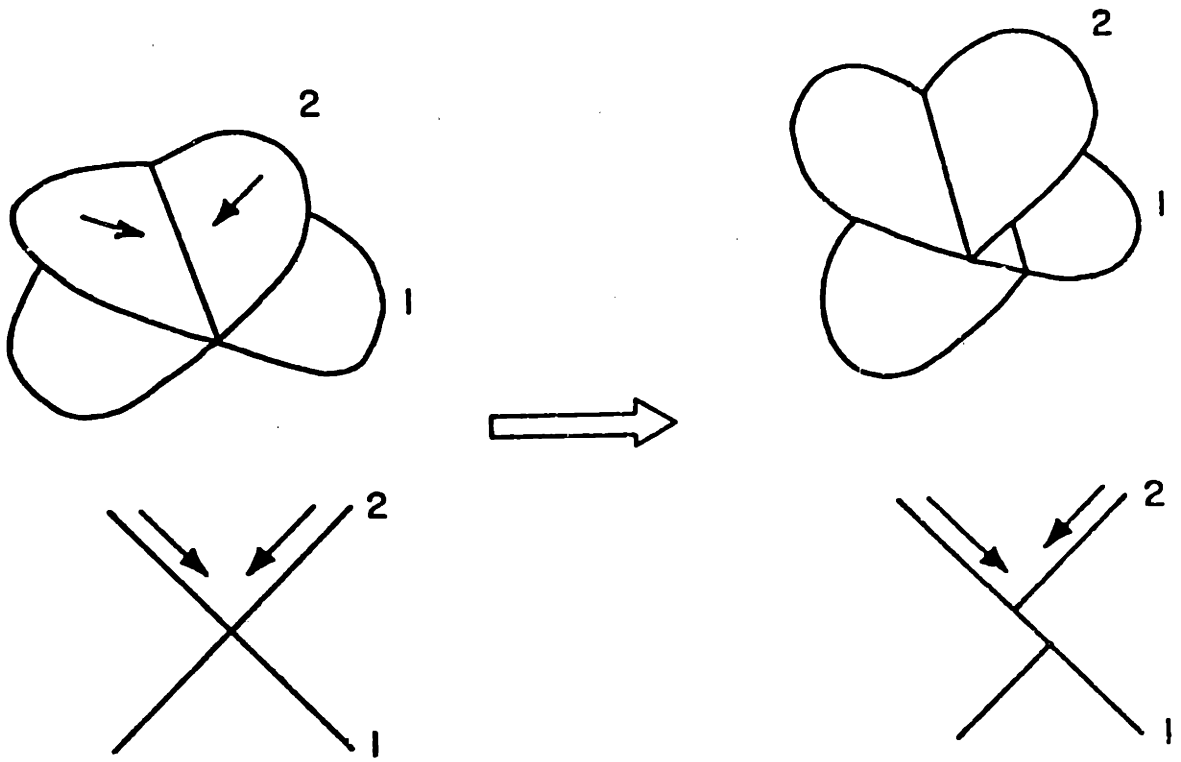

Shear deformation appears possible on both joints 1 & 2

No shear deformation possible on joint 2

Figure 4.4.4 Interference between Intersecting Rock Joints

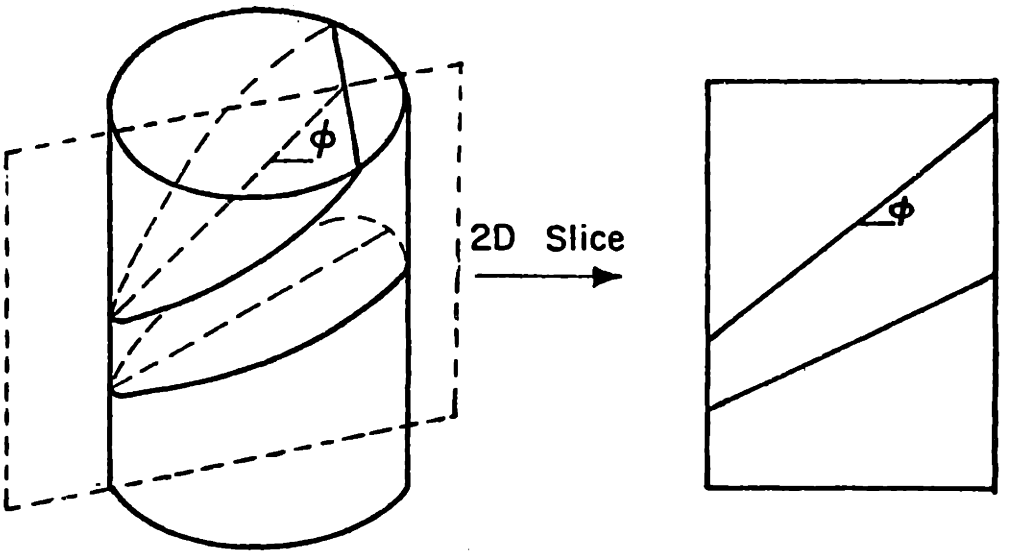

a) TWO DIMENSIONAL

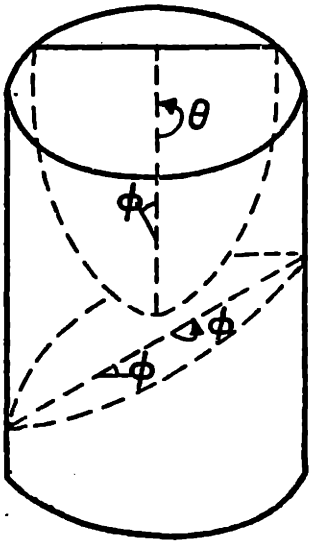

b) THREE DIMENSIONAL

Figure 4.4.5 Two and Three Dimensional Geometrical Parameters

straints on joint deformation. The neglect of these kinematic constraints results in a conservative overestimation of shear deformation on joints.

4.4.3 Parameters

Rock mass descriptors required by the constrained cylinder rock mass model include joint geometry and material property parameters discussed in Chapter 3.

Joint geometry parameters required include joint spacing S and joint orientation. Joint lengths are assumed to be greater than the cylinder diameter, and joints are assumed to be 100% persistent. For the two-dimensional cases of the model, joint trends are assumed parallel, so geometry can be described completely by a one parameter orientation distribution such as the Fisher Distribution and a mean orientation (Figure 4.4.5a). Three-dimensional cases of the model require mean orientation, major and minor axes, and a bivariate orientation distribution such as the Bivariate Fisher or Bingham distributions. (Figure 4.4.5b). Joint spacing can best be represented by the exponential distribution, as shown in Section 3.4.1. (Recall that the differences between 2- and 3-dimensional cases are only in geometry, not stress.)

Material property parameters required include the Young's Modulus of Elasticity E, and Poisson's ratio ν, for intact rock, and joint stiffnesses k_s and k_n for rock joints. These values can all be determined experimentally, although determination of stiffness values is difficult (see Appendix A). Due to the lack of knowledge of appropriate distributional forms, deterministic estimates are used for material properties. Uncertainty

of material properties can be examined through sensitivity studies.

4.4.4 Limitations of Model

Serious limitations of the constrained cylinder model resulting from model assumptions include the necessity for small strain levels, and a uniform stress field. Other limitations result from the difficulty of establishment of appropriate boundary conditions and the difficulty involved in establishment of some input parameters, particularly stiffness values k_s and k_n.

4.4.5 Advantages of Model

The constrained cylinder model has several advantages. The most obvious is its easy adaptation to the use of probabilistic inputs. Another major advantage is the model's implicit recognition of the fact that rock is a discontinuum, and that the deformation process along joints is different from the deformation process in intact rock. While intact rock behavior may be approximated by elastic theory, non-recoverable strains on joints clearly do not obey the laws of elasticity. Non-recoverable, non-linear elastic displacement along joints are modeled separately from recoverable, elastic deformations in intact rock. In addition the model has the singular advantage that all input parameters are commonly measured, generally accepted geological quantities. Application of the model does not therefore require the establishment of a completely new set of geological descriptors. Finally, the model is flexible

enough to be adapted to many different boundary conditions.

4.4.6 Mathematical Development

This section develops mathematical representations for intact rock and rock joint deformation. Further development of aspects of the deformation process dependent upon boundary conditions is given in Section 4.4.7.

Intact Rock

Deformation of intact rock is assumed to be elastic. Deformation is calculated by integration of strains derived from elastic solutions. Elastic strain solutions are of the form

(4.4.1) $[\sigma] = [C]\{\varepsilon\}$ where $[\sigma]$ is the stress matrix
$[C]$ is the modulus matrix
$\{\varepsilon\}$ is the strain matrix

For three dimensions,

$$(4.4.2) \qquad \begin{bmatrix} \sigma_{11} & \sigma_{12} & \sigma_{13} \\ \sigma_{21} & \sigma_{22} & \sigma_{23} \\ \sigma 31 & \sigma 32 & \sigma 33 \end{bmatrix} = \begin{bmatrix} C_{11} & C_{12} & C_{13} \\ C_{21} & C_{22} & C_{23} \\ C_{31} & C_{32} & C_{33} \end{bmatrix} \begin{Bmatrix} \varepsilon_{11} & \varepsilon_{12} & \varepsilon_{12} \\ \varepsilon_{21} & \varepsilon_{22} & \varepsilon_{23} \\ \varepsilon_{31} & \varepsilon_{32} & \varepsilon_{33} \end{Bmatrix}$$

Elasticity theory is discussed in Section 2.2.1

Vertical deformations can be found by integration of vertical strains

(4.4.3) $$\delta_i = \int_0^H \varepsilon_v(x)\,dx$$ where δ_i = vertical deformation

H = height of cylinder

$\varepsilon_v(x)$ = vertical strai at elevation x

For uniform stress fields, strain is independent of vertical location and

(4.4.3) $$\varepsilon_v(x) = \varepsilon_v$$ where ε_v = vertical strain for all x

so, $$\delta_i = H\,\varepsilon_v$$

H = cylinder height

δ_i = total intact rock vertical deformatior

Calculation of vertical strain ε_v depends upon boundary conditions are stress field assumption.

Rock Joints

Calculation of rock joint deformation is considerably more complicated than calculation of intact rock deformation. Joint deformation as defined in the model is controlled by shear and normal stiffnesses and the stresses in shear and normal to the joint.

Given principal stresses σ_1 and σ_3 as shown in Figure 4.4.1, stresses on the joint plane are found by Mohr's Circle. The Mohr Circle (see Figure 4.4.6) allows shear and normal stress traction vectors on any plane to be found from principal stresses. Here we have principle stresses σ_1 on the

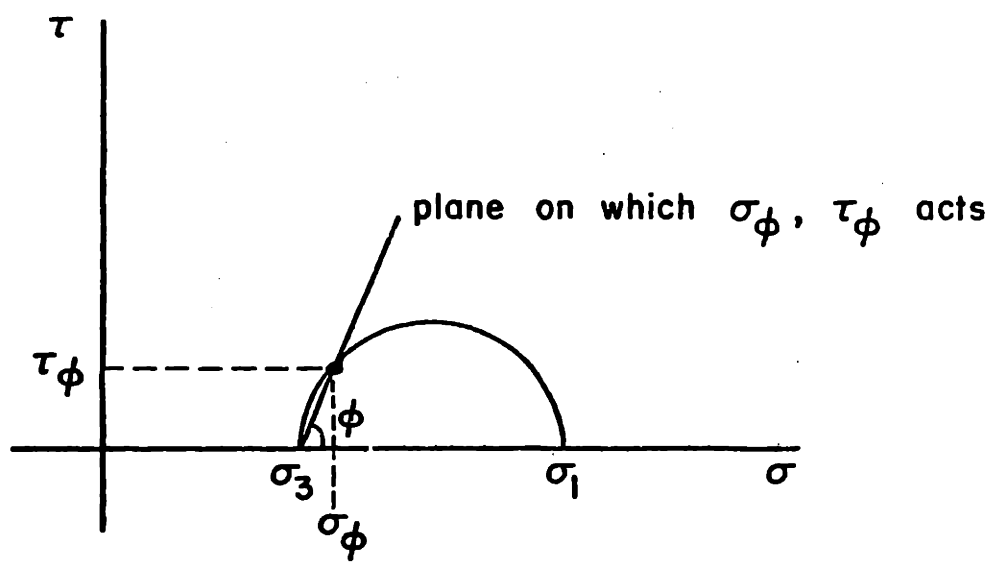

Figure 4.4.6 Mohr's Circle of Stresses

horizontal plane and σ_3 on the vertical plane. For a joint plane oriented at an angle ϕ from the horizontal,

(4.4.5) $\sigma_N = \sigma_1 \cos^2\phi + \sigma_3 \sin^2\phi$ where σ_N = normal stress

$\tau_s = (\sigma_1 - \sigma_3)\sin\phi\cos\phi$ τ_s = shear stress

According to assumptions made in the stiffness theory, joint shear and normal displacements are related to shear and normal stiffnesses by

(4.4.6) $\delta_N = \sigma_N/k_N$ where δ_s, δ_N = shear and normal displacement

$\delta_s \quad \tau_s/k_s$ τ_s, σ_N = shear and normal stresses

k_s, k_N = shear and normal stiffnesses.

Combining the previous equations,

(4.4.7)

$$\delta_N = \sigma_N/k_N = [\sigma_1 \cos^2\phi + \sigma_3 \sin^2\phi]/k_N$$

$$\delta_s = \tau_s/k_s = [(\sigma_1 - \sigma_3)\sin\phi\cos\phi]/k_s$$

Vertical displacements on individual joints are found by vectorial addition of the shear and normal displacements. (See Figure 4.4.7)

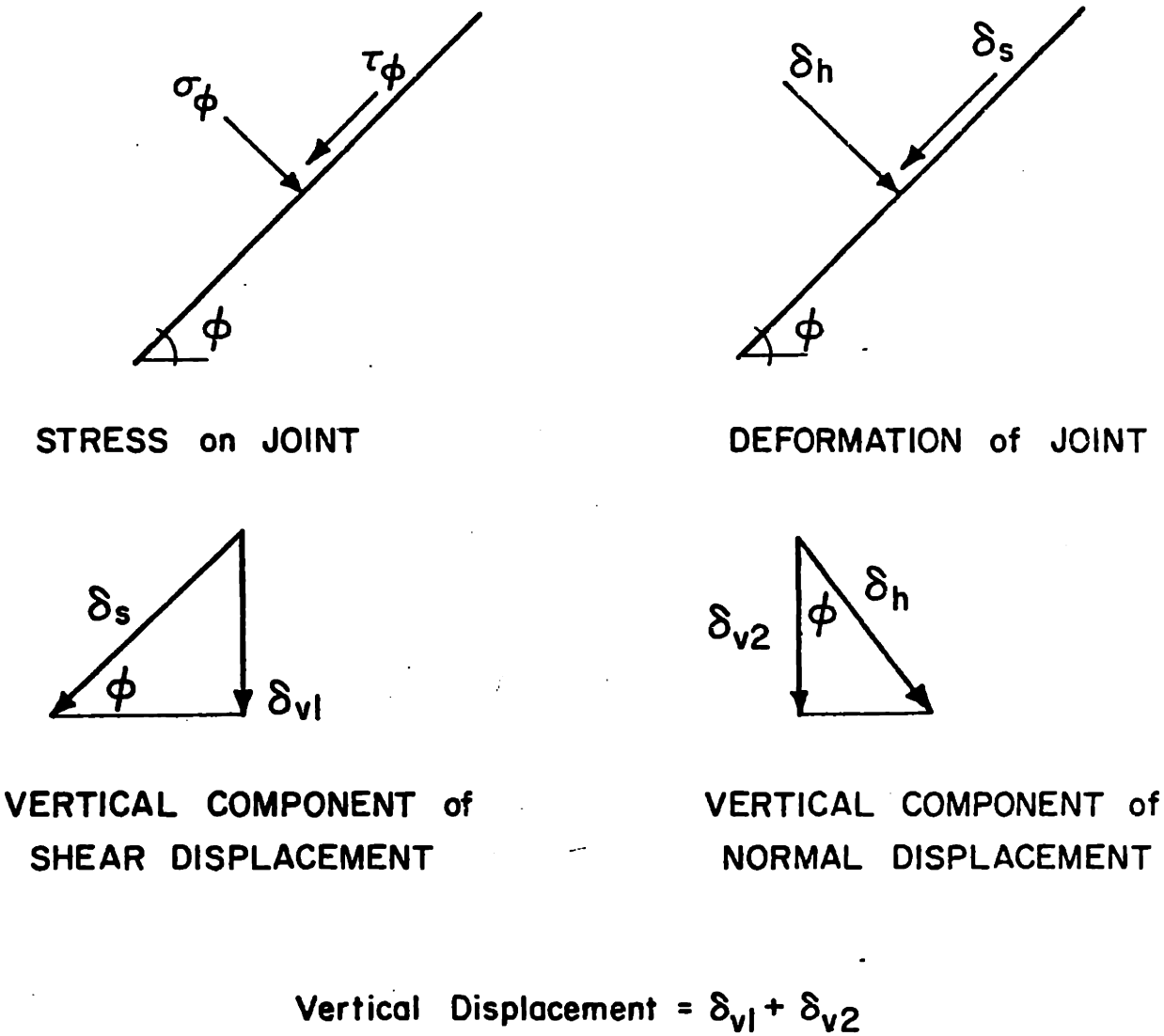

Vertical Displacement = $\delta_{v1} + \delta_{v2}$

Figure 4.4.7 Calculation of Vertical Displacement by Vectorial Addition

(4.4.8) $$\delta_v(\phi) = \delta_N \cos\phi + \delta_s \sin\phi$$

$$= [\sigma_1 \cos^2\phi + \sigma_3 \sin^2\phi]\frac{\cos\phi}{k_N} + [(\sigma_1 - \sigma_3)\sin\phi\cos\phi]\frac{si}{k}$$

By assumption of independence of settlement of different joints, the total settlement due to joint displacement can be calculated from

(4.4.9) $$\delta_j = \sum_{i=1}^{N} \delta_v(i)$$

where δ_j = total vertical joint displacement

N = number of joints

$\delta_v(i)$ = vertical displacement of joint.

By assumption of independence of intact rock and rock joint displacements, the total rock mass vertical deformation is found by simple summation:

(4.4.10) $$\delta_t = \rho = \delta_i + \delta_j = H\,\varepsilon_v + \Sigma\,\delta_v$$

4.4.7 Model Cases

The following four sections present possible variations on the model based upon different boundary conditions. Boundary conditions (Figure 4.4.8) are presented in order of increasing complexity. The first case involves a two dimensional cylinder* with zero lateral confining stress, σ_3 . This

*Cylinders with simplified geometry such that analysis can be conducted in two dimensions (see Figure 4.4.5) will henceforth be called "two dimensional cylinders."

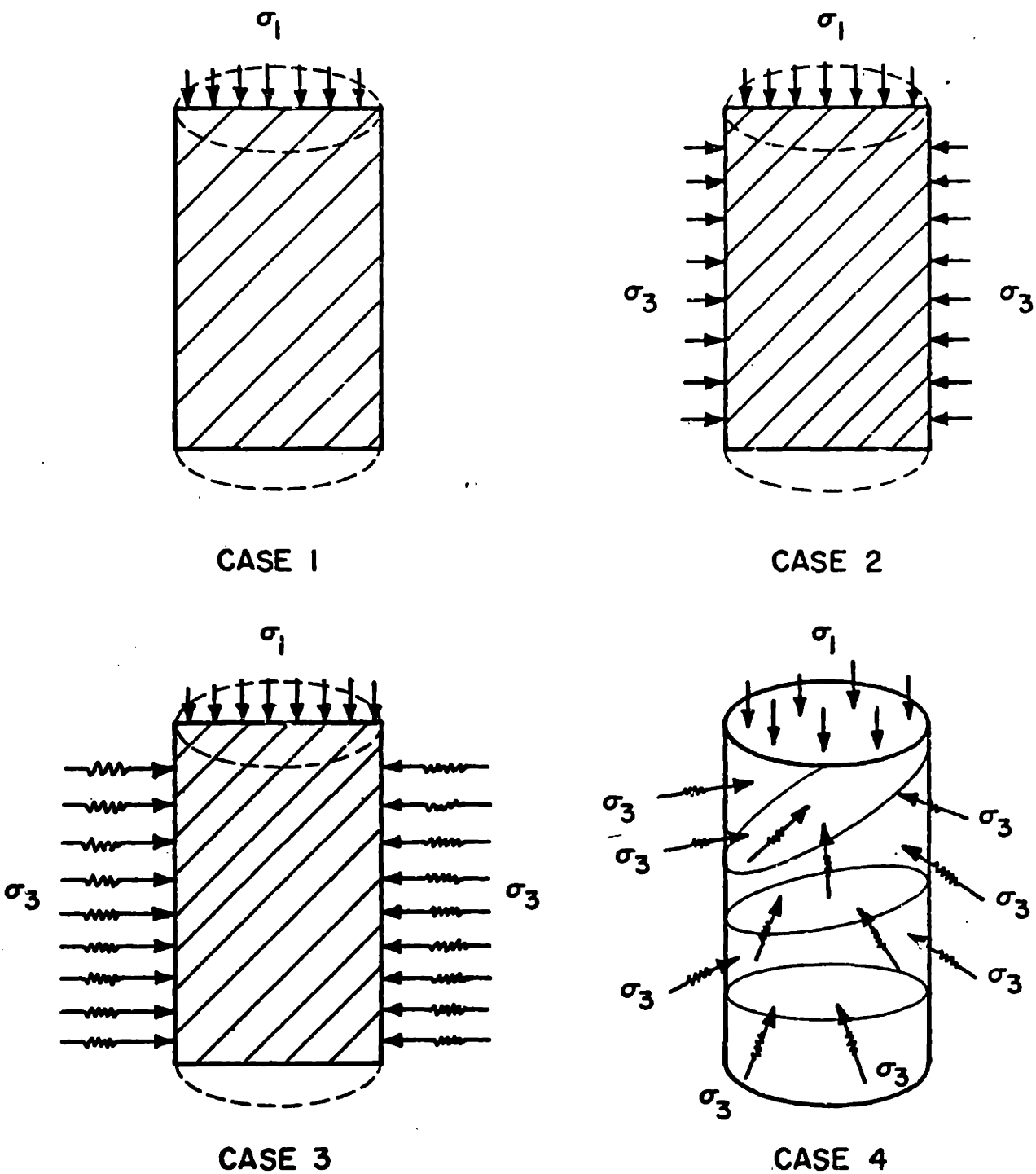

Figure 4.4.8 Constrained Cylinder Model Cases

models an unconfined compression test. The second case utilizes a two dimensional cylinder with constant lateral confining stress. This models a standard triaxial compression test. In the third case, the lateral confining pressure, σ_3, is related to lateral deformations through a spring constant K such that σ_3 increases with lateral deformation. The fourth case mantains tha same boundary conditions as the third case, but extends the geometry to three dimensions.

In development of all cases, input parameter distributions are left unspecified. The distribution of joint spacings is represented by $f_s(s)$, and the distribution of joint orientations is represented by $f_\phi(\phi)$. This usage allows maintenance of the generality of the models. Proposed solution methods (closed form distribution, second moment, Monte Carlo), however, are based upon joint geometry distributions proposed in Chapter 3. Computer program RQD2S, described in Einstein, Baecher, et. al. (1979), is an example of how solutions can be implimented.

Case 1 -- Unconstrained 2D Cylinder

The first case maintains simplified two-dimensional geometry. Displacements are all assumed to be coplaner, so all calculations can be done in two dimensions; in addition, simple boundary conditions are used. Vertical stress σ_1 is kept constant, and horizontal stress σ_3 is constrained to zero. Boundary conditions and geometry are shown in Figure 4.4.9. This set of boundary conditions models unconfined

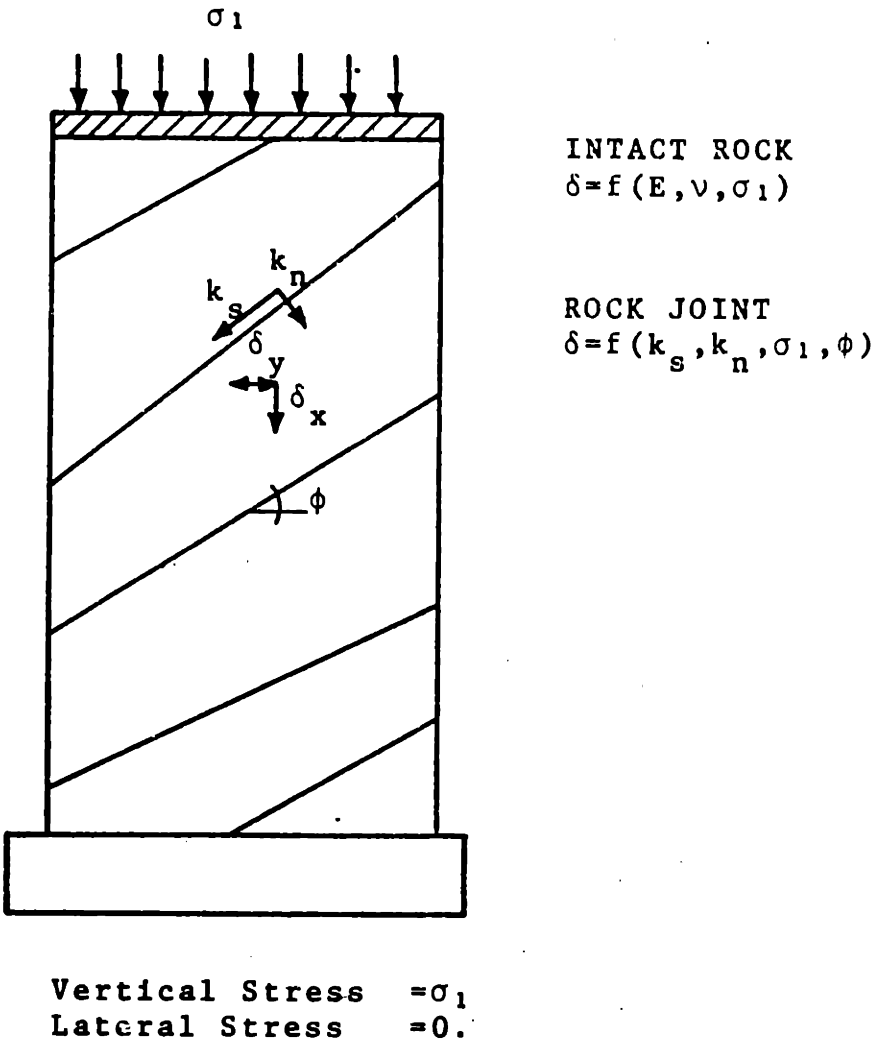

Figure 4.4.9 Unconstrained 2-D Cylinder Boundary Conditions and Geometry

compression tests. Both horizontal and vertical deformations are unconstrained.

Deformation of the intact portion of the rock model is determined from elastic theory. The general model solution for intact rock deformation,

$$(4.4.11) \qquad [\sigma] = [C]\{\varepsilon\} \qquad \text{where } [C] = f(\nu, E)$$

reduces to

$$(4.4.12) \qquad \varepsilon = \sigma_1/E_i$$

for the simple boundary conditions of this model.

Total rock mass vertical deformation due to intact rock deformation can therefore be expressed as

$$(4.4.13) \qquad \delta_i = H\varepsilon = H\sigma_1/E_i \qquad \text{where } H = \text{cylinder height}$$

Deformation of individual rock joints is modeled by the general equation from the previous section

$$(4.4.14) \qquad \delta_j = [\sigma_1\cos^2\phi + \sigma_3\sin^2\phi]\frac{\cos\phi}{k_N} + [(\sigma_1 - \sigma_3)\sin\phi\cos\phi]\frac{\sin\phi}{k_s}$$

For the given boundary conditions, this reduces to

(4.4.15) $$\delta_j(\phi) = \sigma_1 \cos^3\phi/k_N + \sigma_1 \sin^2\phi/k_s$$

The expected value of total rock mass vertical deformation due to rock joints is,

(4.4.16) $$E[\delta_j] = E^{-1}[f_s(s)] \int \delta_j(\phi) f_\phi(\phi) d\phi$$

The standard deviation of total joint vertical deformation is found by application of the equation for standard deviation.

(4.4.17) $$SD\ [x] = [E[x^2] - E^2(x)]^{\frac{1}{2}}$$

In this case,

(4.4.18) $$SD[\delta_j] = [E^{-1}[f_s(s)]] \int \delta_j^2(\phi) f_\phi(\phi) d\phi - E^2[\delta_j]]^{\frac{1}{2}}$$

Total deformation is found by adding intact deformation δ_i and joint deformation $\delta_j(\phi)$

$$\delta_{TOTAL}(\phi) = \delta_i + \delta_j(\phi)$$

The boundary conditions of this case are extremely simple. This results in both advantages and disadvantages. The advantage of simplicity is that it decreases the number of

parameters needed, and increases the tractability of the solution. This disadvantage of simplicity is that it limits the applicability of results. The model is useful primarily as a first pass to determine general trends.

Case 2-2D Triaxial Cylinder

The unconstrained model give as case 1 can be generalized considerably by removal of the stipulation that lateral stress $\sigma_3 = 0$. Case 2 assumes a constant lateral confining stress.

$$\sigma_3 = \text{constant} \tag{4.4.19}$$

This is shown in Figure 4.4.10.

Intact rock deformation for a triaxial case solved from elastic theory reduce to

$$\varepsilon_v = \frac{1}{E}(\sigma_1 - 2\nu\sigma_3) \tag{4.4.20}$$

for the total deformation of intact rock,

$$\delta_i = \varepsilon_v H = \frac{H}{E}(\sigma_1 - 2\nu\sigma_3) \tag{4.4.21}$$

This differs from the previous case in that here vertical displacement are limited by lateral stresses.

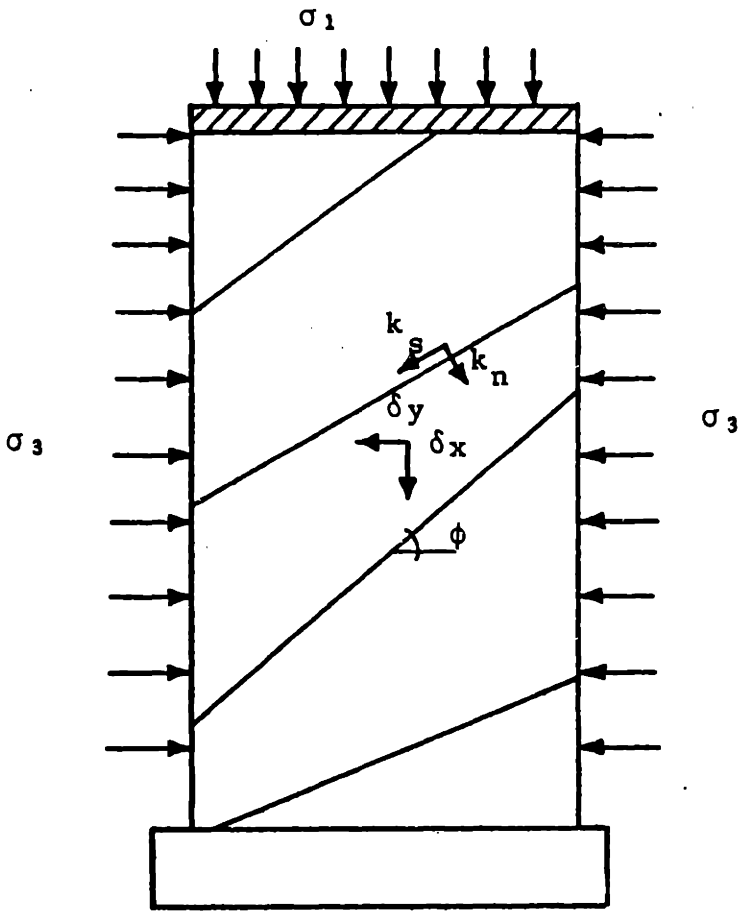

Figure 4.4.10 Triaxial 2-D Cylinder Boundary Conditions and Geometry

Deformation of individual rock joints is modeled by the general equation from the previous section.

$$(4.4.22) \qquad \delta_j(\phi) = [\sigma_1 \cos^2\phi + \sigma_3 \sin^2\phi]\frac{\cos\phi}{k_N} + [(\sigma_1 - \sigma_3)\sin\phi\cos\phi]\frac{\sin\phi}{k_s}$$

Increased lateral stress, in fact, increases settlement due to normal joint displacement, the first term in the above equations. Lateral stress, however, reduces shear displacement, the second term. The net effect of lateral stress can be expected to be a decrease in vertical deformation, however, since shear stiffnesses are generally lower than normal stiffnesses.

Total rock mass vertical deformation δ_j due to rock joints can be found by second moment, just as in the previous section,

$$(4.4.23) \qquad E[\delta_j] = E^{-1}[f_s(s)] \int \delta_j(\phi) f_\phi(\phi)\, d\phi$$

$$SD[\delta_j] = [E^{-1}[f_s(s)] \int \delta_j^2(\phi) f_\phi(\phi)\, d\phi - E^2(\delta_j)]^{\frac{1}{2}}$$

Total rock mass deformation is the sum of intact and rock joint vertical deformation,

$$\delta_{TOTAL} = E(\delta_j) + \delta_i$$

This case's limitations are considerably different from the previous case's. Where the previous realization was limited by the simplicity of its boundary conditions, this case is limited by the difficulty of obtaining values for the additional parameters required for more complete description - σ_3 and ν. Lateral stress σ_3 is very difficult to obtain in situ. Standard values for ν exist but the uncertainty of values is considerable.

In addition, the assumption of constant σ_3 may be questionable. According to the boundary condition, lateral deformation in intact rock and along rock joints does not affect lateral stresses. In reality, however, lateral deformations do increase confining stress σ_3.

The greatest advantage of the case is that it realisticly models a triaxial condition which may occur in rock masses. In addition, although σ_3 and ν may be difficult to determine, they are still commonly measured and recognized properties.

Case 3-2D Cylinder Contained by Springs

The third case incorporates the effect of lateral deformation upon lateral confining stress into the boundary conditions. From the lateral component of each joint's deformation, a different confining stress σ_3 is calculated according to the formula

(4.4.24) $$\sigma_3 = \sigma_{30} + K\delta_y$$

where σ_{30} = lateral stress fo zero deformation

K = spring constant

δ_y = lateral component joint displacemen

For computational convenience, lateral confining stress for the intact rock portions is held constant at σ_{30}. These boundary conditions are illustrated in Figure 4.4.11.

Since lateral confinement conditions for the intact rock portion are unchanged from Case 2, the intact rock deformation remains the same.

$$\delta_i = \frac{H}{E}(\sigma_1 - 2\nu\sigma_3) \tag{4.4.25}$$

Rock joint deformations are calculated by simultaneous solution of the equations for lateral stress and for lateral deformation. The general equation for lateral deformation is,

$$\delta_y = [\sigma_1\cos^2\phi + \sigma_3\sin^2\phi]\frac{\sin\phi}{k_N} + [(\sigma_1-\sigma_3)\sin\phi\cos\phi]\frac{\cos\phi}{k_s} \tag{4.4.26}$$

Solving (4.4.24 and 4.4.26) simultaneously for σ_3,

$$\sigma_3 = \frac{[\frac{\sigma_{30}}{K} + \sigma_1\cos^2\phi\sin\phi(\frac{1}{k_N} + \frac{1}{k_s})]}{[\frac{1}{K} - \frac{\sin^3\phi}{k_N} + \frac{\sin\phi\cos^2\phi}{k_s}]} \tag{4.4.27}$$

Vertical joint displacement can then be calculated simply from the general joint displacement equation,

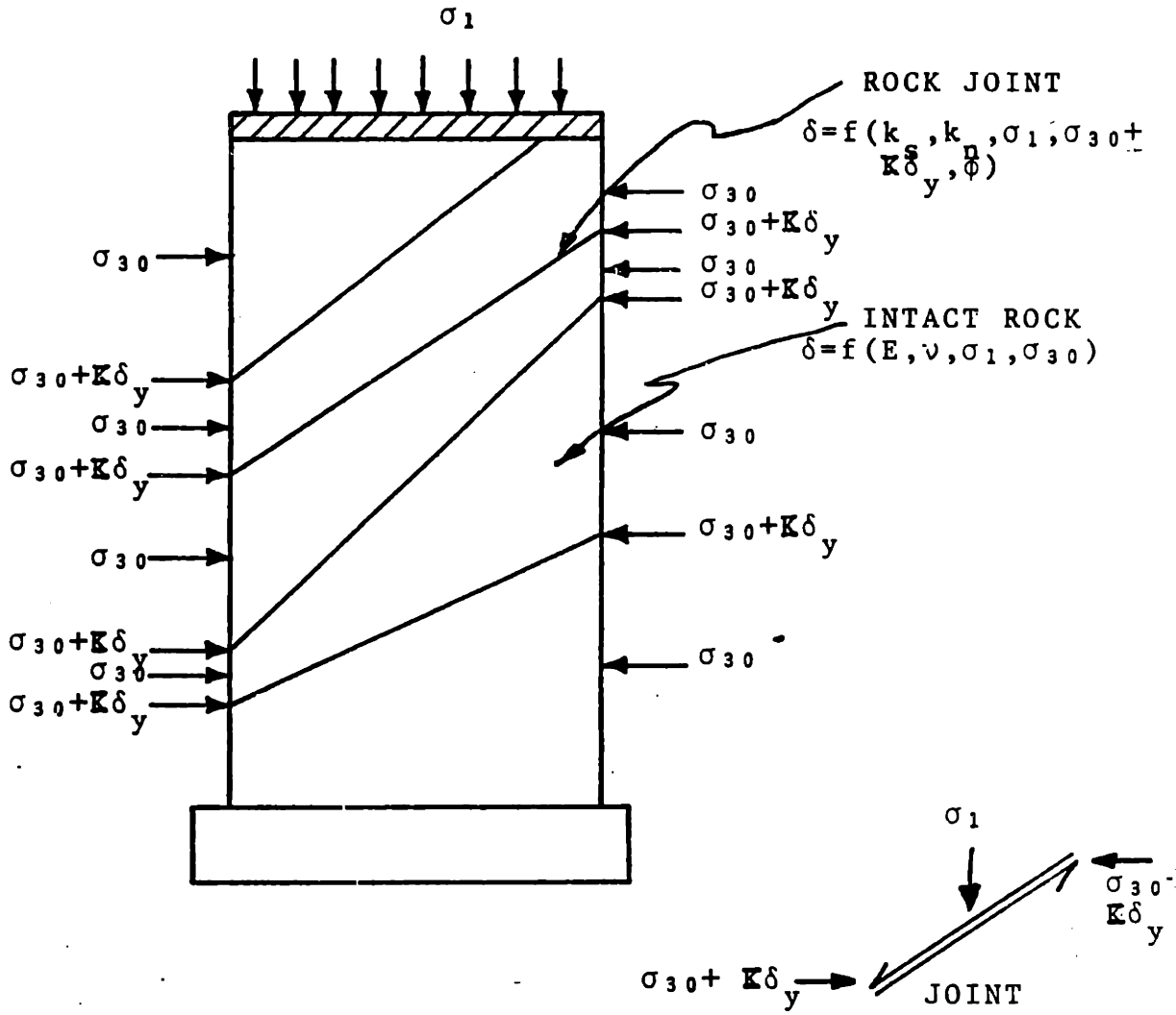

Figure 4.4.11 Strain Dependent 2-D Cylinder Boundary Conditions and Geometry

$$(4.4.28) \qquad \delta_j(\phi) = (\sigma_1\cos^2\phi + \sigma_3\sin^2\phi)\frac{\cos\phi}{k_N} + (\sigma_1-\sigma_3)\sin\phi\cos\phi\frac{\sin\phi}{k_s}$$

This equation is closed form, so it can be solved by simple application of second moment methods just as in the previous two realizations

$$(4.4.29) \qquad E[\delta_j] = E^{-1}[f_s(s)] \int \delta_j(\phi) f_\phi(\phi) d\phi$$

$$(4.4.30) \qquad SD[\delta_j] = [E^{-1}[f_s(s)]\int \delta_j^2(\phi) f_\phi(\phi) d\phi - E^2[\delta_j]]^{\frac{1}{2}}$$

Total vertical deformation is found from intact and joint deformation,

$$\delta_{TOTAL} = \delta_i + E[\delta_j(\phi)]$$

This case's primary limitation is the use of the parameter K, which is related solely to the model. K is not a rock mass property but exists solely to solve a problem in the model. It is not possible to determine K independently of the model. K can only be determined by adjustment of values until model results match those found in the field.

Other limitations include those mentioned for the previous cases.

The advantage of this case is its ability to take variable lateral stress effects into account, however crude that adaptation may be.

Case 4-3D Cylinder Constraints by Spring

In the previous 3 cases, analysis was conducted entirely in two dimensions. This was accomplished by restricting all joint trends to the same vertical plane, and assuming that the controlling stresses σ_1 and σ_3 acted in that plane. In this fourth case joint trends are not restricted (Figure 4.4.12).

The removal of the restriction to two dimensions increases the amount of information necessary for a complete joint geometry description. In addition to dip, azimuth must be described for every joint orientation. Representation of joint spacings is unchanged.

Analysis of the 3-D Cylinder is not significantly more complicated than analysis of the 2-D Cylinder. Two important assumptions maintain simplicity:

1) $\sigma_{30} = \sigma_{20}$
2) Joints undergo shear deformation only in the direction of maximum dip. Lateral stresses acting on joints are related only to lateral displacements in the direction of maximum dip.

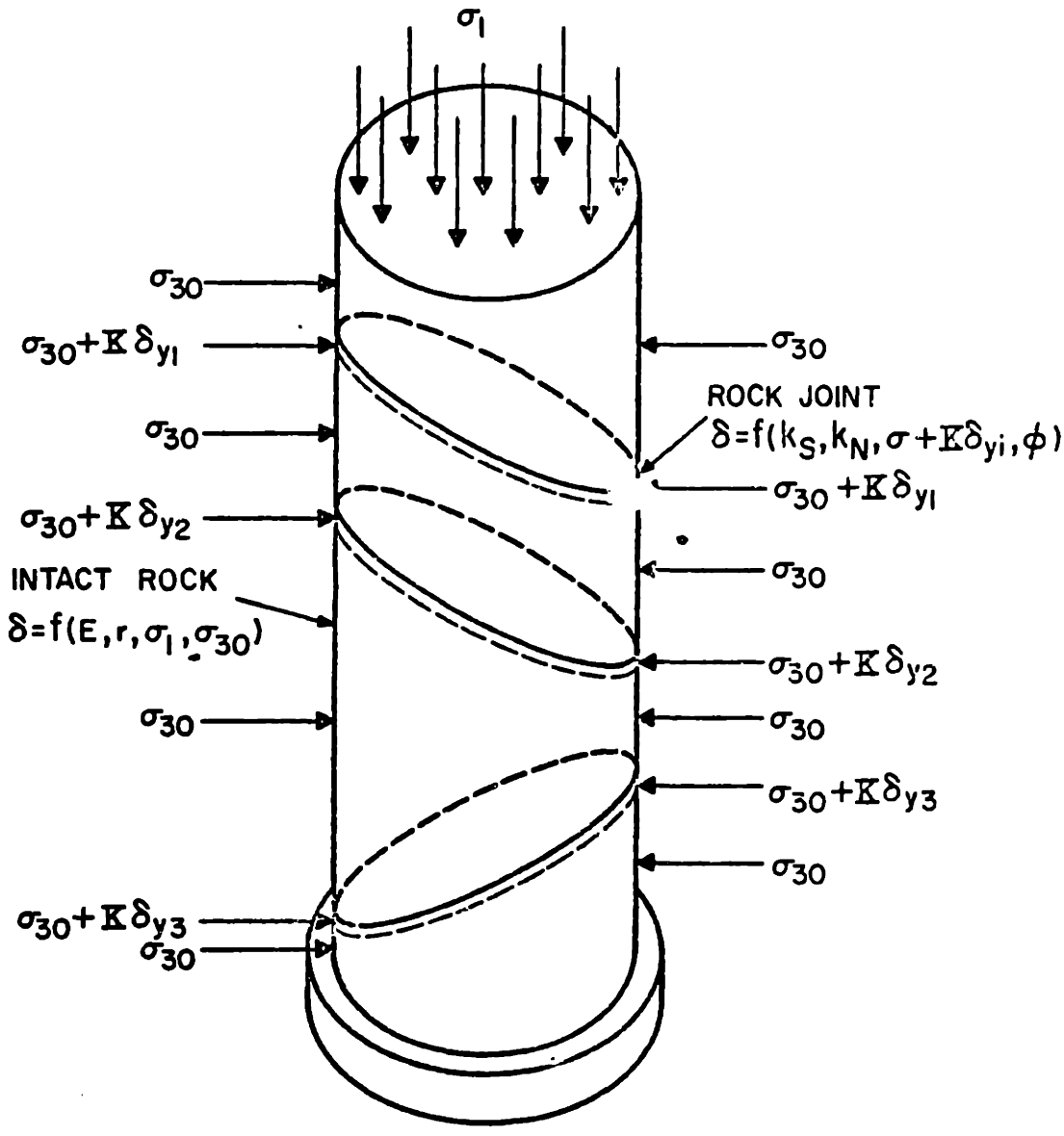

Figure 4.4.12 Boundary Conditions & Geometry-Strain Dependent 3 Dimensional Cylinder

$$\sigma_3 = \sigma_{30} + K\delta_\phi$$ where δ_ϕ = lateral displacement in dip direction.

With these assumptions, analysis can be conducted just as it was for the 2D constrained cylinder.

The 3-D constrained cylinder is slightly more general than the 2-D cylinder, since it allows for the presence of different azimuths(θ). It is also slightly more difficult to use than the 2-D cylinder, since both ϕ and θ must be modeled. For studies of most parameters, the 2-D cylinder is probably sufficient, since the addition of the third dimension does not significantly modify the analysis. For more complete modeling, however, the 3-D cylinder is better.

4.5 Model 2-Boundary Element Model

4.5.1 Description of Model

Figure 4.5.1 illustrates the concept of the Boundary Element Model. The boundary element model depicts the rock mass as a two dimensional elastic half space with "boundary elements" or inclusions with different linear or non-linear elastic properties. Boundary elements are arranged through Monte Carlo simulation to depict joints in two dimensions,as will be explained.

Boundary conditions for the Boundary Element Model are more intuitively satisfying than those of the constrained cylinder model. The boundary element model representation of

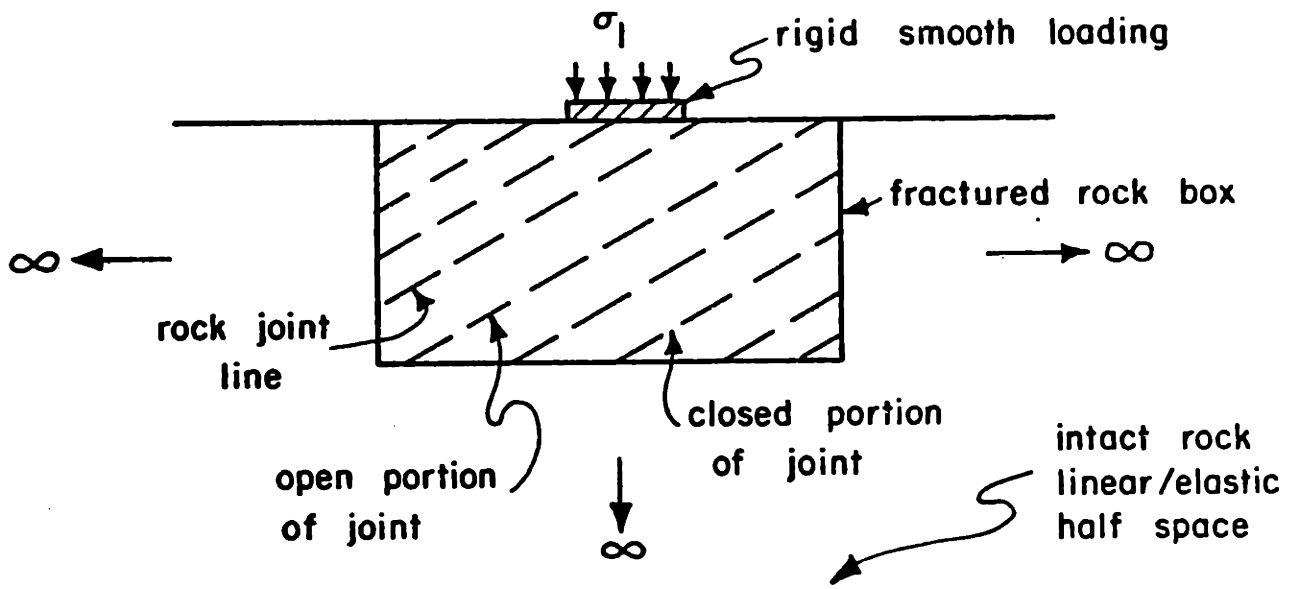

Figure 4.5.1 Boundary Element Model Concept

rock as an elastic half space avoids the use of oversimplified relation to describe lateral stresses required by the cylinder model. Boundaries are set at infinity, so no lateral confinement need be assumed. Elastic assumptions account fully for th affect of lateral deformations upon lateral stress.

Joints are simulated in the boundary element method as follows:

1) A box representing the fractured region of the rock mass is constructed within the linear elastic half space.

2) Values for spacing joint orientation, joint length and persistence are generated by Monte Carlo simulation with assumed distributions. Simulated spacings are equal to spacings between joint lines not between open joint sections. Joint line spacing can be found from persistence and joint spacing by $S_p = S_j\ 100/P$ where S_p is the spacing between joint lines, S_j is the simulated spacing between open joint, P is persistence expressed as a percent (Figure 5.4.2).

3) A point is located along the left hand edge of the fracture box, at a distance equal to the first simulated spacing from the surface. A joint line is then placed through that point with a dip equal to the first simulated dip. The joint line is then divided into open and closed portions with random open and closed lengths according to simulated joint lengths.

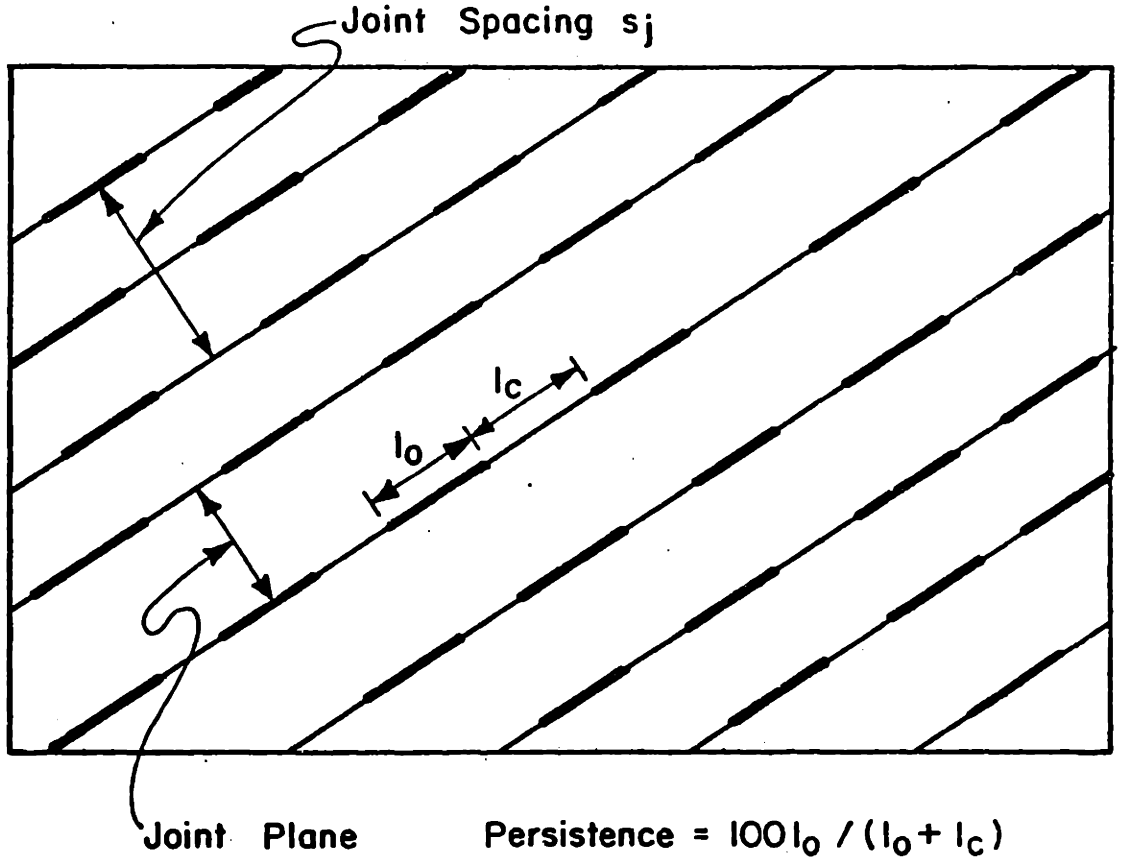

Persistence = $100 l_o / (l_o + l_c)$

l_o = open joint length

l_c = closed joint length

$$s_p = 100 s_j / p$$

Figure 4.5.2 Spacing-Persistence Relationship

Open lengths are determined from joint length distributions. Closed lengths and determined from joint length and persistence by $l_o = \frac{P}{100-P}$.
where l_o = open length, l_c = closed length, P = persistence.

4) A second point is located at a distance equal to the second spacing length multiplied by the secant of the second dip angle from the first point, and a joint line constructed through that point according to the process described in 3 and 4.

5) This process is repeated until the bottom of the box is reached.

6) Joint placement is then continued by the same process based on points along the bottom edge of the box. These points are spaced at a distance equal to the simulated spacing multiplied by the secant of the simulated dip angle.

The joint placement process is illustrated in Figure 4.5.3.

4.5.2 Assumptions and Consequences

Boundary conditions, deformation mechanisms, and the joint placement process are all assumed in the boundary element model Critical assumptions include the following:

1) Rock joints and intact rock are both elastic and continuous. Stress distributions within the rock mass are therefore elastic, and stress concentrations at edges are those predicted by elastic theory. This

1. CONSTRUCT FRACTURED ROCK BOX

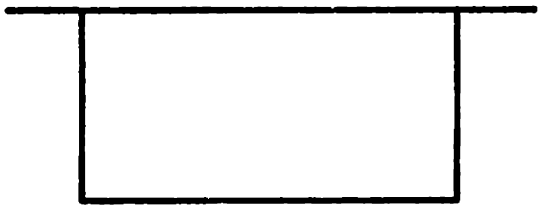

2. LOCATE FIRST JOINT LINE WITH FIRST DIP

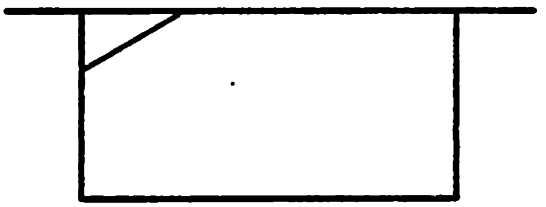

3. CREATE OPEN AND CLOSED PORTIONS OF JOINT FROM SIMULATED LENGTHS AND PERSISTENCES

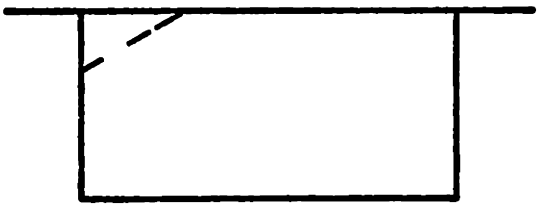

4. LOCATE SECOND JOINT AT DISTANCE $s_i \cos\Phi/p$ FROM FIRST

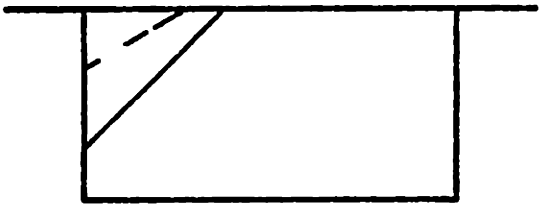

5. REPEAT PROCESS TO BOTTOM OF FRACTURED ROCK BOX

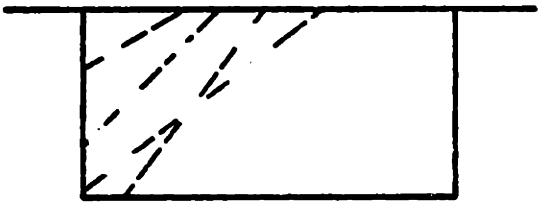

6. CONTINUE ALONG BOTTOM OF BOX AT SPACINGS $s_i \sin\Phi/p$

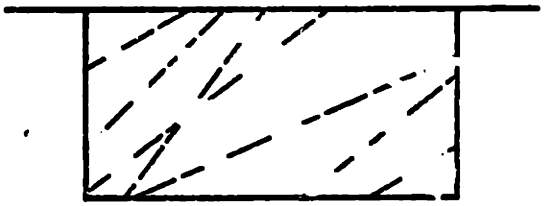

Figure 4.5.3 Joint Placement Process

is in extreme contrast to the cylinder model, which assures a uniform stress distribution for the sake of simplicity.

2. Rock joint deformation obeys linear or non-linear elastic theory. Joint deformation is therefore controlled by elastic constant E, G_s, ν, and any non-linear elastic constants (Figure 4.5.4). These constants are very rarely measured for joints, and are therefore very difficult to apply. Elastic theory, in addition, is limited to small, reversable, compatible strains. Elastic joint elements can not therefore account for irrecoverable strains or incompatible breakages.

3. Intact rock deformations obey linear elastic theory. Intact rock elastic parameters E and ν are commonly measured and represent no problem. Elastic theory limits intact rock deformation to small, recoverable, compatible strains. This does not present a significant constraint for intact rock which generally suffer only small recoverable, compatible strains.

4. Joints exist only along infinite joint lines with open and closed portions describable by a distribution of persistences. The assumption of infinite joint lines is questionable since the nature of joint geometry depends upon the process of formation of the joint. In many cases, joints are of finite length, and are 100%

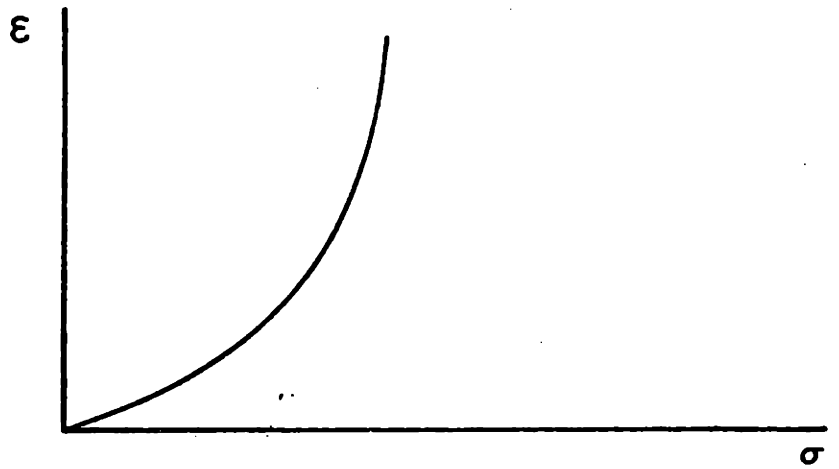

$$\varepsilon = \sigma^2/F$$

where F = nonlinear elastic constant

Figure 4.5.4 Non-Linear Elastic Behavior

persistent. This is not accounted for in the joint geometry model. The persistence concept, as discussed in Chapter 3, is questionable, and its effect upon the model is unknown.

5. Rock jointing only effects deformability within a certain distance from the loading, so jointing beyond that distance (outside fracture box area) can be ignored. This assumption is necessary to limit the number of joints to be simulated to a finite number. The effect of the assumption is probably minimal, provided that the fractured box incloses the entire Bousinesq stress bulb. The fracture box should therefore be set up to include the entire stress bulb.
6. The rock mass can be modeled as an elastic half space. Stresses throughout the rock mass are therefore dependent only upon the applied surface loading σ_1. Lateral stresses σ_3 are developed entirely from stress distributing effects in the elastic model. This is a desirable property, since the determination of an appropriate value for σ_3 was a significant limitation of the cylinder model. The boundary element model does, however, allow determinations of stresses induced under the loading.

4.5.3 Input Parameters

Input parameters required by the model include joint geometry parameters and material properties.

Model joint geometry is determined by Monte Carlo simulation. The simulation requires input distributions of spacing, orientation, persistence, and joint length. The joint spacing distribution input may be of any form. The mean spacing used in simulation, however, is the mean spacing between joint lines not between open joints. Spacing of open joint lines determined from spacing of open joints and average persistence by

(4.5.1) $s_l = s_j \times 100/P$ where s_l = spacing of joint lines

s_j = spacing of open joints

P = persistence expressed as a percentage.

The joint length distribution used in the model is a distribution of lengths of open portions of joint lines. The orientation distribution requires only a distribution of dips, such as the Fisher distribution, because the model is two dimensional.

Material property parameters required include intact rock elastic properties E and ν and rock joint elastic properties E, G_s and ν. Rock joints may be described by non-linear or linear elastic properties. If non-linear properties are desired, the non-linear stress strain relation must be input. The effect of variation of material property parameters can be determined by sensitivity studies.

4.5.4 Limitations

The boundary element model is limited by three major factors. These are: elastic assumptions, Monte Carlo methods, and computer capabilities.

Elastic assumptions limit the applicability of the model by requiring small, recoverable, compatible strains throughout the rock mass. A severe limitation arises from the difficulty of determination of elastic properties for rock joints. Rock joint properties are not generally measured in terms of elastic parameters. (Elastic parameters can however be back-figured from stiffnesses and joint widths.)

Monte Carlo methods require larger numbers of iterations to provide reasonable estimates of behavior. This can be extremely expensive at current computation costs. Additional difficulties of Monte Carlo methods are discussed in Section 4.3.2.

The greatest limitation to the applicability of the boundary element model is the huge quantity of computer core required for computation. This limits the types of computers which can handle the method and dramatically increases the cost of computation. High computation cost limits the number of realizations which can be run and the accuracy of resulting estimates of behavior and sensitivity studies.

4.5.5 Advantages

The advantages of the boundary element model include the

its consistency of material behavior relationships.

The boundary element model describes joint geometry in extremely high detail. Joint Orientations, Length, Persistence and Spacings are all taken into account. This results in consistant probabilistic estimates of behavior.

The use of elastic properties thorughout the model eliminates the need for compatibility between joint and intact rock deformations. The model is ultimately a continuous model and therefore takes compatibility of strains into account implicitly.

The boundary element method can provide an excellent model for jointed rock mass behavior. Implimentation is now primarily limited by computer capabilities. As computers become faster and more sophisticated, the boundary element model will provide great insight into the mechanism of rock mass deformation, and will help improve estimates of rock mass deformability.

4.6 Conclusions

The two models presented in this chapter demonstrate the way in which rock mass models can incorporate probabilistic descriptions of rock mass properties to provide a more complete description of deformation. Both models take the spatial variability of joint geometry into account, and both can be used to study the effects of uncertainty and variability in both joint geometry and in material properties.

Probabilistic models, such as those presented here have many advantages. They can predict the range of deformations behavior to be expected. They can take the importance of

extremes of parameters into account. They can provide uncertain estimates of behavior based upon uncertain estimates of parameters. They are limited primarily by the assumptions required and by the difficulty involved in adequately predicting input parameter values and distribution. They require more assumptions and information than deterministic models.

The following chapter will demonstrate the use of these models to predict engineering behavior and to study the effects of different geological situations upon engineering behavior. This will illustrate the advantages and limitations of probabilistic models most graphicly.

CHAPTER 5

EXAMPLES OF APPLICATION OF PROBABILISTIC MODELS

5.1 Introduction

In the previous chapter, two general probabilistic models for rock deformation were developed. This chapter will show how such probabilistic models can be applied, and will demonstrate the advantages of probabilistic models. Studies in this chapter will use the first model developed in the previous chapter, the constrained cylinder model.

Two related problems of rock mass deformation will be used as examples of the application of probabilistic models. First, the model will be used to study the effects of joint geometry and material properties on rock mass deformation. Then, the model will be used to study the relationship between Deere's RQD, a rock mass index property, and rock mass deformability as expressed by a ratio of the apparent elastic modulus of the rock mass, $\hat{E}$, to the elastic modulus for intact rock, E.

5.2 Chapter Structure

Sections 5.3 and 5.4 are parameter studies of deformation behavior. Studies in both sections use the constrained cylinder with springs model presented in Section 4.4.7. In Section 5.3 deterministic parameters are used, and in Section 5.4 probabilistic parameters are used. Section 5.5 compares the result of Sections 5.3 and 5.4 on the basis of their different

parameter representations. Section 5.6 compares effects of different boundary conditions upon deformability predictions. The validity if assumptions used in the constrained cylinder model is studied on the basis of model results in section 5.7. The constrained cylinder model is used to study the correlation between RQD and deformability in Section 5.8. Conclusions are drawn in Section 5.9.

5.3 Parameter Study of Rock Mass Deformation Model-Deterministic Assumptions

In this section, the constrained 2D cylinder with springs (Section 4.4.4) will be used. Rock joint geometry will be assumed to be deterministic: all joints will be assumed to be parallel with dip ϕ.

(5.3.1) $$f_{\phi}(\phi) = 1/\pi$$

Rock joints will also be assumed to have a true mean spacing, s_m according to the constrained cylinder model. According to the constrained cylinder model, form of spacing does not affect results. No distributional form need be assumed.

Model geometry and parameters to be studied are illustrated in Figure 5.3.1. Model parameters to be studied include dip ϕ, joint stiffnesses k_s and k_n, and joint spacing s_m. Throughout this model study, mass deformability will be represented by the ratio of apparent mass modulus $\hat{E}$ to intact modulness E.

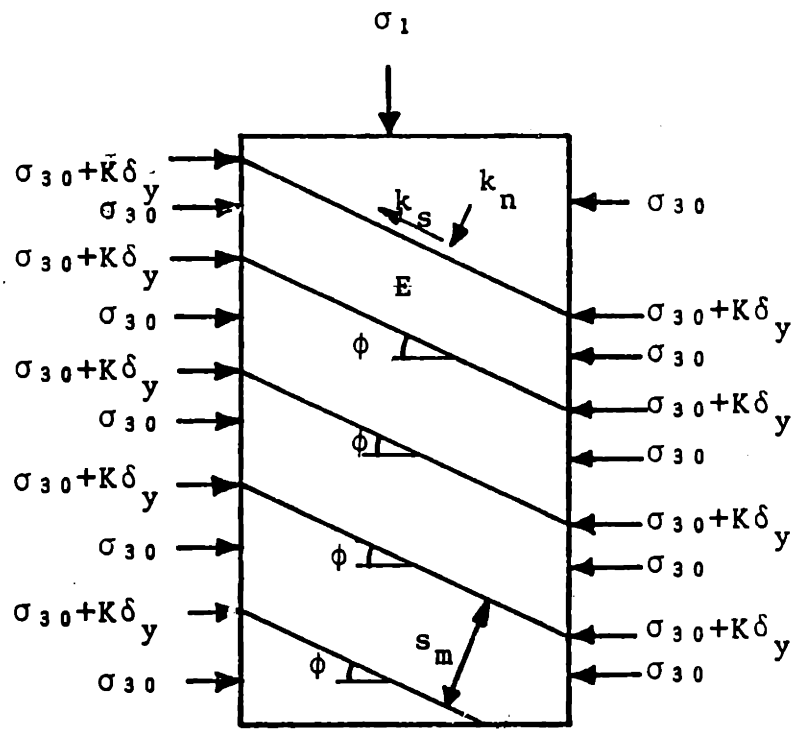

Vertical Stress	$=\sigma_1$
Horizontal Stress on Rock Joint	$=\sigma_{30}+K\delta_y$
Horizontal Stress on Intact Rock	$=\sigma_{30}$
Lateral Deformation of Rock Joint	$=\delta$
Joint Normal Stiffness	$=k_n$
Joint Shear Stiffness	$=k_s$
Rock Joint Dip	$=\phi$
Mean Rock Joint Spacing	$=s_m$
Intact Rock Modulus of Elasticity	$=E$

Figure 5.3.1 Constrained Cylinder Model with Parameters to be Studied (Deterministic Geometry)

Figure 5.3.2 shows deformability as a function of mean joint orientation for different values of joint spacing. Both spacing and orientation, as would be expected, have considerable effect upon deformability. Spacing directly effects deformability because as spacing decreases, the number of joints increases as

(5.3.2) $\lambda = 1/s_m$ where λ is the number of joints per unit length and s_m = mean joint spacing.

The effect of orientation is more difficult to predict. For horizontal joints, deformation only occurs normal to the joint, and deformability is minimized. For vertical joint deformation also occurs only normal to the joint. In addition, since joint normal deformation is horizontal, the joint makes no contribution to total mass vertical deformation. For near vertical "steep" joints, however, joint deformation occurs both in the normal and shear directions to the joints, and deformation is maximized. Thus Figure 3.3.2 shows the lowest deformability for vertical and horizontal joints, and the highest deformability for steep joints.

Figure 5.3.3 shows deformability as a function of joint orientation for several values of joint stiffnesses k_s and k_n. As would be predicted from results above, shear stiffness has

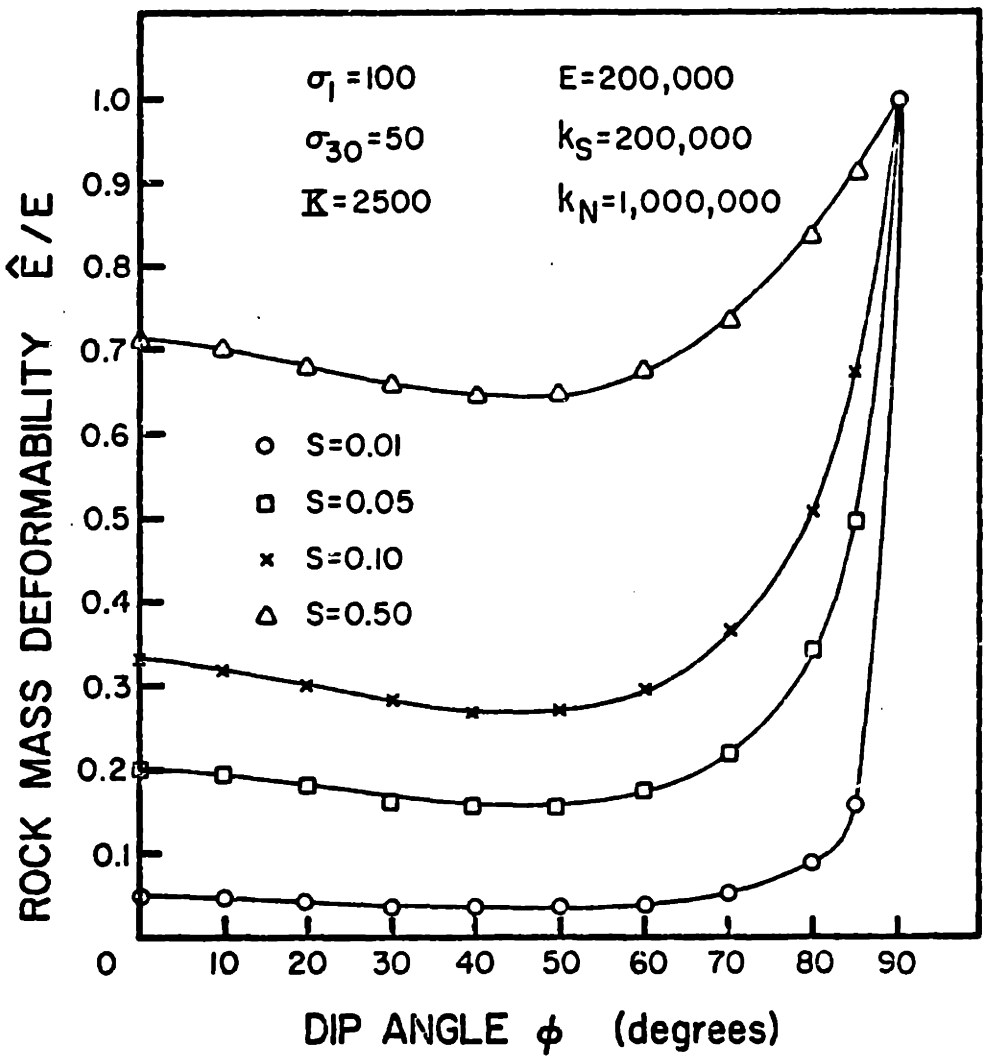

Figure 5.3.2 Rock Mass Deformability as a Function of Dip ϕ and spacing s (Deterministic Geometry)

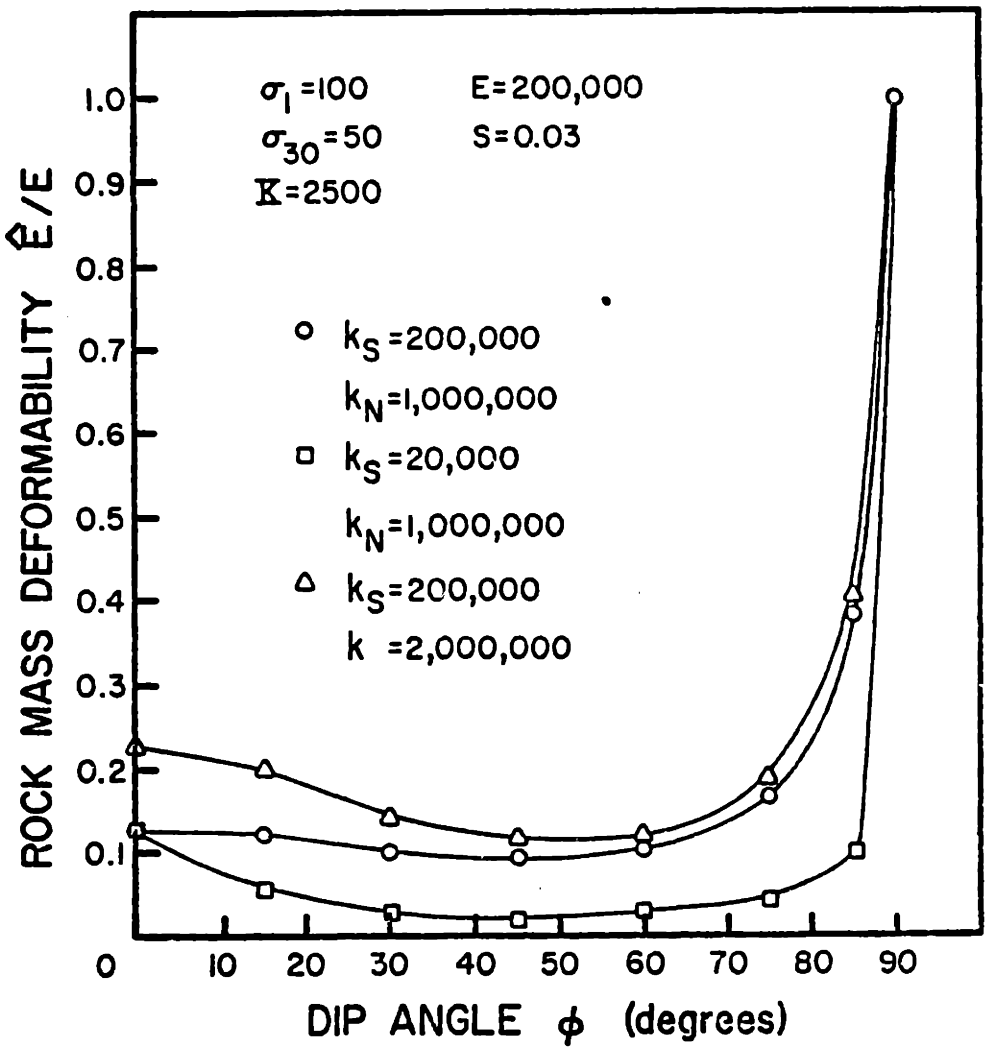

Figure 5.3.3 Rock Mass Deformability for Different Values of Stiffness (Deterministic Geometry)

little effect for vertical or horizontal joints. No shear stress occurs on these joints, so shear stiffness has no effect.

The interesting thing about Figure 5.3.3 is that, while stiffness values have considerable effect upon the actual value of deformability, they have little effect upon the shape of the deformability - dip relationship.

The results shown in Figures 5.3.2 and 5.3.3 provide insight into the effects of joint stiffness, joint orientation, and joint spacing on rock mass deformability. They demonstrate the importance of joint orientation in joint deformation. The importance of joint orientation is not generally recognized. They also show that joint stiffnesses and joint spacing can have considerable effect on deformability.

The application of these results to real rock mass behavior is limited by the validity of model assumptions and rock mass descriptions, as will be shown.

The effect of joint orientation on deformability, for example, also depends to a considerable extent upon boundary conditions. For fixed boundaries, for example, shear deformation could not occur on joints, so orientation would be unimportant. This is shown in Figure 5.3.4

Orientation's importance in the deformation process also depends upon the use of a deterministic description of orientation. For perfectly parallel joints, it is possible to have radically different deformations values for joint oriented at 80 or 90 degrees for the horizontal. Joints at 80° have very high

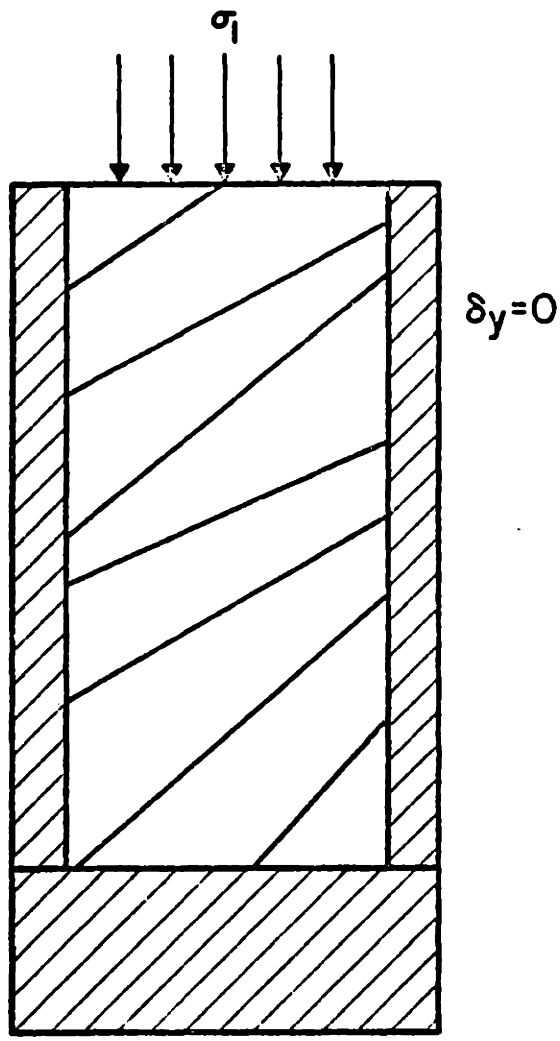

NO HORIZONTAL MOVEMENT POSSIBLE
SHEAR DISPLACEMENT ON JOINT CONSTRAINED

$\hat{E} \cong E$

Figure 5.3.4 Rock Mass Model with Fixed Boundaries

shear stresses and therefore high deformablity. Joints at 90 degrees, on the other hand, have zero shear stress and minimal deformability. For nonparallel joints or joints with uncertain orientation, however, joints oriented near the vertical would have a more moderate deformability, and considerable variability depending upon the mix of 90° and 80° orientations. Where joint orientations have considerable scatter, the principal joint orientation might, in fact, be of very little consequence. This will be explored in the next parameter study.

The effect of joint spacing depends heavily upon the assumption of a uniform stress field within the rock mass. Increased joint intensity directly increases deformability according to the model. This is in part because joint intensity has no effect upon the stress field in the model. If jointing affected the stress field,* results could be very different.

5.4 Parameter Study of Rock Mass Deformation - Probabalistic Assumptions

In this section, the constrained 2D cylinder model with springs will again be used. Rock joint geometry will be

---

* Research by Goodman & St John(1978) and Maury (1970) indicates that significant stress concentrations do in fact occur in jointed rock masses.

represented probabilisticly. Joint orientation will be represented by the Fisher distribution:

$$f_\phi(\phi) = \frac{\kappa}{2\pi \sinh \kappa} e^{\kappa \cos\phi} \sin \phi \tag{5.4.1}$$

Joint spacing will be modeled by the exponential distribution, as recommended in Section 3.4.1.

Model geometry and parameters to be studied are illustrated in Figure 5.4.1. Model parameters to be studied include dip ϕ, joint stiffnesses k_s and k_n, Fisher distribution dispersion parameter κ, and mean joint spacing s_m. As before, mass deformability will be represented by $\hat{E}/E$.

Figure 5.4.2 shows deformability as a function of mean joint orientation for a few values of Fisher distributiuon dispersion parameter κ. As was predicted in the previous section, increased variability in joint angle results in decreased influence of mean joint orientation upon deformability. For concentrated joint orientation (high κ), behavior approaches that of parallel joints, and mean joint orientation has considerable effect. For diffuse joint orientations, however, mean joint orientation has very little effect. This effect does not appear to be a consequence of the assumption of the Fisher distribution for joint orientation. The same effect would appear with a moving average of joint orientations with inncreasingly broad windows, or with any other diffuse distribution.

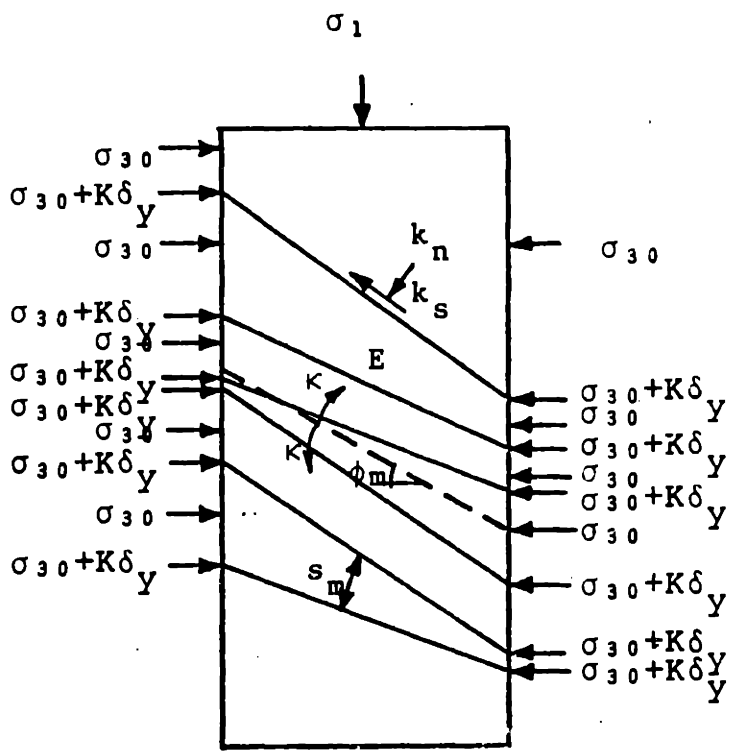

Vertical Stress	=	σ_1
Horizontal Stress on Rock Joint	=	$\sigma_{30}+K\delta_y$
Horizontal Stress on Intact Rock	=	σ_{30}
Lateral Deformation of Rock Joint	=	δ_y
Joint Normal Stiffness	=	k_n
Joint Shear Stiffness	=	k_s
Mean Rock Joint Dip	=	ϕ_m
Rock Joint Dip Dispersion	=	
Mean Rock Joint Spacing	=	s_m
Intact Rock Modulus of Elasticity	=	E

Figure 5.4.1 Constrained Cylinder Model with Parameters to be studied- Pro abilistic Orientation

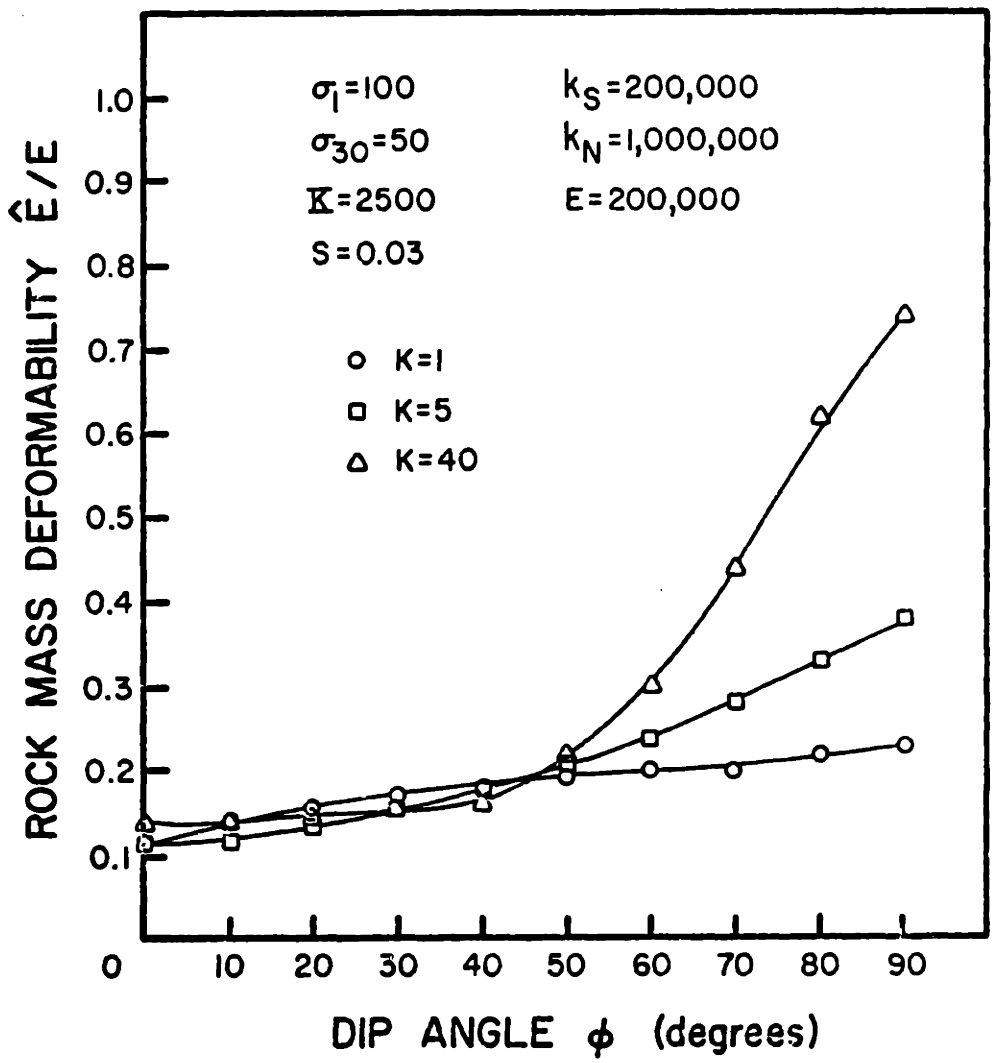

Figure 5.4.2 Rock Mass Deformability as a Function of Mean Dip ϕ and Dispersion κ (Probabilistic Geometry)

Although variability of spacing is modeled by the exponential distribution, the actual distributional form is unimportant As the model was developed in Section 4.7, only the expected number of joints per unit length, not the distribution of spacing is important. The expected number of joints per unit length, λ is found from mean joint spacing by

(5.4.2) $$E[\lambda] = 1/s_m \quad \text{where } s_m = \text{mean joint spacing}$$

Figure 5.4.3 shows deformability as a function of mean spacing. The effect of joint spacing upon deformability is similar for deterministic description of spacing (Figure 5.3.2) and probabalistic description of spacing. This is because of the unimportance of the distributional form of spacing.

The use of a probabilistic description for orientation results in a distribution of predicted deformabilities. Figure 5.4.4 shows that for increased dispersion (decreased κ), the standard deviation of deformability increases. The largest uncertainty for deformability occurs for large dip angles. This is because of the large difference in deformation values for different dips at large dip (see Figure 5.3.2).

Joint stiffness is varied in the curves in Figure 5.4.5. As in the previous section, changes in joint stiffness change only the magnitude of deformability, not the form of the deformation relation. Lower stiffnesses result in increased

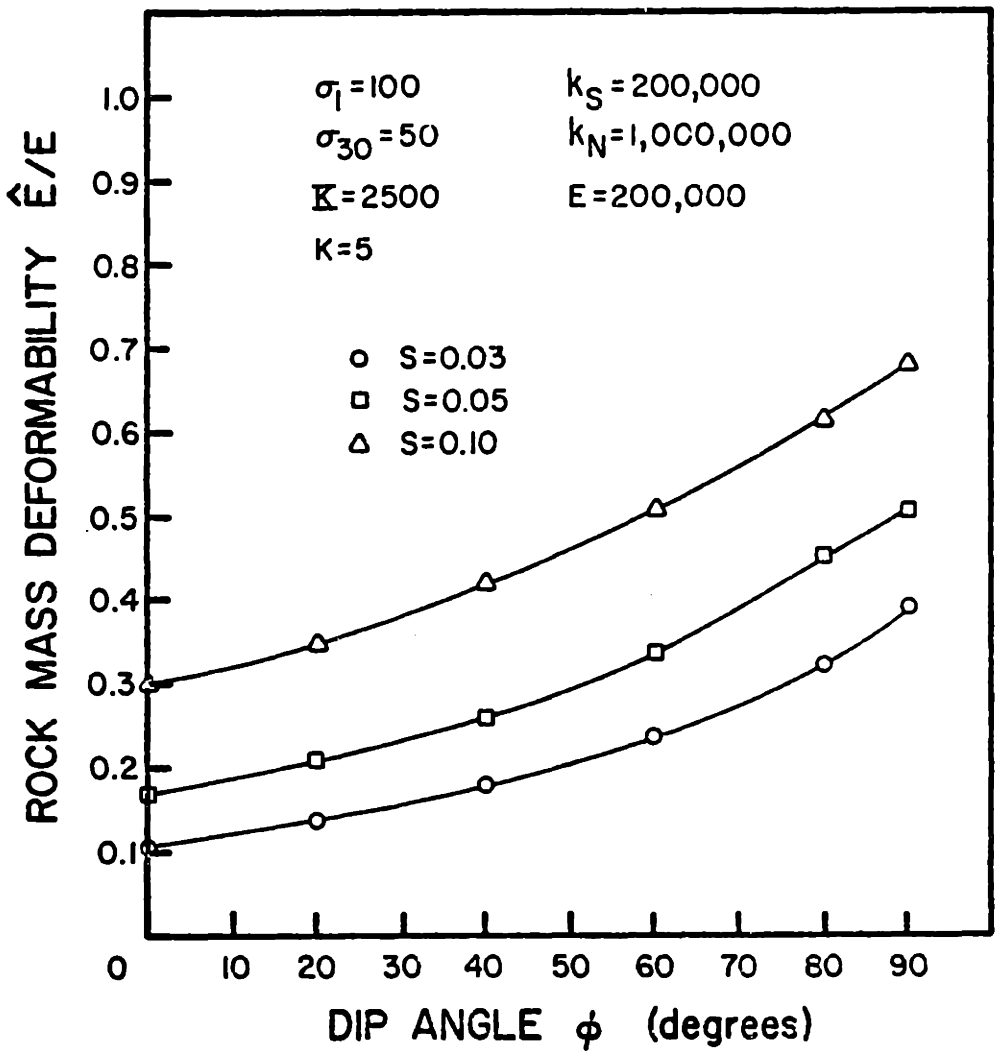

Figure 5.4.3 Rock Mass Deformability as a Function of Dip ϕ and Spacing s (Probabilistic Geometry)

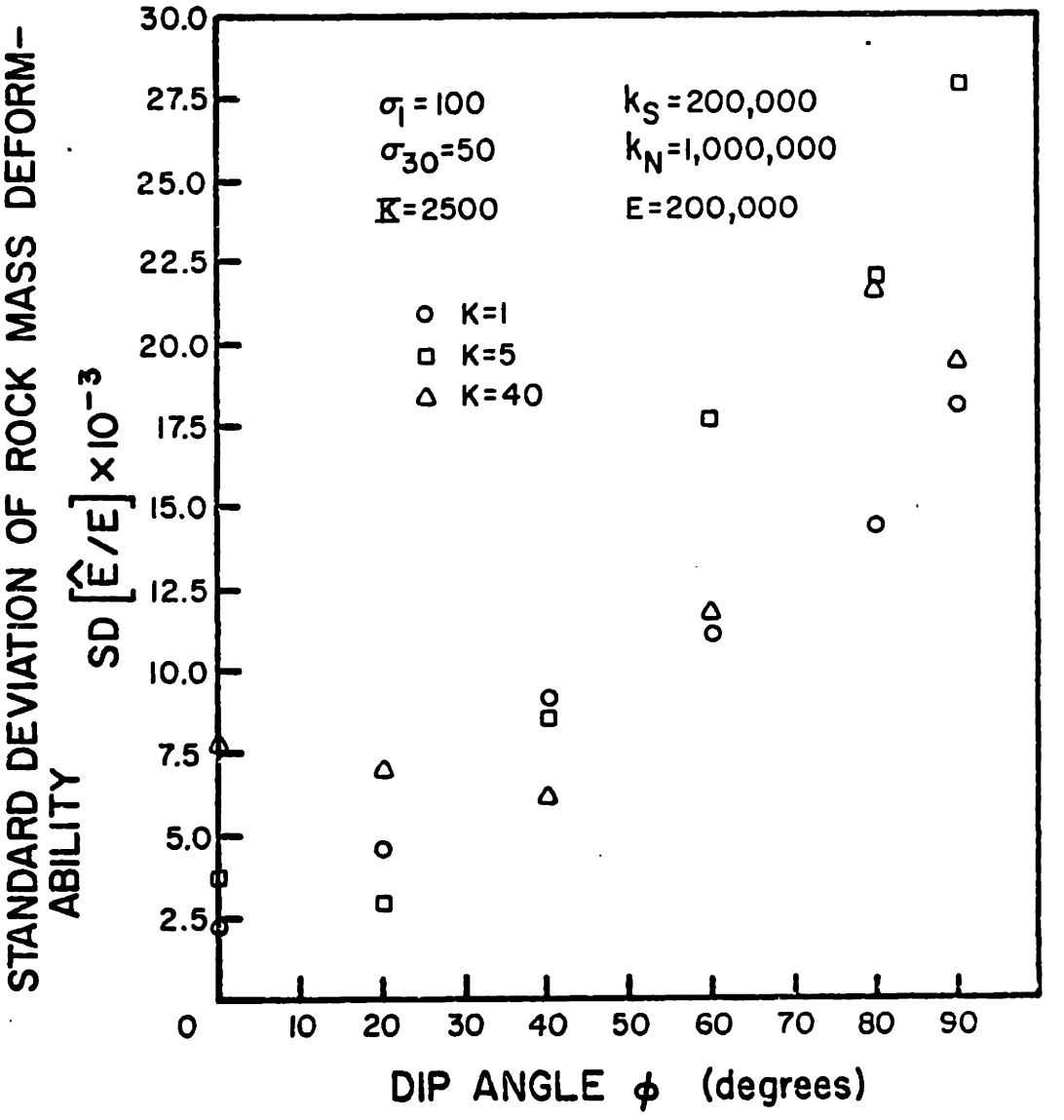

Figure 5.4.4 Standard Deviation of Rock Mass Deformability as a Function of Dip ϕ and Dispersion κ (Probabilistic Geometry)

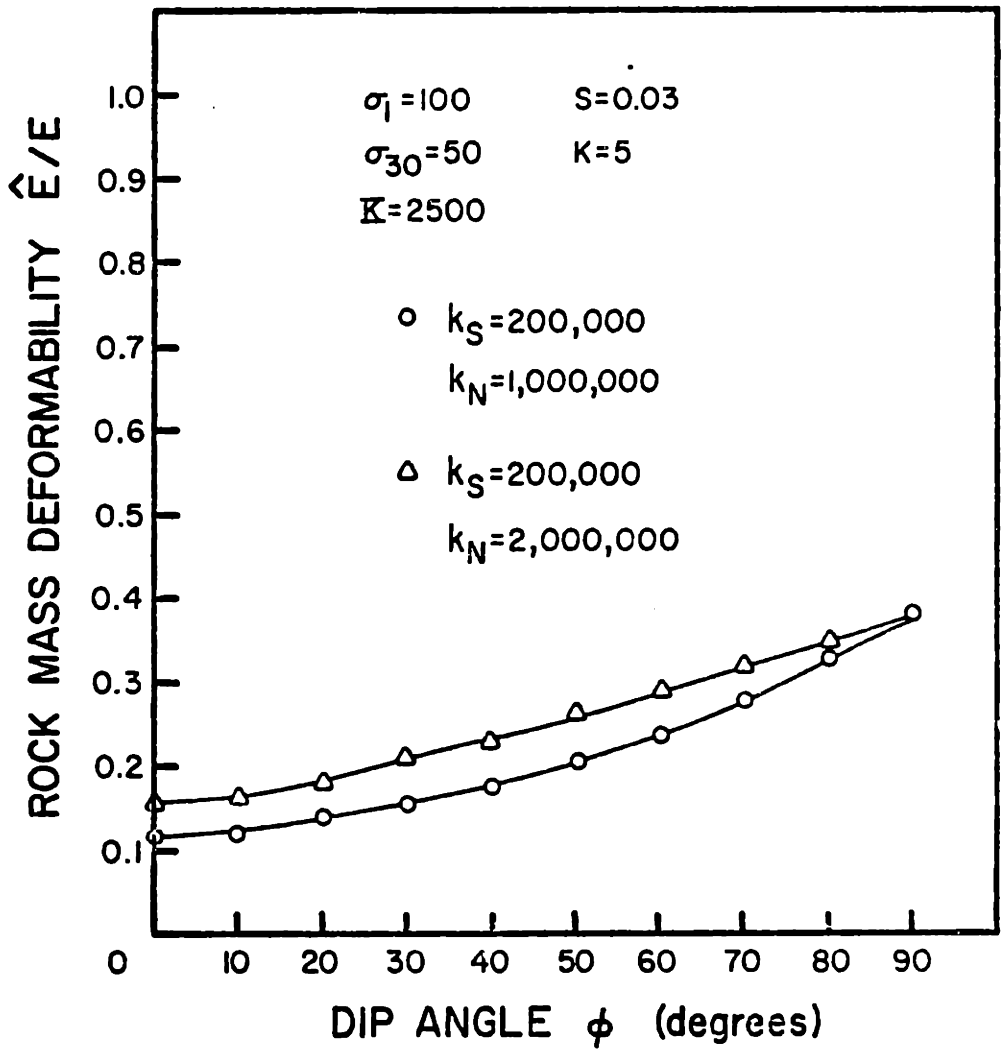

Figure 5.4.5 Rock Mass Deformability for Different Values of Stiffness (Probabilistic Geometry)

deformability, but the effect is proportional for all mean spacings and mean orientation and does not change the character of the model behavior.

The use of probabilistic joint orientations resulted in a substantial change in results. Maximum deformabilities predicted for given stiffnesses decreased, and mimimun deformabilities increased. This demonstrates the importance of input assumptions in model studies. While the actual probabalistic assumptions used for orientation and spacing may not have been critical, the use of probabalistic description was.

The assumption of independence of individual joint deformations is critical to the behavior of the model with probabilistic input parameters. Where joint orientations are variable, it is possible for joints to intersect, and to interfere with each other's deformation. This is illustrated in Figure 5.4.6. If this behavior were accounted for, increased joint intensities might not result in proportional increases in deformation, since disproportionate interference might occur. Particular joint orientations might also suffer disproportional interference. In the model, however, these effects do not appear because interference in assumed not to occur at any level of joint intensity or joint orientation. This demonstrates the importance of one of the limitations of the model.

The use of the model with probabilistic input assumptions results in probabilistic predictions of behavior. Although the

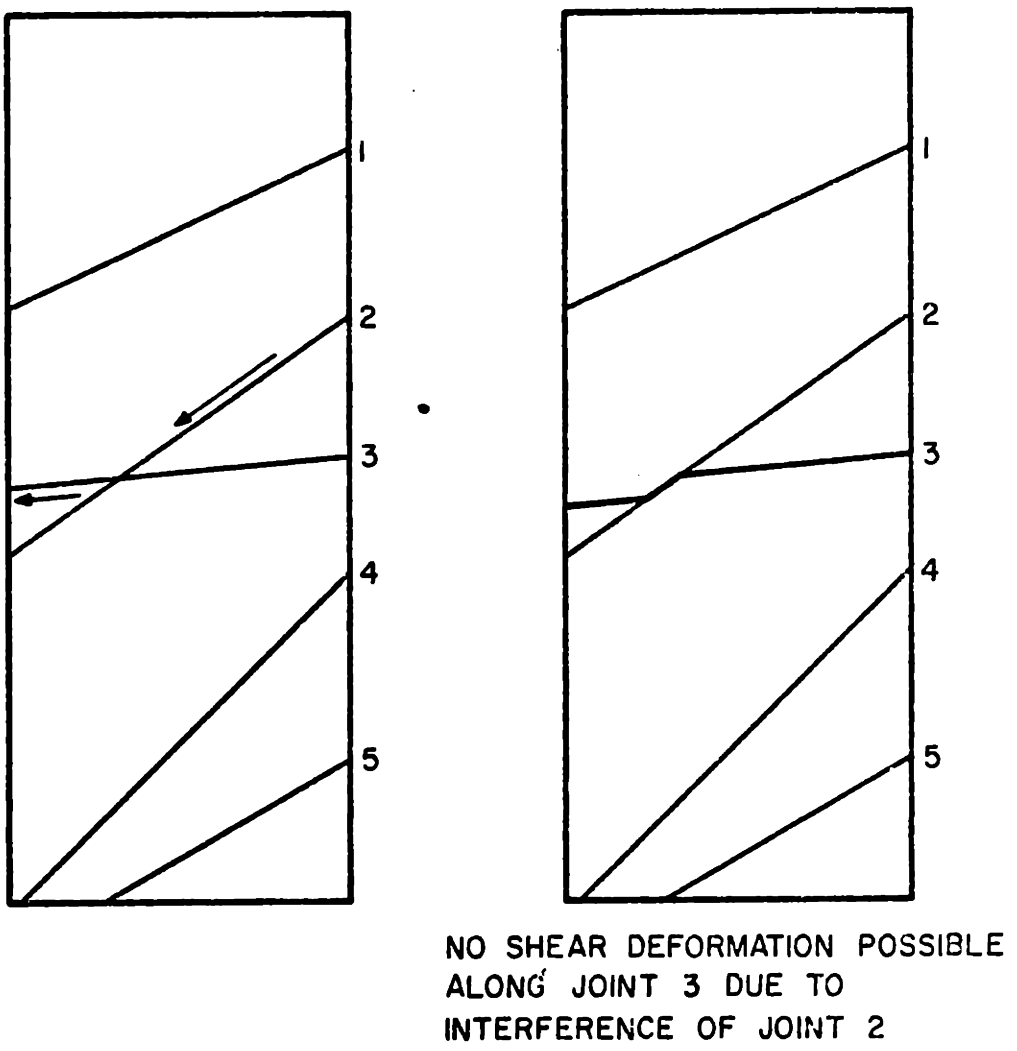

Figure 5.4.6 Joint Interference-
Non-Parallel Joints

model results in distributions of predicted behavior, only second moments are calculated because of the difficulty of analytic solution and the lack of justification for Monte Carlo solutions. These probabilistic predictions, however, only account for two of the many sources of uncertainty and variability discussed in Chapter 4. The combined effect of spatial variability of input parameters and input parameter uncertainty is incorporated into model prediction. Uncertainty of model constitutive relations and assumptions, descriptional forms, and boundary conditions are not considered. These can only be considered by weighing results obtained with different constitutive relations, assumptions, parameter descriptions, and boundary conditions by their uncertainty or the confidence placed in them.

5.5 Comparison of Probabilistic and Deterministic Results

Figure 5.5.1 dramatically demonstrates the difference in deformability predictions obtained with probabilistic and deterministic inputs to the same model. Despite the fact the mean value for input parameter remains unchanged between probabilistic and deterministic implementations, the expected value of deformability changes.

In rock mass deformation, extreme values of parameters may have as much effect on results as mean values. Therefore deterministic models based solely upon central tendencies may fail completely to predict behavior. Accurate prediction

of results clearly requires acknowledgement of the effect of extreme values.

On the other hand, the effect of joint geometry parameters such as dip ϕ are much more clearly represented in the deterministic model results. Deterministic models are useful for the isolation of individual parameter effects. It is important to recognize, however, that these individual parameter effects may be masked in actual behavior because of parameter variation and uncertainty.

Spatial variability of rock mass joint geometry clearly plays a large role in rock mass deformation. This can be seen in deterministic results, where a small change in joint geometry can result in a large change in deformability. It can also be seen in probabalistic results, where changes in dispersion result in substantial changes in deformability.

5.6 Effect of Boundary Conditions

The constrained cylinder model for rock mass deformation allows one to use many different boundary conditions. Use of the model requires selection of an appropriate set of boundary conditions. Application of model results requires confidence in the validity of selected boundary conditions and an understanding of the sensitivity of the model to boundary conditions. If the model is extremely sensitive to boundary conditions, it is essential that exactly the right set of boundary conditions be selected. If the model is not so sensitive to boundary

conditions, selection of correct boundary condition is less important.

In this section, we will compare model results for three different sets of boundary conditions. If different boundary conditions lead to radically different model results, the applicability of the model when boundary conditions cannot be accurately determined will be limited.

Figure 5.6.1 shows deformability predictions for the constrained cylinder model with three different boundary conditions. In Figure 5.6.1a, the cylinder is assumed to have a constant vertical stress σ_1. In Figure 5.6.1b, the cylinder is assumed to be under constant triaxial stresses σ_1 (vertical) and σ_3 (horizontal). In Figure 5.6.1c, vertical stress σ_1 is assumed to be constant, but horizontal stress σ_3 is assumed to vary with lateral deformation as:

$$\sigma_3 = \sigma_{30} + K\delta y \tag{5.6.1}$$

These three boundary conditions were discussed in Section 4.7 and are schematically shown in Figure 5.6.2.

Results in Figure 5.6.1 show that, while boundary conditions do change model results, they do not significantly change the nature of model behavior. Deformability still increases with decreased joint spacing. Deformability still varies substantially with joint orientation.

It is possible, therefore, to assume that in the range

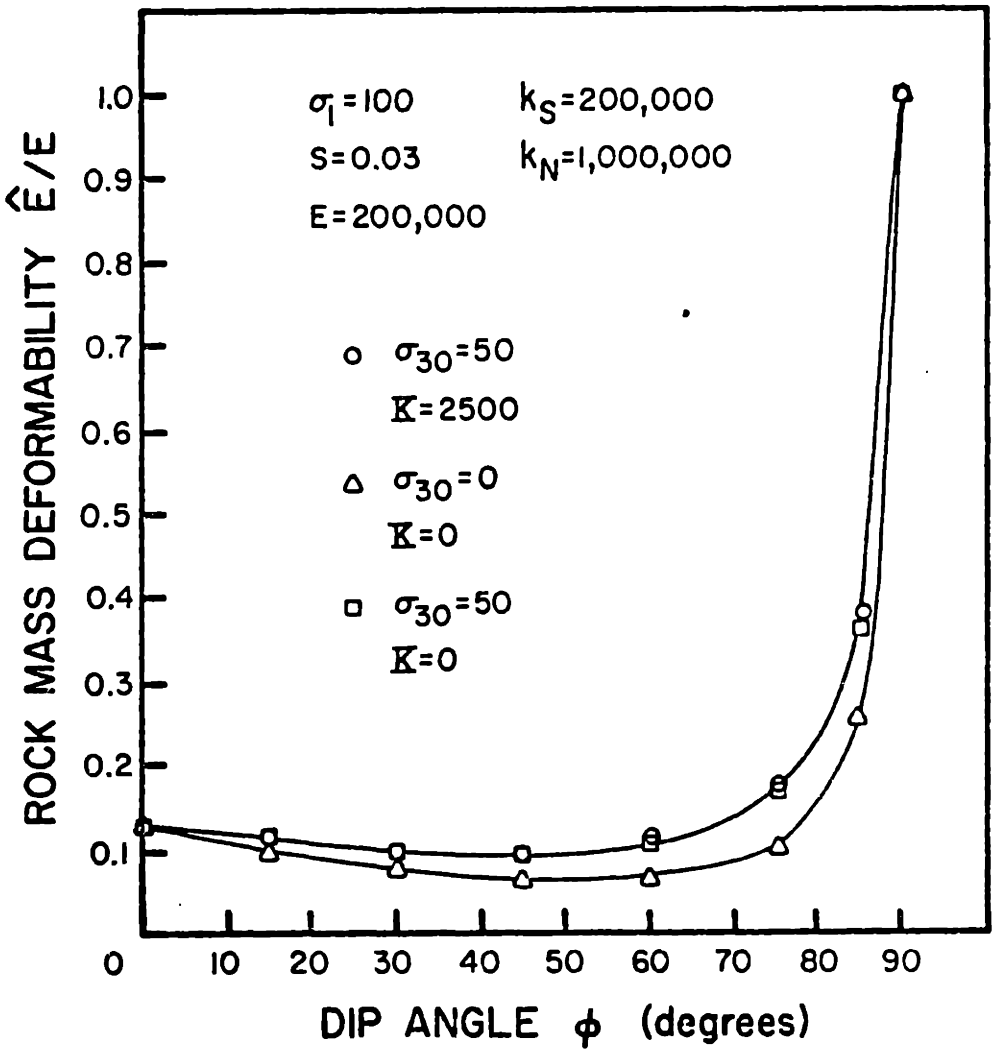

Figure 5.6.1 Rock Mass Deformability for Different Boundary Conditions (Deterministic Geometry)

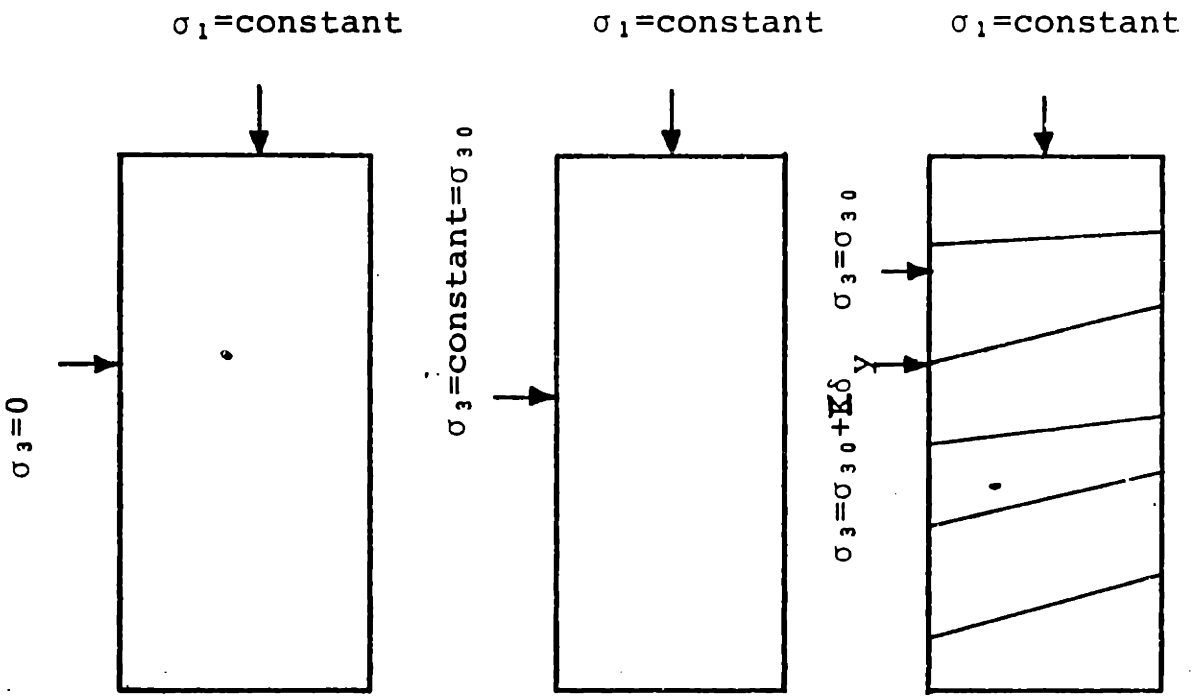

Figure 5.6.2 Unconfined Cylinder, Constant Stress Triaxial, and Lateral Strain Dependent Triaxial Boundary Conditions

investigated boundary conditions are not of primary importance. The boundary conditions which best match observed behavior can therefore be assumed. The most flexible boundary conditions are the triaxial stresses with strain dependent lateral stresses, since they can be reduced to either of the other boundary condition assumptions.

While model results indicate that boundary conditions are not important, it is important to realize that this is due to model assumptions. The validity of this conclusion depends upon the validity of underlying assumptions. The result that lateral stress assumptions are not critical to behavior may in part be due to the assumption of a uniform stress field, and in part to the assumption of no rotation of principal stress directions. Under the assumption of a uniform stress field, lateral stresses affect more the magnitude of deformations than the relation between deformations for different joint geometry conditions. Under the assumption of invariant principal stress directions, changes in the magnitude of lateral stresses cannot affect the basic joint deformation process, since the deformation process is dependent more on the direction of principal stresses than upon their magnitude.

Boundary conditions assumptions clearly affect model predictions. Deformability is greatest under uniaxial unconfined loading. The effort of joint orientation is also most pronounced for that condition. The effect of joint orientation

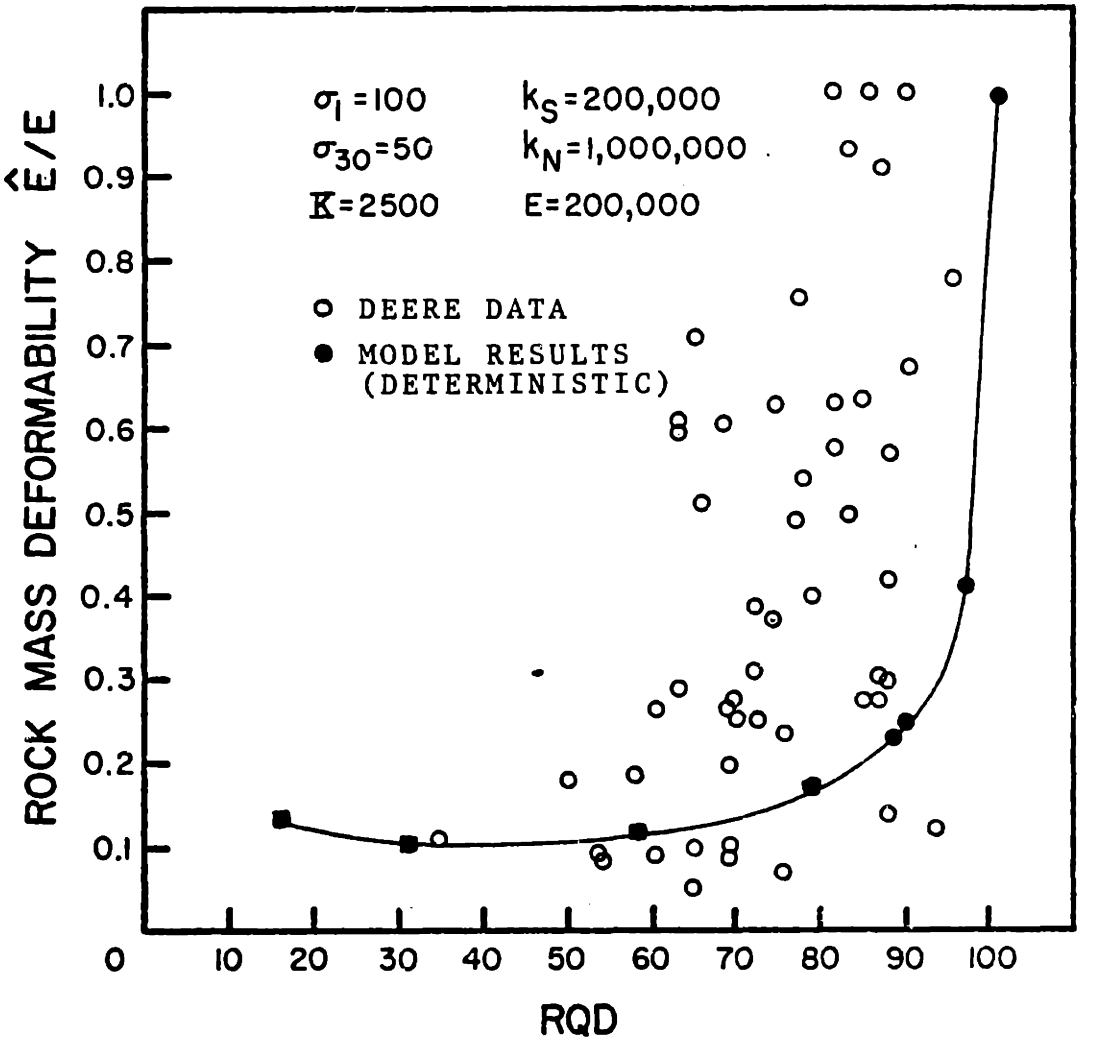

Figure 5.8.5 Rock Mass Deformability Relation to RQD: Model Results and Deere's (1967) Correlation

is muted to some extent for triaxial loading when lateral confining stress increases with lateral strain. Deformability is also least for loading with strain dependent lateral stress. Boundary conditions, however, are still only a secondary effect compared to dip orientation, joint spacing, and method of analysis.

5.7 Validity of Assumptions

Results in Sections 5.3-5.6 depend entirely upon the validity of model assumptions. In this section, model results will be discussed in regard to their relation to model assumptions. Three assumptions will be considered. These include small strains on rock joints, independence of individual joint deformations, and input parameter variablity.

The assumption of small strains along joints is contradicted by results shown in Figure 5.3.2. For steep, non vertical dip angles, strains along joints are in fact quite substantial. This could result in incompatibility of strains, reorientation of joint planes, and many other effects avoided by the assumption of small strains. For large dip angles, the validity of the model must be questioned, because the critical model assumption of small joint strains is violated.

The independence of individual joint deformations is critical to the analysis of the rock mass model. Since large strains occur along joints, however, this assumption is brought into doubt. If individual joint deformations are not, in fact,

independent, then the effect of dip angle ϕ , joint spacing s and boundary conditions on rock mass deformability is distored by the model. The magnitude of this distortion depends upon how inaccurate the model assumption is. Figure 5.4.6 illustrates the problem of interference.

The use of probabilistic descriptions of joint geometry appears to be very important, since the results of analysis are different for probabilistic and deterministic geometries. The particular distributions chosen for analysis, however, appears to be less important than the degree of dispersion of the distribution. For example, the assumption of a Fisher distribution for dip appears to have the same effect on results as the assumption of a moving average in Section 5.3.

5.8 RQD-$\hat{E}$/E correlation

Deere's correlation between RQD and modulus ratio $\hat{E}/E$ will be studied in this section. The constrained cylander model model is convenient for study of Deere's correlation because the inputs used for the deformation model can also be used in the probabalistic description of RQD (Section 3.4.5). The exponential distribution can be assumed for joint spacing in both the deformability model and the RQD model. Identical distributions for orientation can also be used in both models. Here, Deere's correlation will be studied with both deterministic parallel joints at an orientation ϕ , and with probabilistic

Fisher distributed sub-parallel joints with mean orientation ϕ_m and dispersion κ.

Deterministic Joint Orientation

Figure 5.8.1 and 5.8.2 show RQD and deformability $\hat{E}/E$ as functions of mean spacing s_m and orientation ϕ for parallel joints. RQD is calculated according to the formula in Section 3.4.4. Deformability is calculated form the constrained cylinder model with springs (Section 4.7.4). Both RQD and $\hat{E}/E$ are highly dependent upon both spacing and orientation. Figure 5.8.3 shows RQD plotted against $\hat{E}/E$ for all combinations of orientation and spacing. Surprisingly enough, RQD and $\hat{E}/E$ appear to be clearly correlated even for widely different spacings and orientations. Figure 5.8.4 shows the relationship between RQD and $\hat{E}/E$ for several different values of joint stiffnesses k_s and k_n. The actual RQD-$\hat{E}/E$ curve is different for different values of k_s and k_n, but the shape of the curve is not. This indicates that, according to the model, the form of the RQD-$\hat{E}/E$ correlation is general, and only the specific values depend upon geology.

These results, which tend to support the use of Deere's correlation, are subject to the same limitation as the probabilistic description of RQD and the constrained cylinder model for rock mass deformation.

Both models are limited by input parameter assumption of deterministic dip ϕ and probabilistic exponentially spaced joints with mean spacing S_m. In addition, the rock

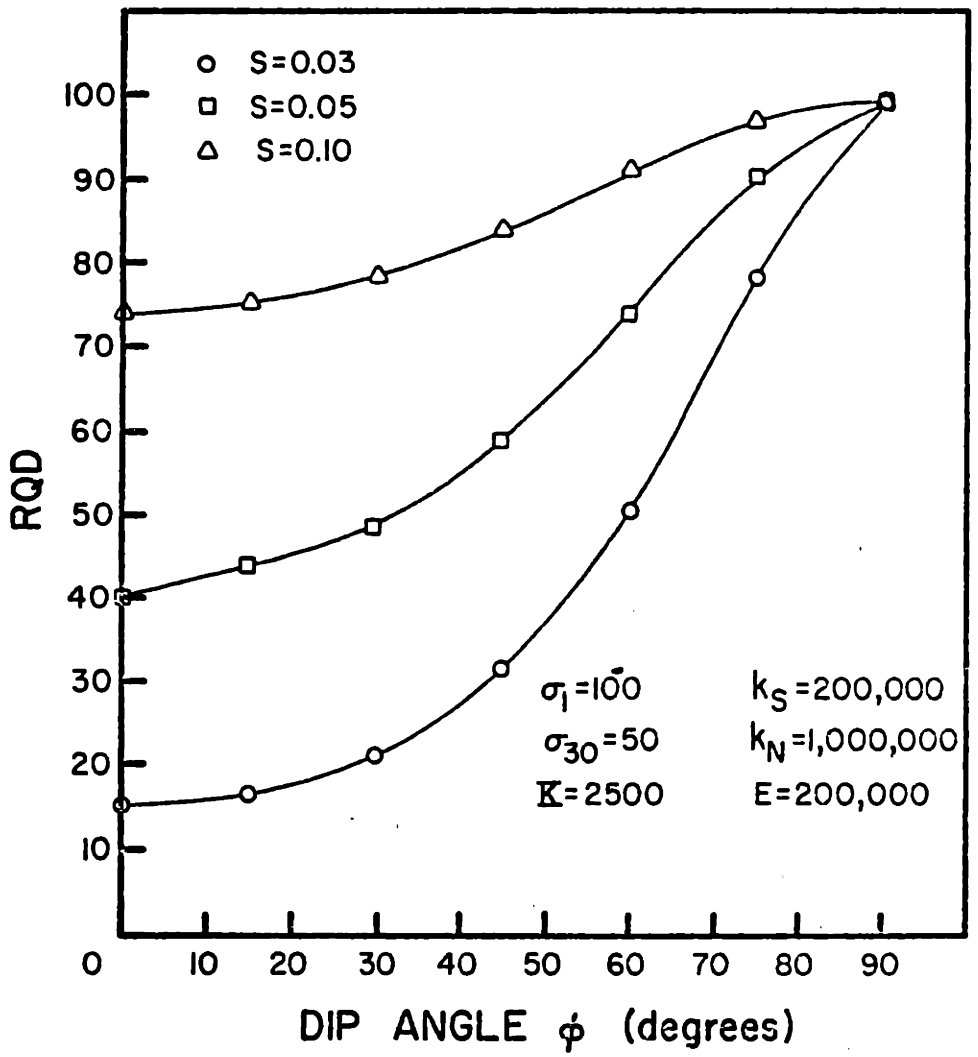

Figure 5.8.1 RQD as a Function of dip ϕ and spacing s (Deterministic Geometry)

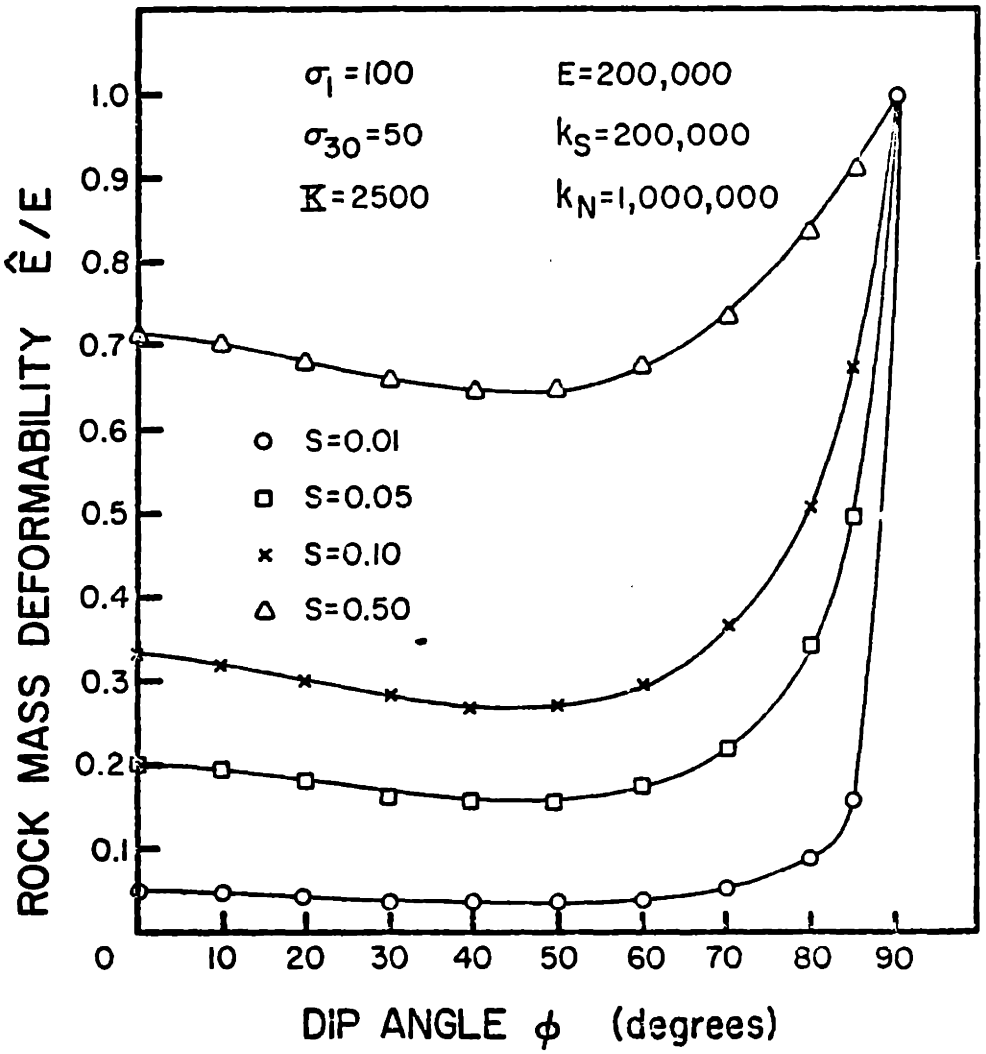

Figure 5.8.2 Rock Mass Deformability as a Function of Dip ϕ and spacing s (Deterministic Geometry)

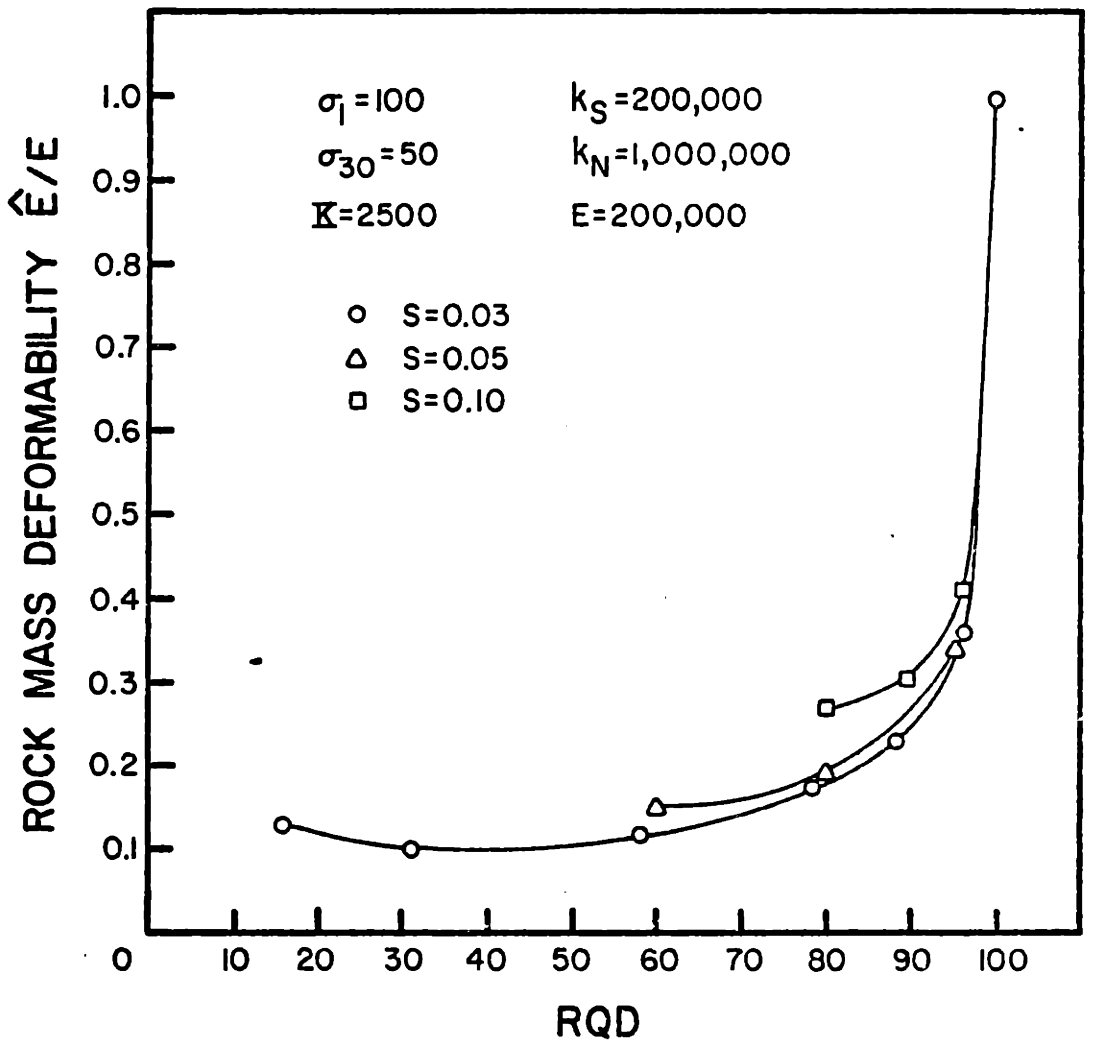

Figure 5.8.3 Rock Mass Deformability Predicted from RQD for Different Values of Dip ϕ and spacing s (Deterministic Geometry)

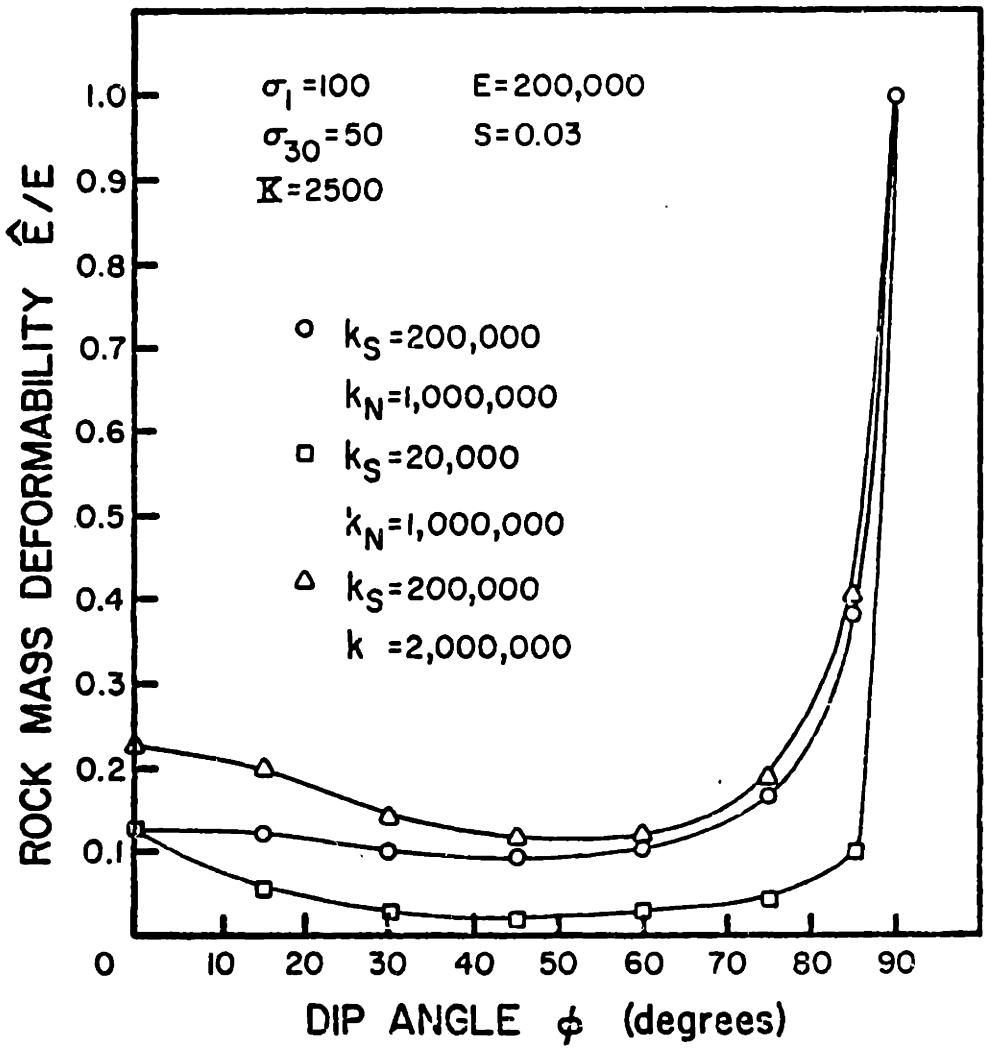

Figure 5.8.4 Rock Mass Deformability for Different Values of Stiffness (Deterministic Geometry)

deformation model is limited by considerations of strain compatability, stress field, and strain level as discussed in Section 4.4.4.

The agreement between model correlations and Deere's correlation, however, are striking. Deere's correlation and the model correlation are shown superimposed in Figure 5.8.5. This agreement does not confirm Deere's correlation, especially considering all of the models' limitations; but it does lead to greater confidence in the correlation.

Probabalistic Joint Orientation

Figures 5.8.6 and 5.8.7 show RQD and $\hat{E}/E$ as function of orientation and dispersion κ for joints distributed according to the Fisher distribution. Both RQD and $\hat{E}/E$ relations are again highly dependent upon ϕ . RQD is plotted against $\hat{E}/E$ for different spacings, orientation, and dispersion levels in Figure 5.8.8. Here, there is considerable scatter in the correlation. Still, the general shape of the RQD-$\hat{E}/E$ correlation for Fisher distributed joints is similar to that obtained by Deere. The variance in the correlation is small for low RQD but for high RQD the variance can be quite large. This indicates that for low quality rock masses, the correlation can be used with considerably more confidence, than for high quality rock masses.

Comparison of Deterministic and Probabalistic Results

It is interesting to examine the difference between results

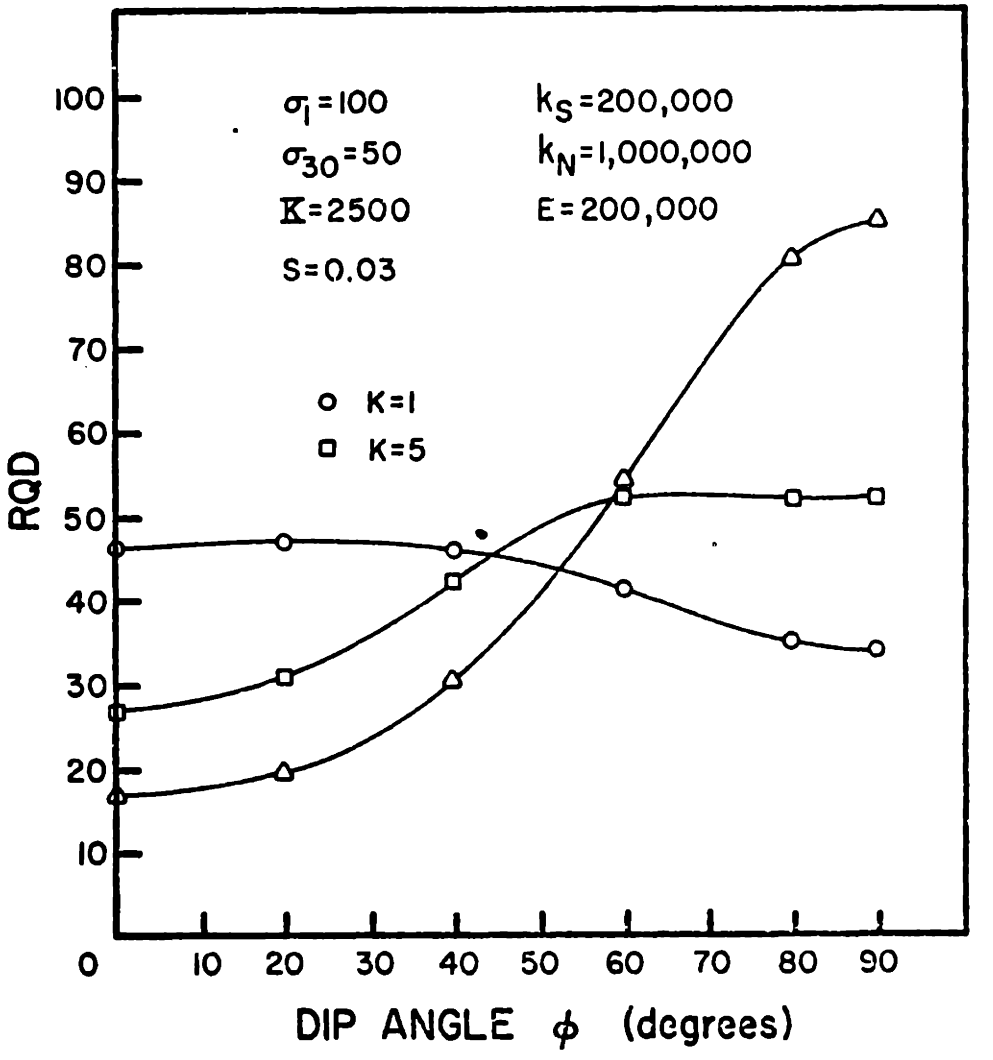

Figure 5.8.6 RQD as a Function of Dip ϕ and Dispersion κ (Probabilistic Geometry)

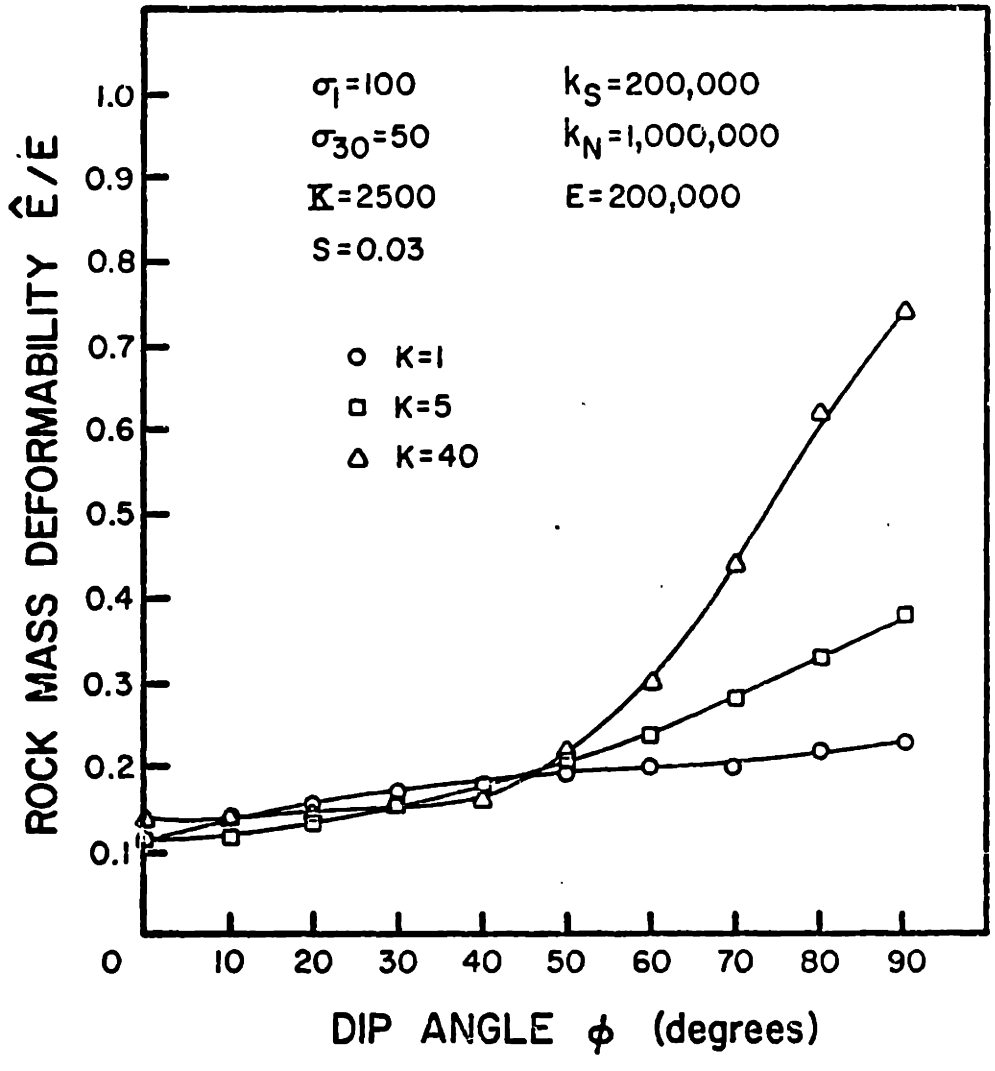

Figure 5.8.7 Rock Mass Deformability as a Function of Mean Dip ϕ and Dispersion κ (Probabilistic Geometry)

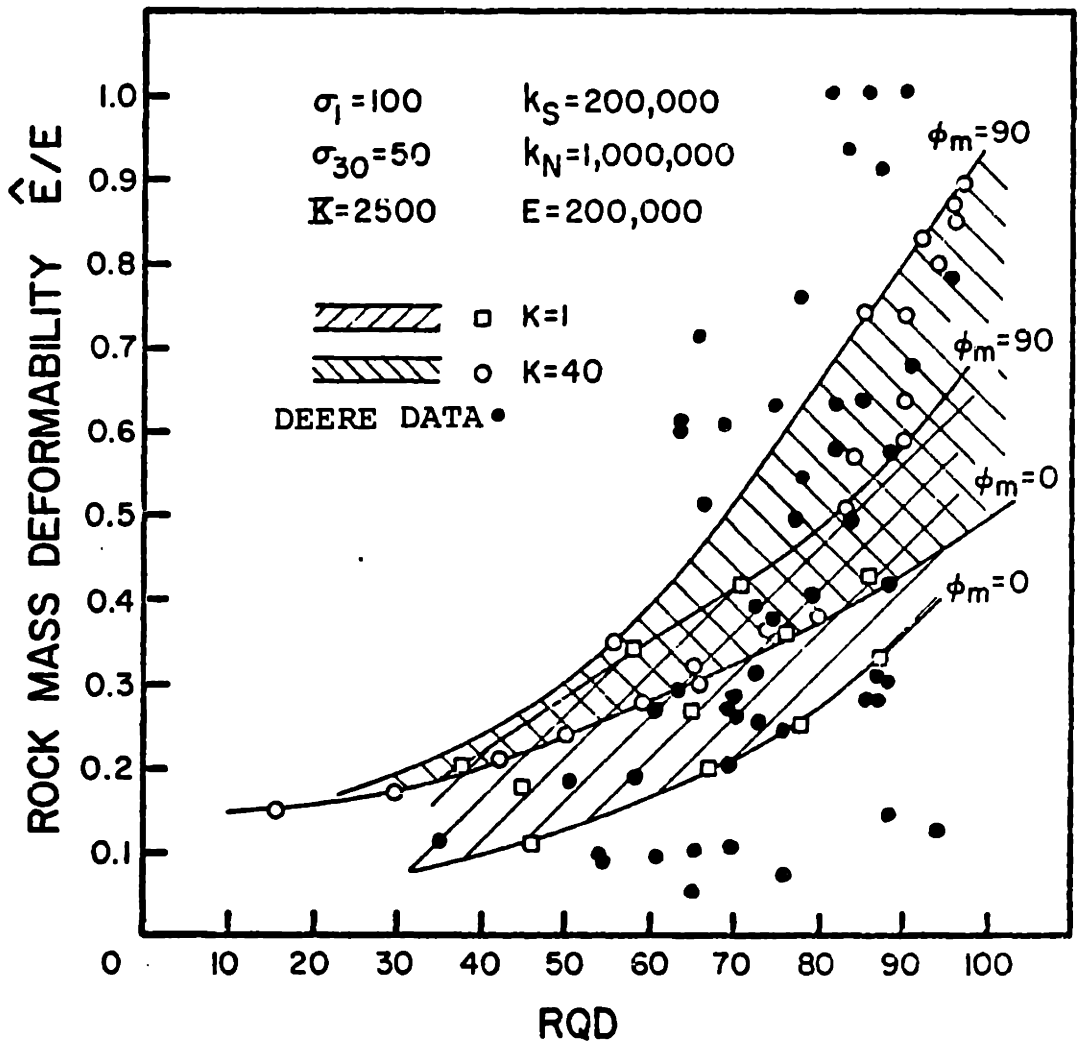

Figure 5.8.8 Rock Mass Deformability Predicted from RQD (Probabilistic Geometry)

obtained from deterministic and probabilistic description of rock joints. With deterministic description, results are extremely similar to Deere's, while with probabilistic description only the general trend of Deere's correlation appears. There are several possible explanations for this. The most obvious explanation is that Deere's correlation was developed from rock masses in which joints were almost perfectly parallel, so that his results do in fact arise from deterministic data. This is possible, considering the limited number of sites upon which Deere's work was based. Another explanation is that the Deere's correlation is correct and that the rock mass deformation model works for parallel joints but fails for Fisher-distributed joints because of strain compatability problems and interference between joint deformations in the probabalistic models.

The differences between the probabilistic model RQD-$\hat{E}$/E correlation and Deere's correlation could also be due to errors in Deere's correlation. Deere's correlation depends upon in-situ measurements subject to considerable error, and may not represent general rock mass deformation behavior. Deere's correlation may represent measurement bias rather than a true correlation.

General agreeement between the <u>trend</u> of the probabilistic RQD-$\hat{E}$/E model and Deere's correlation, however, indicates that the trend of Deere's correlation is correct, but is subject to

greater uncertainty for large RQD, as indicated by Figure 5.8.8. The actual RQD-$\hat{E}/E$ curve appears to depend upon stiffness and the degree of variability of the rock joint geometry.

5.9 Conclusions

Examples of application of the constrained cylinder model with both deterministic and probabilistic input assumptions demonstrate the advantages of the use of deterministic and probablistic models.

Deterministic models most clearly show parameter effects and boundary condition effects, since the effect of individual parameter values can be studied. In addition, deterministic models can show the effect of parameter uncertainty by comparison of results for different possible parameter values.

Probabalistic models, on the other hand, incorporate the effect of parameter uncertainty and spatial variability directly. Therefore, probabalistic models can graphically illustrate the importance of uncertainty and variability, and the sensitivity of results to the level of uncertainty or variability.

Models are useful for the study of parameter effects. Model studies in this Chapter show the influence of stiffness, joint orientation, and joint spacing on rock mass deformation. Models are also useful for the study of deformation mechanisms, and for the study of the underlying mechanism of correlation. Model studies in this chapter explored the deformation mechanism of jointed rock masses, and the mechanism behind the

correlation between RQD and deformability. Models can also be used to check the validity of boundary conditions and assumptions used in the models. Boundary conditions and assumptions where both studied in this chapter, and the limitations of model results were thereby clarified.

CHAPTER 6

SUMMARY AND CONCLUSIONS

6.1 Summary

Probabilistic models for jointed rock mass deformation were developed and the implications of the models for prediction of rock mass deformability were studied.

The probabilistic models were based upon improved probabilistic descriptions of rock masses and upon analysis of the mechanism of rock mass deformation. Rock masses were described probabilisticly by assumption of appropriate distributions for rock joint geometries. The mechanism of rock mass deformation was analyzed by separation of the deformation into intact and joint components.

Probabilistic models were used to study the rock deformation process, to analyze the effect of probabilistic assumptions upon model behavior, and to study the mechanism behind a commonly used empirical method for prediction of rock deformability, Deere's RQD - Deformability correlation.

6.2 Conclusions

Rock mass deformation is currently predicted primarily by simple empirical correlations. Understanding of rock mass deformation, and therefore our ability to predict, can be improved through the development and study of realistic models.

6.2.1 Rock Mass Models

The usefulness of current rock mass models is limited because they

- o Depend upon deterministic assumptions of rock mass properties.
- o Use parameters not commonly or easily measured.
- o Amalgamate the behavior of intact rock and rock joints so that the effect of joints cannot be independently assessed.
- o Assume overly simple material properties.
- o Do not incorporate spatial variability.

Improved models for rock masses developed here

- o Use probabilistic descriptions of rock masses.
- o Separate the influence of intact rock and joint, and model each according to observed behavior.

6.2.2 Description of Rock Masses

Rock masses can best be described probabilisticly. Probabilistic description allows incorporation of the effects of spatial variability and parameter uncertainty. Rock joint geometry plays an important role in deformation and it is therefore important to describe it as fully as possible. The appropriate distribution for spacing and trace length appears to be the exponential. No adequate distribution has been found for joint orientation. The Fisher distribution, however, appears to be adequate for two-dimensional modeling purposes of

axisymmetric cases because it is a reasonable representation for spherical orientation data and because of its mathematical convenience.

6.2.3 Models for Rock Mass Deformability

Probabilistic models developed on the basis of measurable rock properties, accurate probabilistic descriptions, and a coherent analysis of the mechanics of both intact rock and rock joints:

- o Allow the determination of the sensitivity of deformability to different measurable engineering and geologic properties
- o Facilitate the study of the roles of intact rock and rock joints in rock-mass deformation.
- o Can be used to study the role of joint geometry and spatial variability upon behavior.

6.2.4 Examples of Model Use

Model studies demonstrated that:

- o Rock mass deformability is extremely sensitive to joint geometry. Spacing, orientation and spatial variability are all major influences.
- o Joint stiffness has a major effect upon deformability but the effect is secondary to that of joint geometry.
- o Deere's RQD - Deformability correlation and other empirical methods for predicting RQD can be analyzed through the use of appropriate models. Deere's RQD is con-

sistent with current results in the case of parallel joints. For disperse joints, however, the variance of the correlation increases dramaticly.

REFERENCES

1. Agterberg, E.P. (1976) Geomethematics, Elsevier, New York.

2. Arnold, K.J. (1941) An Spherical Probability Distributions, Ph.D. dissertation, M.I.T.

3. Baecher, G.B. and N.A. Lanney (1978) "Trace Length Biases in Joint Surveys," 19th U.S. Symposium on Rock Mechanics, pp 56-65.

4. Baecher, G.B., N.A. Lanney and H.H. Einstein (1977) "Statistical Description of Rock Properties and Sampling," 18th U.S. Symposium of Rock Mechanics 5C1-8.

5. Baecher, G.B., H.H. Einstein, W.S. Dershowitz, E.G. Glynn, N.A. Lanney, G.L. Maloney (1978), Risk Analysis for Rock Slopes in Open Pit Mines, M.I.T. Civil Engineer-Technical Report A78-7.

6. Baecher, G.B., H.H. Einstein, et al. (1979), Final Report: Risk Analysis for Rock Slopes in Open Pit Mines. M.I.T. Civil Engineering Technical Report.

7. Barton, N. (1975), "Suggested Methods for the Description of Rock Masses and Discontinuities," 2nd Draft, ISRM Working Paper, Category 19, 110.

8. Barton, N. (1976), "The Shear Strength of Rock and Rock Joints," Int. Jour. of Rock Mechanics and Min. Sci. and Geomech.Abstr.Vol. 13, No. 9, 9/76, pp 255-279.

9. Benjamin, J.R. and C.A. Cornell (1970), Probability, Statistics, and Decision, for Civil Engineers, New York, McGraw Hill.

10. Beiniawski, Z.T. (1975), "Case Studies: Prediction of Rock Mass Behavior by the Geomechanics Classification." Second Australia-New Zealand Conference on Geomechanics, Brisbane, 1975. The Institution of Engineers-Australia National Conference Publication 75/4.

11. Beiniawski, Z.T. (1978), "Determining Rock Mass Deformability: Experience from Case Histories," Int. J. Rock Mech. and Mining Sci. and Geomech. Absts. Vol. 15 10/78 pp 237-248.

12. Billings, M. (1972), Structural Geology, Prentice Hall, Englewood Cliffs, New Jersey.

13. Bingham, C. (1964), Distributions on the Sphere and on the Projective Plane. Unpublished Ph.D. dissertation, Yale University, New Haven, Ct.

14. Bingham, C. (1974), "An Antipodally Symmetric Distribution on the Sphere," The Annuals of Statistics, Vol. 2, No. 6 (1974), pp 1201-1225.

15. Bingham, M.S. and K.V. Mardia (1975), "Maximum Likelihood Characterization of the von Mises Distribution," In GP Patil et al. (eds) Statistical Orientations in Scientific Work, V.3, pp 387-398. D. Reidel Pub. Co., Dodrecht, Holland.

16. Borowicka, H. (1936), "Influence of Rigidity of a Circular Foundation Slab on the Distribution of Pressures over the Contact Surface", Proc. First Int. Conf. Soil Mech. and Fdn. Eng., 1936, Vol. 2, p 144.

17. Boughton, N. (1968), "Correlation of Measured Foundation Modulus with the in-situ Rock Properties," Madrid-68 International Symposium of Rock Mechanics.

18. Boussinesq, J. (1883), Comptes Rendues, V. 97, p 843.

19. Breitenberger, Ernst (1963), "Analogues of the Normal Distribution on the Circle and the Sphere," Biometrica Vol. 50, No. 1 (1963) pp 81-88.

20. Bridges, M.C. (1976), "Presentation of Fracture Data for Rock Mechanics," 2nd Australia-New Zealand Conference on Geomechanics, Brisbane, pp 144-148.

21. Bridges, M.C. (1977), "Statistical Analysis of Clusters of Orientations," Unpublished Ph.D. dissertation.

22. Burman, B.C. and R.D. Hammett (1976), "Design of Foundations in Jointed Rock Masses," in Second Australia-New ZealandConference on Geomechanics, p 83-88.

23. Call, R.B., J. Savely, D.E. Nicholas (1976), "Estimation of Joint Set Characteristics from Surface Mapping Data." 17th U.S. Symposium of Rock Mechanics pp 2B2-1 - 2B2-9.

24. Calladine, C.R. (1969), Plasticity, Pergainon Press.

25. Cawsey, David, C. (1977), "The Measurement of Fracture Patterns in the Chalk of Southern England." Engineering Geology, Vol. 11 (1977), pp 201-215.

26. Chayes, F. (1949), "Statistical Analysis of Fabric Diagrams," in H.W. Fairbairn, Structural Petrology of Deformed Rocks, Addison-Wesley Press, Cambridge, MA, pp 297-326.

27. Chayes, F. (1954), "Effect of Change of Origin on Mean and Variance of Two-Dimensional Fabrics." American Journal of Science. Vol. 252, (9/1954) pp 567-570.

28. Coon, D. F. and A.H. Merritt (1970), "Predicting In Situ Modulus of Deformation Using Rock Quality Indexes," in Determination of the In Situ Modulus of Deformation of Rock, ASTM STP 477, American Society for Testing and Materials, pp 154-173.

29. Crandall, S.H. and N.C. Dahl (1959), An Introduction to the Mechanics of Solids. New York; McGraw Hill,

30. Cruden, D.M. (1977), "Describing the Size of Discontinuities," Int. J. Rock Mech. Min. Sci. and Geomech. Abstr. Vol. 14, pp 133-137.

31. Cruden, D.M. and H.A.K. Charlesworth (1976), "Errors in Strike and Dip Measurements." Geological Society of America Bulletin. Vol. 87, (7/1976) pp 977-980.

32. Deere, D.U. (1964), "Technical Description of Rock Cores for Engineering Purposes," Rock Mechanics and Engineering Geology, V. 1., N 1, 1964, pp 17-21.

33. Deere, D.U., A.J. Hendron, D.F. Patton, E.J. Cording (1967), "Design of Surface and Near Surfaces Construction in Rock," in Failure and Breakage in Rock. Proc. 8th Symposium Rock Mechanics AIM & ME, p 237-302.

34. Druker, D.C. (1959), "A Definition of Stable Inelastic Material," Transactions ASME Journal Appl. Mech. Vol. 26, No. 1.

35. Duncan, J.M. and R.E. Goodman (1968),"Finite Element Analyses of Slopes in Jointed Rocks," U.S. Army Waterways Experiment Station, Vicksburg, Miss. 5-68-3.

36. Fisher, Ronald, Sir (1953), "Dispersion on a Sphere," Proc. Royal Society of London, Series A, Vol. 217 A (7 May 1953) pp 295-305.

37. Fung, Y. (1965), Foundations of Solid Mechanics, Prenctice Hall, Englewood Cliffs, NJ.

38. Fung, Y. (1977), A First Course in Continuum Mechanics, Prentice Hall, Englewood, NJ.

39. Glynn, E.F. (1979), A Probabilistic Approach to the Stability of Rock Slopes, Ph.D. Dissertation, M.I.T., 2/79.

40. Goodman, R.E., R.C. Taylor, and T.L. Brekke (1968), "A Model for the Mechanics of Jointed Rock," ASCE JSMFD v. 94, SM3, pp 632-659.

41. Goodman, R.E. (1970), "The Deformability of Joints," in Determination of the In Situ Modulus of Deformation of Rock, ASTM STP 477, American Society for Testing and Materials pp 174-196.

42. Goodman, R.E. and JM. Duncan (1971), "The Role of Structure and Solid Mechanics in the Design of Surface and Underground Excavations in Rock." Proc. Conf. on Structure, Solid Mechanics, and Engineering Design, Pt 2, paper 105, p 1379 (Wiley).

43. Goodman, R.E. F.E., Heuze, Y. Ohnishi (1972), "Research on Strength - Deformability - Water Pressure Relationships for Faults in Direct Shear. Final Report on ARPH Contract H0210020. 4/72.

44. Goodman, R.E., T.K. Van and F. Heuze (1972), "The Measurement of Rock Deformability in Boreholes," Proc. 10th Symp. on Rock Mech. (AIME) pp 523.

45. Goodman, R. (1976), Methods of Geological Engineering in Discontinuous Rocks, West, St . Paul, Minnesota, 472 pp.

46. Goodman, R.E. and C. St. John (1978), "Static Finite Element Analysis of Jointed Rock," in Numerical Methods in Geotechnical Engineering, Christian and Desai, eds. McGraw Hill, New York.

47. Hungr O. and D.F. Coates (1978), "Deformability of joints and its relation to rock foundation settlements." Canadian Geotechnical Journal, Vol. 15, 1978, pp 239-249.

48. Iida, Ryuichi (1968), "Mechanical Study on Displacement of Rock Mass," MADRID-68 Int. Symp Rock Mech., Madrid, pp 335-341.

49. Jennings, J.E. (1970), "A Mathematical Theory for the Calculation of the Stability of Open Cast Mines," Proceedings, Symposium on the Theoretical Background to the Planning of Open Pit Mines, Johannesburg, South Africa, p 87-102.

50. Jizba, Z. Dened (1953), "Mean and Standard Deviation of Certain Geologic Data," American Journal of Science Vol. 251 (12/1953), pp 899-906.

51. Kelker, D. and C.W. Langenberg (1976), "A Mathematical Model for Orientation Data from Macroscopic Cylindrical Folds," Mathematical Geology, Vol. 8, No. 5, (1976), pp 549-559.

52. Kiraly, L. (1969), "Statistical Analysis of Fractures (Orientation Density) Geologische Rundshau, Vol. 59 pp 125-151.

53. Kulhawy, F.H. (1978), "Geomechanical Model for Rock Foundation Settlement," ASCE J. G.E.D., 2/78, pp 211-227.

54. Kulhawy, F.H. (1975), "Stress Deformation Properties of Rock and Rock Discontinuities," Engineering Geology V. 9, (1975), pp 327-350.

55. Lanney, N.A. (1978), Statistical Description of Rock Properties and Sampling, SM Thesis, M.I.T., 253 pp.

56. Maranhoa, N. (1968), "Geometrical Characterization of Jointing of Rock Masses," Second International Congress of the International Association of Engineering Geology, V. 1-3.1-3.10.

57. Mardia, K. V. (1972), Statistics of Directional Data, Academic Press.

58. Mardia, K.V. (1975), "Characteriztion of Directional Data," in GP Patil et al. (eds) Statistical Orientations in Scientific Work, Vol. 3, pp 365-385. D. Reidel Pub. Co., Dodrecht, Holland,

59. Mardia, K.V. (1975), "Distribution Theory for the von Mises - Fisher Distribution and Its Applications," in G.P. Patil et al. (eds) Statistical Orientations in Scientific Work. Vol. 1, pp 113-130. D. Reidel Publ Co., Dodrecht, Holland.

60. Maury, L. (1970), "Distribution of Stresses in Discontinuous Layered Systems," Water Power, May/June.

61. McMahon, B.K. (1971), "A Statistical Method for the Design of Rock Slopes," Proc. 1st Australia-New Zealand Conf. on Geomechanics, V. II-B, pp 803-808.

62. Müller, L. (1933), "Unter Suchunger Uber Statistiche Kluftmessung," Geol. u. Bau., 5: 185.

63. Obert, L. and W.F. Duvall (1967), Rock Mechanics and Design of Structure in Rock, Wiley, New York.

64. Pell, PJN (1975), "Predicted Displacements of the Rock Foundations of a Major Arch Bridge," Sixth Regional Congerences for Africa on Soil Mechanics and Foundations Engineering, Durham, South Africa, 9/75, pp 207-212.

65. Phillipes, A. (1956), Introduction to Plasticity, Ronald, New York.

66. Pincus, H. J. (1961), "Analysis of Aggregates of Orientation Data," Bull. Geol. Soc. of America, 62: 81-130.

67. Priest, S.D. and J. Hudson (1976), "Discontinuity Spacings in Rock," Int. J. Rock Mech. and Min. Sci., V. 13, pp 135-148.

68. Roberds, William and H.H. Einstein (1977), A General Purpose Elasto-Visco-Plastic Critical State Behavior Model. M.I.T. Civil Engineering Report R77-8

69. Roberds, W. and H.H. Einstein (1978), "Comprehensive Model for Rock Discontinuities," ASCE Journal of the Geotechnical Engineering Division, Vol. 104 GT5.

70. Robertson, A (1970), "The Interpretation of Geologic Factors for Use in Slope Stability," Proc. Symp. on the Theoretical Background to the Planning of Open Pit Mines..., Johannesburg, South Africa, pp 55-71.

71. Robertson, A.M. and D.R. Piteau (1971), "The Determinations of Joint Populations and their Significance for Tunnel Stability," in W. Cook (ed) The Technology and Potential of Tunneling.

72. Rocha, M. (1964), "Mechanical Behavior of Rock Foundations in Concrete Dams," Eight Int. Cong. on Large Dams, 1964, V. 1, pp 785-831.

73. Rodrigues, F. Peres (1968), "Determination of Shear Throughout the Rock and Slide Along Joints," MADRID-68 International Symposium on Rock Mechanics, Madrid, 1968, pp 175-182.

74. Rosso, R.S. (1976), "A Comparison of Joint Stiffness Measurements in Direct Shear, Triaxial Compression, and In Situ," Int. J. Rock Mech. Min. Sci. and Geomech. Abstr., Vol.13, pp 167-172.

75. Scott, R.F. (1963), Principals of Soil Mechanics, Addison Wesley, Reading, MA.

76. Seeler, Karl (1978), The Influence of Joint Intensity on the Strength of a Rock Model, M.I.T. Master of Science Thesis, 2/1978.

77. Shanley, R.J. and Mahtab, M. (1975), "FRACTAN: A Computer Code for Analysis of Clusters Defined on a Unit Hemisphere," USBM RI8671.

78. Shanley, R.J. and M.A. Mahtab (1976), "Delineation and Analysis of Centers in Orientation Data,: Mathematical Geology, Vol. 8, No. 1 (1976), pp 9-23.

79. Stagg, K.G. and O.C. Zienkiewicz (1968), Rock Mechanics in Engineering Practice, Wiley, New York.

80. Steffen, O.K.H. and J.E. Jennings (1974), "Definition of Design Joints for Two-Dimensional Rock Slope Analyses." Proceedings, Third ISRM Congress, VII part B pp 827-832.

81. Terzaghi, Ruth D. (1964), "Sources of Error in Joint Surveys, Geotechnique , V. 15, No. 3, pp 287-304.

82. Timoshenko, S. (1955), Strength of Materials, Van Nostrand, New York.

83. Timoshenko,S.and, N. Goodier (1951), Theory of Elasticity McGraw Hill, New York.

84. Timoshenko,S and, D.M. Young (1951), Engineering Mechanics, McGraw Hill, New York.

85. Veneziano, D. "Probabilistic Model of Joints in Rock," Manuscript submitted for publication in Geotechnique.

86. Vistelius , A.B. (1966), Structural Diagrams, Pergamon Press 176, p.

87. von Mises, R. (1918), "Uber die Ganzzahligkeil der Atomgewicht und verwandte Fragen." Physikal. Z. V 19 pp 490-500.

88. Watson, G.S. (1956), "Analysis of Dispersion on a Sphere," Monthly Notes of the Royal Astronomical Society Geophysical Supplement, Vol. 7, No. 4, (8/1956) pp. 153-161.

89. Watson, Geoffrey,S. (19), "The Statistics of Orientation Data," Journal of Geology, Vol. 74, pp 786-797.

90. Watson, Geoffrey,S.(1970), "Orientation Statistics in the Earth Sciences," Bulletin Geol. Inst. Univ. Upoala, Nova Scotia, Vol 2. No. 9, pp 73-89.

91. Watson, G.S. and E. Irving (1957), "Statistical Methods in Rock Magnesium," Monthly Notes of the Royal Astronomical Society Geophysical Supplement. Vol. 7., No. 6, (11/1957) pp 289-300.

92. Wu, T.H. and E.M. Ali (1978), "Statistical Representation of Joint Roughness," Int. J. of Rock Mech. and Min Sci. and Geomech. Abstr., V. 15, no. 5, 10/78, pp 259-262.

93. Yip, C.K. (1979), Shear Strength and Deformability of Rock Joints, SM Thesis, M.I.T., 6/79.

APPENDIX A

ROCK MASS DEFORMABILITY LITERATURE

This appendix presents a summary of published results relevant to the study of rock mass deformability models. No attempt is made to provide a rigorous survey, but most important research is presented and discussed.

Research covered by this appendix is divided into four sections. Section A.1 presents some different methods used to describe rock jointing, Section A.2 provides further discussion of RQD, an important index parameter for rock jointing. Section A.3 describes field experimental and empirical methods for determining rock mass deformability. Section A.4 presents experimental studies of rock joint stiffnesses and their results.

A.1 Description of Joints

Rock joints, strictly speaking, include only regular rock fractures across which no movement has occurred (Billings, 1972). Here the term joint will be used to include all types of discontinuities in rock. These include joints, sheared zones, crushed zones, seams, cleavage planes and openings along bedding, schistocity and foliation planes. (Goodman, 1970) This, most general sense is used throughout this survey.

Joint planes have a variety of geometries. They are normally planar and regular, though they can sometimes be curved (Billings, 1972). Figure A.1.1 illustrates sedimentary joint plane types according to Bassarab(1970).

Rock joints are generally imbedded in rock masses, so observations must be made either at the surface of the rock mass in a line or circle survey or in a boring into the rock mass. Problems of biase resulting from these forms of observation are discussed by Terzaghi (1964), Baecher, Lanney and Einstein (1977), and Baecher and Lanney (1978), Robertson (1970) and Cruden (1977). Despite these biases, however, borings and surface surveys provide our only source of information.

Boring results are a useful source of information about joints in situ. Borings can be used to obtain brief lithological descriptions of rock masses and a qualitative description of joints and faults. Core recovery, the percentage of any core which actually reaches the surface, is an indication of rock joint intensity, subject to drilling procedures. Thus boring logs should contain information about the type of drilling since it may effect results (Coon & Merritt, 1970). Recovered cores reveal the nature of rock joints within the rock mass. Coon and Merritt (1970) separate broken surfaces in cores into four categories:

1) Clean, irregular surfaces which can be rejoined almost perfectly (breaks during coring)

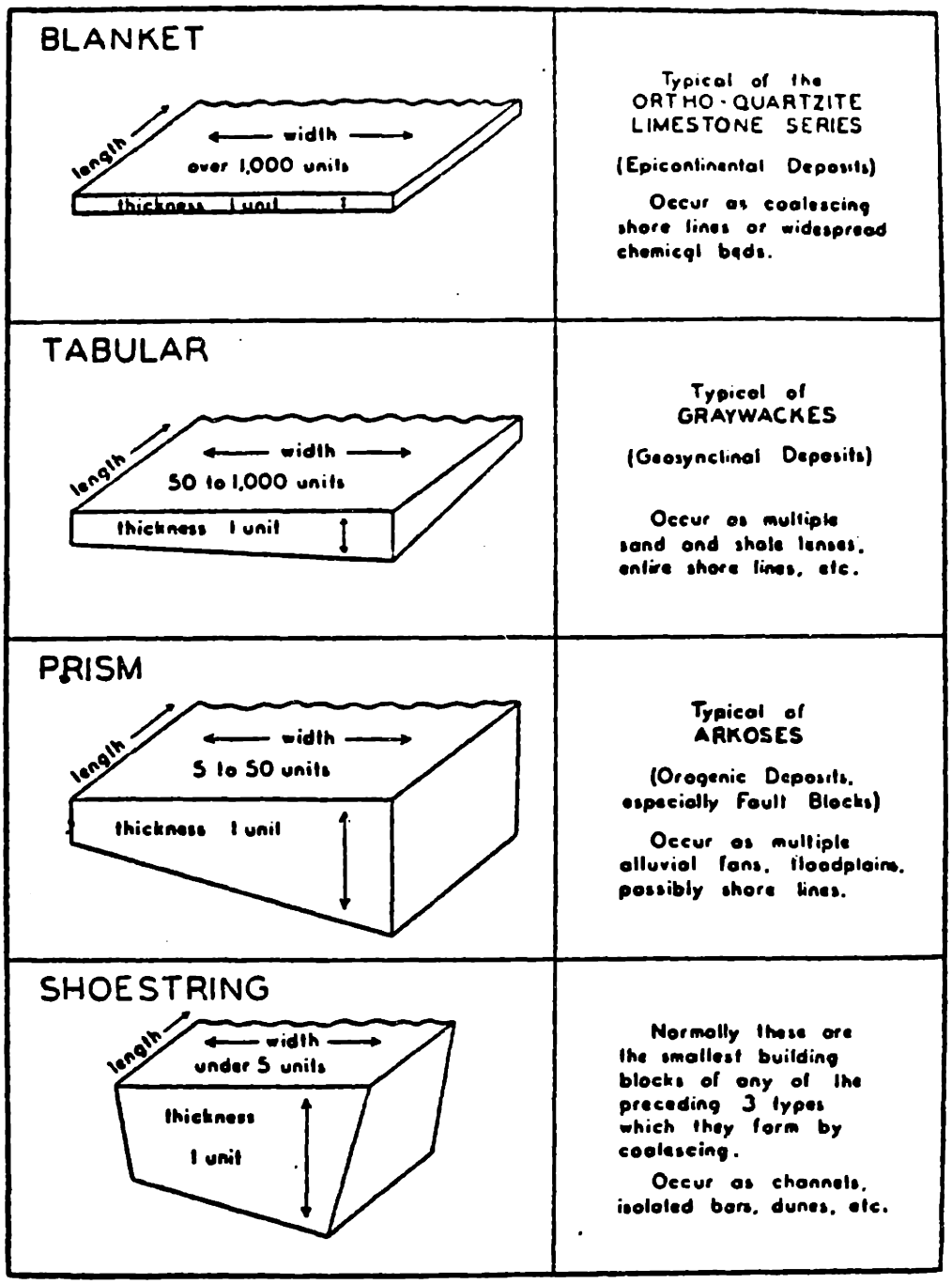

Figure A.1.1 Sedimentary Joint Plane Types
Bassarab (1975)

2) irregular, rounded surfaces resulting from grinding ir in the core barrel

3) smooth surfaces which cannot be rejointed, but show nc sign of weathering (foliation, bedding plane)

4) surfaces showing weathering, hydrothermal alteration, or slickensides (fractures joint, shear zones).

Fracture frequency, the number of joints per unit length would be an excellent measure of joint intensity if it could be measured directly in rock cores. (Deere, 1967) Unfortuna core recovery is rarely good engough to determine fracture fre quency directly. Fracture frequency can be correlated to som index properties such as RQD, discussed below.

In 1967, Deere developed the concept of a modified core recovery ratio which would be correlated with fracture freque He called his index, Rock Quality Designation. Deere (1967) defines RQD as follows:

> "The RQD is a modified recovery percentage in which all pieces of sound core over 4 in. long are counted as recovery. The smaller pieces are considered to be due to close shearing, jointing, faulting, or weathering in the rock mass and are not counted."

RQD is lower for higher fracture frequencies and higher for lower frequencies, regardless of drilling procedure, and thus has a clear advantage over unmodified core recovery. Deere's procedure includes breaks caused by the drilling proces as fractures,since they are indicative of rock weakness. Such breaks generally occur, according to Deere, along pre-existing planes of weakness.

> "The RQD ... evaluates fractures in the core caused by the drilling process, as well as natural fractures previously existing in the rock mass. For example, when the core hole penetrates a fault zone or a joint, additional breaks may occur which, although not natural fractures are caused by the natural planes of weakness existing in the rock mass. These breaks should be included in estimating rock quality." (Deere, 1967)"

Deere's RQD is still sensative to drilling porcedure, but to a smaller extent then core recovery ratio.

Deere used experimental data to relate RQD to fracture frequency. The resulting relationship is shown in Figure A.1.2. Deere observed that fracture frequency and RQD were related most clearly for unweathered rock masses degraded only by fracturing.

Other than core and surface logging, the only practical method available for exploring joint in rock masses is geophysical testing. Geophysical tests include sonic and seismic logging of boreholes, continuous velocity logging, up-hole and cross-hole seismic surveys, and seismic refraction testing at the surface and in tunnels. These are discussed in detail in testbooks such as Stagg & Zienkewicz (1968) and in Coon and Merritt (1970). Deere (1967) prefers Seismic Pulse Attenuation Velocity ratio as a geophysical measurement of joint properties, and has correlated it to his RQD (Figure A.1.3). Velocity Ratio is found by sending a constant energy seismic pulse from one borehole to another, at many different levels in the borehole, and measuring received pulses. Velocity ratio is the ratio of received to transmitted pulse, and is an indication of rock quality. In perfect rock, received velocity

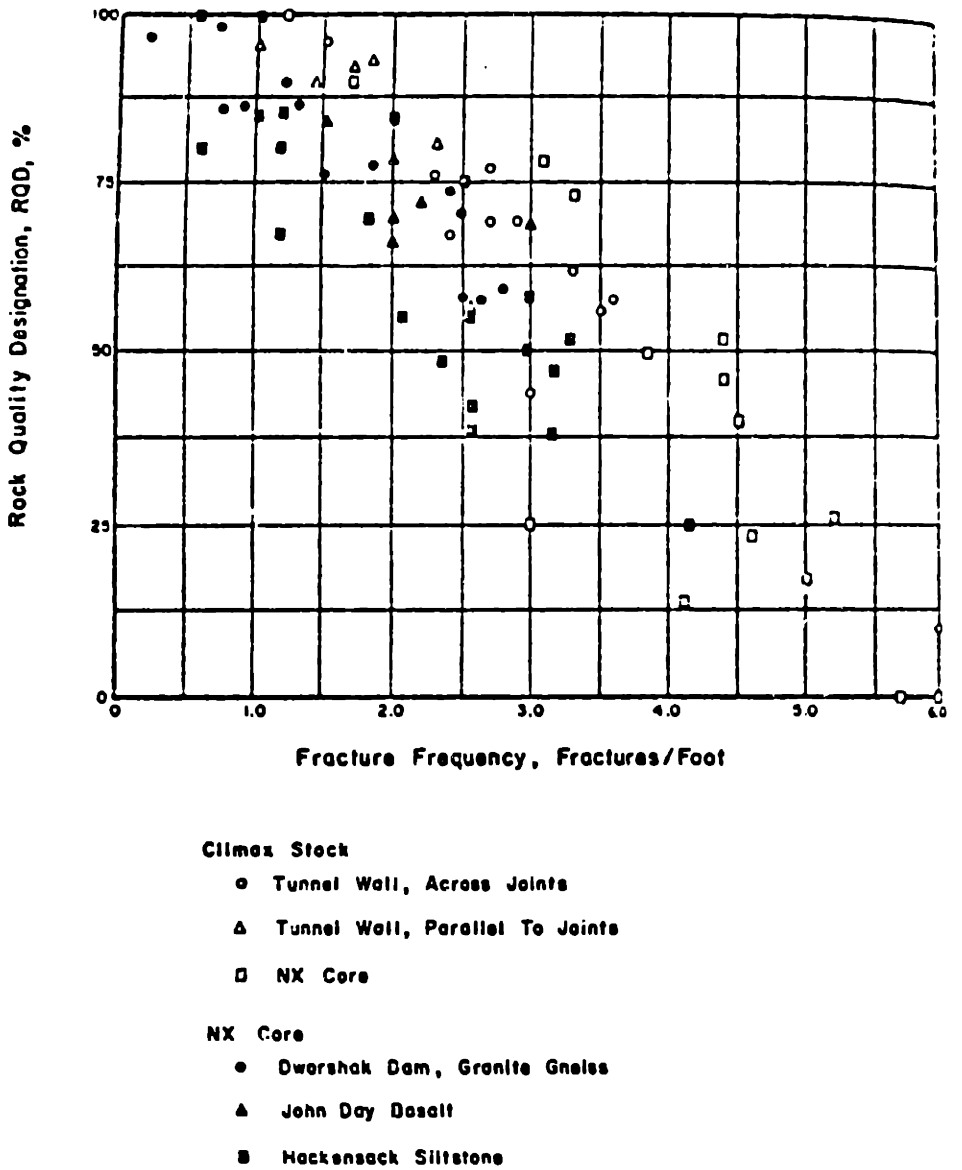

Fig. 6—Correlation of rock mass quality indices: fracture frequency and RQD

Figure A.1.2 RQD-Fracture Frequency Relationship (Deere, 1967)

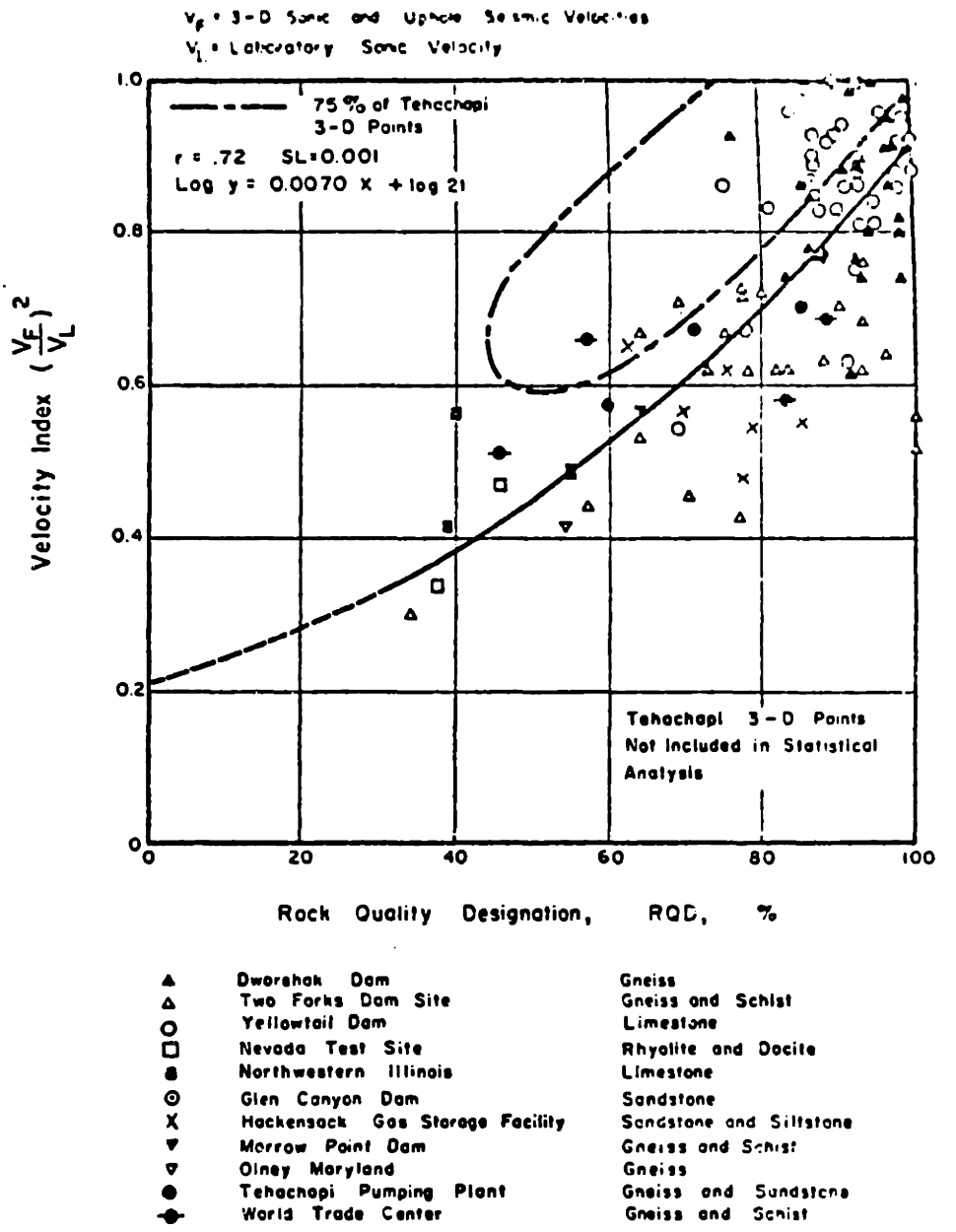

Figure A.1.3 RQD-Velocity Ratio V_F/V_L Correlation (Deere,1967)

equals transmitted velocity (VR = 1). For completely broken rock almost no signal would be received (VR = 0). Velocity Ratio is therefore correlated with fracture frequency.

RQD is generally accepted as an index property for rock joint intensity. Many correlations have been developed between RQD and rock mass behavior on design. The next section discusses RQD in greater detail.

A.2 RQD

While RQD is clearly correlated to joint density λ (where $\lambda = 1/s_m$ and s_m = mean joint spacing) other joint attributes such as orientation and joint opening must also be considered. At the Nevada Test Site, Deere measured RQD's at two different orientations in the Climax Stock granite formation with only one principal jointing direction. Parallel to the joint system, he found an RQD of 85%. Across the joint system, he found an RQD of 63% (Deere, 1967). This shows that RQD is clearly related to orientation. Little attention has been given to this fact in the literature. The question of RQD-orientation relationships is discussed in greater detail in Chapter 3. Although core recovery and therefore RQD is affected to a certain extent by joint opening or width, the effect is usually minimal. Therefore joint width must be measured separately. Mathematical models for RQD generally show only the relationship of RQD to fracture frequency or mean spacing s_m. The mathematical definition of RQD in

discrete form is (Kulhawy, 1973):

$$RQD = 100 \sum_{i=1}^{N} x_i/L \qquad \text{(A.2.1)}$$

where N = expected number of joints = $L/E[s]$

x_i = length of recovered piece of over 0.1m

L = total length of core, typically 1.5m.

In continuous, integral form,

$$RQD = 100 \int^{N} \frac{sf(s)ds}{L} \qquad \text{(A.2.2)}$$

where f(s) = distribution of joints of greater than o.1m.

Most rock mass models assume constant spacing equal to the mean spacing. Kulhawy (1978) pointed out that these models result in RQD values of either 0% or 100% only, depending upon whether the joint is longer or shorter than 0.1m (4").

This dilemma is avoided by models derived from:

1) Spacing-RQD curves derived from empirical results;
2) Statistical or probabilistic models;
3) "Simple physical/geometric models," which could be "hypothesized to relate RQD to the number of discontinuities per core run."

The first method was adopted by Deere (1967). His results are shown in Figure A.1.2. A statistical model was developed by Priest and Hudson (1975) based upon the assumption

of an exponential distribution for spacing. Their method is expanded in Chapter 3. Kulhawy apopted the third approach, and developed a geometrical model.

Priest and Hudson developed their model for RQD as follows. Given a distribution of discontinuity spacings $f_s(s)$, a scanline of length L, and a mean spacing λ^{-1}, the total number of discontinuities is λL.

Therefore the number of intact lengths between x and $x+\Delta x$ is $\lambda L f(x)dx$. From the definition of RQD (equation A.2.1) RQD in the continuous case can be represented by

$$\text{(A.2.3)} \qquad RQD^* = \int_t^L \lambda L s f(s)ds/L$$

where t=minimum length of intact core counted in RQD. With an exponential distribution of spacing,

$$\text{(A.2.4)} \qquad RQD^* = 100\lambda^2 \int_t^L x e^{-x} dx$$

For large L, terms containing $e^{-\lambda L}$ can be ignored and

$$\text{(A.2.5)} \qquad RQD^* = 100\ e^{-\lambda t}(\lambda t+1)$$

For the standard RQD, minimum length t=0.1m.

(A.2.6) RQD* $RQD^{*}=100e^{-0.1\lambda}(0.1\lambda+1)$

Kulhawy (1978) developed his model on the premise that "discontinuities can be represented by an accumulation of uniformly spaced discontinuity sets, and that the superimposition of those sets account for the randomness of spacing found in the rock mass."

Kulhawy implimented his model assumption by genetating uniformly spaced joint sets containing i, i=1,2,.... , ∞ discontinuities. Each joint set has a spacing L/i where L, the core length, is assumed to be 1.5 meters. These joint sets are added together starting from i = 1 until the desired average spacing is obtained. RQD can then be calculated. The model is peresented graphicly in

Figure A.2.1. The spacing-RQD curve resulting from the model is shown in Figure A.2.2.

Kulhawy attempted to take sampling problems into account. The two sampling processes are shown in Figure A.2.3. In the first process, he assumes that the bottom 10% of the cores are always lost. In the second process, he assumes that the sample may begin anywhere in the top half of the core. Results of these sampling assumptions are shown in Figure A.2.3.

Kulhawy's model is fit against Priest and Hudson's model and Deere's empirical results in Figure A.2.4. Although correspondence between the three models appears to be good, there are reasons to prefer Priest and Hudson's probabilisticly based model to Kulhawy's. Kulhawy's model depends upon an ad hoc assumption about the jointing process. This assumption has not been verified and is not suggested by analysis of jointing such as Billings (1972). Priest and Hudson's assumptions of exponential spacing can be derived from the assumption that joint location is perfectly random. Thus, it is based on a stochastic process model. Furthermore, equation (A.2.3) can be in principle applied to any spacing distribution.

A.3 Rock Mass Modulus of Deformation

The modulus of deformation (σ applied/ε resulting) of rock masses is considerably less than the modulus of intact rock. This is, in part, because while laboratory specimens may ade-

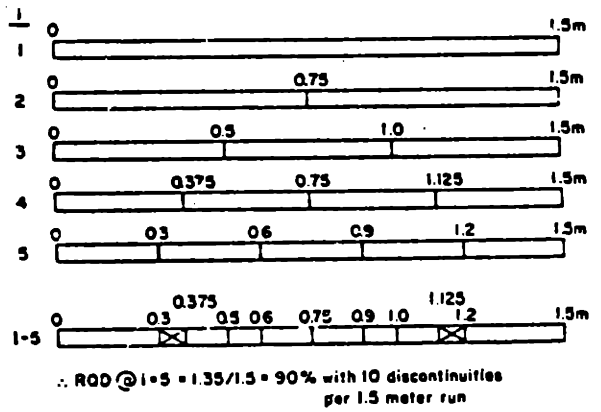

Figure A.2.1 Model for RQD Process(Kulhawy,1978)

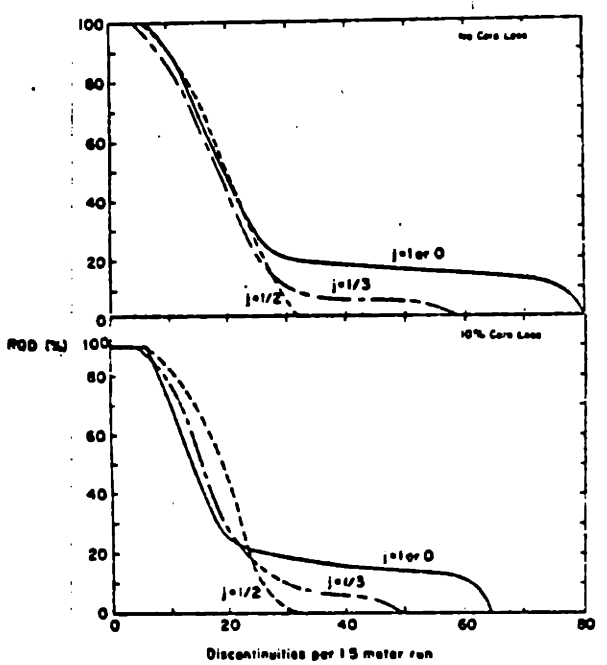

FIG. 8.—Variation of RQD with Number of Discontinuities per 1.5-m Run

Figure A.2.2 Spacing-RQD Correlation Predicted from Model (Kulhawy,1978)

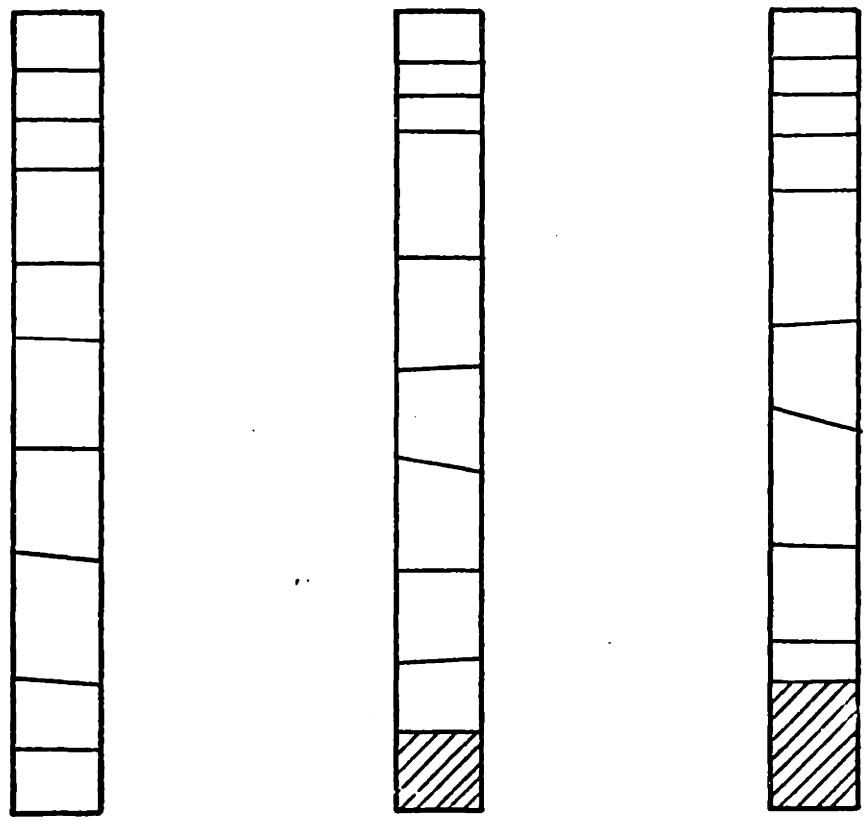

Perfect Sampling: No Loss.

Bottom 10% Lost

Random Percentage of Bottom Lost.

Figure A.2.3 Alternative RQD Sampling Process Models

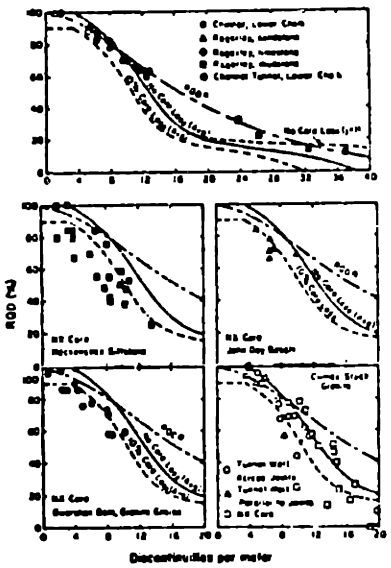

FIG. 10.—Correlation of Proposed RQD Model with Several Data Sets (Data from Refs. 4 and 13)

Figure A.2.4 Comparison of Kulhawy(1978) Model for RQD with Empirical Results (Deere,1967) and Mathematical Model (Priest & Hudson,1975)

quately represent the intact rock material itself, they do not include rock defects such as joints and faults, which have a very profound effect upon deformability. Slippage and rotation of rock blocks along discontinuities often create surface deflections greater than the deformation of the intact blocks themselves (Coon and Merritt, 1970). Mass or in situ modulus can be determined by three different methods. These include field tests, correlations with index properties, and mathematical and physical models. Models are discussed in Chapter 2.

A.3.1 Field Tests for Rock Mass Deformability

Field tests are discussed extensively in Stagg and Zienkewicz (1968) and in Deere (1967). Two common field tests for rock deformability are plate jacking tests and pressure chamber tests.

Plate jacking tests consist of the application of load to a rock mass surface through a metal plate attached to a loading jack. Both load and deformation are then measured. Results of a typical plate jacking test are given in Figure A.3.1.

The size of the plate and the loading path used can have very significant effects upon the results of plate jacking tests. For instance, small plates have a small zone of influence and as a result tend to test only the rock mass near the loading surface. In addition, since stress-deformation in rock can be non-linear, stresses must be tested at design levels. In addition, $\hat{E}$, the mass modulus, can be calculated from the loading, unloading, or reloading portions of Figure A.3.1. Coon and

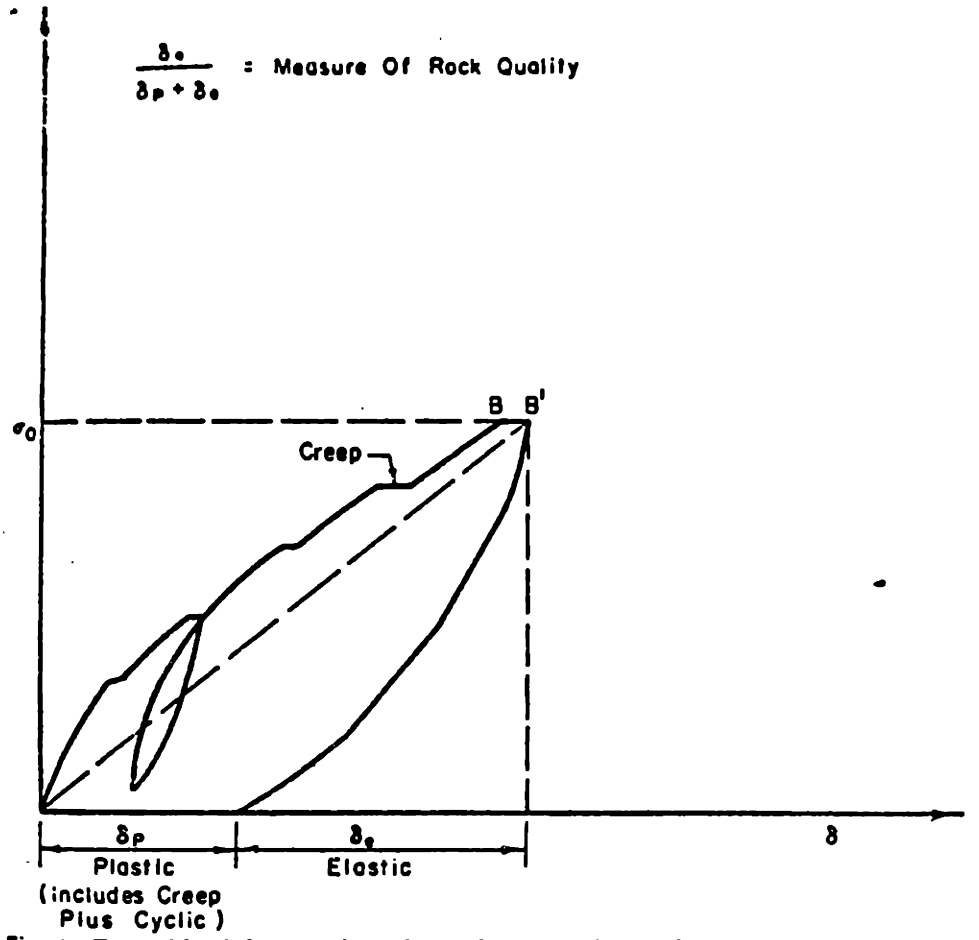

Fig. 10—Typical load-deformation relationship for a plate jacking or pressure chamber test.

Figure A.3.1 Typical Plate Jacking Test Results (Deere, 1967)

Merritt (1970) recommend the use of the reloading curve.

For small, cast iron plates, Deere (1967) presents the following relationship for mass modulus, based upon

$$\hat{E} = \frac{1}{2}\,\frac{P(1-\nu^2)}{\delta a} \qquad \text{(A.3.1)}$$

where P = total applied force
ν = Poisson's ratio
δ = displacement
a = radius of loading plate.

the Boussinesq solution. Small plates have the advantage of low cost, allowing repeated testing. Repeated testing improves both the statistical reliability of results and the ability to obtain information about spatial variation. Small plates have the disadvantage, however, of a small influence zone, and of shear deformations at the edge of the loading plate at high stress levels.

Both of these problems can be solved by use of large plates, but at the expense of many of the small plate advantages. Larger plates are more costly and therefore less repeatable. They are also more difficult to analyze because of uneven stress distributions resulting from the imperfect rigidity of larger plates. Borowicka (1936) found solutions for analysis of large plates with unequal stress distributions. Rocha (1955) developed a special apparatus which maintains even stress under a large loading plate by a hydraulic feedback system.

Pressure chamber tests are generally conducted on tunnel sections at least 5-6 diameters long, plugged and lined with an impermeable liner, and loaded by hydraulic pressure or flat-jacks along the tunnel perimeter. Deformations are read with diametrical extensometers or strain gauges. Modulus is found from pressure applied (P), and radial deformation d, based upon an assumption of Poisson's ratio

(A.3.2) $$E = \frac{P}{d} \frac{a^2}{r} (1 - \nu)$$

where E = Young's Modulus of Deformation

P = applied pressure

d = radial deformation

a = radius

r = distance of deformation measure from tunnel center

ν = Poisson's ratio

(Deere, 1967)

The pressure chamber test has many advantages. Unlike plate load tests, pressure chamber tests have substantial zones of influence and can be performed at stress levels comparable to those needed for design. Analysis of pressure chamber test results is easier than analysis of plate jack tests. The primary disadvantages of pressure chamber tests are restrictively high costs and technical problems involving pressure application, liner flexibility and permeability.

A.3.2 Empirical Correlations for Rock Mass Deformation

The use of index property-engineering property correlations is extensive in engineering. It is only natural that, when engineering properties are difficult to measure, correlations are sought with easily-measured index properties. In soil mechanics, important index properties such as Atterberg Limits and blow count are correlated to important engineering properties such as undrained strength s_u and deformability m_v. In rock mechanics, most index properties are taken from core logs and geophysical tests. Important correlations that have been made between core log indices and rock deformation include RQD (Deere, 1967), geomechanics classification (Bieniawski, 1975), and Joint Weathering Index (Boughton, 1968). The most important geophysical index correlation with deformation is velocity ratio (Deere, 1967).

Figure A.3.2 shows the correlation found between RQD and modulus ratio $\hat{E}/E$ developed by Deere (1967), and expanded by Coon and Merritt (1970). The correlation was based upon tests done at Dworshak dam using 20' NX cores for calculation of RQD and 34 uniform pressure pad plate jacking tests for $\hat{E}$. $\hat{E}$ was found by unconfined compression tests on intact core specimens. Deere weighted RQDs according to the stress level on each joint under the plate jacking test according to the Boussinesq stress distribution (Figure A.3.3) so that the effect of each joint upon RQD would be proportional to the effect of that joint upon plate jacking test results. Deere's correlation suffers from all the problems inherent in RQD and in plate jack testing, as

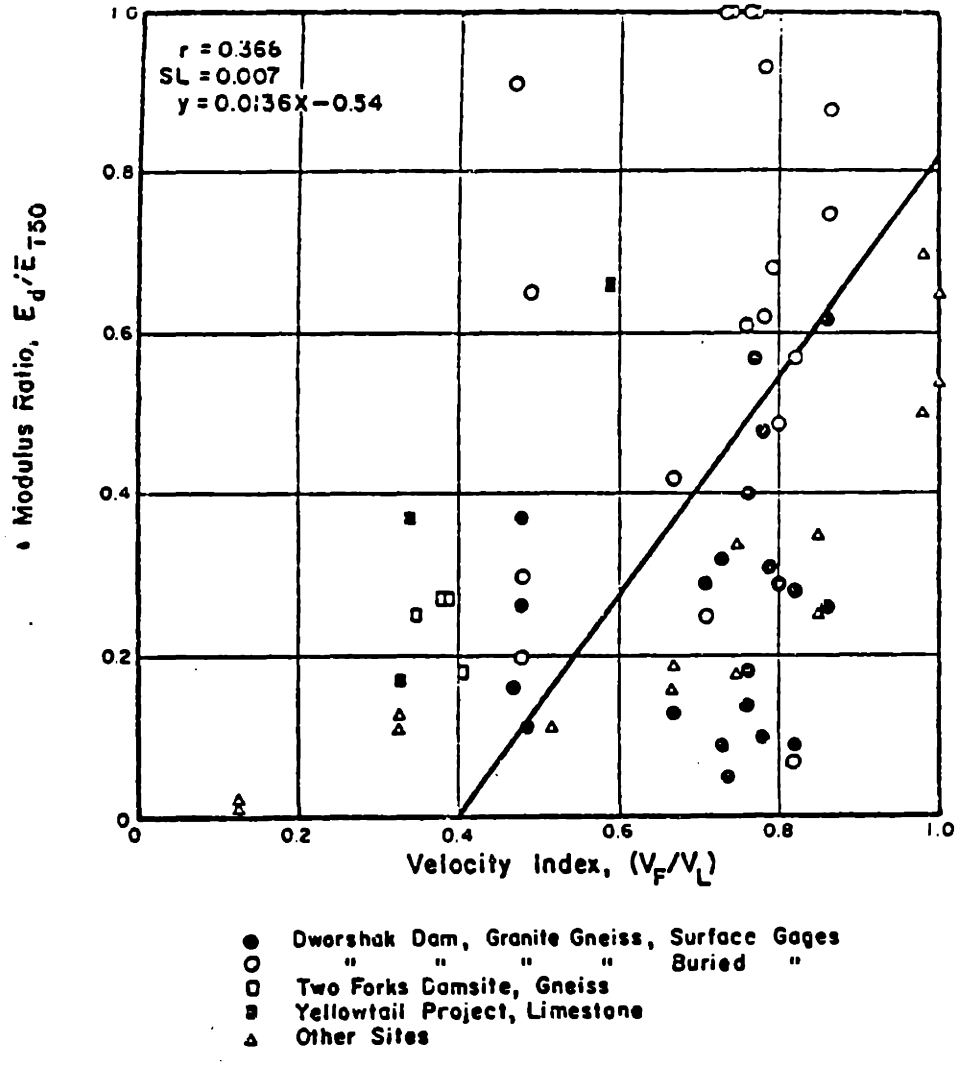

Figure A.3.2 RQD correlation to Modulus Ratio $\hat{E}/E$ from Field Tests (Coon & Merritt, 1970)

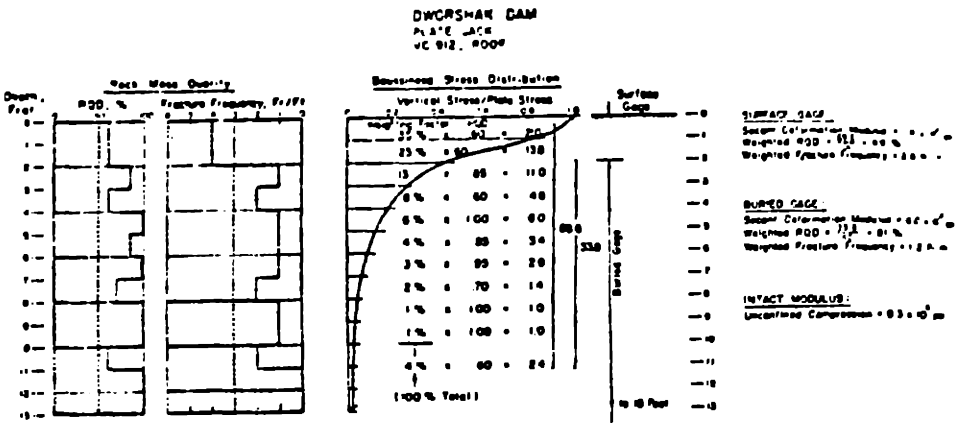

Fig. 14—Illustration of a method for obtaining a weighted rock quality beneath a plate jacking test.

Figure A.3.3 Method for Weighting RQD According to Stress Distribution(Deere,1967)

discussed above. In addition, there are problems due to variations in rock joint properties such as spacing and width, which affect $\hat{E}$ but are not fully described by RQD.

The shape of the $\hat{E}$/E-RQD curve is unusual, because it is basically bilinear, while such curves would be expected intuitively to be smooth polynomials. For RQDs less than 60%, the deformability appears to be ten times greater than that of intact rock, while for RQD greater than 60%, deformability varies from 5 to 1 times the deformability of intact rock. Thus, it appears that the higher the rock quality, the higher the variance in deformability. This is a most unexpected result, and indicates that RQD is an insufficient index for deformabiltiy - more information is needed to make an accurate prediction.

Plate load tests, as was stated earlier, are very sensitive to deformations at the very surface. RQD is not particularly sensitive to surface conditions, so some noise enters Deere's relation. In addition, deformation is sensitive to joint width, which is not adequately described by RQD, and to joint orientation, which may be included in RQD to some extent.

Still, $\hat{E}$/E-RQD correlation is reasonably good, and has been used in practice. An example of a practical use of RQD to find a deformation modulus of a use in design can be found in Pell (1975).

The velocity ratio V_F/V_L is well correlated with RQD. The velocity ratio should, therefore, be correlated to deformation modulus about as well as RQD. Figure A.3.4 from Deere (1967) shows the correlation. Note that it is significantly

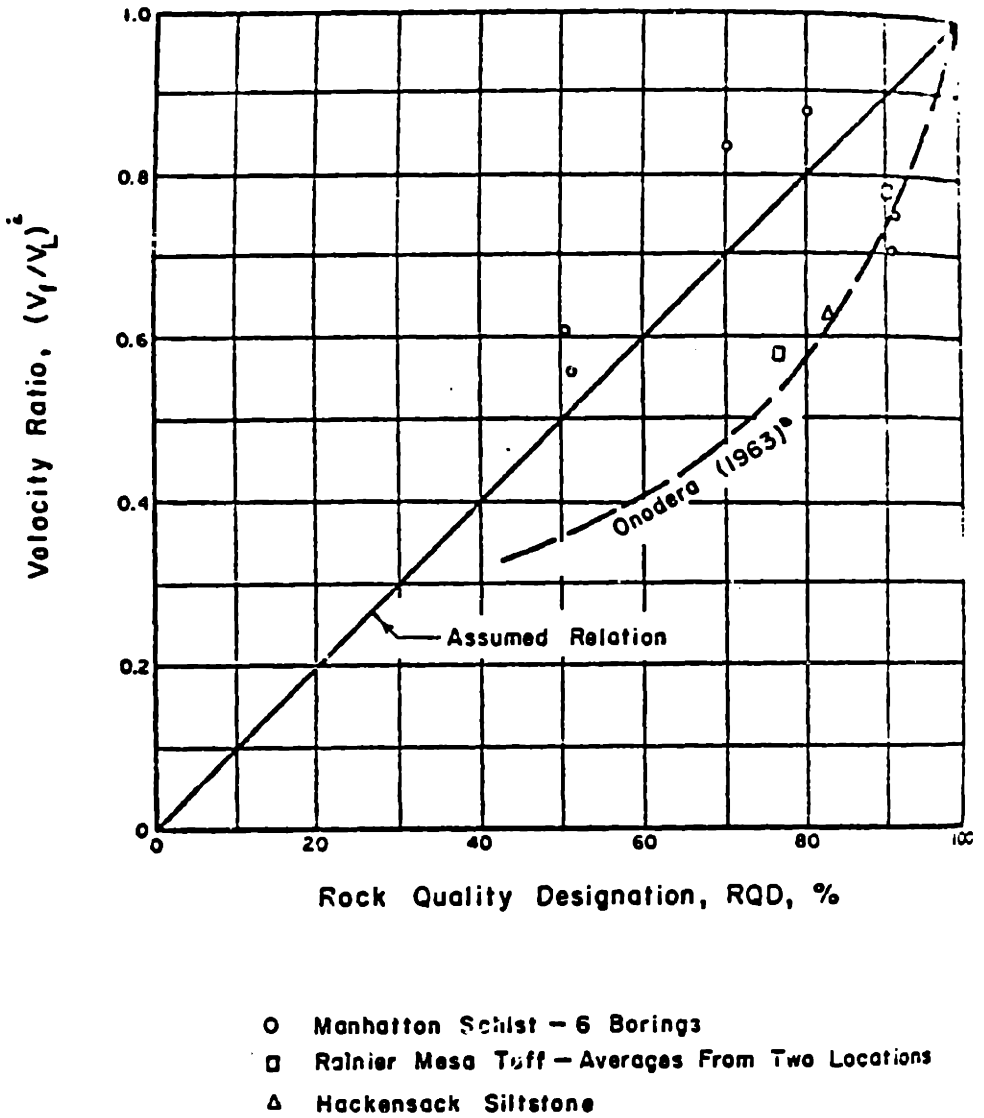

Figure A.3.4 RQD Correlation to Velocity Ratio (Deere,1967)

inferior to that of RQD. Several explanations have been put forward to explain this. Coon and Merritt attribute the discrepancy to the fact that RQD and plate load tests both measure small-scale effects, while velocity ratio measures effects over considerably larger volumes. According to their argument, smaller scale velocity indices weighted according to stress distributions would provide results comparable to those for RQD.

Another possible explanation is that joint orientation, which strongly affects deformability, is incorporated into RQD, while it is not incorporated comparably into velocity ratio, since RQD measures joints intersected by a vertical boring, while geophysical methods measure joints intersected by semi-horizontal soundings. This is illustrated in Figure A.3.5.

Another index which has been correlated with deformability is the Geomechanics Index (Bieniawski, 1975). The Geomechanics Index is a composite measure of a large number of subjective and objective measures of rock quality. The system for calculating Geomechanics Index is shown in Figure A.3.6. The Geomechanics Index is unbelievably well correlated to deformation modulus ratio $\hat{E}/E$, as shown in Figure A.3.7. This is, perhaps, due to the nature of the Geomechanics Index, which allows adjustment of subjective values and weighting to assure a good correlation, at least in those results which are published. There is no fundamental reason why many of the factors in the Geo-

TABLE I

GEOMECHANICS CLASSIFICATION OF JOINTED ROCK MASSES

A. CLASSIFICATION PARAMETERS AND THEIR RATINGS

1	Strength of intact rock material	Point-load strength index	> 8 MPa	4 - 8 MPa	2 - 4 MPa	1 - 2 MPa	Use of uniaxial compressive test is better		
		Uniaxial compressive strength	> 200 MPa	100 - 200 MPa	50 - 100 MPa	25 - 50 MPa	10-25 MPa	3-10 MPa	1-3 MPa
	Rating		15	12	7	4	2	1	0
2	Drill core quality RQD		90% - 100%	75% - 90%	50% - 75%	25% - 50%	< 25%		
	Rating		20	17	13	8	3		
3	Spacing of joints		> 3 m	1 - 3 m	0.3 - 1 m	50 - 300 mm	< 50 mm		
	Rating		30	25	20	10	5		
4	Condition of joints		Very rough surfaces Not continuous No Separation Hard joint wall rock.	Slightly rough surfaces Separation < 1 mm Hard joint wall rock	Slightly rough surfaces Separation < 1 mm Soft joint wall rock	Slickensided surfaces OR Gouge < 5 mm thick OR Joints open 1-5 mm Continuous joints	Soft gouge > 5 mm thick OR Joints open > 5 mm Continuous joints		
	Rating		25	20	12	6	0		
5	Ground water	Inflow per 10m tunnel length	None		< 25 litres/min	25 - 125 litres/min	> 125 litres/min		
		Ratio joint water pressure / major principal stress	OR 0		OR 0.0 - 0.2	OR 0.2 - 0.5	OR > 0.5		
		General conditions	OR Completely dry		OR Moist only (interstitial water)	OR Water under moderate pressure	OR Severe water problems		
	Rating		10		7	4	0		

B. ADJUSTMENT FOR JOINT ORIENTATIONS

Strike and dip orientations of joints		Very favourable	Favourable	Fair	Unfavourable	Very unfavourable
Ratings	Tunnels	0	-2	-5	-10	-12
	Foundations	0	-2	-7	-15	-25
	Slopes	0	-5	-25	-50	-60

C. ROCK MASS CLASSES AND THEIR RATINGS

Class No	I	II	III	IV	V
Description	Very good rock	Good rock	Fair rock	Poor rock	Very poor rock
Rating	100 ← 90	90 ← 70	70 ← 50	50 ← 25	< 25

D. MEANING OF ROCK MASS CLASSES

Class No	I	II	III	IV	V
Average stand-up time	10 years for 5 m span	6 months for 4 m span	1 week for 3 m span	5 hours for 1.5 m span	10 minutes for 0.5 m span
Cohesion of the rock mass	> 300 kPa	200 - 300 kPa	150 - 200 kPa	100 - 150 kPa	< 100 kPa
Friction angle of the rock mass	> 45°	40° - 45°	35° - 40°	30° - 35°	< 30°
Caveability of ore	Very poor	Will not cave readily Large fragments	Fair	Will cave readily Good fragmentation	Very good

Figure A.3.6 Geomechanics Classification Index System (Bieniawski,1975)

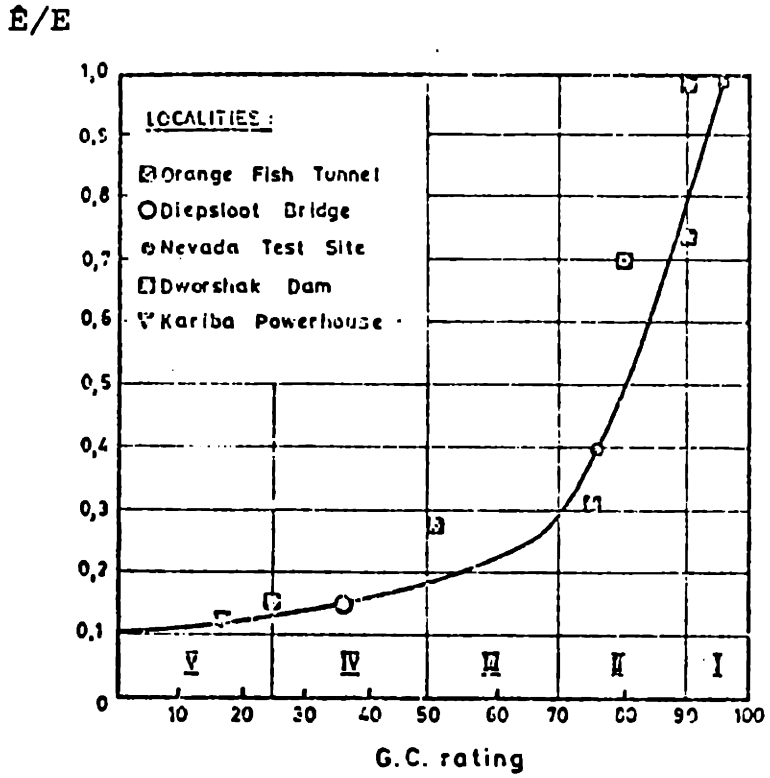

Figure A.3.7 Geomechanics Classification Correlation with Modulus Ratio Ê/E (Bieniawski,1975)

mechanics Index should play an important role in deformation. Still, it is possible that, within a given site, the Geomechanics Index may be a good measure of relative deformability of different rock masses.

The final major index which has been correlated to $\hat{E}/E$ is the "Joint Weathering Index," JWI, (Boughton, 1968). The Joint Weathering Index involves the logging of each joint in a core and the weighting of each joint according to factors based upon the degree of weathering of that joint. Figure A.3.8 shows the weighting factors which are used for different degrees of weathering. For purposes of correlation with deformability, joints are also weighted according to the stress concentration expected on that joint according to the Boussinesq stress bulb. The correlation between JWI and $\hat{E}/E$ is shown in Figure A.3.9. The JWI is well correlated to deformability and, from a theoretical point of view, presents a very attractive solution. It provides for the most complete joint description of any index. It allows great flexibility, and correlates very well with experimental results. Difficulties with the JWI arise for the impractically high level of detail necessary in core logging and the difficulty involved in obtaining substantial data for correlation.

A.4 Joint Stiffnesses

Joint stiffnesses are perhaps the most difficult of rock mass properties to determine. But since joint stiffnesses play such an important role in rock deformation, it is essential

TABLE I

ROCK CLASSIFICATION

Classification	*Joint Weathering Index*	*Description*	
		Dolerite Rock	*Quartzite Rock*
A	0	Fresh.	Fresh.
B	40	Fresh rock, stained joint.	Fresh rock, stained joint.
C	80	Signs of decomposition in feldspars adjacent to joint. Some clay on joint face.	Slight weathering at joint, deposition of iron oxides, some breakdown of mineralisation, scattered mica or chlorite on joint face.
D	90	Some decomposition of feldspars through whole of rock. Clay over whole joint face.	Joint faces largely covered with weathering products or platy minerals. Includes presence of: — carbonaceous material. — clay or rock flour. — mica or chlorite covering joint face.

Figure A.3.8 Joint Weathering Index Weighting Factors (Boughton, 1968)

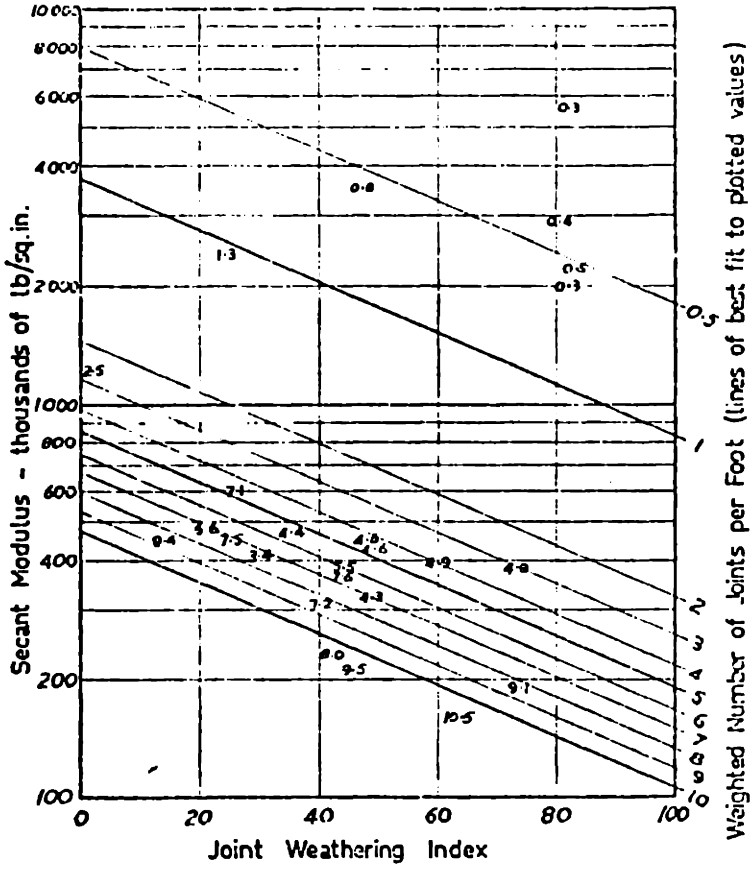

FIG. 3. *Test results*

Figure A.3.9 Joint Weathering Index Correlation with Rock Mass Modulus of Deformability (Boughton,1968)

that we understand what joint stiffnesses are, how they are determined, and what they mean.

A.4.1 Definition

Joint stiffness is normally considered to be the relationship between stress and deformation along joints. Shear stresses are related to shear displacements according to shear stiffness k_s; and normal stresses are related to normal displacements according to normal stiffness k_n:

(A.4.1) $$k_s = \sigma_s/\delta_s = \tau/\delta_s$$

$$k_n = \sigma_n/\delta_n$$

where k_s, k_n = shear, normal stiffness

σ_s, σ_n = shear, normal stress

$\tau = \sigma_s$

In fact, deformations are affected by off-diagonal stiffness terms k_{sn}. Thus, in matrix notation,

$$[\sigma] = [K]\{\delta\}$$

(A.4.2) $$\begin{bmatrix} \sigma_{ss} & \sigma_{sn} \\ \sigma_{ns} & \sigma_{nn} \end{bmatrix} = \begin{bmatrix} k_{ss} & k_{sn} \\ k_{ns} & k_{nn} \end{bmatrix} \begin{Bmatrix} \delta_s \\ \delta_n \end{Bmatrix}$$

It should be noted that this is very similar to the notation for elastic deformation,

$$[\sigma] = [C]\{\varepsilon\} \tag{A.4.3}$$

According to elastic theory, stress is related to strain, not deformation. Thus, stiffnesses are, in fact, improper moduli according to elastic theory. Over certain stress ranges, however, the concept of stress-deformation stiffnesses can be accepted as a simplifying approximation. This approximation, however, explains in part the difficulty involved in obtaining accurate and reliable values for stiffness.

A.4.2 Experimental Determination of Stiffness

Joint stiffnesses are determined experimentally by applying loads to joints and measuring loads and resulting displacements in both shear and normal directions. The method of load application frequently has a significant effect upon results, however, so it is important to understand the different procedures used. The most commonly used experimental procedures are the laboratory triaxial and direct shear tests and *in situ* direct shear tests.

In the triaxial test, intact rock samples are subjected to increasing axial stress until failure occurs and a "joint" is formed. The "joint" is then sheared by increased confining and axial stress, and loads and deformations are recorded. Typcial results are shown in Figure A.4.1. The advantage of

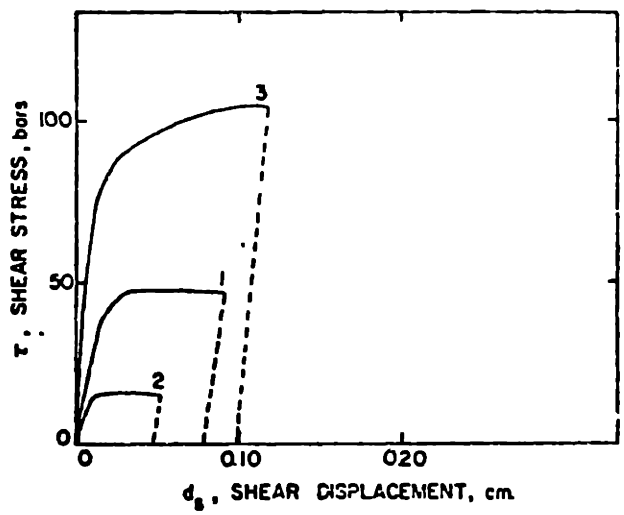

Fig. 3. Typical results of a jointed triaxial test. (See Table 1).

TABLE 1

Test Portion	σ_3, Confining Pressure bars	K_s, Shear Stiffness Kb/cm
1	35	3.3 ± 1.5
2	10	2.2 ± 1
3	70	9.5 ± 3

Figure A.4.1 Typical Results of Triaxial Test on Rock Joint (Rosso, 1976)

the test is that it allows derivation of stress-displacement properties along the joint, and that it allows testing on a truly undisturbed joint, since the joint is formed during the test, within the structure of the testing apparatus. Boundary conditions can be relatively well controlled and monitored in the triaxial test, and edge effects can be minimized. The major criticism of the test is that it tests a clean, unweathered joint, which is very different from most joints encountered in the field. In addition, there is some question about stress distributions within the rock sample during shearing because of the constraint on sample rotation imposed by the apparatus.

Laboratory direct shear tests are conceptually very simple but are in fact very difficult to analyze. In the lab direct shear test, a rock sample is taken with an "undisturbed" joint intact. The sample is then subjected to normal and shear loadings, and the top block is slid over the bottom block. Figure A.4.2 shows a stress-deformation curve resulting from a direct shear test. Unfortunately, although the results of the direct shear test appear to be simple, they are not. As the top block is pulled over the bottom block, substantial moments are produced. The stress distribution acting on the joint may therefore be very different from that applied to the sample. High cost simple shear tests eliminate that problem, but have not yet been perfected. The remaining problem is that of obtaining an undisturbed, intact rock joint for testing. This

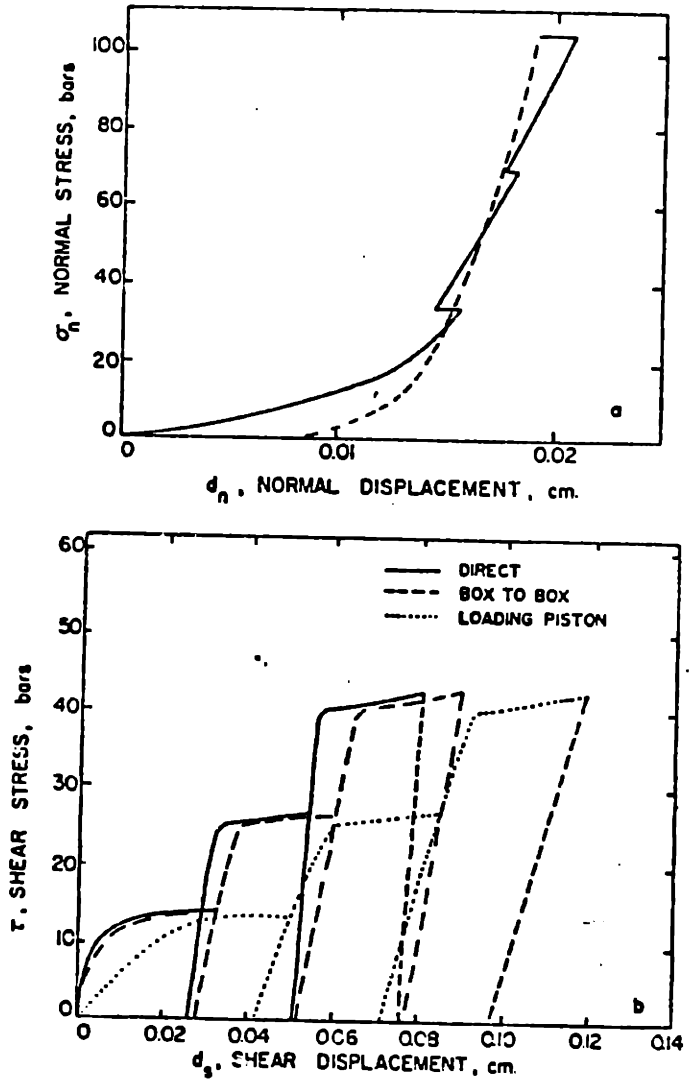

Fig. 6. Results of a direct shear test on a rock sample containing a natural open fracture where three different measurement methods were used to determine the shear displacement. (See Table 2.)

TABLE 2

	Measurement Method		
σ_n bars	Loading Piston K_s Kb/cm	Box to Box K_s Kb/cm	Direct K_s Kb/cm
35	.64±.2	2.4±.5	4.3±.5
70	1.5±.5	2.7±.5	4.9±.5
105	2.0±.5	3.2±.5	7.6±.5

Figure A.4.2 Typical Results of Direct Shear Test on Rock Joint (Rosso, 1976)

can only be avoided by in situ testing.

In situ direct shear tests are carried out on blocks formed by selective excavation of a natural joint. The joint block is confined by a reinforced concrete or steel-concrete frame. Stresses are applied shear and normal to the joint. The joint need not be horizontal. The large mass of the block avoids the problems of uneven stress distribution and large overturning moments. In addition, in situ joints are as undistrubed as possible. The major drawback to in situ testing is the high cost. In addition, the selective sampling of easy-to-get-to sections of joint for in situ testing may not be representative.

A.4.3 Stiffness Values

This section presents stiffness values obtained by the different experimental methods described above. Table A.4.1 contains values of k_s compiled by Goodman (1970) from various sources. His values for k_s vary from 0.8 to 600 ksc/cm. Hunger and Coates (1978) compiled the values of k_s and k_N shown in Table A.4.2. Rosso (1976) used triaxial and direct shear tests on identical samples at different stress levels. His results are shown in Table A.4.3. Table A.4.4 shows stiffness values compiled by Kulhawy (1978).

A.4.4 Discussion

As Rosso's measurement of stiffness values at different stress levels dramatizes, constant stiffness factors are an imperfect representation of joint behavior. Stiffness values change with stress level. Goodman (1970) showed that stiffness

TABLE 4—*Results of laboratory direct shear tests on artificial specimens with mica-filled joints.*

Test Number	Amplitude of Roughness, cm	Thickness of Seam, cm²	Cross Section Area, cm²	Normal Stress at Start of Test, kg/cm²	Tangential Stress, kg/cm²		Tangential Displacement, cm		Shear Stiffness, kg/cm³		Curve Type
					Yield	Peak	Yield	Peak	Yield	Peak	
1	0.41	0	31.7	7.6	...	6.18	...	0.203	...	30.4	4a
2	0.41	0	31.7	7.6	...	6.80	...	0.244	...	27.9	4a
3	0.41	0.1524	31.7	7.6	...	4.33	...	0.241	...	18.0	4a-4b
4	0.41	0.524	31.7	7.6	...	4.26	...	0.226	...	18.8	4a-4b
5	0.41	0.3048	31.7	7.6	3.05	3.28	0.102	0.165	29.9	19.8	4b-4a
6	0.41	0.3048	31.7	7.6	...	3.06	...	0.305	...	10.1	4b-4a
9	0.41	0.3048	31.7	7.6	1.75	2.58	0.114	0.297	15.4	8.7	4b-4a
7	0.41	0.508	31.7	7.6	1.43	2.05	0.140	0.291	10.2	7.1	4b
8	0.41	0.508	31.7	7.6	1.83	1.98	0.203	0.241	9.2	8.2	4b

Table A.4.1 Goodman(1970) Stiffness Values

CAN. GEOTECH. J. VOL. 15, 1978

TABLE 2. Summary of the average measured values (10^4 MN/m^3) of the unit shear stiffness coefficient k_{ss} and the off-diagonal coefficient k_{ns}

Specimen number	k_{ss} at 50% τ_p	k_{ss} at τ_y	k_{ss} average	k_{ns} at 50% τ_p	k_{ns} at τ_y	k_{ns} average
Ottawa limestone						
1	1.2	0.3	0.4	4.9	0.6	0.8
2	1.1	0.4	0.4	4.4	0.7	1.0
3	24.6	1.0	1.5	−3.5	−5.6	−4.8
4	2.9	0.6	0.9	−30.0	11.7	23.7
5	36.8	0.7	1.0	1.3	0.4	0.5
6	2.2	0.6	0.8	−3.3	2.8	7.9
7	32.4	1.7	2.5	33.5	1.8	2.7
8	1.6	0.3	0.5	−1.0	−1.2	−1.1
9*	20.2	0.8	1.2	—	—	—
10	23.0	1.5	2.2	—	—	—
Nepean sandstone						
11	8.3	1.1	1.6	50.0	8.8	12.4
12	1.4	0.5	0.6	−7.9	11.1	7.5
13	2.1	1.0	1.2	−3.1	69.6	−6.5
14	21.1	1.4	2.1	7.7	2.5	3.3
15	26.8	1.5	2.2	3.5	1.4	1.8
16*	25.6	1.7	2.5	—	—	—
17	23.5	2.9	4.2	31.4	6.2	8.6
18	28.2	0.6	0.9	4.0	1.6	1.5
19*	7.1	1.6	2.2	—	—	—
20	23.0	3.8	5.1	17.1	3.6	5.0
Overall average values						
Limestone	2.60	0.54	0.75	113.00	1.14	1.72
Sandstone	5.15	1.04	1.42	22.80	3.16	4.21
Limestone saw cut	21.59	1.07	1.57	—	—	—
Sandstone saw cut	12.52	1.66	2.32	—	—	—

*Artificial (saw cut) discontinuities.
NOTE: τ_p = peak shear stress; τ_y = yield shear stress (yield point defined as point of maximum curvature of test plots); 1 MN/m^3 = 3.68 lb/in^3.

Table A.4.2 Hungr & Coates(1978) Stiffness Values

Figure A.4.3 Rosso(1974) Stiffness Values

PRINT ON THE FOLLOWING PAGE IS ILLEGIBLE

...of discontinuities under direct shear conditions

Test designation	Specimen description	Discontinuity thickness (cm)	Discontinuity area (cm^2)	Range of normal stress (MN/m^2)	Secant shear stiffness K_s (GN/m^3) Yield Range	Yield Avg.	Peak Range	Peak Avg.	Cohesion, C (MN/m^2) Maximum C	Residual C_r	Angle of friction φ Maximum φ	Residual φ_r	Curve type	Reference
...0 14.6 run 3 - U. Illinois	Berea sandstone dry, sawed joint	–	82	0.26	–	–	–	29.80	-		–	-	2a	Goodman (1968)
...14.7 run 7 U. Illinois	Limestone dry, sawed joint	–	82	10.40	-	–		8.73	–	–	–	–	2a	Goodman (1968)
JP2 U.C. Berkeley	Rose sandstone dry, rough saw cut	–	5	2.43	–	-	-	1.29	–	–	-	–	2b	Mahtab (1969)
Blackingstone Imperial Col.	Granite dry, rough joint from breaking beam	–	144-205	1.18-1.42	1.26-1.67	1.42	0.99 1.57	1.32	–	–	–	–	3a	Goodman (1968)
Delgado – Imperial Col	Slate dry, natural cleavage surface	–	500	4.37	-	0.88	-	0.79	–	–		-	3b	Goodman (1968)
Vouglans Dam	Limestone oolitic, compact to stylolitic		575	0.49	-	6.08	1.68 4.61	2.78	–		–	–	4a	Goodman (1968)
Lamouriere 1965	Marl layers in limestone sat.	0.1-0.3	605-730	0.47-0.56	2.16 3.73	2.84	0.51 3.73	2.13	-		-	-	1,4a	Goodman (1968)
Lamouriere 1964	Marly partings in limestone - sat.	0.1-5.0	51-63	0.24-0.77	2.16-3.34	2.74	0.85 5.69	2.89	..A	0	A	38.4	1	Goodman (1968)
Vouglans Dam	Limestone with marly joints - dry	0.025 2.0	28-47	0.49-1.47	–	-	2.26 23.55	9.75	0.92	0.11	46.6	37.8	1	Goodman (1968)
L'Aquila Meridional Apennine	Sandstone marl contact			0.10-0.98	0.33 2.08	0.84	0.11 0.17	0.15	0.20	0.15	45.0	38.0	3	Baklovin (1970)
Brescia Meridional Prealps	Phyllitic schist fractures			0.20 1.47	0.41 0.97	0.65	0.14 0.40	0.22	0	0	45.0	40.0	3	Baklovin (1970)
B-2 Sarajevo	Limestone slightly rough bedding		1600	0.15 3.63	0.83 4.12	2.17	0.20 1.37	0.81	1.23	0.57	36.9	29.8	3a	Goodman (1968)
B-3 Sarajevo	Limestone rough bedding surfaces		1600	0.30 3.36	0.33 14.90	5.93	0.25 7.35	3.06	0.89	0.23	53.5	43.2	3a	Goodman (1968)
D-2 Sarajevo	Limestone rough unfilled fractures		1600	1.52 4.00	0.24 13.80	8.46	1.26 2.61	1.98	2.69	0.88	19.0	31.8	3a	Goodman (1968)
Malrasset Mills	Foliated gneiss and mylonite	4.0-5.0	10.6-24.6	0.39 2.94	1.46 4.71	2.55	0.69 3.69	2.36	1.17	0	53.0	46.3	3a	Goodman (1968)
Delgado Imperial Col.	Porphyry dry, natural joint surface		500	3.24 10.10	0.96 1.64	1.30	0.26 1.94	1.02	0.74	0	39.0	35.5	3b	Goodman (1968)
B-1 Sarajevo	Limestone mylonite along bedding	–	1500	0.21-2.38	1.04-8.04	3.90	0.28 5.69	1.25	0.51	0.29	37.3	35.5	4a	Goodman (1968)
Vouglans Dam	Moist marly joint in limestone	1.5 3.0	980-1243	0.53-2.99	1.18 3.33	2.65	0.41 4.71	1.70	0.36	0.08	26.0	25.2	4a	Goodman (1968)
B-1 Sarajevo	Limestone thin shale seams along bedding		1500	1.23 2.80	1.55 12.90	6.96	0.32 8.33	3.08	0.49	0.49	30.6	30.6	4b	Goodman (1968)
Vouglans Dam	Marly joint sat	1.3 3.2	1030 1240	0.49-2.94	0.09 2.74	1.41	0.92 1.86	0.78	0	0	23.4	23.4	4b	Goodman (1968)
D-1 Sarajevo	Limestone smooth unfilled fractures		1600	0.88-2.40	0.41 2.36	1.07	0.20 1.28	0.51	0	0	38.4	36.3	4c	Goodman (1968)
Tronto Gran Paradiso Massiccio	Granitic gneiss fractures	–	-	0.20 0.78	0.29 0.38	0.33	0.09 0.12	0.11	0	0	40.0	40.0	4c	Baklovin (1970)
Vouglans Dam	Limestone with marly joints sat.	0.025 0.2	24-40	0.49 1.47		1.47	0.14 31.60	7.41	0	0	55.8	39.6	1,3a 4a,b,c	Goodman (1968)
1P Krivoklat	Bedding plane in greywacke	0.5-0.8	2265	1.24	–	-	–	0.23	–	–	–		4b	Goodman (1968)
2P Krivoklat	Bedding plane in greywacke	>0.1	3110	1.01	–	–	–	1.21	–	–	–	–	4b	Goodman (1968)
3P Krivoklat	Bedding plane in greywacke	Closed, clean	3000	0.43	–	–	–	2.26	–	–	–	–	4b	Goodman (1968)
Vouglans Dam	Marly sand filled joint	0.1-0.2	44000	0.98	-	–	–	2.34	–	–	-	–	4b	Goodman (1968)
R-1 Kariba IV Dam	Vertical fault	Thick, uneven	-	0.37-1.07	–	-	0.17 0.23	0.20	–	–	–	-	4c	Goodman (1968)
SLL Khasun Dam	Closely jointed shale zone in limestone	0.2-0.5	50000	0.02[f]	-	–	0.01-0.02	0.02	–	–	–	-	4c	Goodman (1968)
SLS Khasun Dam	Shale interbed – wet	0.2-0.5	50000	0.02-0.03	-	–	0.01-0.02	0.02	–	-	–	–	4c	Goodman (1968)
C-2 Dolesice Dam	Schistosity plane in amphibolite	–	5000	0.12	-	–	–	0.59	–	–	–	–	–	Goodman (1968)
Jaina Dam	Unbonded basalt – sandstone contact	–	307900	0.13	-	–	–	0.11	–	-	-		–	Goodman (1968)
Overall summary or average		Closed – 5.0	5-307900	0.02 10.40	0.09 14.90	3.02	0.01 31.60	2.82	0.61	0.18	39.3	35.7		

...ies – laboratory direct shear tests over limited stress range.
...es laboratory direct shear tests.
...ies – in-situ block direct shear tests.

A – data too scattered and/or too little spread.

Avg Normal stiffnesses, K_n (in GN/m^3) are: 35.1 for DLL-3, 1.96 for DIS 4, 0.24 for DIS-6, 0.26 for DIS-7.

Table A.4.4 Kulhawy(1978) Stiffness Values

TABLE 8.—Summary of Discontinuity Shear Stiffness Values (Data from Ref. 10)

Test (1)	Test designation (2)	Specimen description (3)	Discontinuity: Thickness, in centimeters (4)	Discontinuity: Area, in square centimeters (5)	Shear Stiffness, K_s, in giganewton per cubic meter: Range (6)	Shear Stiffness, K_s, in giganewton per cubic meter: Average (7)
DLL-1*	10–14.6 run 3—University of Illinois	Berea sandstone—dry, sawed joint	—	82	—	29.80
DLL-2	6–14.7 run 7—University of Illinois	Limestone—dry, sawed joint	—	82	—	8.73
DLL-3	QP2—University of California, Berkeley	Boise sandstone—dry, rough saw cut	—	5	—	1.29
DLL-4	Blackingstone—Imperial College	Granite—dry, rough joint from breaking beam	—	144–205	0.99–1.57	1.32
DLL-5	Delgado—Imperial College	Slate—dry, natural cleavage surface	—	500	—	0.79
DLL-6	Vouglans Dam	Limestone—oolitic, compact to stylolitic	—	575	1.68–4.61	2.78
DLL-7	Larouviere—1965	Marl layers in limestone—saturated	0.1–0.3	605–730	0.51–3.73	2.13
DL-1*	Larouviere—1964	Marly partings in limestone—saturated	0.1–5.0	51–63	0.85–5.69	2.69
DL-2	Vouglans Dam	Limestone with marly joints—dry	0.025–2.0	28–47	2.26–23.55	9.75
DL-3	L'Aquila Meridional Apennine	Sandstone—marl contact	—	—	0.11–0.17	0.15
DL-4	Bresica Meridional Prealps	Phyllitic schist fractures	—	—	0.14–0.40	0.22
DL-5	B-2 Sarajevo	Limestone—slightly rough bedding	—	1,500	0.20–1.37	0.84
DL-6	B-3 Sarajevo	Limestone—rough bedding surfaces	—	1,600	0.25–7.35	3.06
DL-7	D-2 Sarajevo	Limestone—rough unfilled fractures	—	1,600	1.26–2.61	1.95
DL-8	Malpasset Mill6	Foliated gneiss and mylonite	4.0–5.0	10.6–24.5	0.69–3.69	2.36
DL-9	Delgado—Imperial College	Porphyry—dry, natural joint surface	—	500	0.26–1.94	1.02
DL-10	B-1 Sarajevo	Limestone—mylonite along bedding	—	1,500	0.28–5.69	1.25
DL-11	Vouglans Dam	Moist marly joint in limestone	1.5–3.0	980–1,243	0.41–4.71	1.70
DL-12	B-1 Sarajevo	Limestone—thin shale seams along bedding	—	1,500	0.32–8.33	3.08
DL-13	Vouglans Dam	Marly joint—saturated	1.3–3.2	1,030–1,240	0.02–1.86	0.78
DL-14	D-1 Sarajevo	Limestone—smooth unfilled fractures	—	1,600	0.20–1.28	0.51
DL-15	Torino Gran Paradiso Massiccio	Granitic gneiss fractures	—	—	0.09–0.12	0.11
DL-16	Vouglans Dam	Limestone with marly joints—saturated	0.025–0.2	24–40	0.14–31.60	7.41
DIS-1*	1P Krivoklat	Bedding plane in greywacke	0.5–0.8	2,265	—	0.23
DIS-2	2P Krivoklat	Bedding plane in greywacke	>0.1	3,510	—	1.21
DIS-3	3P Krivoklat	Bedding plane in greywacke	Closed, clean	3,660	—	2.26
DIS-4	Vouglans Dam	Marly sand filled joint	0.1–0.2	44,000	—	2.34
DIS-5	K1 Kerobe IV Dam	Vertical fault	Thick, uneven	—	0.17–0.23	0.20
DIS-6	SLL Khajuri Dam	Closely jointed shale zone in limestone	0.2–0.5	50,000	0.01–0.02	0.02
DIS-7	SLS Khajuri Dam	Shale interbed—wet	0.2–0.5	50,000	0.01–0.02	0.02
DIS-8	C-2 Dolesice Dam	Schistosity plane in amphibolite	—	5,000	—	0.59
DIS-9	Jupia Dam	Unbonded basalt—sandstone contact	—	307,900	—	0.11
	Overall summary or average		Closed—5.0	5–307,900	0.01–31.60	2.42

*DLL series—laboratory direct shear tests over limited stress range.
*DL series—laboratory direct shear tests.
*DIS series—in-situ block direct shear tests.
Note: 1 GN/m³ = 3.681 lb/cu in.

values are also sensitive to many other factors. Normal stiffness values are sensitive to normal stress and the initial aperture of the joint. Shear stiffnesses are sensitive to normal stress level, shear stress level and aperture.

Kulhawy (1975) developed relations between stiffness and stress level. These relations take the non-linear (stress-dependent) behavior into account.

$$k_{sT} = k_{si}\left(1 - \frac{\tau R_{fi}}{c_j + \sigma_N \tan\phi_j}\right)^2 \tag{A.4.4}$$

$$k_{si} = k_j \, (\gamma_w) \left(\frac{\sigma_N}{Pa}\right)^{nj}$$

$$k_s = k_N \, / \, (2(1 + \nu))$$

where k_{sT} = tangent shear stiffness

k_{si} = initial tangent shear stiffness

τ = mobilized shear stress

R_{fi} = failure ratio $\approx$ 1 (chosen to fit data)

σ = normal stress on discontinuity

ϕ_j = discontinuity friction angle

k_j = stiffness number (chosen to fit data)

n_j = stiffness exponent (chosen to fit data)

Pa = atmospheric pressure

γ_w = density of water

c_j = joint cohesion

Hunger and Coates (1978) explain non-linear stiffness as the effect of sliding in shear, closure under compression, and opening under tension. They developed iterative finite element techniques to simulate these effects.

Ultimately, however, the dependence of stiffness on stress level and non-linearity is the result of the improper nature of stiffness as a stress-deformation modulus. It is perhaps better, in the long run, to develop techniques for expressing joint behavior in terms of elastic or plastic parameters E, ν and G, rather than in stiffness values which are sensitive to stress, and which can be used only with complex correction factors.

APPENDIX B

ORIENTATION LITERATURE

The study of rock deformation models depends heavily upon the representation of joint orientations. It is worthwhile, therefore, to examine different approaches taken in the literature. Orientation description methods included in this Appendix are used to develop and fit mathematical models for orientation in Appendix C.

Four aspects of orientation description are presented here. First, different graphical methods for presenting rock joint orientations are presented and discussed. Next, systems developed for grouping joints into statistically homogeneous joint sets are given. Then, the mathematical treatment of orientation distributions is developed. Finally, a few of the biases in sampling for orientation are briefly dealt with and one system for correcting bias is presented.

B.1 Graphical Representation of Orientation Data

Rock joint orientations can be expressed mathematically in terms of dip (ϕ) and dip direction (θ). Dip direction may also be represented as strike or azimuth. Figure B.1.1 illustrates the meaning of (θ,ϕ) as a point in three space.

Large amounts of orientation data are cumbersome to evaluate. Graphical representations for collections of orientation data were therefore developed.

The most intuitive representation for groups of data is the frequency polygon, such as that used by Cawsey (1977).

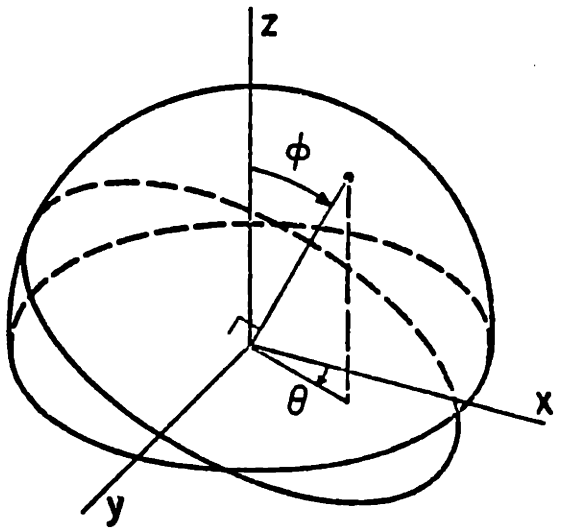

Figure B.1.1 Meaning of Orientation (θ,ϕ) as a Point on Surface of Sphere

Figure B.1.2 shows frequency polygons for dip. The frequency polygon shows the number of occurrences of each dip value within the joint sample. The advantage of frequency polygons is that they are easy to read and to plot. Unfortunately, they have several weaknesses. They treat strike and dip separately despite the fact that θ and ϕ are clearly correlated. It is impossible therefore to evaluate the joint probability of orientations (θ,ϕ). In addition, frequency polygons misrepresent distributions of dip and strike because orientations which are in fact only two degrees apart may show up as being completely different due to shifts of dip from left to right hemisphere. This is illustrated in Figure B.1.3. Another problem with frequency polygons is that they ignore the fact that orientations are distributed on a sphere, not on a planar surface. This is discussed in greater detail in Section 3.4.

Rose diagrams show orientation frequency on a circular bar chart. Rose diagrams are similar to frequency polygons in that they ignore the spherical nature of orientation data, and in that they separate strike from dip. Rose diagrams, however, solve the problem of orientation value shifts between hemispheres by plotting on a circle. An example of a rose diagram is given in Figure B.1.4.

Rectangular plots of joint data such as those used by Robertson & Piteau (1971) plot frequency, dip direction and dip simultaneously, and thus avoid many of the problems of frequency polygons. A computer-generated rectangular plot is shown in Figure B.1.5. Rectangular plots contain data without

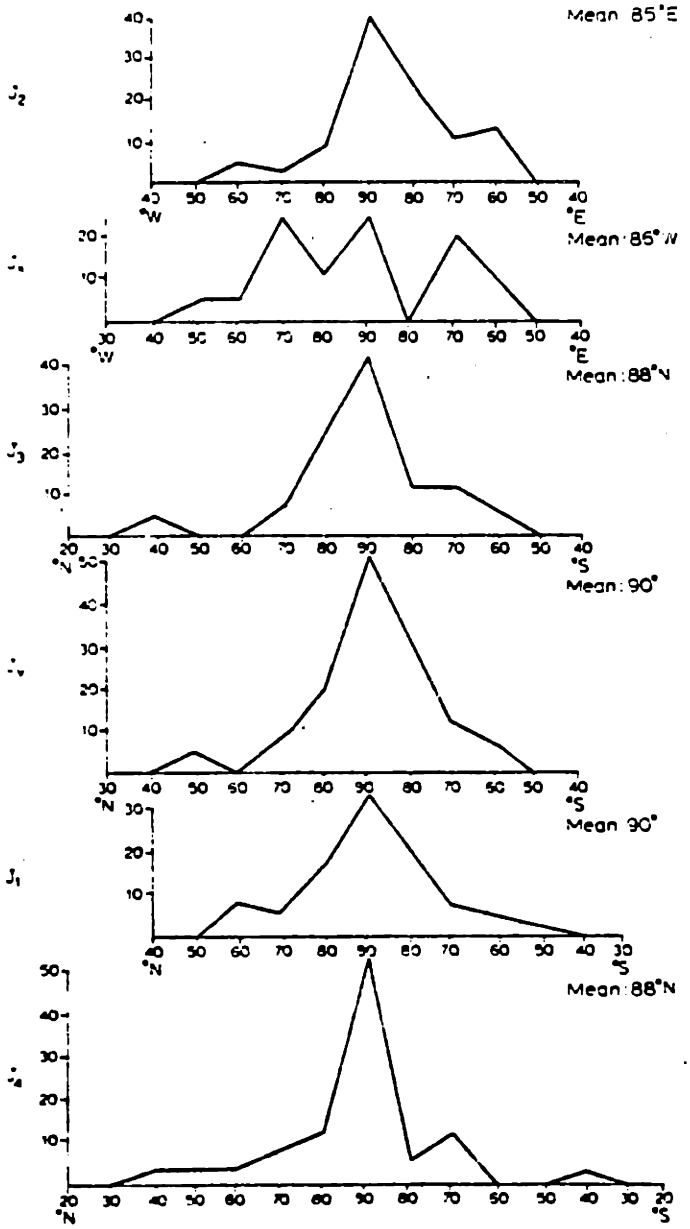

Fig.11. Frequency polygons of percentages of joints plotted against their angles of dip

Figure B.1.2 Frequency Polygons for Strike and Dip

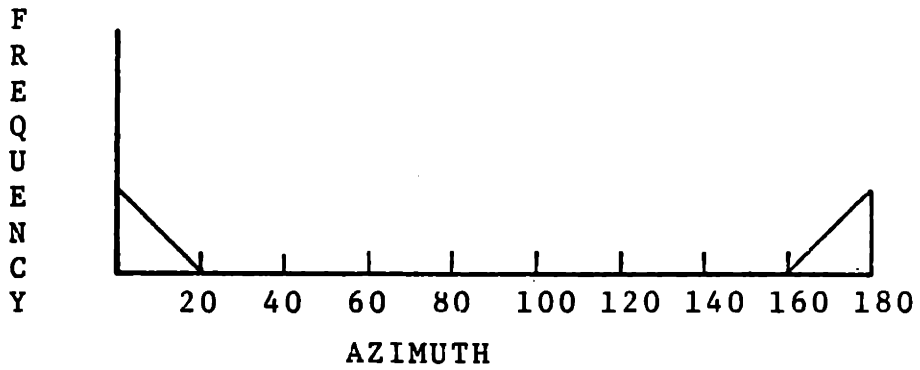

Both peaks are part of the same joint set. When dip is near 90°, strike may appear as Θ+0 or
-Θ+180.

Figure B.1.3 Non-circulatity Problem of Frequency Polygons

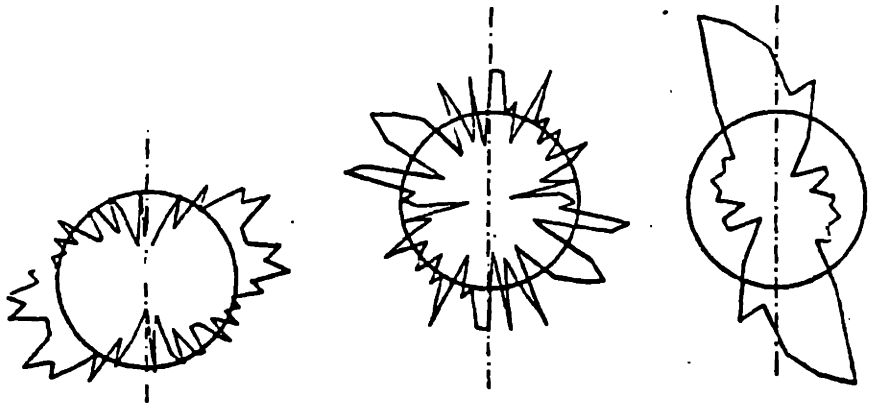

FIG. 22-2. Types of compass rose diagrams. After Schmidt (234).

Figure B.1.4 Rose Diagram (Chayes,1949)

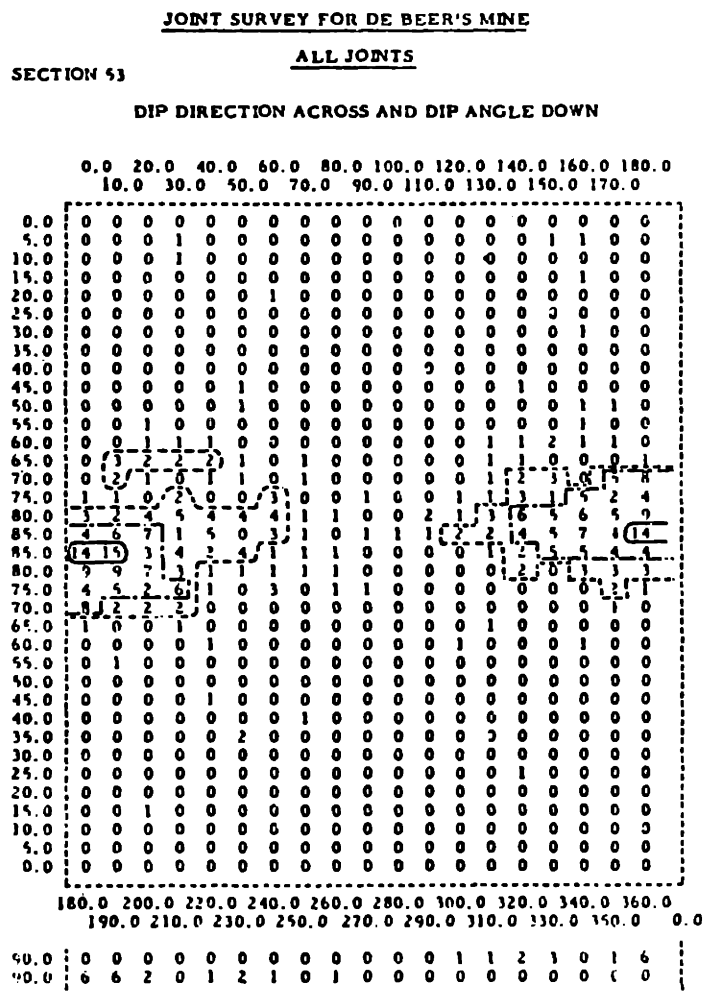

Fig. 2 — The Rectangular Plot as adapted for the Computer

Figure B.1.5 Computer Generated Rectangular Plot (Robertson & Piteau,1971)

any loss in information, since intervals can be set to represent data at any desired level of detail. Rectangular plots keep strike and dip measurements together so that joint probabilities can still be expressed. The disadvantages of rectangular plots are that they maintain the spatial distortion inherent in a linear two-dimensional plot of three-dimensional data, and that they do not make an allowance for the circular nature of orientation data. Orientations of 1° and 359° are plotted 358° apart, although they are in fact only two degrees apart.

Stereonets (described in Billings, 1972) plot joint orientations on a projection of a spherical surface. As a result, they minimize problems of distortion (equal area nets are used for statistical work) and of representation of circular data. Still, small east-west differences in orientation may cause large apparent differences on the stereonet. A stereonet is shown in Figure B.1.6. The difficulty of stereoplot analysis involves the conceptual difficulty in interpreting data plotted on a projective plane. Since areas on the projected plane represent areas on the surface of the sphere, interpretation of results requires some transformation. Point density contours are used to represent frequency on the plot. Despite these difficulties, however, stereonets are the most logical, consistent and complete method for presenting orientation data.

An innovative and useful method for plotting joint data was developed by Steffan and Jennings (1974). Steffan and

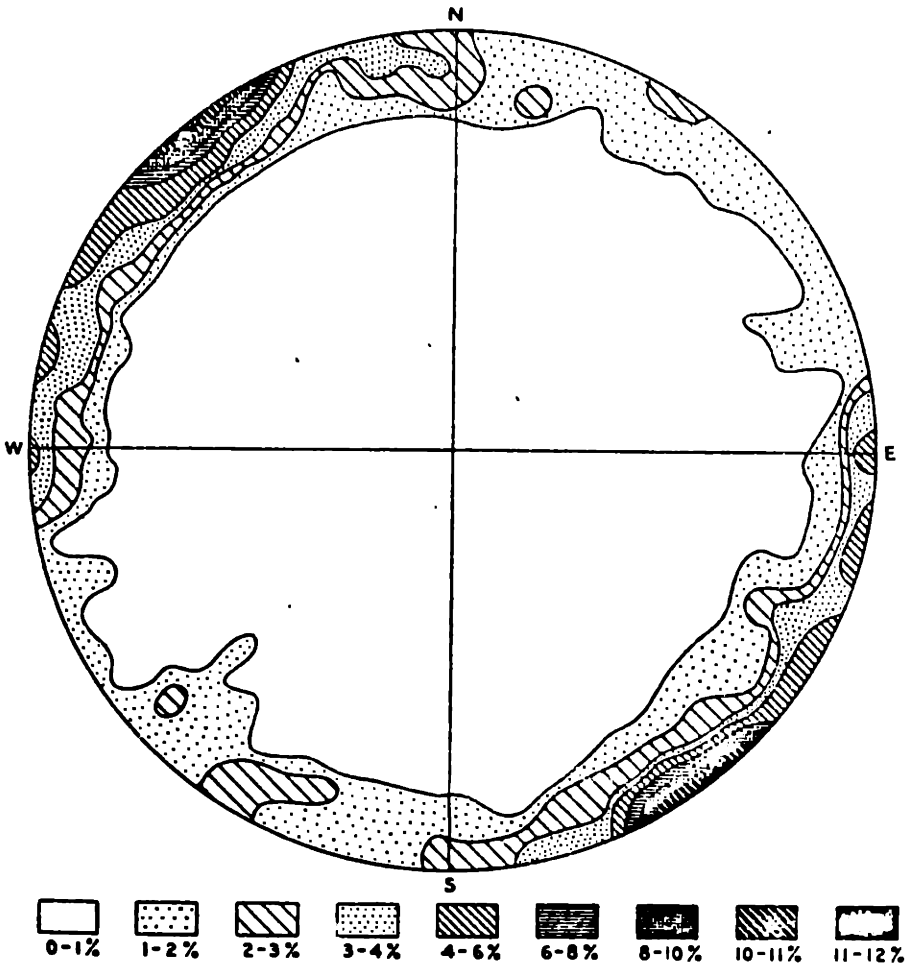

Fig. 7-6. Contour diagram of 311 joints in Adirondack Mountains. Plotted on lower hemisphere. (After Balk.[5])

Figure B.1.6 Stereonet (Billings, 1972)

Jennings actually plot the strike line of every joint in relation to the sampling line. This allows the actual spatial relationship between joints to be observed, and allows visual inspection of jointing patterns. Their plot is shown in Figure B.1.7.

B.2 Clustering

Rock joints generally exist in joint sets, groups of joints having similar properties. Joint sets are usually defined as having a principal orientation and some scatter about that orientation. Statistically homogeneous joint sets also have common distributions of spacing and length, and common conditions of roughness, gouge, and material properties. In order to describe all members of a joint set by set characteristics rather than individually, joint sets must be isolated from each other and from random, ungrouped joints. This process is called clustering. Clustering is frequently related to the method used for graphical representation of joints, so there are at least as many ways of clustering joints as there are ways to represent joint orientation distributions graphically.

Cawsey (1977) used his joint frequency polygons to cluster joints by strike alone. He disregarded dip entirely in his clustering technique, which involved simple visual inspection of the strike frequency polygon. His method is illustrated in Figure B.2.1. His method ignores not only the fact that dip is as important as strike in differentiating clusters, but also the fact that joints with radically different strikes may belong

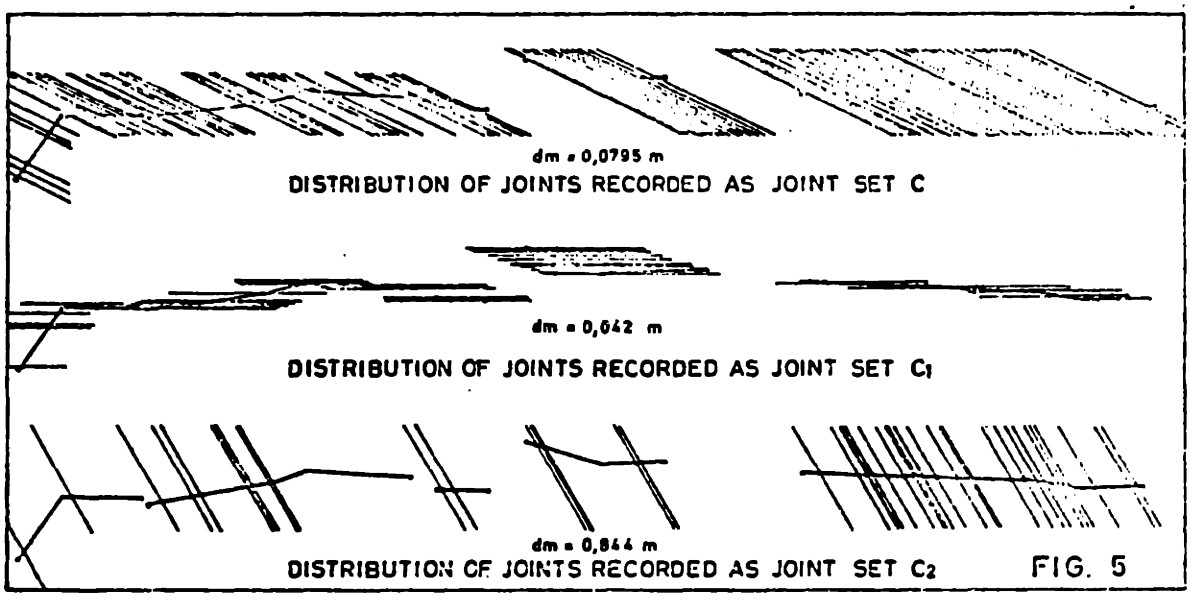

Figure B.1.7 Strike Line Plot(Steffan & Jennings, 1974)

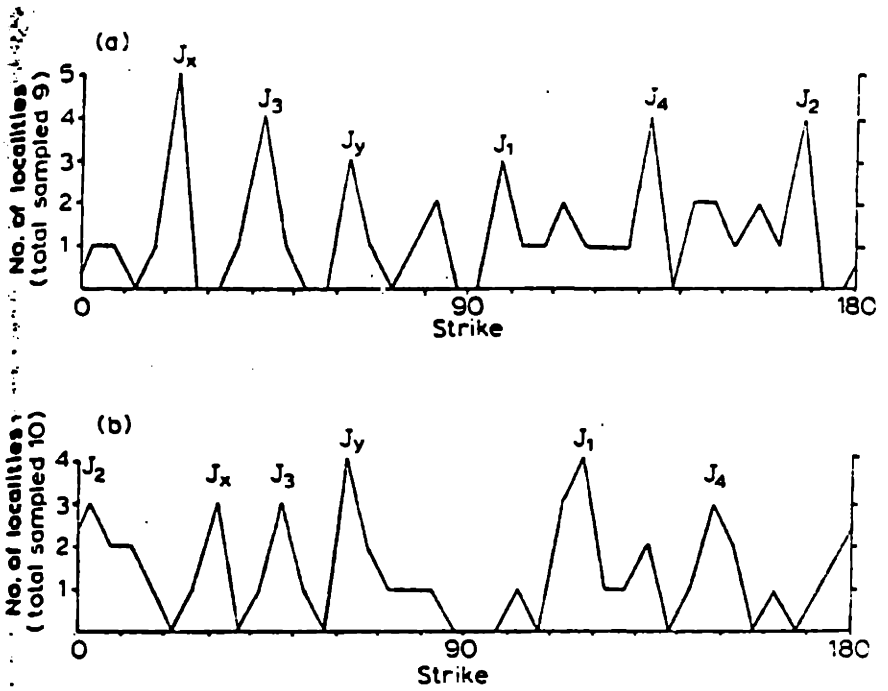

Fig.3. Frequency polygons of number of stations at which dominant joint sets are developed plotted against their strike for (a) the northern group of localities sampled in the Chilterns and (b) the southern group of localities sampled in the Chilterns.

Figure B.2.1 Clustering from Frequency Polygons (Cawsey, 1977)

to the same set because of the circularity of strike measurements. This is illustrated by the stereoplot in Figure B.2.2.

Robertson and Piteau (1971) used rectangular plots to cluster data as illustrated in Figure B.2.3. This method is better than Cawsey's, because it involves both strike and dip in the clustering algorithm. Still, the method suffers from all the weaknesses of the rectangular plot method in terms of the circular nature of orientation data and the distortion inherent in a flat representation of spherical data. Robertson and Piteau, however, use a correction factor to weight their data according to spherical projection areas, and thus eliminate the latter objection. Still, the technique relies upon subjective evaluation of cluster boundaries, and fails where joint sets overlap.

The most commonly used joint clustering routines are based upon stereographic projections. That is because only stereographic projection allows visual inspection of point densities on the sphere and accounts for the circular nature of orientation data. The simplest application of stereonets for clustering is clustering based solely upon contour lines. All points falling within a certain group of concentric contours are grouped into a cluster (Billings, 1972). This technique has the advantage of being based upon clearly definable spherical point density considerations. In addition, clusters can be grouped even when joint poles occur in both eastern and western hemispheres because concentric lines wrap around the projection.

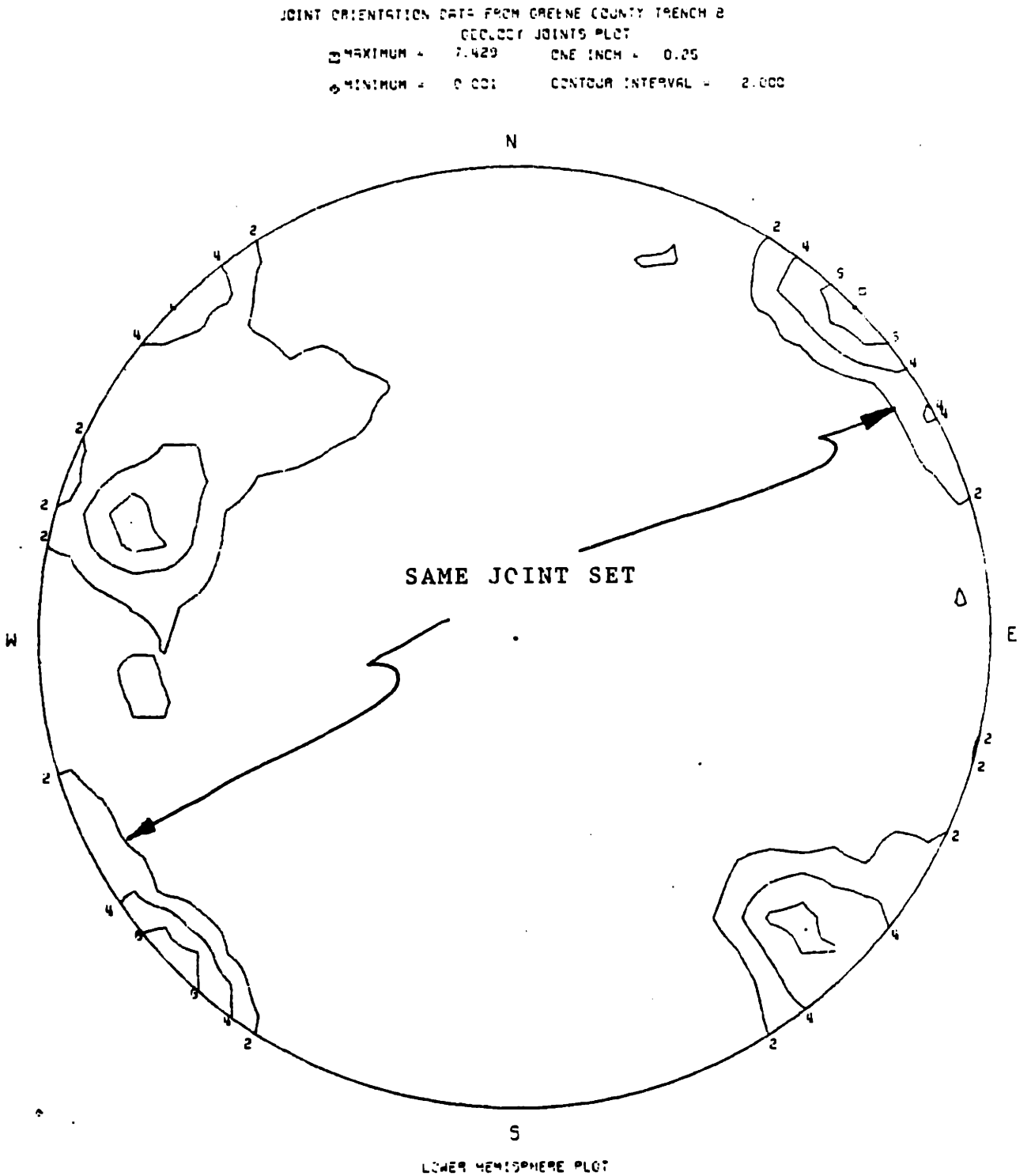

Figure B.2.2 Stereoplot of Joint Cluster Divided between Two Hemispheres

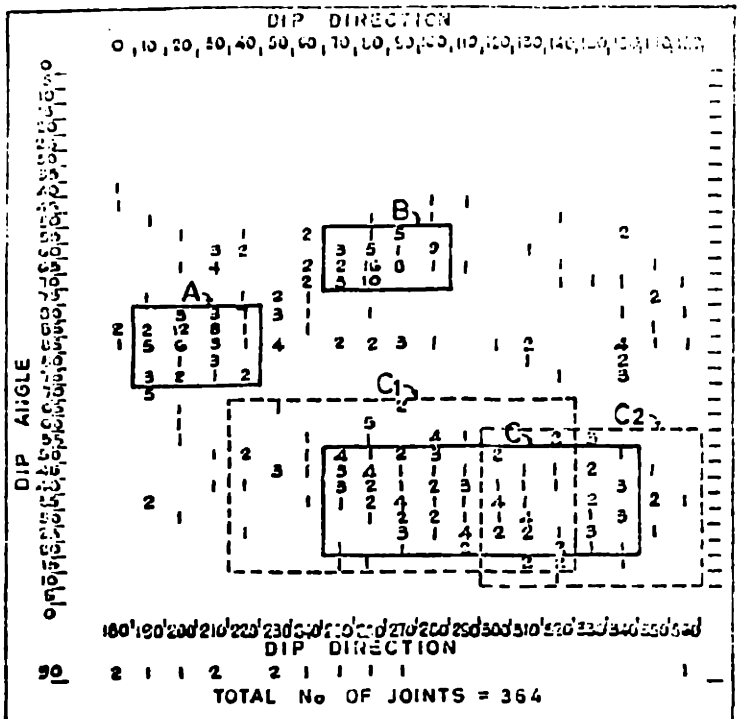

FIG. 3 RECTANGULAR PLOT OF JOINT DATA

Figure B.2.3 Clustering from Rectangular Plot(Steffan & Jennings, 1974)

This is illustrated in Figure C.2.1. The difficulty with the method is that it does not cluster disperse points and cannot separate clusters which are overlapping.

Maranhao (1968) developed a simple numerical technique for clustering points based upon stereographic projection. Maranhao plotted orientations on the upper hemisphere, which he divided into 60 equal area cells. Any cell with more than the average number of points and all cells adjacent to it were put into a cluster. Although Maranhao reported that his method worked very well for him, the method obviously fails when joint sets overlap and where joint sets are asymmetrical and do not extend equally in all directions from the densest cell.

Shanley and Mahtab (1976) developed a similar system. Their clustering algorithm is as follows: First, they set up spheres of radius r about each point on a stereonet. Then all centers of spheres containing k or more observations are labeled "dense". Finally, all non-dense points are added to adjacent points until every point is part of a cluster. Parameters r (radius) and k (center density) are found by optimizing an objective function description the clustering system. Shanley and Mahtab used the objective function,

$$\text{(B.2.1)} \qquad F(\text{Partition}) = \sum_{j=1}^{M} \sum_{i=1}^{N_j} d^2(x_j', \bar{x}_j) + \sum_{i=1}^{M-1} \sum_{i=1}^{M} d^2(\bar{x}_i, \bar{x}_j)$$

where $d(x_i, x_j)$ = distance from x_i to x_j

M = number of clusters in partition system

N_j = number of points in cluster j of partition system P

x_{ij} = ith element of cluster j

$\bar{x}_j$ = center of gravity of cluster j.

The objective function is intended to minimize the total variance of clusters within the particular partition system.

The advantages of this system are clear. It groups all data within a site into clusters according to a reasonably rational standardized system. And, for sites with few, well-defined joint sets, it performs quite well. Unfortunately, it fails completely for sites containing adjacent or overlapping joint sets. It also fails for sites containing a significant number of random joints which are not, in fact, members of joint sets.

B.3 Distributions of Orientation Data

Orientation data is distributed on a sphere, and therefore requires a completely different set of statistical distributions from the Pearson-type distributions used for planar data. Spherical orientation distributions are discussed in detail in Section 3.4.4. Here, the development of those distributions, and the assumptions underlying the selection of those distributional forms, are presented.

Figure B.3.1 shows the diverse range of orientation distributions that are observed in nature. Any general orientation distribution would have to be able to model all of those forms.

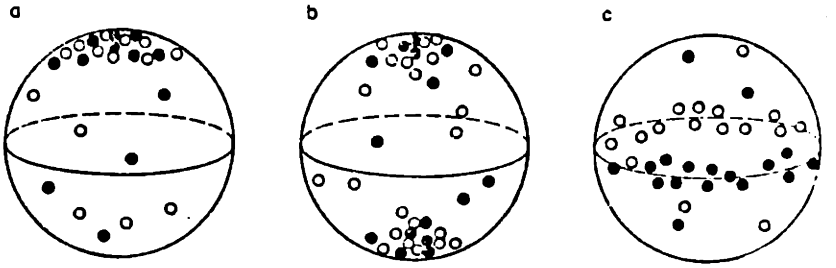

FIG. 8.3. Configurations of sample points from (a) unimodal (b) bimodal and (c) girdle distributions. (An open circle denotes a point on the other side).

Figure B.3.1 Observed Types of Orientation Distributions (Mardia,1972)

The goal of spherical distribution development has not, however, been the development of a general distribution for observed phenomena. Instead, effort has been concentrated on the development of an analog for the normal distribution on the sphere.

The normal distribution on the plane is an especially attractive form, and it is understandable that an analog on the sphere should be desired. The normal distribution has the singular advantage that the sample mean and standard deviation are also mean and standard deviation for the best fit normal. The sample mean provides a maximum likelihood estimate for location in the normal distribution. In addition, the Central Limit Theorem states that any sum of a sufficiently large number of random events will eventually approach a normal distribution.

Unfortunately, as was eloquently noted by Jizba (1953), the mathematical mean for orientation data cannot be found. This is because the mean of orientation data is not invarient with respect to frame of reference (Figure B.3.2). As the reference frame is shifted, the "mean" shifts.

Fisher (1953) developed an analog for the normal on the sphere based upon a theory of random errors similar to that used by vonMises (1918) in developing the circular normal and by Gauss in developing the normal distribution. Fisher assumed that the "fundamental distribution of elementary errors on the surface of a unit sphere" is,

(B.3.1) $$f(\phi) \propto \exp(\kappa \cos\phi)$$

REFERENCE FRAME ONE

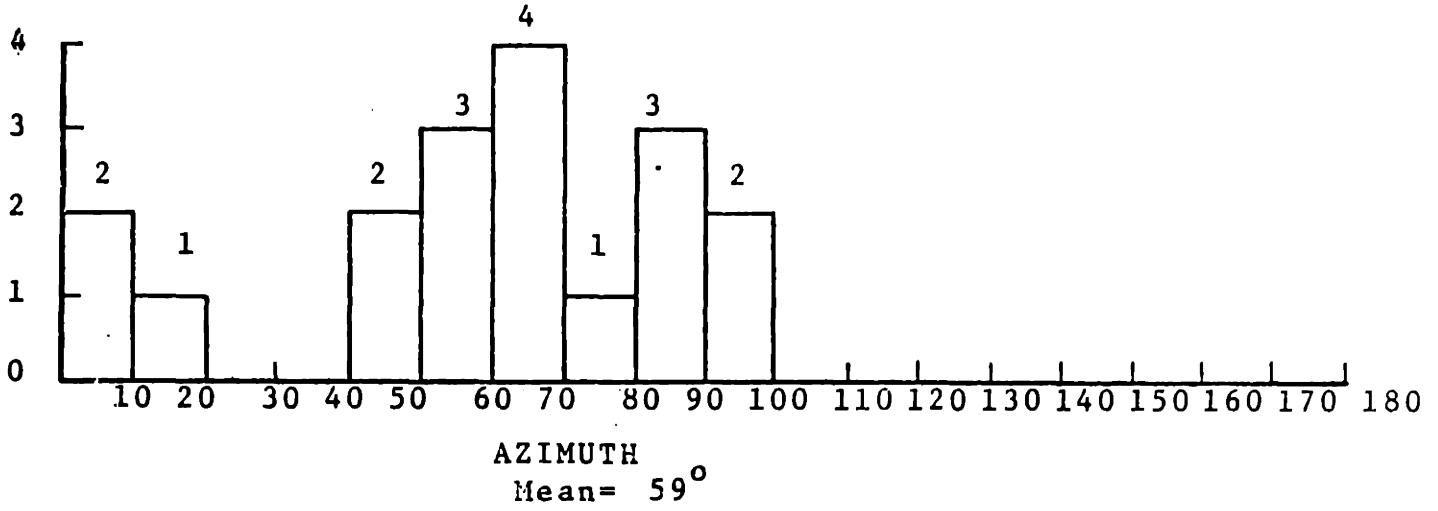

REFERENCE FRAME TWO
(Shift 40°)

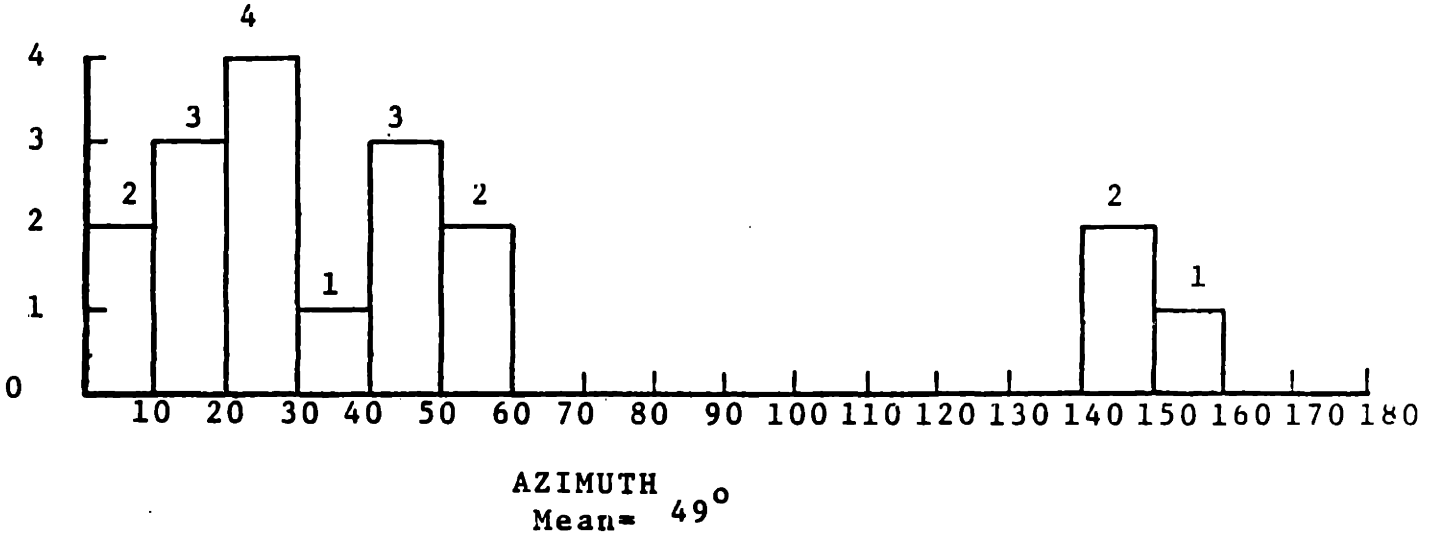

Figure B.3.2 Reference Frame and Mean Orientation

where κ is a measure of precision, and ϕ is the angle of a point from the mean pole (Figure 3.4.17). The frequency distribution (pdf) for this distribution is

$$\text{(B.3.2)} \qquad df(\phi) = \frac{\kappa}{2\sinh\kappa} e^{\kappa\cos\phi}\sin\phi d\phi$$

When $\kappa = 0$, the distribution becomes the uniform distribution on the sphere. Fisher found that the maximum likelihood estimate for κ could be found from

$$\text{(B.3.3)} \qquad \coth\kappa - \frac{1}{\kappa} = \frac{x}{N} \qquad \text{where } x = \sum_{\text{all}\,\phi}\cos\phi$$

N = number of observations

For $\kappa > 3$, this can be approximated by

$$\text{(B.3.4)} \qquad \kappa = \frac{|R|}{N}$$

where R = resultant vector of observations. $R = \Sigma l^2 + m^2 + n^2$ where l,m,n are direction cosines.

Figure B.3.3 illustrates the Fisher distribution on the surface of a sphere.

Breitenberger (1963) used two different solutions to find analogues for the normal. Since the normal distribution's strength is based in part upon its relation to the mean of sampl d ta, Breitenberger searched for analogues for the mean which

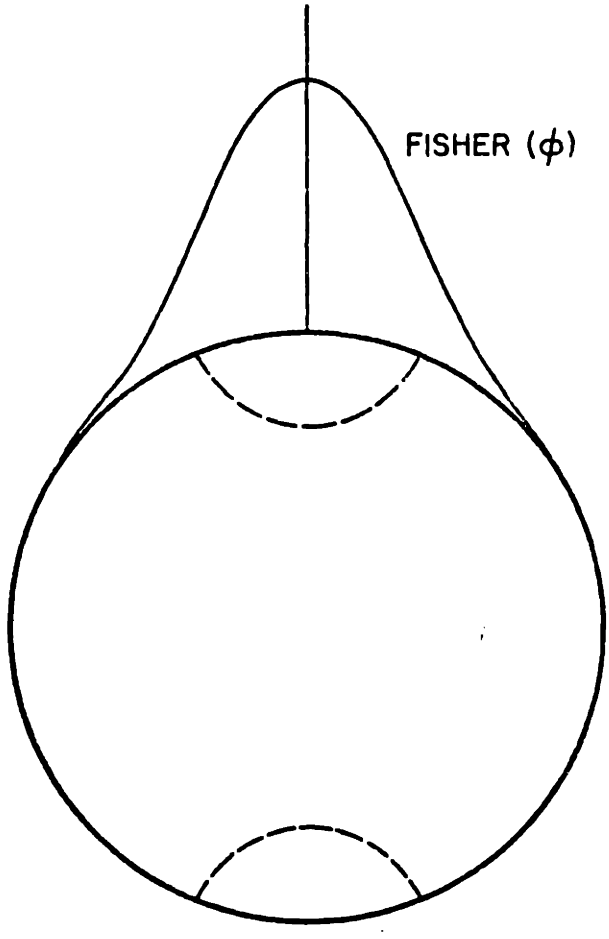

Figure B.3.3 Fisher Distribution on Surface of Sphere

are invariant with reference frame on the sphere. He found two analogues, the center of mass and the least polar moment of inertia.

From the center of mass, Breitenberger developed the distribution

(B.3.5) $$f(\theta,\phi) = \frac{\kappa}{4\pi \sinh\kappa} \exp\{\kappa\cos\phi\}$$

The pdf of this distribution is, of course, the Fisher.

(B.3.6) $$f(\theta,\phi) = \frac{\kappa}{4\pi \sinh\kappa} \exp\{\kappa\cos\phi\}\sin\phi d\phi d\theta$$

From the least polar moment of inertia, Breitenberger developed

(B.3.7) $$f(\theta,\phi) = \frac{\exp(-1/2\ \kappa\ \sin^2\phi)}{4\pi\ {}_1F_1\ (1;3/2;-1/2\kappa)}$$

when ${}_1F_1$ $(1;3/2;-1/2\kappa)$ is the confluent hypergeometric function and κ is a dispersion parameter. For large κ, $f(\theta,\phi)$ approaches the normal distribution on a plane. The pdf of this distribution is

(B.3.8) $$f(\theta,\phi) = \frac{\exp(-1/2\ \kappa\ \sin^2\phi)}{4\pi\ {}_1F_1\ (1;3/2;-1/2\kappa)} \sin^2\phi d\phi$$

Note that Breitenberger's techniques are basically an extension of Von Mises (1918) work on the circle.

Arnold (1941) used heat flow models to derive a hemispherical normal distribution. His work was performed as an M.I.T. Ph.D. dissertation and involves an inordinate amount of algebraic manipulation of heat flow and center of gravity theories to derive a distribution identical to Fisher's on the sphere.

Bridges (1977) attempted to extend Fisher's and Arnold's work on an analogue of the normal distribution to an analogue of the bivariate or elliptical normal distribution. He used complex graphical constructions on the sphere to develop an elliptical distribution with a form similar to the Fisher.

Bingham (1964) was the first to develop distribution for spherical data with a goal of generality rather than a goal of modeling the normal. His distribution is the only one which can model girdle and small circle distributions as well unimodal and bimodal clustered distributions. His distribution is

$$\text{(B.3.9)} \qquad f(\theta,\phi) = \frac{\exp(\kappa_1 \cos\phi \sin\phi + \kappa_2 \cos\phi \cos^2\theta)\sin\phi}{4\pi \; {}_1F_1\,(1/2;3/2;[{}^{\kappa_1}\kappa_2{}_0])}$$

where ${}_1F_1\,(1/2;3/2;[{}^{\kappa_1}\kappa_2{}_0])$ is a practically insoluble function, the confluent hypergeometric function of matrix argument and κ_1 and κ_2 are dispersion parameters.

Unfortunately, there is no easy method for finding maximum likelihood estimates for κ_1 and κ_2.

Maranhao (1968) objected to the entire method used for developing orientation distributions. He claimed that the use of spherical distributions introduced "exaggerated correction factor and that planar normal distributions could be used perfectly well for orientation data. Further, he stated that it is very importa to test for preferred orientations in a statistically significant manner as part of the distribution fitting process. He also made the claim, contradicted by all of the above studies, that most researchers fail to see joint density diagrams as pdf's.

Maranhao then proceeded to fit the bivariate normal distribution to 14 cases of orientation data clusters; and to test his fit by the χ^2 test. His fits passed the 95% significance level in all 14 cases.

This result would seem to confirm his claim that use of spherical distributions is unnecessary. However, as noted by Cruden and Charlesworth (1976) and others, for large κ, the Fisher distribution is equivalent to the planar normal distribution. For small κ, it is unreasonable to expect that the planar normal could fit spherical data. Since Maranhao did not publish his data, it is impossible to determine whether his data did in fact have large κ.

B.4 Orientation Sampling Bias

This section will briefly report studies of biases encounter in sampling for joint orientation, and a method for compensation

for these biases developed by Robertson and Piteau (1971).

Ruth Terzaghi (1964) was the first to recognize the seriousness of orientation sampling biases. She noted that whether a joint is observed in a sampling line or borehole is directly related to the orientation of that joint. Both strike and dip affect the probability of sampling of an individual joint. Terzaghi developed the relation

(B.4.1) $$N_\alpha = \frac{L\sin\alpha}{d}$$

where N_α = number of joints intersected in line survey

L = sample length

d = sample spacing

α = dip angle

to describe the effect of dip upon sampling.

Vistelius (1966) and Müller (1933) both developed relations between true dip, errors in dip measurement and errors in strike measurements.

Vistelius' relation is

(B.4.2) $$\sin\phi = \sin\gamma/\sin\delta$$

where ϕ = true dip

γ = error in dip measurement

δ = error in strike measurement

This relation is based upon the sensitivity of Brunton compass measurements to alignment with the true dip.

Müller's relation is

(B.4.3) $$\sin\phi = \tan\gamma/\tan\delta$$

Cruden and Charlesworth (1976) examined both the Vistelius and Muller hypotheses. They developed analytic techniques to explain the effect of true dip upon measurement errors, and collected empirical data. Figures B.4.1 and B.4.2 show empirical dip and strike and dip error measurements. In five test sets, Muller's hypothesis passed the χ^2 test at the 95% level for 4 out of 5 samples. Vistelius' hypothesis passed for all 5 samples. Cruden and Charlesworth concluded that:

1. Error in strike measurement is directly proportional to error in dip measurement.
2. Error in strike and dip measurements are inversely proportional to the sine of the true dip.

The only known attempt to apply corrections for errors and biases in sampling is Robertson and Piteau (1971). They modified the joint counts in each cell of their rectangular plot for sample bias by

(B.4.4) $$N'_{\theta\phi} = N_{\theta\phi}[\cos(\theta_1 - \theta)\cos|(\phi_1 + \phi - 90)|]^{-1}$$

where $N_{\theta\phi}$ = number of joints in rectangular cell centered at (θ,ϕ), and (θ_1,ϕ_1) are the orientation of the sample line.

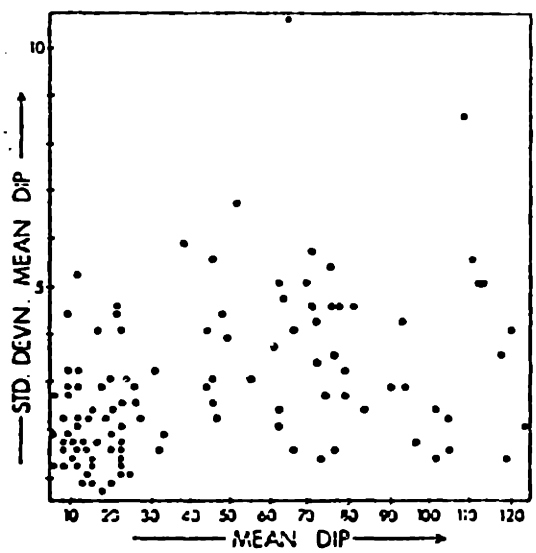

Figure 3. Variation in the standard deviation of dip with mean dip.

Figure B.4.1 Dip Measurement Error as a Function of Dip (Cruden & Charlesworth,1976)

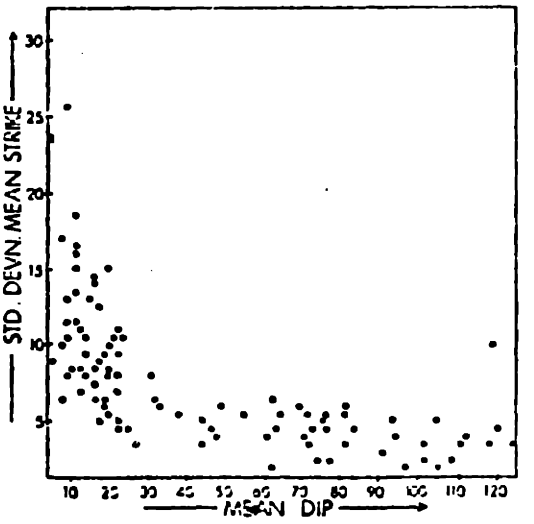

Figure 4. Variation in the standard deviation of strike with mean dip.

Figure B.4.2 Strike Measurement Error as a function of Dip (Cruden & Charlesworth,1976)

It is not known where they obtained their correction formula. Robertson and Piteau also corrected cell counts for survey length,

$$N''_{\theta\phi} = N'_{\theta\phi} \quad L_s/L \tag{B.4.5}$$

where L_s = sample line length

L = joint length,

and for the error introduced by using a rectangular plot instead of a proper spherical projection

$$N'''_{\theta\phi} = N''_{\theta\phi} \,/(\cos(90-\phi)) \tag{B.4.6}$$

Unfortunately, the correction factors modified the data in many cases by more than a factor of 5, so that the validity of final results is very much in question.

APPENDIX C

FITTING ORIENTATION DATA

This Appendix describes the use of computer program system FRAC2 to fit orientation distributions to joint orientation data. The manual for the computer program is given in Einstein, Baecher, et. al.(1979). Orientation distributions fit here are discribed in greater detail in Sections 3.4.4 and B.3 .

C.1 Introduction

The literature contains few attempts to fit distribution to orientation data. In general, mathematical distributions have not been fit systematically to orientation data. Research has generally been limited to a single orientation distribution. Mahtab (1975) used data from one porphory copper deposit to test the fit of the Bingham distribution. Maranhao (1968) used data from several different sites to test the fit of the Bivariate normal distribution. Mahtab's results were mixed, with about 50% of the joint clusters fit at the 95% confidence level. Maranhao's results indicated that the Bivariate normal distribution fit in all cases.

This Appendix presents a systematic attempt to fit orientation distributions to joint orientation data. A large variety of data sets were used in the study, and most known distributions were tested for quality of fit by both χ^2 and likelihood methods. Section C.2 describes the procedures used in the study. Results are presented in Section C.3. Section C.4 contains conclusions.

C.2 Fitting Procedures

The orientation distribution fitting process consists of three phases. In the first phase, data is converted to a standar format, and sorted into data clusters. In the second, maximum likelihood estimators for distribution parameters are determined for each distribution to be tested. In the final phase, the goodness of fit of each distribution is determined, and results are printed.

Five distributions are fit in this fitting program. They are the Arnold, Bingham, Bivariate Fisher, Fisher, and Bivariate Normal distributions. Mathematical forms for the distributions are shown in Table C.2.1.

Phase 1: Data Format Conversion and Clustering

Joint orientation data is taken in many different forms. These forms include strike-dip, azimuth-dip, and dip direction-dip. For purposes of analysis, it is convenient to have all data in the same format. The format chosen is upper hemisphere pole dip direction-dip. Table 3.4.1 shows the different forms and conversions between them.

Each data site generally contains several clusters of joint orientations. A joint cluster, as defined in Section B.2 is a group of joints having statistically homogeneous properties. Joints are commonly clustered on the basis of similar joint orientations. The procedure used for clustering in this study is as follows:

DISTRIBUTION	MATHEMATICAL FORM	MAXIMUM LIKELIHOOD ESTIMATORS
Arnold	$f(\theta,\phi)=\dfrac{e^{\kappa\cos\phi}\sin\phi}{e^{\kappa}-e^{-\kappa}}$	$\kappa=\dfrac{\lvert R\rvert}{N}$ R=Resultant Vector N= No. of Joints
Bingham	$f(\theta,\phi)=C_1e^{(\kappa_1\sin^2\theta+\kappa_2\cos^2\theta)\sin^2\phi}\sin\phi$	$\begin{vmatrix}\kappa_1 & & \\ & \kappa_2 & \\ & & 0\end{vmatrix}={}_1\bar{F}_1(\frac{1}{2};\frac{3}{2};\begin{vmatrix}\mu_1 & & \\ & \mu_2 & \\ & & \mu_3\end{vmatrix})$ where μ_i= eigenvalues of covariance matrix ${}_1\bar{F}_1$= inverse hypergeometric function of matrix arguments
Bivariate Normal	$f(\theta,\phi)=(2\pi\sigma_\theta\sigma_\phi)^{-1}\exp\{-\frac{1}{2}(\frac{\bar{\theta}^2}{\sigma_\theta^2}+\frac{\bar{\phi}^2}{\sigma_\phi^2})\}$	$\bar{\theta},\bar{\phi}$ = sample mean azimuth,dip $\sigma_\theta;\sigma_\phi$=sample standard deviations
Bivariate Fisher	$f(\theta,\phi)=C_1e^{(\kappa_1\sin^2\theta+\kappa_2\cos^2\theta)\cos\phi}\sin\phi$	κ_1,κ_2 by log-likelihood maximization
Fisher	$f(\theta,\phi)=\dfrac{e^{\kappa\cos\phi}\sin\phi}{1-e^{-2\kappa}}$	$\kappa=\dfrac{\lvert R\rvert}{N}$ R=Resultant Vector N=No. of Joints

Table C.2.1 Mathematical Forms of Distributions Fit

1. Plot all joints on stereonets.
2. Visually determine joint cluster boundaries on the basis of pole density.* (See Figure C.2.1)
3. Segregate joints into clusters on the basis of boundaries determined in Step 2.

Visual clustering techniques are used because of the failure of mathematical techniques such as those presented in Section B. to adequately separate adjacent joint sets.

Phase 2: Maximum Likelihood Estimation of Distribution Parameters

Once joint data have been divided into clusters, best estimates must be determined for distribution parameters. Maximum likelihood estimators are determined as follows:

1. Determine major and minor axes of data set. This is done on the basis of the eigenvectors of the covariance matrix of joint pole direction cosines.
2. Rotate data points into frame of reference of data set axes.
3. Determine maximum likelihood estimators for Fisher, Arnold, and Bivariate Normal distributions analytically. For the Fisher and Arnold distributions, the maximum likelihood estimator of dispersion κ is

*Pole density curves plot lines of equal joints per unit area on the surface of the sphere. Points with highest pole densities can be considered to be cluster mean poles. All joints within the density curves around the poles are then considered to be members of the joint clusters. Where density curves contain mor than one distinct high density point, joints are divided graphically into clusters around each high density point.

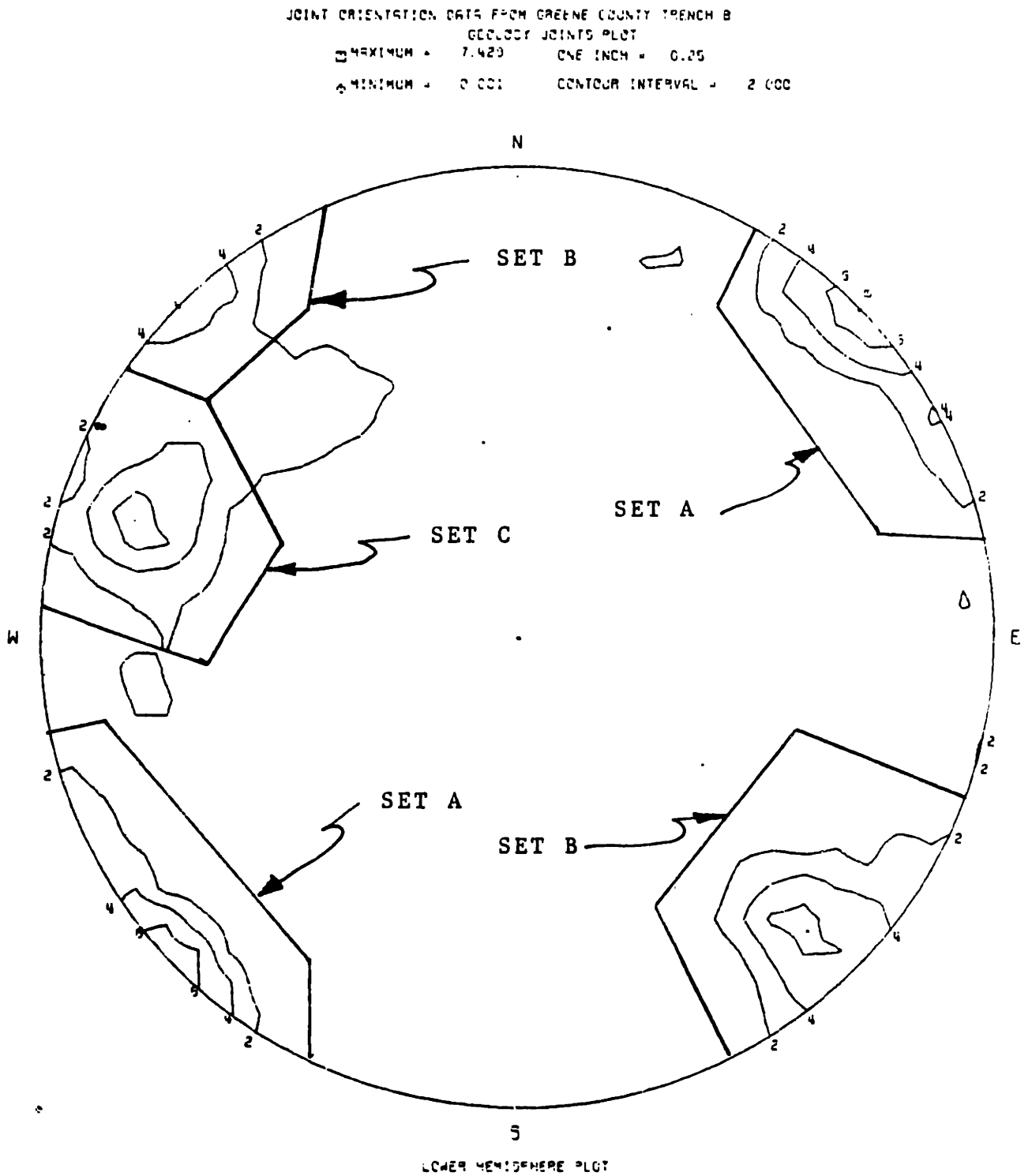

Figure C.2.1 Determination of Joint Cluster

$\kappa = \frac{|R|}{N}$ where R = resultant vector

N = number of data points in cluster.

For the normal distribution, the maximum likelihood estimators of the distribution parameters are the mean and standard deviation.

4. Determine maximum likelihood estimators for Bingham and Bivariate Fisher distributions by maximization of log likelihoods

$$\kappa_1, \kappa_2 \rightarrow \max\left[\sum_{i=1}^{N} \ln[f(\theta_i, \phi_i, \kappa_1, \kappa_2)]\right] \tag{C.2.1}$$

where N = number of data points

(θ_i, ϕ_i) = ith data points

$f(\theta, \phi, \kappa_1, \kappa_2)$ = distribution being fit.

Maximum likelihood estimators for the Bingham distribution are available in the closed form, but require calculation of confluent hypergeometric functions of matrix arguments. Confluent hypergeometric functions are very difficult to calculate when $\kappa > 10$, which is frequently the case.

Phase 3: Goodness of Fit Test

Two tests are conducted to determine the relative goodness of fit of the distributions. The χ^2 test is used to determine whether the fit of each distribution is significant at the 95% confidence level. The Log likelihood method allows determination

of the relative but not the absolute validity of different distributions.

1. χ^2 Test: The χ^2 test involves the determination of the difference between the actual number of data points in any given zone and the number of points predicted by the fit distribution. The test requires the arbitrary selection of zones over which the test is to be conducted. Here, zones were defined such that the average zone would contain 5 predicted data points. The number of zones, Z, is determined from

$$Z = N/5$$

The χ^2 statistic is

$$\chi^2 = \sum_{i=1}^{Z} (O_i - P_i)^2 \qquad \text{(C.2.2)}$$

where O_i = observed number of points in Zone 1

P_i = predicted number of points in Zone 1.

2. Log Likelihood Method: The log likelihood method involves comparison of log likelihoods for each distribution. The log likelihoods calculated during determination of maximum likelihood parameter estimators for Bingham and Bivariate Fisher distributions are used for those distributions. Log likelihoods are calculated in the same manner for Arnold, Fisher, and Normal distributions as they were for Bingham and

Bivariate Fisher. The best fitting distribution is tha which has the highest log likelihood.

C.3 Results

Distributions were fit to joint clusters from 5 sites. The sites are described in Baecher et al. (1978). Results are shown in Table C.3.1. No distribution fit data at the 95% confidence level of the χ^2 test for more than 4 clusters. The distributions which provided the best fit according to the log likelihood criterion are the Bingham and Bivariate Fisher distributions.

C.4 Conclusions

From Table C.3.1, it is impossible to select the best distribution to describe joint orientation data. No distribution performs adequately. Several explanations are available for the failure of the distributions tested.

The simplest explanation is that joint orientation distributions are generally of a form other than those tested. If this is the case, further work on the development of spherical distributions is required. Another possiblilty is that true rock joint orientations fit one or more of the distributions tested but that measurement and sampling biases (see Section B.4 result in distributions of <u>observed</u> joint orientations different from those tested. If this is the case, further research into joint orientation measurement and sampling biases would be desirable. A third possibility is that joint data clustering

LOG LIKELIHOODS

Joint Set	Fisher	Fisher Bi-Variate	Bingham	Pass χ^2 Test
MILLSAB1	-558.7	-520.3	-480.	NONE
MILLSAB2	-80.0		-8.	NONE
MILLSC1	-294.8	-144.	-107.	NONE
GREENEB1	-127.1	-31.5	-47.	NONE
GREENEB2	-71.5	-60.1	-282.	NONE
GREENEA1	-442.2	-322.9	-283.	NONE
GREENEA2	-131.	-90.7	-326.	NONE
GREENET2			-29.	NONE
GREENET3	-89.4	-68.5	-51.	NONE
BLUEHILLS1	-125.0	-122.0	-114.	ALL
BLUEHILLS2			-20.	NONE
BLUEHILLS3	-20.	-20.0	-91.	NONE
DUVALL1	-567.6	-554.8	-517.	NONE
C1901.1	-444.5	-287.7	-272.	NONE
C1904.2	-236.1	-141.7	-149.	BINGHAM
COKA.1	-79.4	-57.6	-37.	NONE
COKA.2	-62.3	-27.0	-27.	ALL
C6205.1	-383.6	-298.9	-280.	NONE
C6205.2	-251.8	-91.4	-140.	NONE
C2005.1	-574.7	-574.8	-555.	NONE
C2005.2	-119.9	-45.4	-41.	BINGHAM,BIV. F.
MILLSC2	-294.8	-144.	-107.	NONE
TOTAL BEST FITS:		7.	13.	

Note: Best Fit is highest loglikelihood.
Normal Distribution was fit on direction cosines and results are therefore not comparable. Magnitude of log-likelihood is related to number of observations, so it is not possible to compare values between different sets. Arnold Distribution results are indistinguishable from Fisher results.

Figure C.3.1 Results of Goodness of Fit Tests of Orientation Distributions